Calcium carbonate surface/bulk scaling mechanisms and kinetics in a once-through in-situ flow visualization rig

A thesis submitted

By

Olujide Samuel Sanni

Submitted in accordance with the requirements for the degree of

Doctor of Philosophy
The University of Leeds
School of Mechanical Engineering
September, 2016

The candidate confirms that the work submitted is his own and that appropriate credit has been given where reference has been made to the work of others.

This copy has been supplied on the understanding that it is copyright material and that no quotation from the thesis may be published without proper acknowledgement.

Acknowledgement

Abstract

Scale management is usually a complex mixture of prediction, inhibition and sometimes removal strategies. Investigations into scale formation have largely been focused on precipitation in the bulk solution by assuming that surface scaling always results from pre-precipitated crystals in the bulk solution. Recent observations have shown that bulk and surface scaling do not share the same trends with respect to crystal growth kinetics and inhibition as such the relationship between these two scaling processes are being given attention in the literature. Despite much recent attention on scale formation on surface, there is still not a full mechanistic understanding of how scale layers build on component surfaces. Most of the previous studies have been carried out in a closed system where the saturation ratio was decreasing as a function of time. As such, the understanding of the precipitation/deposition system needs a suitable methodology to build an accurate surface deposition kinetic model.

The objectives of this study are to develop a once-through flow rig system suitable to distinctively study bulk precipitation and surface scaling processes and also to improve on the understanding of surface scale deposition mechanisms and kinetics at constant supersaturation. The *in-situ* flow rig is designed to combine measurement of turbidity in the bulk and real-time visualization of scale build up on a solid surface. Calcium carbonate ($CaCO_3$) surface and bulk scaling deposition were followed *in-situ* and in real-time in a newly developed flow rig that allows assessment and control of various scaling indices and parameters. The kinetics and mechanisms of $CaCO_3$ surface scaling are evaluated from images taken with time using the image analysis protocols to determine the surface coverage, number of particles and average size of the crystal.

Brines with different values of saturation ratio (SR) 15, 25, 45, 60, 70 and 90 were tested at 25°C and 40°C. The effects of SR, flow rates and temperature on scale deposition were studied. The flow rates used are 10ml/min, 20ml/min

and 40ml/min. Also, the influence of SR and inhibitor concentration on surface inhibition efficiency of Polyphosphinocarboxylic acid (PPCA) were studied.

The newly developed set-up allows for a mechanistic understanding of scale build up on the surfaces in flowing conditions at constant SR and helps to improve the understanding of both bulk precipitation and surface deposition scaling kinetics. Results show that at low SR, the residence time from the mixing point to sample was shorter than the induction time for bulk precipitation and, as a result, there are no crystals in the bulk solution as the flow passes the sample. Therefore, in contrast to popular thinking, the study has shown that crystals present on the surface are not always the result of a secondary deposition process occurring after the precipitation mechanism which occurs in the bulk solution. The determination of surface crystallization mechanisms and kinetics allow for the correct type and dosage of inhibitor to be selected. Addition of inhibitors at the bulk minimum inhibition concentration (MIC) actually aggravates surface scaling

Table of content

List of Figures

List of Tables

Publications

O. Sanni, O. Bukuaghangin, T. Charpentier, N. Kapur, A. Neville (2016), "Using a Real-Time Visualisation Technique for the Assessment of Surface Scale Kinetics and Mechanisms of Inhibition," SPE International Oilfield Scale, 179896 (Aberdeen, UK: SPE 2016), Society of Petroleum Engineers

O. S. Sanni, T. Charpentier, N. Kapur, A. Neville (2016) "$CaCO_3$ Scale Surface Nucleation and Growth Kinetics in a Once-Through in situ Flow Rig as a Function of Saturation Ratio (SR)," Corrosion 2016, Paper No.07642 (Vancouver, Canada: NACE, 2016), NACE International.

O. Sanni, T. Charpentier, N. Kapur, A. Neville (2015), "Study of Surface Deposition and Bulk Scaling Kinetics in Oilfield Conditions Using an In-Situ Flow Rig," Corrosion 2015, Paper No. 05916 (Dallas, US: NACE, 2015), NACE International.

Nomenclature

β: Geometric factor

γ: Free surface energy (J.m^{-2})

σ: Interfacial energy (J.m^{-2})

$f(\theta)$: Correction factor

V_m: Molecular Volume (m^3.mol^{-1})

k: Boltzmann constant (1.3805.10^{-23}J.K^{-1})

a: geometric factor

K_{sp}: Solubility product

SR: Saturation Ratio

t_{ind}: Induction time (s)

t_r: Relaxation time (s)

t_n: Period of nucleation (s)

t_g: Growth time (s)

t_{surf}: Surface induction time (s)

t_{bulk}: bulk induction time (s)

A: Empirical constant

T: Temperature (K)

N_A: Avogadro number (6.023.10^{23} mol^{-1})

R: Gas constant (8.3143 J.mol^{-1}.K^{-1})

ΔG: Overall excess free energy (kJ.mol^{-1})

ΔGS: Volume free energy (kJ.mol^{-1})

ΔGV: Surface excess free energy (kJ.mol^{-1})

r:: Equivalent radius of the crystal (m)

r_c: Critical radius (m)

J: Nucleation rate (Number of nuclei/s.m^3)

$K1$: Kinetic constant (pre-exponential term of the nucleation rate)

p: Number of ion in the critical size cluster

S: Supersaturation ratio

K: Constant

N: Number of crystals

D: Constant

αN: Slope of log N versus (log S)$^{-2}$ function

m: mass of solid deposited (g)

$A(t)$: Surface area of a crystal (cm^2)

km: Coefficient of mass transfer

c: Solute concentration (mol.l^{-1})

c^*: Equilibrium saturation concentration

kc: Crystal growth constant

[Ca]: Molar concentration of calcium (mol.l^{-1})

[Ca]$_{eq}$: Molar concentration of calcium at equilibrium (mol.l^{-1})

g: Kinetic order of growth

i$_{res}$: residual current (μA)

V$_s$: Scaling rate

$T\lambda$: Turbidity

I_o: Intensity of the incident ray

I_L: Intensity of the transmitted ray after an optical path length L

A: complex function of the wavelength use and the relative refractive index of the solid with respect to the solvent (for Turbidity)

N_0: particles per unit volume of solution

v: volume of each particle

l: Length of profile used for the measurement of surface roughness parameters

θ: Contact angle (°)

γS: solid surface free energy

γSL: solid/liquid interfacial free energy

γL: liquid surface tension

u: terminal velocity (m.s)

g: acceleration due to gravity (m.s^{-2})

μ: viscosity of the fluid (N.s/m^2)

ρ: Density (kg.m^{-3})

Re: Reynolds number

t: Time

N_0: Active nucleation sites (μm^{-2})

SI: Saturation Index

SR: Saturation ratio

S(t): Surface Coverage (%)

S_{ext}(t): Extended surface coverage (%)

Chapter 1 Introduction

Several industries are plagued by various inevitable challenges that quietly loom as very serious threats to sustainable production resulting in a huge financial drain to the economy. In the oil and gas industry, formation of mineral scale or scaling is one major challenge that is usually encountered.

Mineral scale formation is the deposition of sparingly soluble inorganic salts from aqueous solutions. Scaling can also be regarded to as 'precipitation fouling', which is the accumulation of unwanted material on solid surfaces to the detriment of function. Fouling material can consist of either living organisms (biofouling) or non-living substances (inorganic or organic) [1, 2].

For the purpose of this study, scaling is defined as a solid layer deposition on a surface that arises primarily from the presence of dissolved inorganic salts in the flowing solution that exhibits supersaturation under the process conditions [3]. Scale formation is one of the factors which needs to be taken into account in the earliest stage of design, equipment development, and choice of a proper material and production of specific equipment. The possibility of scale formation on surfaces is also one of the criteria to look at before implementing new chemicals in the industry. Insufficient attention to scale formation problems can lead to such undesirable circumstances as: decreasing performance of the equipment, significant decreasing productivity, economical costs, and time consumption for mechanical removal of already formed scale [1, 2, 4].

Three main approaches that are used to mitigate scaling are

- Prediction: analyzing the mechanisms and conditions that lead to the precipitation and deposition of scales viz- a-viz the thermodynamic and kinetic processes. In order to manage a potential scale problem, it is

important to know where and how much calcium carbonate ($CaCO_3$) scale will be deposited during oil and water production [5].

- <u>Inhibition</u>: preventive methods such as developing different types of inhibitors as well as modification of the material surfaces. It is the most common method of preventing scale in industry [6].

- <u>Removal</u>: mechanical and/or chemical means that has to do with removing the present fouling layer to restore as best the original productivity [2].

The various scales typically encountered in industry according to the water chemistry and environmental conditions include [7] :

- Calcium carbonate – (calcite and aragonite) - $CaCO_3$
- Calcium oxalate – CaC_2O_4
- Sulfate salts of calcium (gypsum – $CaSO_4 *2H_2O$)
- Barium sulfate (barite) – $BaSO_4$
- Magnesium hydroxide – $Mg(OH)_2$, magnesium oxides - MgO
- Sodium chloride (halite) – $NaCl$

The consequences of scaling are; lowered heat transfer efficiency, increase in pumping costs, total or partial blocking the water flow and the requirement for frequent system cleaning. Mineral scale has always been a major flow assurance problem in the oil industry [7].

1.1 Mineral scale in the oil industry

Mineral scale is a major problem for the upstream oil and gas industry during production of well fluids. Scale formation in the near-wellbore area, the tubing and in topsides facilities is one of the major challenges associated with oil production and so must be managed. The most severe problems are predominantly encountered during oil and condensate production where the thermodynamic driving force for scale deposition is caused by temperature and pressure changes or mixing of incompatible waters [8]. Oil and gas reservoirs have a natural water layer called the formation water, to achieve

maximum oil recovery, additional water is often injected at high pressure into the reservoirs as shown in Figure 1-1 to help force the oil onto the surface and in the direction of the production wells. The injected water can have a different ionic concentration and composition to the formation water leading to a high risk of scale formation.
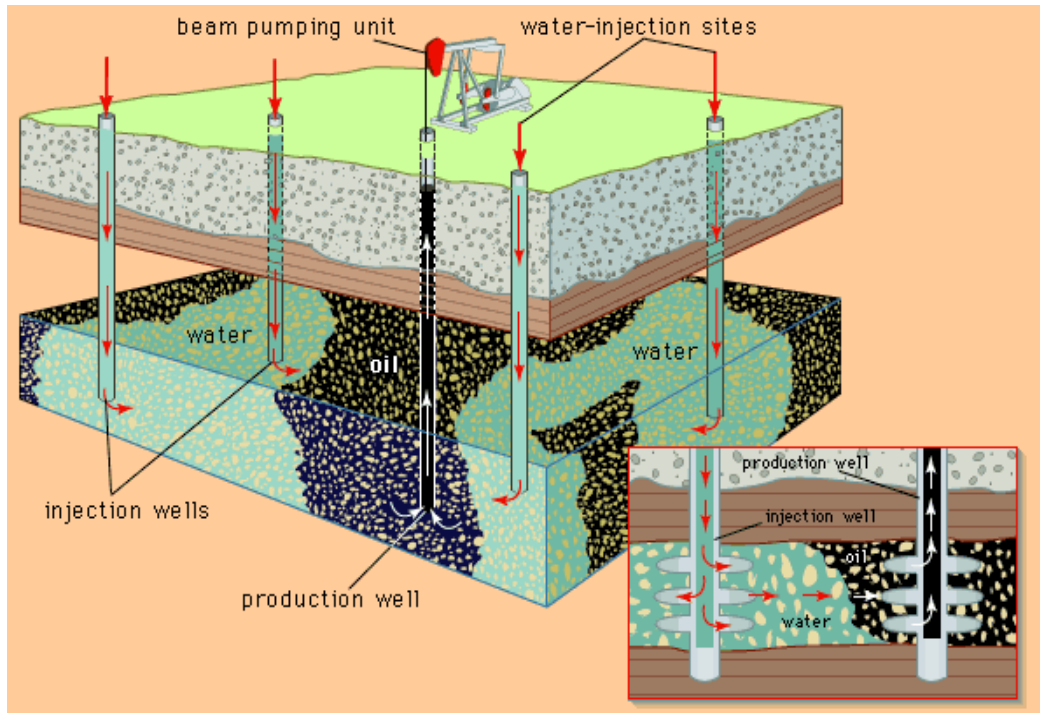
Figure 1-1: Schematic of the secondary oil recovery process [9]

Scale can develop in the formation pores near wellbore-reducing formation porosity and permeability. It can block flow by clogging perforations or forming a thick lining in production tubings, see Figure 1-2. It can also coat and damage downhole completion equipment such as safety valves. Scaling occurs anywhere along the production conduit narrowing the internal diameter and blocking flow and can even occur as far along as the processing facilities.

Dealing with scale problems costs the industry hundreds of millions of dollars per year in lost production [10]. $CaCO_3$ scale growth in production tubing (Figure 1-2) obstructs more than 40% of the flowing area of the tubing and prevents access to lower sections by well remediation

(a)	(b)
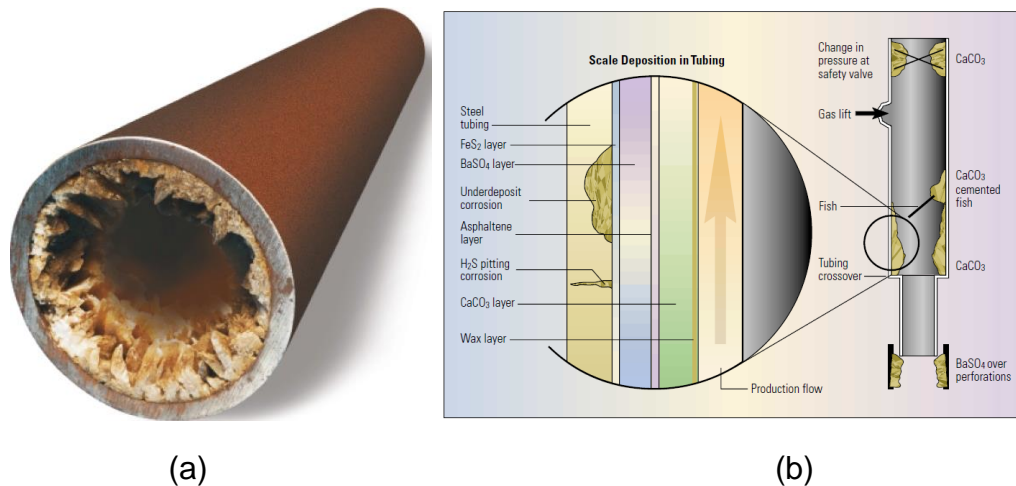
Figure 1-2: (a) Scale deposition in a pipe [11] (b) Scale formation in tubing [11]

Materials used in the oilfield production, transport and refining processes are potentially sensitive to scale occurrence. As a consequence, many different parts of the network are replaced prematurely. Moreover, pipes that are largely affected with scale require rigorous and expensive maintenance [12, 13].

The different scales that are usually found in the oil industry are calcium carbonate (amorphous, calcite and aragonite) and sulfate salts of calcium (gypsum), strontium (celestite), and barium (Barite) [6]. Some of the more common ions that frequently occur in oilfield waters and cause precipitation in incompatible waters are ions of calcium (Ca^{2+}), strontium (Sr^{2+}), barium (Ba^{2+}), iron (Fe^{2+}), bi-carbonate (HCO_3^{-}), and sulphate ($SO_4^{\,2-}$) [14].

$CaCO_3$, is one of the most common scales found in oilfield production wells and surface facilities [15]. It is a sparingly soluble inorganic compound formed in aqueous phase during oil and gas productions [2]. Formation water usually contains bicarbonate ions as well as calcium ions. In most cases, the scaled-up wells are caused by the formation of sulfate and carbonate scales of calcium and barium due to their relative hardness and low solubility [16].

The concept of crystallisation, mechanisms of $CaCO_3$ scaling (nucleation and growth), various factors that affect scaling, scale inhibition, thermodynamics

and kinetic studies of $CaCO_3$ scale, surface for preventing scaling amongst all are extensively presented under the literature review (see chapter 2).

1.2 Background and objectives

1.2.1 Background

There is a considerable interest to investigate surface crystallization in order to have a full mechanistic understanding of scaling and consequently the possible treatments to eliminate the formation of deposits [17]. The growth of calcium carbonate ($CaCO_3$) on various surfaces has been thoroughly examined with several models developed in many studies but most of these studies were based primarily on thermodynamic considerations. However, effective prediction of scaling requires a reliable thermodynamic model for the prediction of the scaling tendency and a kinetic model for the prediction of scaling rate [18].

As earlier described, scaling can be regarded as crystallization/precipitation fouling process and therefore the development of antifouling surfaces is an area of interest. The scaling process on a surface has been assumed, for a long time, to be similar to the biofouling process with migration of the foulant towards the surface. Nevertheless the crystallisation process has been shown to be different [19, 20].

There is no predictive model that has been developed based on surface deposition measurements. Models based on bulk measurements to predict scale thermodynamics and kinetics have previously been developed. The relationship between these two processes have received little attention while only a few authors have recently tried to link both. Moreover, the majority of the studies have focused on "off-line" or static conditions and the crystallisation has not been recorded in real-time [21, 22].

An *in-situ* technique developed by Euvrard *et al* [17] was based on electro-crystallization. It yielded some extremely important information regarding the

kinetics of scale formation. So far there has been one study which employ such an *in-situ* method for deposition from a supersaturated solution. The study which considered combined bulk precipitation and surface deposition *in-situ* from supersaturated solution was carried out in a closed system where the saturation was decreasing with time [23]. The understanding of the precipitation/deposition system needs experimental work conducted in a once-through system. Such a suitable methodology for the building of an accurate deposition kinetic model would result in a reliable prediction which could be translated to different flow scenarios.

Against this background, the present work aims is to develop a system that enables surface deposition and bulk precipitation measurement at constant saturation ratio in order to increase the mechanistic understanding of how scale layers build on component surfaces.

1.2.2 Objectives

Three main objectives of the current work, are described below:

- To design and develop a once-through *in-situ* visualization flow rig and associated analysis protocols that enable the combined assessment of bulk precipitation and quantification of surface scaling in flowing conditions. This will ultimately enable both bulk and surface scaling mechanisms to be studied and how one relates to the other under constant driving force to be considered.

- To understand the mechanisms and kinetics of $CaCO_3$ surface scaling in terms of nucleation and growth processes at different SR, flow rates and temperatures. This will allow to decoupling the thermodynamic and kinetic parameters in fouling mechanisms and ultimately be able to develop a better scale management strategy.

- To demonstrate the mechanisms and assess the effectiveness of scale inhibitor (PPCA) on both bulk precipitation and surface scaling at different SR values under the same set of conditions. This will allow the

6

effectiveness of current bulk scale inhibitors (SI) on surface scaling to be assessed.

The objectives of the study are to improve the knowledge of surface deposition mechanisms and kinetics. This would have a significant impact on predicting the formation of scale and improving inhibition strategy especially on topside facilities.

1.3 Outline and overview

The first chapter gives an insight into scale formation processes and the problems it poses to industry especially the oil industry. The different types of inorganic scale, the approaches that are used to mitigate against scaling, the background as well as the objectives of the work are also highlighted.

A literature review on the explicit description of calcium carbonate scaling and the various factor affecting its formation is given in the second chapter. A literature review is also presented in Chapter Three on scale removal and inhibition techniques, current study and investigation techniques and an overview of the current techniques use to study calcium carbonate mineral scale is presented.

The fourth chapter fully describes the methodology in which the design of the rig, the image analysis protocols for image processing and analysis of the surface deposition data, the apparatus, brine solutions, sample used, and experimental overview are presented. The commissioning of the rig is presented in Chapter Five which also includes the optimisation of the technique, repeatability and scale uniformity tests as well as some initial images visualization and processing. Results from the assessments of scale kinetics and mechanism are presented in Chapter Six and Chapter Seven. Chapter Six presents observations of bulk precipitation and surface scaling at both low SR and high SR and the effects of varying SR. Chapter 7 gives the

results obtained *in-situ* and in real time for the bulk and surface kinetics at different flow rates, temperature and inhibitor injection.

The discussion presented in Chapter Eight with reference to past and current work includes: bulk precipitation versus surface scaling, mechanisms and kinetics of surface scale formation at constant SR, quantification of surface induction and growth rate, correlation of surface scaling with deposition flux and temperature as well as the effects of inhibitors injection at different SR. A general summary of the study, conclusions and recommended future work are given in Chapter Nine.

Chapter 2 Literature Review

2.1 Scale formation

Drilling and oil recovery processes in production and injection wells at any location from downhole to topside facilities are usually associated with disturbance to thermodynamic and chemical equilibria leading to scale formation [10, 24]. Scale would occur if the water contains ions which are capable of forming compounds of limited solubility and if there is a change in the physical condition or water composition that lowers the solubility below the concentration present [25].

Scale formation, referred to as the crystallization of sparingly soluble substances, crystallization by precipitation, or simply precipitation are usually the result of nucleation and growth processes which, can either proceed consecutively (in series) or simultaneously (in parallel) throughout the whole, or during only part of the crystallization [26].

Scale formation processes lead to either precipitation in the bulk and/or the deposition on a surface. For precipitation to occur from a solution, the solution must contain more ions than it can dissolve, a phenomenon known as 'Supersaturation'. It is an important factor which controls the precipitation of salts from solution. Therefore, scale could be any precipitation, sedimentation or deposition of a compound which forms once the solubility of these precipitates exceeds the saturation limit [27]. The processes involved in the precipitation of scale are shown in Figure 2-1.

2.1.1 Supersaturation

The rate of scale formation process can be a function of the level of supersaturation at which it takes place. The low solubility of sparingly soluble materials leads to the development of high supersaturation and consequently leads to precipitated products [26]. This means that the solution has to contain

more solute entities (molecules or ions) dissolved than it would contain under the equilibrium (saturated solution) [28].
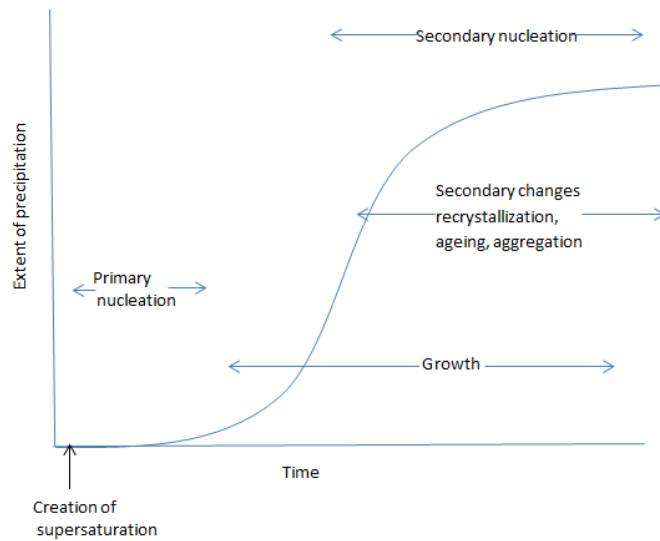
Figure 2-1: Processes involved in precipitation [28]

Supersaturation can be regarded to as the "thermodynamic driving force" for scale formation. The scaling tendency for a giving solution can be quantified by its saturation ratio (SR) which is the excess of the actual concentration of dissolved ions over the solubility product [29-32].

$$SR = \frac{\text{IAP}}{K_{sp}}$$
(2.1)

Where IAP denotes the product of ion activity and K_{sp} is the solubility product.

Supersaturation ratio for ionic compound based on activity is given as:

$$SR = (\frac{IAP}{K_a})^{1/\gamma}$$
(2.2)

K_a is the activity based solubility product, γ is the activity cooefficient.

The solubility of a salt is the mass of the salt dissolved in a known weight or volume of fluid [10] and it is a measure of its ability to stay in the liquid phase

without precipitation under given conditions. The value of K_{sp} for calcite is given as 4.55 x 10^9 at 25°C (298K) and 1.06 x 10^9 at 80°C (353K) [33].

For salts, there are different numbers of charge on the cations and anions, the generalized equation is

$$M_mX_x(s) \leftrightarrow mM^{z+}(aq) + xX^{z-}(aq) \tag{2.3}$$

Where m and x are the number of cations with charge z^+ and number of anions with a charge of z^- respectively. M^{z+} and X^{z-} are the ionic activities of the species.

For salt dissolution, which is important in scaling studies, the equilibrium constant K_{eq} is given as [27]

$$K_{eq} = \frac{[M^{z+}]^m \, [X^{z-}]^x}{[M_mX_x]} \tag{2.4}$$

The activity of pure solid = 1, therefore (2.3) becomes

$$K_{eq} = K_{sp} = [M^{z+}]^m[X^{z-}]^x \tag{2.5}$$

Where solubility product, K_{sp} is the equilibrium constant for the dissolution of salt. If the salt is dissolving into a dilute solution, the ionic activities are equal to their concentrations in mol/m^3.

Saturation ratio, SR, for a salt measures the degree of supersaturation.

From (2.1)

$$SR = \frac{IAP}{K_{sp}} = \frac{[M^{z+}]^m[X^{z-}]^x}{K_{sp}} \tag{2.6}$$

SR = 1: represents an equilibrium state where both scale precipitation and dissolution rate are balanced.

SR < 1: This represents an undersaturated solution. Scale formation is practically not possible and the solution is likely to dissolve any deposit.

1< SR ≤ 40: The solution is supersaturated and there is an inherent tendency for scale to form which means that scaling is thermodynamically possible.

SR > 40: There is spontaneous precipitation of $CaCO_3$ [31]

The scaling tendency can also be expressed in terms of Saturation Index (SI), which is the logarithm of Saturation Ratio (SR)

$$SI = \log_{10} SR \tag{2.7}$$

The saturation index of a solution changes for different fields because of its dependence on temperature and pressure as well as ionic strength [28, 34].

Once supersaturation is attained, the process of scale formation which involves nucleation and growth would proceed. Nucleation is usually preceded by the induction process.

2.1.2 Induction time

Before precipitation, the supersaturated solution is in a metastable state where spontaneous nucleation is impossible and the solution needs to reach an unstable state for nucleation to occur, this process is known as the induction time (t_{ind}) [35].

The concept of induction presupposes a time lapse between the establishment of supersaturation and the first changes in the system physical properties. Thus, the induction time is sometimes referred to as the 'waiting time' or 'incubation period' for scaling. It is the time between supersaturation state and the detection of the first crystal particles [26, 36].

Induction time corresponds to the appearance of visible crystals, an increase in turbidity, a concentration decrease or a decrease in solution conductivity [26]. The total induction time can be a combination of the relaxation time (t_r), in which there is distribution of molecular clusters for the system to reach a quasi-steady-state; nucleation time (t_n), to form a stable nucleus and growth time (t_g), for the nucleus to attain a visible size [35].

The induction period in a homogeneous liquid system represents the sum of the times necessary for critical nucleus to be formed, t_i and for the critical nucleus to grow to a detectable size, t_g [37].

$$t_{ind} = t_i + t_g \tag{2.8}$$

Models relating the induction time and the initial concentration of the solution have been proposed [36]. Further works improved the correlation by considering several other parameters such as temperature, interfacial tension, the saturation index, the activation energy for nucleation.

Sohnel and Muhlin [38], established a model to discuss the molecular interpretation of induction times from the standpoint of classical nucleation theory as follow:

Crystal nuclei with a critical size must be formed before the new solid phase is visible.

$$\ln t_{(ind)} = \frac{B}{T^3(\Delta G/RT)^2} - \ln A \tag{2.9}$$

$$\ln(t_{ind}) = \frac{B}{T^3(\log SR)^2} - \ln A \tag{2.10}$$

According to the model there exists a free energy barrier, ΔG^o to the formation of the crystal nuclei. ΔG^o is proportional to $(\ln SR)^{-1}$ where SR is the saturation ratio. The Gibb's free energy, ΔG of the supersaturated solution is equal to $-RT \ln S$ (where R=gas constant, T= temperature, A is an empirical constant (dimensionless) and B is given by:

$$B = \frac{\beta \gamma^3 V_m^2 N_A^2 f(\theta)}{(1.3R)^3} \tag{2.11}$$

Where β is a geometric factor of $16\pi/3$ (for the spherical nucleus), $f(\theta)$ is a correction factor according to the type of nucleation taking place, V_m is the molecular volume (6.132×10^{-23} cm^3 for calcite), T is the absolute temperature

(Kelvin), R the gas constant (8.3146 J/mol.K), γ is the surface energy (mJ/m^2) and N_A is Avogadro's number (6.022 X 10$^-$23/mol).

The induction time is a function of ΔG^o and thus a function of S. The expected correlation between the induction period of the nucleation is an inverse relation, the greater the supersaturation, the shorter the induction time [31, 39]. The appearance of the first nuclei marked the end of the induction period and immediately signalled the nucleation process.

2.1.3 Nucleation

Nucleus formation or nucleation primarily involves the creation of a new crystal phase. Mostly, the change of phase A to phase B will not commence immediately the process becomes thermodynamically possible but after at least one phase B nucleus is formed in phase A. It is only after then that phase B can increase in volume [26, 35]

The different mechanisms found responsible for nucleation are based on whether there is the presence or absence of foreign particles, which makes nucleation to either occur spontaneously or induced artificially [35, 40, 41]. A broad classification is shown in the Figure 2-2 below.
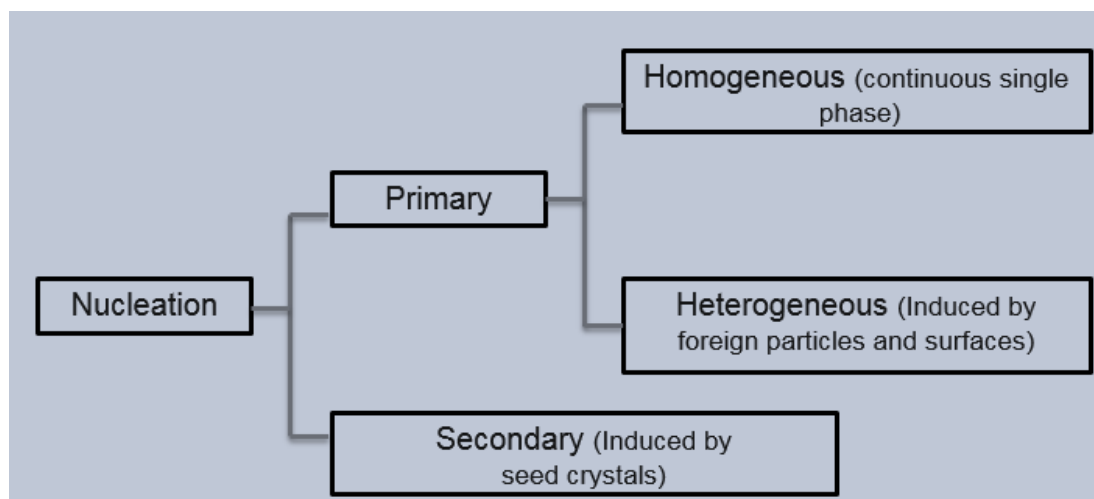
Figure 2-2: Types of nucleation [35]

2.1.3.1   Primary nucleation

Primary nucleation usually predominates in a supersaturated solution. It can either be homogeneous or heterogeneous depending on whether the formation of a new phase occurs with or without any influence or the presence of foreign particles and surfaces. While homogeneous nucleation is not brought about by the presence of foreign particles heterogeneous nucleation requires that a foreign body be present [35]. Figure 2-3 depicts the homogeneous and heterogeneous nucleation processes. Generally, at high supersaturation degree, homogeneous nucleation predominates while heterogeneous nucleation play a major role at low supersaturation because the presence of impurities or foreign particles actually lowers the critical saturation value for heterogeneous nucleation [10, 35, 42, 43].
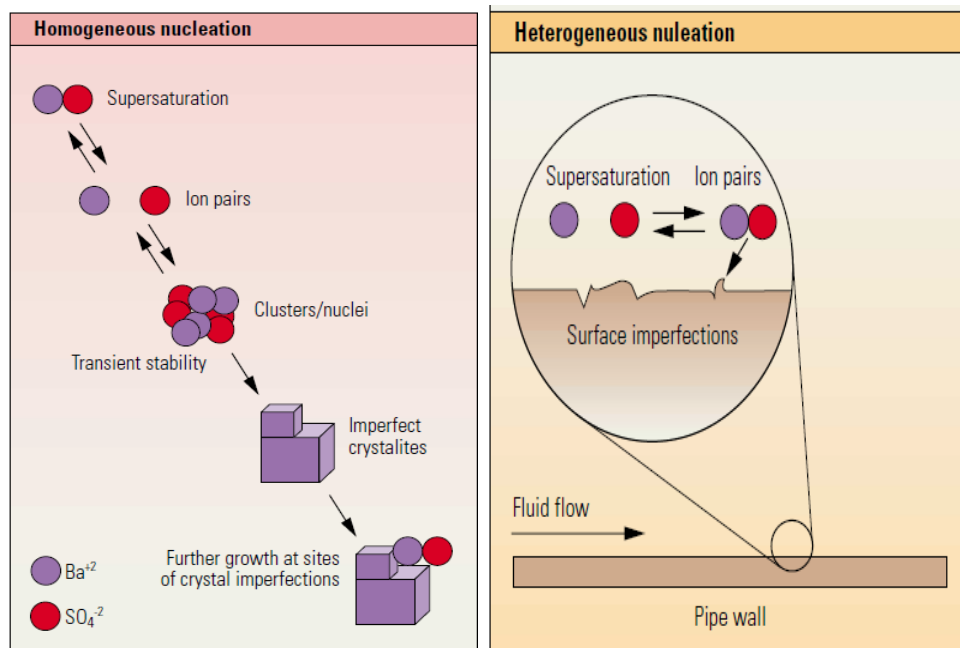
Figure 2-3: Process of homogeneous and heterogeneous nucleation [11]

The free energy changes associated with the process of homogeneous nucleation is expressed by the classical theory of nucleation [35, 44] as follows:

$$\Delta G = \Delta G_S + \Delta G_\upsilon = 4\pi r^2 \gamma + \frac{4}{3}\pi r^3 \Delta G_\upsilon \qquad \textbf{(2.12)}$$

Where ΔG is the overall excess free energy between a small solid particle of solute and the solute in solution, r =radius of the solute (sphere), ΔG_S = surface excess free energy (a positive quantity proportional to r^2) ΔG_υ = volume excess free energy particle of solute (a negative quantity proportional to r^3), γ = interfacial tension (J/m^2). The maximum value of ΔG, ΔG_C corresponds to the critical nucleus,r_c

By setting

$$\frac{d\Delta G}{dr} = 0 \tag{2.13}$$

$$r_c = \frac{-2\gamma}{\Delta G\upsilon} \tag{2.14}$$

$$\Delta G_c = \frac{16\pi\gamma^3}{3(\Delta G_V)^2} = \frac{4\pi\gamma r_c^2}{3} \tag{2.15}$$
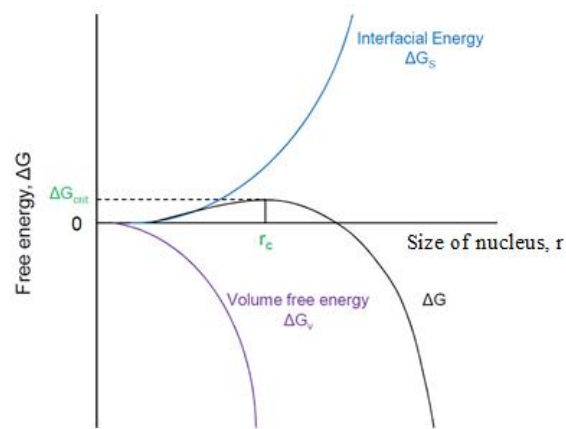
Figure 2-4: Free energy diagram for nucleation and critical radius [35]

The nucleation rate is the number of nuclei formed per unit time and volume. The expression of nucleation rate is given in form of the Arrhenius reaction velocity equation commonly used for the rate of a thermally activated process:

$$J = K_1 \exp(\frac{-\Delta G_c}{KT}) \tag{2.16}$$

Where J = Nucleation rate (Number of nuclei/s.m^3); K_1 = Frequency factor in nucleation rate equation. K (m^{-3}/s) = Boltzmann constant (J/K); T = temperature (K) and ΔG_C = free energy change for the critical cluster size formation given by:

$$\Delta G_c = \frac{16}{3} \frac{\pi a \gamma^3 \upsilon^2}{3(KT \ln SR)^2} \tag{2.17}$$

Where a, is the geometric factor, γ is the interfacial energy (J/m^2), υ denotes molecular volume of crystal (6.132 x 10^{-23} cm^3.mol^{-1} for calcite), and SR = saturation ratio.

From the classical nucleation theory, the rate of nucleation and size of the critical nucleus are mainly dependent on supersaturation. Homogeneous nucleation theory predicts that very rapid changes take place over a narrow supersaturation interval [35].

A major theory for homogeneous nucleation which is less dependent on the supersaturation and assumes a constant size of critical cluster was also suggested by Nielsen and Christoffersen [45].

$$J = K (S - 1)^P \tag{2.18}$$

P = number of ions in the critical sized cluster; S: Supersaturation ratio; K: Constant

The equation was used to obtain the number of particles formed by homogeneous nucleation [46].

$$\log N = D - \alpha_N / (\log S_\alpha) \tag{2.19}$$

Where N = number of crystals, D = a constant, α_N= slope of log N versus (log S)$^{-2}$ function where S is the supersaturation and S_α is the supersaturation based on ion activity [35].

Homogeneous nucleation has been extensively studied as most models assume homogeneous nucleation in a static system; however true homogeneous nucleation can only be achieved under carefully controlled laboratory conditions. In reality other processes such as heterogeneous nucleation in a flowing system may take place [36].

The presence of impurities in a system can considerably affect the rate of nucleation of a solution and crystal growth tends to initiate on a pre-existing fluid-boundary surface. Heterogeneous nucleation sites include surface defects, such as pipe surface roughness, existing scale or perforations in production liners, or even joints and seams in tubing and pipelines. As the presence of a foreign body can induce nucleation, the overall free energy associated with the formation of a critical nucleus under heterogeneous conditions, $\Delta G'_{crit}$, must be less than the corresponding free energy change ΔG_{crit}, associated with homogeneous nucleation:

$$\Delta G'_{crit} = \varphi \Delta G_{crit} \tag{2.20}$$

The factor φ (a function of the contact angle) is less than unity.

As seen in equation 2.12 and 2.15, the interfacial tension of crystals is an important factor in the nucleation process.

The interfacial energy diagram for three phases in contact is shown in Figure 2-5.
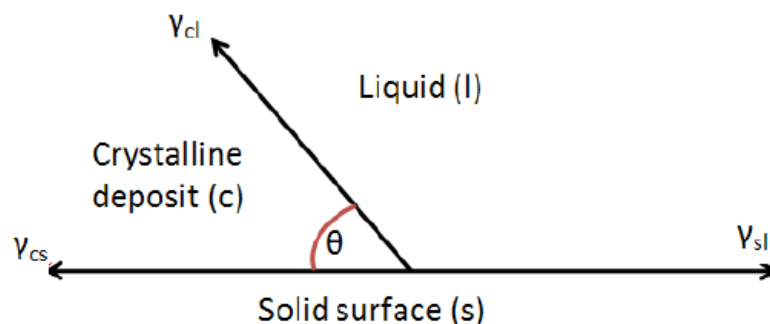
Figure 2-5: Interfacial energy diagram

Resolving the forces,

$$\cos\theta = \frac{\gamma_{sl} - \gamma_{cs}}{\gamma_{cl}} \qquad\qquad \textbf{(2.21)}$$

Where γ_{sl}, γ_{cs} and γ_{cl} represent the interfacial tensions of the solid-liquid, solid-crystalline and crystalline-liquid interfaces respectively.

The factor φ in equation (2.20) can be expressed as

$$\varphi = \frac{(2 + \cos\theta)(1 - \cos\theta)^2}{4} \qquad\qquad \textbf{(2.22)}$$

In the case of complete non-affinity between the crystalline solid and solid surface (corresponding to that of complete non-wetting in liquid-solid systems):

$\theta = 180°$, $\cos\theta = -1$ and $\varphi = 1$, equation (2.20) becomes

$$\Delta G'_{crit} = \varphi\Delta G_{crit} \qquad\qquad \textbf{(2.23)}$$

The overall free energy of nucleation is the same as that required for homogeneous or spontaneous nucleation. In the case of partial affinity corresponding to the partial wetting of a solid with a liquid

$0 < \theta < 180°$, $\varphi < 1$ and equation (2.20) gives

$$\Delta G'_{crit} < \varphi\Delta G_{crit} \qquad\qquad \textbf{(2.24)}$$

The overall excess free energy required is less than that for homogeneous nucleation resulting.

When there is complete wetting or complete affinity

$\theta = 0°$, $\cos\theta = 1$ and $\varphi = 0$ and equation (2.20)

$$\Delta G'_{crit} = 0 \qquad\qquad \textbf{(2.25)}$$

In this case, the free energy of nucleation is zero, corresponding to the seeding of a supersaturated solution with crystals of the required crystalline product where no nuclei have to be formed in the solution.

A new phase is usually formed in the presence of another solid phase within the system. Different foreign particles may support nucleation to different degrees; each particle brings about the formation of new crystals at different supersaturation. The critical supersaturation for heterogeneous nucleation also depends on the type of concentration of admixture present [26]. Recently, attention in the oil industry has been shifted to understanding the relationship between heterogeneous nucleation and growth on pipeline surfaces (adhesion) rather than homogeneous nucleation and growth from bulk solution [47].

2.1.3.2   Secondary nucleation

The formation of a solid phase can be initiated by the presence of solid phase of the crystalizing material itself, this implies that there is a prior presence of the new phase being formed. The mechanisms involved in secondary nucleation were categorised into three, namely: apparent secondary nucleation; in which the nuclei are brought into the system along with inoculating crystals, real secondary nucleation; involving nuclei formation due to crystal solution interactions and contact nucleation; where crystals are formed by collisions between crystals [35].

Secondary nucleation mechanisms have also been identified as involving a three-step process. These include attrition mechanisms to form the secondary part, the removal of these fragments and their growth [48]. Two mechanisms were presented; "surface breeding" and "mechanical breeding". "In "mechanical breeding", the missing parts as a result of mechanical action on parent crystal is replaced by growth while "surface breeding" is a result of growth of the parent crystal.

In precipitation of sparingly soluble substance (scale), primary nucleation mechanisms predominate because the particles formed are too small for secondary nucleation mechanisms to play an important role [26].

Information of nucleation rates is often inferred from the induction time measurements because of the difficulties in the direct measurement of nucleation rates. The process of nucleation from solution involves changes in a number of properties, which may be monitored in order to estimate induction times or to fit nucleation models. The nucleation rate, J is often inferred from the induction time, t_{ind} by the following relation

$$J = \frac{1}{t_{ind}}$$
(2.26)

The model created by Beaunier *et al* [42] and modified by Euvrard *et al* [49] made great progress in understanding the surface nucleation process. Their method assessed the number of crystals as a function of time and enabled the differences between instantaneous nucleation from progressive nucleation to be determined. This model as explained in the methodology chapter is further exploited in this study to assess the nucleation mechanism at constant supersaturation (SR) and for longer test period. Significant research effort is presently being made to understand and quantify the surface scaling processes in the oil and gas and desalination sectors.

2.1.4 Crystal growth

This is the aspect of scale formation involving the increase in size of nucleated crystals to form bigger crystals and the process is greatly influenced by supersaturation ratio as well as temperature. Crystal growth mechanisms have been described in terms of surface energy, adsorption layer and dislocation theories [36, 50]. The growth of a crystal is associated with the smoothness or roughness of its surface and therefore to its surface area and the surface energy. Low surface energy and surface area (smooth surface) have been shown to favour or promote stability while surface discontinuities

and irregularities result in higher surface energy sites and favour the crystal growth [41]. Volmer [51] proposed the first adsorption layer theory by formulating the existence of a mobile adsorption layer which permits growth without nucleation at the crystal surface. Based on the theory, the growth units incorporate on kink sites presents on the crystal surface. However, these theories could not explain growth at a low supersaturation degree but at locally high supersaturation. The first to suggest a theory of crystal growth that could explain growth at low supersaturation was Frank [52].Dislocation theories are based on the existence of irregularity or dislocation in the crystal. Spiral growth would occur by rotation of the ledge formed by the screw dislocation as shown in Figure 2-6.
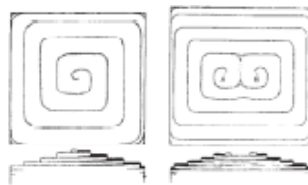
Figure 2-6: Growth of crystals by screw dislocation [52]

Yamanaka *et al* [53] studied the heterogeneous nucleation and crystal growth of $CaCO_3$ on mica surface and on highly oriented pyrolytic graphite (HOPG) substrate by AFM technique. They found that the initial growth process can be divided in three stages: the amorphous, the intermediate, and the crystalline stage. The heterogeneous nucleation of calcium carbonate is believed to be determined by the electrostatic interaction between the adsorbed hydrated calcium ion and the substrate (Figure 2-7).
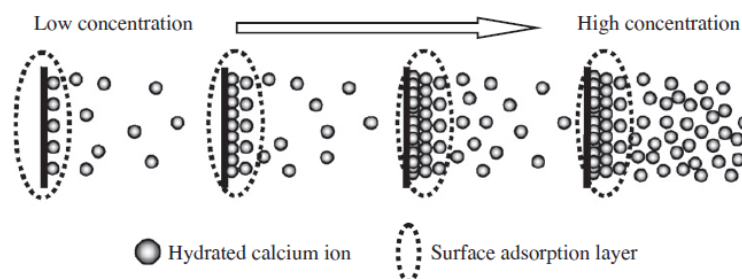
Figure 2-7: Schematic description of adsorbed layer near the mica surface at various concentration of calcium nitrate solution [54].

2.1.4.1   Crystal growth mechanisms and kinetic models.

Nonyes and Whitney [35] suggested that crystal growth mechanisms are predominantly controlled by diffusion processes and also that dissolution is a reciprocal of growth. Further research, however showed a two-step process of diffusion of solute molecules from the bulk solution to the crystal surface and subsequent integration of the molecules into the crystal lattice. The growth rate as quantified by Nonyes and Whitney [35] is as follows:

$$\frac{dm}{dt} = k_m\, A(c - c^*)$$
(2.27)

Where m = mass of solid deposited as a function of time t, A = surface area of the crystal, c is the solute concentration in the supersaturated solution, c* is the equilibrium saturation concentration, and k_m is the mass-transfer coefficient.

The above expression did not have a direct relationship with experimental results [51] thereby leading to the development of another expression (equation 2.27) basically for growth of crystals of $CaCO_3$, which are nucleated and grown in the bulk solution [55].

$$-\frac{d[Ca]}{dt} = k_c A(t)\big([Ca][Ca]_{eq}\big)^g$$
(2.28)

Where k_c is the crystal growth constant, A(t) is the surface area of the growing crystal, [Ca] is the molar calcium concentration, $[Ca]_{eq}$ is the molar concentration of calcium at equilibrium, and g is the kinetic order of crystal growth.

The classical nucleation theory as expressed in equations 2.9, 2.10 and 2.16 shows that temperature and SR are two important parameters that strongly affects the thermodynamic and/or the kinetics of bulk precipitation. The precipitation kinetics is greatly influenced by temperature as Feng *et al* [56] observed the crystallization process to be quicker with an increase in temperature. Mullin and Zacek [35] showed that for a given SR, an increase

in temperature resulted in a decrease in the induction time, this is in agreement with the expression shown in equation 2.29.

$$\log(t_{ind}^{-1}) \propto \gamma^3 T^3 (\log S^{-2})$$ **(2.29)**

Based on the experimentation of the classical nucleation theory, He *et al* [57] developed a semi-empirical and found that at a given temperature, the logarithm of the induction period was proportional to 1/SI and at a given SI the logarithm of the induction period was proportional to 1/T.

The above expressions were focussed on growth of $CaCO_3$ crystals nucleated and grown in the bulk solution. Zhang *et al*, [18] developed a model to predict down-hole scaling by performing tube-blocking tests and correlated the thickness of surface scale observed at the end of the experiments with bulk measurements recorded as a function of time.

2.1.4.2   Growth rate laws

The overall linear growth rate G is defined as the rate of change of a typical dimension of a crystal or particle with time. Half of this value, the rate of change of particle radius (ṙ) is frequently Used

$$\dot{r} = k_r (S - 1)^n$$ **(2.30)**

Where k_r is the growth rate constant and the order n explains the mechanism by which the crystals grow [58].

Basic growth mechanisms may be classified according to the rate law resulting when they are fully responsible for the growth rate [59]. The expressions for the growth rate, G as a function of the relative supersaturation, S, give the linear, parabolic, and exponential rate law respectively as

$$G = k_1(S - 1)$$ **(2.31)**

$$G = k_2(S - 1)^2$$ **(2.32)**

$$G = k_3 S^{7/6}(S-1)^{2/3} \ln(S)^{1/6} e^{[-K/(\ln S)]} \qquad \textbf{(2.33)}$$

The three kinds of kinetics are explained by the following rate-determining mechanism:

(i) Transport (diffusion) or surface adsorption

(ii) Surface integration (spiral growth)

(iii) Surface nucleation (polynuclear growth) - for two-dimensional (2D) nucleation-mediated growth

The growth of very soluble electrolytes which crystallize from aqueous solution usually follow a linear rate law, the rate being proportional to the difference between the concentration and the solubility. The rate is controlled by the transport of the ions in the bulk solution or by the adsorption process [59]. When the crystal growth is surface controlled, the growth units must get adsorbed, move along the surface and integrate into the crystal lattice at a growth site, i.e. a kink in a surface step. Each of these steps may be rate determining. The adsorption rate may be controlled by the partial dehydration of the cations or by the penetration through the hydration layer of the crystal [58, 59].

Sparingly soluble electrolytes mostly grow by a parabolic or exponential rate law at small or moderate supersaturations, and may change to transport control at larger concentrations [59]. Both with parabolic and with exponential rate laws the rates can be accounted for in terms of the classical theories of surface spirals caused by screw dislocation, and surface nucleation, respectively, when it is assumed that the rate-determining molecular mechanism is the integration of the cations into crystal lattice positions at kinks in the surface steps (whether caused by dislocations or surface nucleation) [58, 59]. The polynuclear model assumes that many nuclei continuously appear and grow during the nucleation period, so that the crystals detected are a direct result of nucleation and growth rather than just collision breeding. Examples of the different growth rate laws are shown in Figure 2-8.
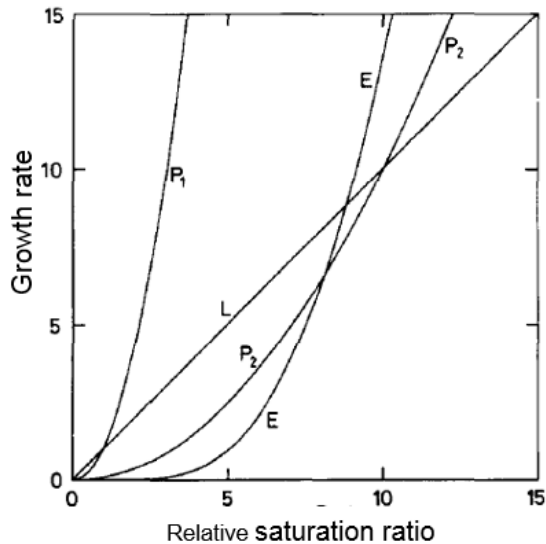
Figure 2-8: Examples of linear (L), parabolic (P1 and P2) and exponential (E) rate laws [59]

Equations 2.32 and 2.33 have almost the same assumption except for the difference in their source of steps which are dislocations and surface nucleation respectively. However, the increase in the density of the steps is stronger for surface nucleation than for dislocation. Models have been developed for the growth of a continuous scale layer [60, 61]. Results obtained previously for vaterite growth in the literature have shown that the particles grow by surface reaction controlled mechanisms characterised by a parabolic rate law [58].

In a seeded growth experiment, Lioliou *et al* [62] obtained a value of n = 2 for the apparent order of the crystal growth process, this was interpreted as indicative that the rate-determining step in the crystal growth process is the diffusion of the growth units on the surface of the growing crystals [35]. A high value of the apparent order suggested a polynuclear type of growth.

Kinetics studies have involved measuring the solution properties or the amount of scale formed ex-situ after the experiment. There have been few significant advances in terms of predicting the scale deposition rate at component surfaces.

26

2.2 Formation of calcium carbonate scale

The stability of $CaCO_3$ scale makes it one of the most common mineral scale found in oilfield operations. $CaCO_3$ scale formation is the results of combination of Ca^{2+} with either CO_3^{2-} or HCO_3^- ions (depending on the pH), which are present in formation water [2, 3].

The formation waters in oilfield reservoir are generally at thermodynamic equilibrium. Scale formation is usually as a result of pressure drop leading to either the release of CO_2 and or change in pH. During production, water is usually drained to the surface and suffers from significant pressure drop and temperature variations. The successive pressure drop leads to the release of dissolved CO_2 with an increase in the pH value of produced water, the water becomes supersaturated with $CaCO_3$ leading to its precipitation [63].
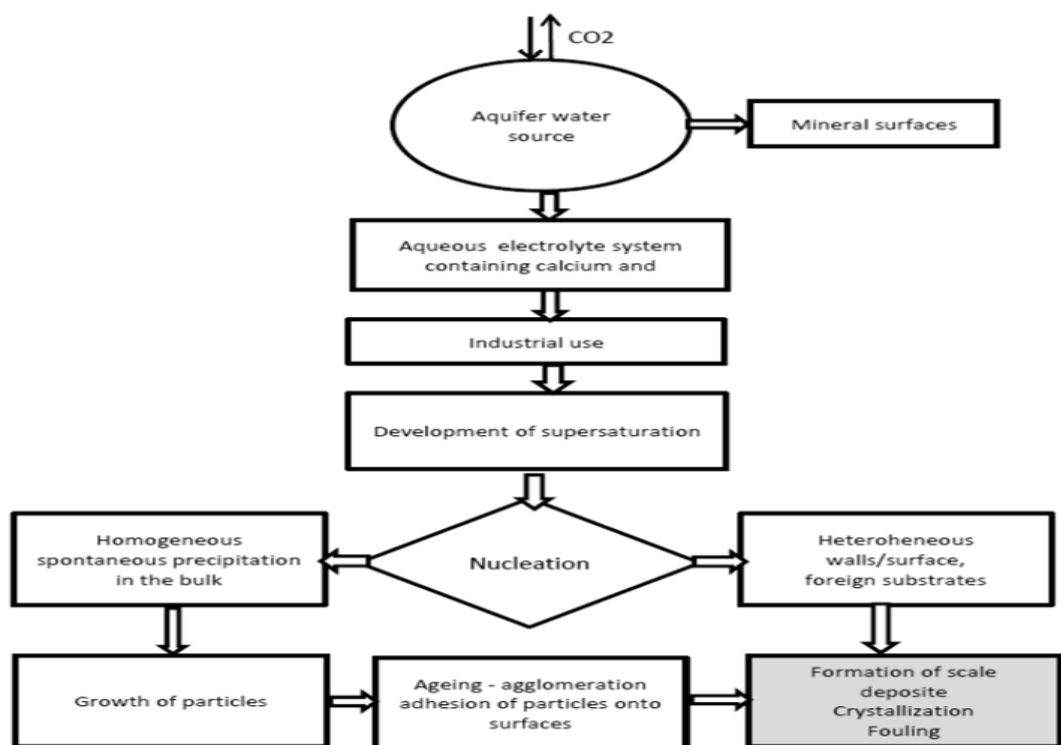
Figure 2-9: Process of calcium carbonate scale formation [3]

2.2.1 Calcium carbonate reactions

The equilibrium relationship for calcium carbonate scale formation is given by the following reactions:

Dissolution of carbon dioxide and carbonate minerals into water as a result of drop in pressure

$$CO_{2(g)} + H_2O \leftrightarrow H_2CO_{3(S)} \tag{2.34}$$

Increase in pH of the system

$$H_2CO_3 \leftrightarrow HCO_3^- + H^+ \tag{2.35}$$

$$HCO_3^- \leftrightarrow CO_3^{2-} + H^+ \tag{2.36}$$
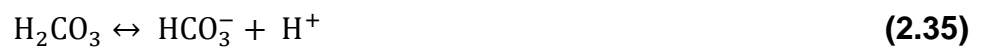
Decrease in calcium carbonate solubility and precipitation

$$Ca^{2+} + CO_3^{2-} \leftrightarrow CaCO_{3(S)} \tag{2.37}$$

The equilibrium between CO_3^{2-}, HCO_3^-, H_2CO_3 as a function of pH can be seen in Figure 2-10.
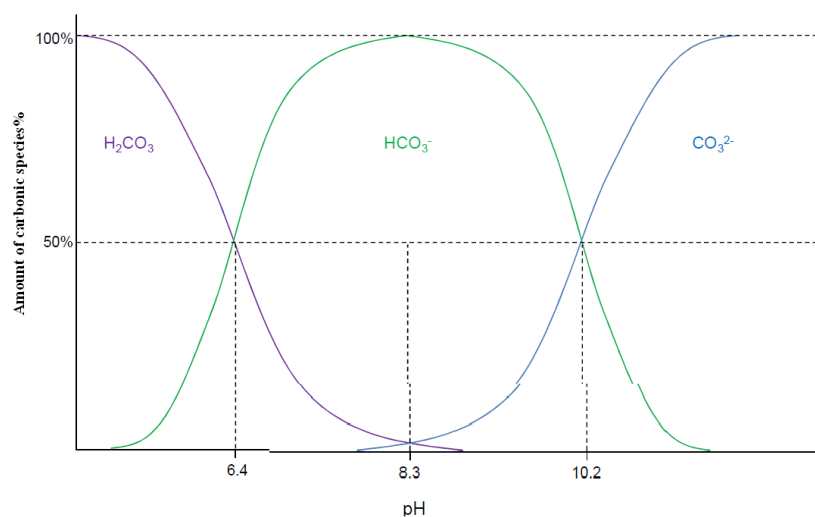
Figure 2-10: Percentage of CO₃²⁻, HCO₃⁻ and H₂CO₃ as a function of pH[64]

28

Depending on the pH, calcium ions will also be able to combine with bicarbonate ions, which is the dominant species over a wide pH range round the neutral:

$$Ca^{2+} + 2HCO_3^- \leftrightarrow CaCO_{3(s)} + CO_{2(g)} + H_2O \qquad \textbf{(2.38)}$$
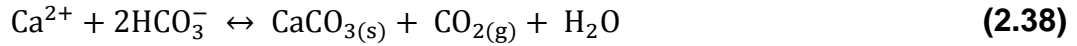
$K_{sp} = 10^{-8}$ mole/L at 20°C.

The activity based chemical equilibrium constant for calcium carbonate is given by

$$K_{eq} = \frac{(a_{CaCO_3})(a_{CO_2})}{(a_{Ca^{2+}})(a_{HCO_3^-})^2} \qquad \textbf{(2.39)}$$

This follows Le Chatelier's Principle which states that if a chemical system at equilibrium experiences a change in concentration, temperature, volume, or partial pressure, then the equilibrium shifts to counteract the imposed change and a new equilibrium is established [65].

A drop in pressure liberates CO_2 from the solution and resulted in CO_2 concentration reduction. More $CaCO_3$ will be produced to maintain the chemical equilibrium K_{eq}. Likewise, the increase in Ca^{2+} ions concentration during enhanced recovery process when incompatible fluids are mixed is compensated by calcium carbonate [$CaCO_3$] precipitation.

2.2.2 Polymorphic phases of calcium carbonate

The different forms or phases in which calcium carbonate can exist are vaterite, aragonite, and calcite (Figure 2-11). These phases have different solubility, morphological and crystallographic characteristics. The development of appropriate conditions (high pH, high calcium and carbonate concentration) leads to the formation of a precursor phase, the amorphous calcium carbonate, which evolves into the more stable anhydrate phases; calcite, aragonite and vaterite [3, 66]
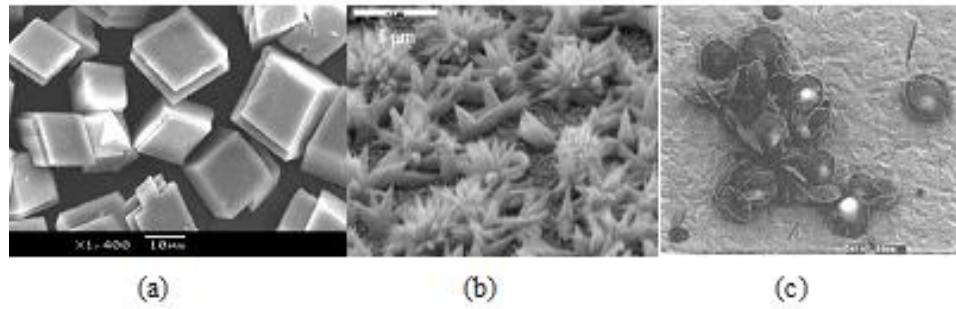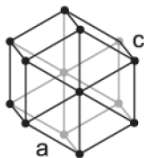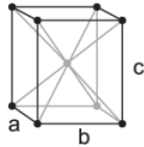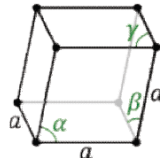
Figure 2-11: Polymorphs of CaCO$_3$ (a) calcite (b) aragonite (c) vaterite [42, 67]

Studies have shown that aragonite and calcite can be found in nature, being the most stable forms whereas, vaterite is the least stable and as a result very rare [66, 68, 69]

Depending on the fluid conditions (composition, temperature, pH, fluid dynamics and substrate), the less stable polymorphs may be stabilized or converted into the thermodynamically most stable calcite, which is generally formed at lower temperature [3, 70, 71]. Aragonite phase precipitate first at above ambient temperature [72] while vaterite appear at moderate temperatures and pressures naturally [73]. Some of the characteristics of the polymorphs are shown in Table 2-1

The crystal structures of aragonite, calcite and vaterite are orthorhombic, rhombohedra and hexagonal respectively [70].

Table 2-1: Characteristics of calcium carbonate polymorphs

	Vaterite	Aragonite	Calcite
State	Metastable (least stable) Porous Microcrystalline	Single crystal porous	Most stable Single crystal Porous
Morphology	Hexagonal Hemispherical	Needle-Like	Cubic to Rhombohedra
Crystal System	Hexagonal $a \neq c$ 	Orthorhombic $a \neq b \neq c$ 	Rhombohedral $\alpha, \beta, \gamma \neq 90°$
Influencing factors	High Supersaturation Low oxygen-concentration Strong tendency to spread laterally	Temp. above 50°C High pH value (>13.5)	Instantaneous-nucleation Room Temperature High oxygen-concentration

Vaterite can first appear under an amorphous calcium carbonate form, without a well-defined structure type, and then gradually transforms into spheroidal crystals. It is very difficult to confirm its physical parameters and solubility product due to its instability. Aragonite is less stable than calcite and exhibits a needle-like habit whereas calcite has well defined equant habit, with very few crystal defects [65, 74].

The crystal morphology of the precipitated phases and by extension the overall characteristics of calcium carbonate scale is very important and has been widely studied. There are many parameters that affect the type of polymorphs formed as well as the overall crystallization reaction of calcium carbonate [34, 75, 76].

2.3　Factors affecting calcium carbonate scale formation

The process of calcium carbonate scale formation in the bulk and surface can be influenced by several factors. These factors can be classified into (a) Physical/Chemical factors and (b) Nature of substrate.

A parameter can influence nucleation itself, the subsequent growth of the nuclei or both processes simultaneously [77, 78].

2.3.1　Physical and chemical factors

This includes the saturation ratio, temperature, pressure, flow velocity, pH, solution composition, impurities.

2.3.1.1　　Effects of saturation ratio

The saturation ratio as discussed under section 2.1.1 is directly associated with the ionic concentrations in bulk solutions (see equation 2.6 and 2.7) and is referred to as the thermodynamic driving force of scale formation [29-32]. Also, equation 2.1 shows the relation between saturation ratio and solubility of a salt as a highly soluble salt will require a higher saturation ratio to form scale.

At equilibrium, "K_{sp}" is equal to the ionic-activity product (IAP), therefore

$$K_{eq} = \frac{[CaCO_3]\,[CO_2]}{[Ca^{2+}]\,[HCO_3^-]^2} \qquad \textbf{(2.40)}$$

From equation 2.6, the Saturation index for calcium carbonate can be expressed as:

$$SR = \left(\frac{IAP}{K_{sp}}\right) = \frac{(a_{Ca^{2+}})(a_{HCO_3^-})^2}{K_{sp,CaCO_3}} \qquad \textbf{(2.41)}$$

Shinya *et al* [54] found that the number of crystals on a mica substrates were affected by the change in initial supersaturation. Growth rate of $CaCO_3$ was observed to reduce from $5.36 \pm 0.18 \cdot 10^{-6}$ kg/m^2·s to $2.6 \pm 0.3 \cdot 10^{-6}$ kg/m^2·s

when the inlet supersaturation decreased from 6 to 4.5 at comparable conditions and a time magnitude of 180 minutes [79]. In other studies, bulk turbidity curve were observed to reach a plateau as SI decreases with time and surface scaling kinetics could only be assessed for the initial stage which resulted in difficulties to achieve a full mechanistic understanding of scale build-up [80, 81].

The typical crystallization turbidity curve in Figure 2-12 is for a batch or closed system where SR was decreasing as a result of reduction in ionic species as scale deposition takes place.
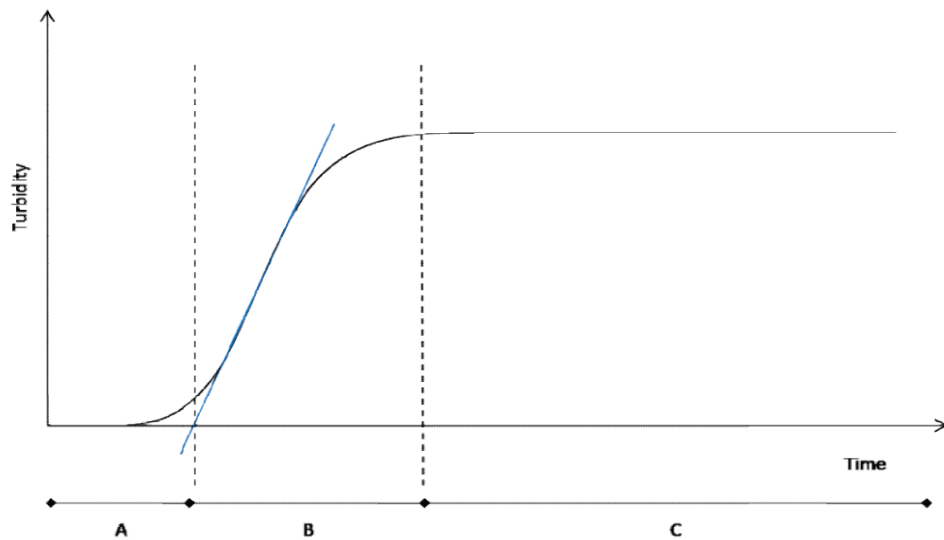
Figure 2-12: Typical turbidity curve

A is the induction time; B is the region where the growth of crystals proceeds at a fast rate. C is where the turbidity has reached a plateau which shows a steady curve with no further increase in crystals (turbidity). The tangent to the slope allows an intersection with the time axis to be assessed which gives the induction time value, with long induction time suggesting slow kinetics.

It has been observed that the induction period of nucleation is inversely proportional to the degree of saturation [31]. This is illustrated in Figure 2-13, where it can be seen that undersaturated solutions (U) will not allow calcium carbonate crystals formation. Slightly saturated solutions (S) allow the

formation and dissolution of nuclei. Higher saturation indices (Labile zone, L) allow the formation of calcium carbonate nuclei and their growth.
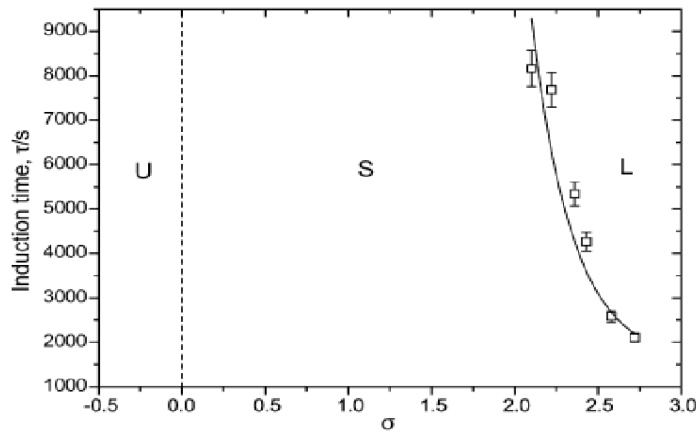
Figure 2-13: Calcium carbonate stability areas and nucleation induction time as a function of the saturation index (σ) [31].

U: under-saturated solution. S: stable supersaturated solution. L: Labile supersaturated solution with calcium carbonate crystals formation.

Brine solutions show different scaling tendencies according to saturation indices. Figure 2-14 shows that the amount of scale formed on a stainless steel surface is observed to be greater for high saturation index than for low saturation index.
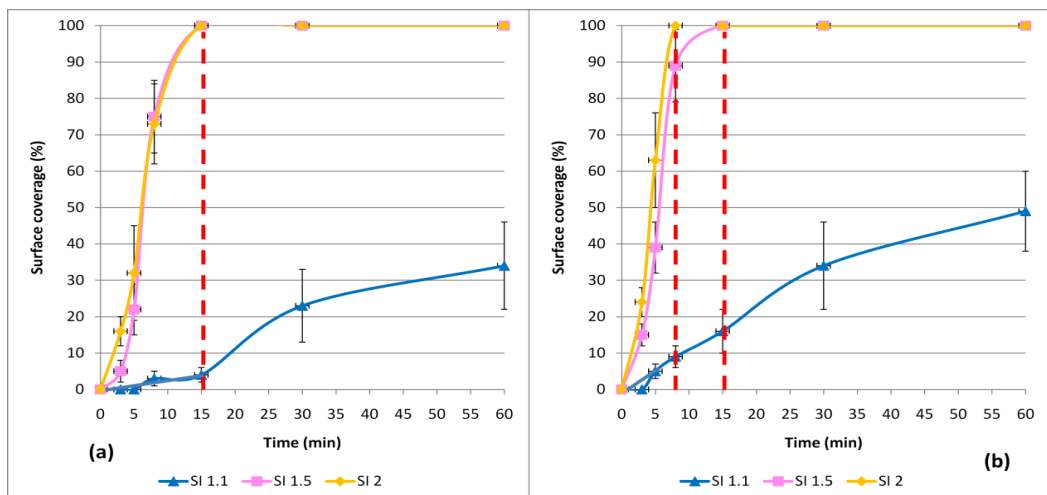
Figure 2-14: Calcium carbonate scale deposition surface coverage in static conditions, at (a) 24^{0}C and at (b) 70^{0}C [81].

2.3.1.2 Effects of temperature

Temperature has a very significant and direct effect on the process of calcium carbonate scale formation as well as the morphology of the calcium carbonate formed [68, 82]. Various studies have been carried out and reported in this regard. Contrary to the behaviour of most materials, calcium carbonate becomes less soluble with increasing temperature. This owe so much to its inverse solubility characteristics [83].
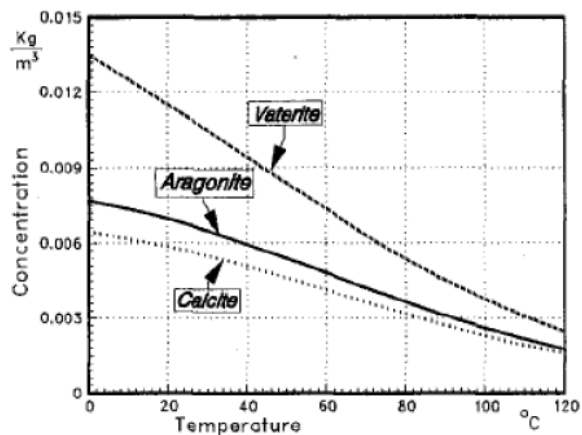
Figure 2-15: Relationship of CaCO$_3$ solubility and temperature[84]

Various studies have all reported complementary temperature range at which the different forms of calcium carbonate will be stable.
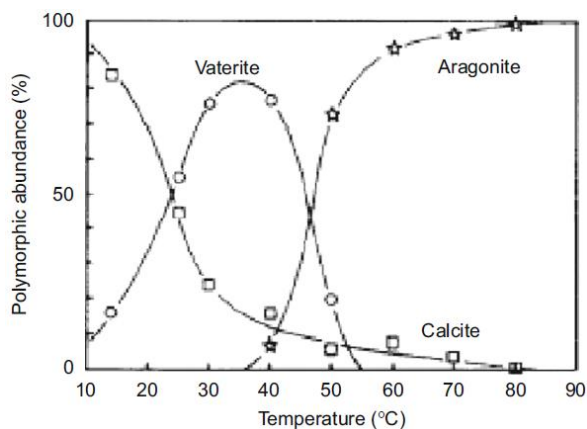
Figure 2-16: CaCO$_3$ forms as a function of the temperature [85].

Calcite predominates at low temperature 25°C while at 30°C, both calcite and aragonite are formed. Between 40°C and 60°C calcite, aragonite and vaterite are formed, vaterite is more stable at 40°C while aragonite is the predominant form at high temperature of 70°C [67, 70, 85].

Temperature has also been shown through different studies to influence the particle size [50], the induction time, which decreases with an increase in temperature [42], nucleation mechanisms; where heterogeneous nucleation occurs at low temperature and homogeneous nucleation predominates at high temperature [86] as well as the kinetics of precipitation; as an increase in temperature leads to faster crystallization [56, 81].

2.3.1.3 Effects of pH

The formation of carbonate scale is greatly dependent on pH as a high pH allows a high saturation index and therefore a high scale formation rate [32, 87].

The equilibrium reactions involving the precipitation of calcium carbonate as discussed in section 2.2.1 can be greatly affected by changes in pH. The bulk solution pH determines the ratio of different carbonic species present in solution. The measurement of pH is an important factor necessary to understand and follow the kinetics of calcium carbonate precipitation because the pH decreases along with the precipitation process as the carbonate ions decreases [64, 88].

Supersaturation can also be controlled by initial pH conditions or by changing the concentration of calcium while maintaining the pH and total carbonate constants [89]. pH has also been shown to affects the particle size, Cheng *et al* [90] and Feng *et al* [56] found that the size of the primary particles decreases with a rise in pH due to the increase in nucleation rate.

2.3.1.4 Effects of pressure

The saturation limit for dissolving the ions will be reduced as a result of pressure drop and this causes an increased precipitation of $CaCO_3$. When pressure is decreased in a chemical system, the equilibrium will try to compensate by increasing the pressure. Because CO_2 is the only gaseous species, the only way to increase pressure is by shifting the equilibrium towards producing more CO_2. A decrease in pressure will then result in more precipitation of calcium carbonate. Pressure drops stimulate calcium carbonate scale precipitation due to a lower solubility. On the contrary, an increase of pressure will lead to a higher solubility for calcium carbonate crystals which will allow it to stay in the liquid phase [91, 92]. This is illustrated by the carbonic system shown in Figure 2-17.
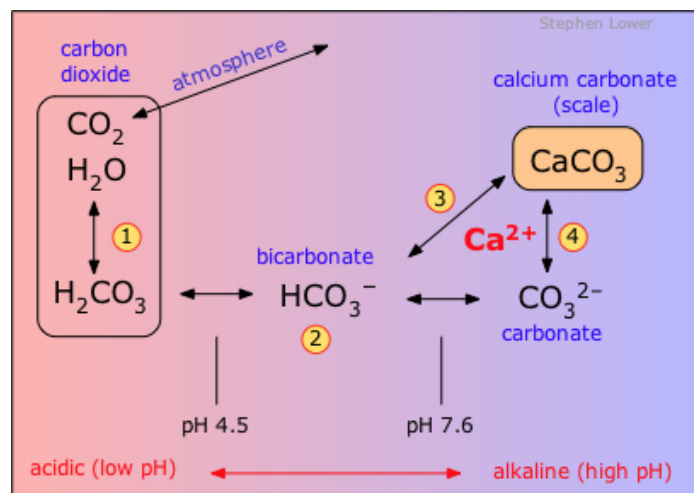
Figure 2-17: Schematic representation of the carbonic system [93]

It is important to monitor the partial pressure of carbon dioxide so as to manage the behaviour of scaling waters. This is because when spontaneous scaling occurs, the pH rises at the same time by loss of the initial free CO_2 and of the one produced by the hydrogen carbonate ions decomposition [94]

2.3.1.5 Effect of flow velocity

Many studies to demonstrate that Calcium carbonate scaling showing a pronounced dependence on velocity have been carried out. Beaunier *et al*

[42] show that the scaling rates was found to be lower at lower flow rate than at higher flow rate as shown in Figure 2-18.
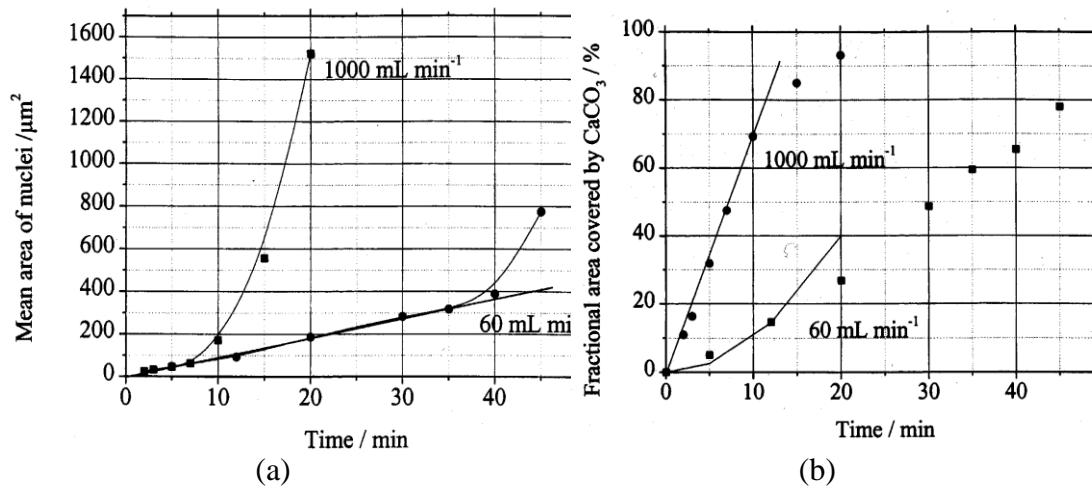
Figure 2-18: Change of (a) mean area of nuclei and (b) mean fractional coverage by scale with time for two flow rates [42]

In fouling, higher velocities can assist in the transportation of ions to the crystallisation interface while also the removal rate can be increased with increased velocities because of higher shear rate at the liquid-solid interface if the hydrodynamic interactions are greater than the adhesive bond between the particle and the substrate [95]. High flow velocities can reduce deposition especially in cases where particulate fouling dominates or where deposits are not well adhered on the surface while in other cases they accelerate fouling [28, 30].

At a heat transfer surface, it is found that the fluid velocity increases inhibition effect and in the absence of inhibitor, increases the fouling tendency which shows that the diffusion of foulant ions affects scaling behaviour. At higher fluid velocity, there will be more inhibitor molecules or ions as well as foulant ions diffusing onto the growing $CaCO_3$ surface [96].

The morphology and structure of the deposit, the size of the particles and the induction time are also affected by the flow rate. Trippa and Jachuck [97] showed that the particle size decreases with increasing flow rate due to better

mixing, Karabelas [98] found that a low velocity promoted a non-compact deposit while Andritsos *et al* [60] observed elongated prismatic calcite due to the flow for a given supersaturation degree.

The induction time was observed to be decreasing with increasing flow rate, and consequently resulted in an increase in the growth rate [99]. A study of calcium carbonate fouling on heat transfer surfaces in cooling water systems found that the induction period increases with decreasing initial surface temperature and fluid velocity [99].

2.3.1.6 Effects of water composition

The water composition can influence the precipitation kinetics of calcium carbonate. Ben Amor *et al* [86] showed that nucleation and growth rates increase when water hardness decreases. Water composition can also influence the type of calcium carbonate formed, its quality as well as its quantity. For instance, presence of organic matter in water can reduce and even stop the formation of nuclei [91].

Spontaneous precipitation of calcium carbonates from artificial seawater which contains significant amount of Mg^{2+} always results in the formation of aragonite even if the solution is inoculated with vaterite or calcite [100].

2.3.1.7 Effects of impurities

$CaCO_3$ precipitation is sensitive to impurity ions which exist in formation and injection waters, such as Mg^{2+}; Ba^{2+}; Sr^{2+}; Mn^{2+} and SO_4^{2-}; and it is well known that these can affect $CaCO_3$ growth rate [101]. The presence of solid particles in the bulk can enhance the scale precipitation and many of these ions have the effect of inhibiting the growth of calcite [102].

Magnesium ions (Mg^{2+}) has the strongest influence on $CaCO_3$ precipitation, often favouring the formation of aragonite over calcite. The nucleation rate as well as the crystal growth rate of $CaCO_3$ scale may be strongly affected by the

presence of Mg^{2+} ions in formation water. It was found that the inhibiting effect of magnesium ions influences the bulk precipitation more than the surface deposition process [30]. This is illustrated in Figure 2-19 and Figure 2-20 below.
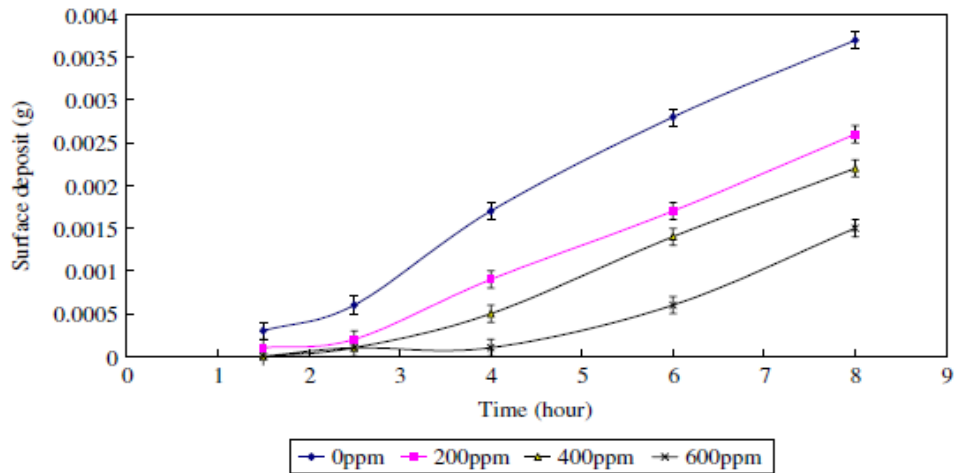
Figure 2-19: Effect of Mg^{2+} on surface deposition under 1500 rpm at 20ᵒC [30]
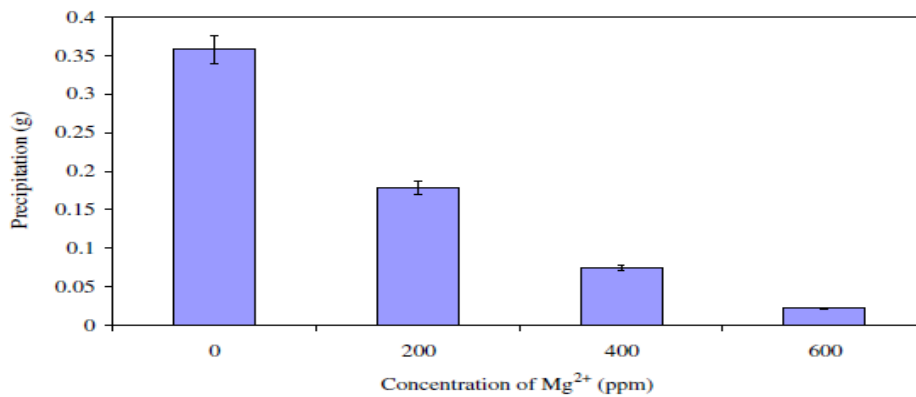
Figure 2-20: Effect of Mg^{2+} on bulk precipitation under 1500 rpm RDE at 20ᵒC [30]

At magnesium ion concentration of 600ppm, a decrease of surface deposition of about 60% was observed while the magnesium inhibition effect on the calcium carbonate precipitation reached a value of 95%.

Many studies, using seeded growth tests, have shown that the calcite growth rate can be inhibited by the presence of Mg^{2+} [103-105]. Devos *et al* [106] showed that aragonite formation is promoted with an increase in magnesium. Other ions in the bulk such as strontium ions (Sr), Copper (Cu) ions, Zinc ions (Zn), Cobalt ions (Co), Barium ions (Ba) can also promote aragonite formation [73, 107].

The inhibition of calcite growth by the presence of Mg^{2+} is caused by Mg^{2+} being incorporated into the calcite crystal lattices at Ca^{2+} ion sites which then affect the morphology of the crystal and hence its growth [108].

Experiments were also carried out to assess the effect of zinc on crystallization of $CaCO_3$ in a high scaling water, a reduction in nucleation rate and a high inhibition of growth was observed [109]. However copper was found to have higher efficiency in inhibiting scale than zinc due to its ability to form a neutral complex that inhibits crystal growth [110].

2.3.2 Nature of substrate material

The nature of the substrate material has a significant effect on deposition, adhesion, form and structure of the deposits [76]. In this vein, various works that have been carried out in order to modify the substrates nature by coatings, ion implantation or ion sputtering and other various surface finishing techniques will be discussed under the antifouling surfaces section. However, it is important to understand the interaction between the inorganic foulant, and the substrates properties such as surface energy, roughness and wettability that influence crystallization rate as well as adhesion strength [111].

2.3.2.1 Surface roughness and contact angle

Roughness is regarded as a measure of the texture of a surface and can be quantified by the vertical deviations of a real surface from its ideal form. Large deviation is equivalent to a rough surface while small deviations mean a smooth surface. Roughness is an important parameter which goes a long way

to determining how a surface interacts with the medium. Rough surfaces have been found to have higher fouling tendency compared to smooth ones [112].

Wettability is another very important property associated with a solid surface and is governed by surface chemical composition and the roughness of the solid surfaces. It also gives an indication of the surface energy of the solid surface [113].

Primarily, wetting is characterised by static contact angle defined as the angle a liquid makes with a solid. Contact angle depends on other factors such as surface roughness, surface preparation and cleanliness. It depends on the properties of the substrate [114].

In studying the effect of surface roughness on calcite deposit formation on mild steel, the adhesion strength of the fouling layer on the metal surface was found to be strongly influenced by the degree of surface roughness and the tensile stress required to break away the scaling layer from a rough surface was several times greater than for a smooth surface [44]. The induction time for scaling is also found to be dependent on surface roughness with very rough stainless steel surfaces showing a minimum induction time [115].
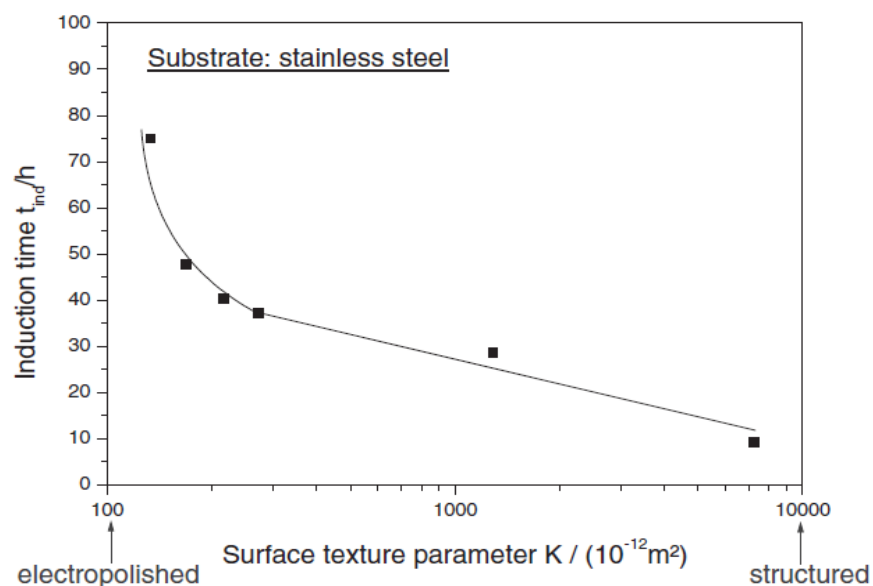
Figure 2-21: Induction time vs surface texture parameter [115].

2.3.2.2   Surface energy

The surface free energy of a solid or liquid is the work required in forming a unit area of a surface. High surface energy as a result of increases in surface area due to roughness leads to greater adhesion. It has been shown that scale adhesion occurs on materials with high surface energy which can vary with presence of impurities while adhesion is lower and induction times are prolonged in systems that have low surface energies [116-118]. Periods of supersaturated $CaCO_3$ solutions held in cells of different materials were measured by Roques and Girou [119] and it was found that the induction periods were lowest for polished stainless steel and highest for poly vinyl chloride (PVC) which had the lowest surface energy.

Chapter 3 Scale removal, control and investigation techniques

The techniques used for the removal of scale in addition to being effective at preventing re-precipitation should also be quick, non-damaging to the wellbore, tubing or formation environment. The type, quantity, physical composition and texture of scale are factors considered before applying the right removal methods because a wrong choice can actually promote rapid recurrence of scale [11].

Calcium carbonate precipitation and deposition can be ameliorated by chemical, physical or biological methods with various level of effectiveness. The control of scale can be divided into those that affect solubility, those that alter the growth mechanism of crystals, and those that change the potential of a surface to foul [120].

3.1.1 Chemical techniques

When calcium carbonate scale exists at locations that are not readily accessible or where conventional mechanical removal methods are ineffective or expensive, chemical removal methods are usually applied. Hydrochloric acid (HCl) is mostly used to dissolve carbonate scale due to the high solubility of carbonate minerals in it [11]. However, spent acid solutions of scale by-products can initiate the reformation of scale. The scale deposit combined with the rapid acid reaction which can hide a problem makes it a challenging method. The use of chelating agent such as Ethylenediamine tetra acetic acid (EDTA), that dissolves and chelate calcium ions breaks the reprecipitation of the scale [11].
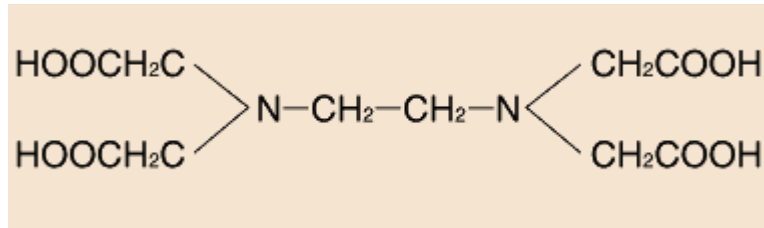
Figure 3-1: Chemical structure of EDTA

The chelating agents isolate and lock up unwanted ions in solution within their closed ring-like structure [11].

3.1.2 Mechanical techniques

Mechanical approaches include the use of explosive string shots which provide high-energy impact loads that could remove scale. The use of drilling rocks and milling steel for thick scale that is too strong for safe explosive removal and abrasive water jetting for soft scale [11].

The problems associated with these mechanical methods include:
- damaging of tubular and cement structure;
- the need to tame the explosives resulting in reducing the amount of explosive loads;
- large cutting size which makes hole cleaning more difficult;
- incompatibility with dissolvers, variation in milling power requirements due to uneven distribution of scale on tubing wall;
- loss of production as a result of dismantling equipment, and high cost [10, 11].

3.1.3 Scale inhibitors

The most common method of preventing scale formation in the oil industry is the use of scale inhibitors which work by preventing either nucleation and/or crystal growth of the scale. The inhibitors are applied either by continuous injection or by periodic scale squeeze treatments [121].

Efficiency of scale inhibition depends on dosage of the inhibitor, its physical properties such as the number of functional groups in the inhibitor molecule, the composition of the polymer and on its molecular weight [122, 123].

3.1.3.1 Conventional inhibitors

The classification of commercial inhibitors for carbonate scaling contain one or more of the following functional groups from which they are formulated:

- Polyphosphonate
- Sulphonated polymer
- Carboxylic acid [6, 101]

3.1.3.1.1 Polyacrylic acid (PAA)

PAA is used as a standard polymer for studying properties of linear polyelectrolytes. It is a generic name for all compounds comprising of synthetic high molecular weight polymers of acrylic acid, an unsaturated carboxylic acid [124].
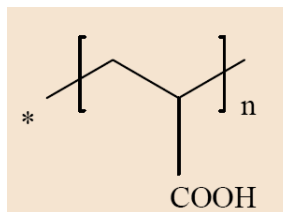
Figure 3-2 PAA molecular structure [96]

PAA can be used in situations of alkaline and high concentration without scale sediment. PAA can disperse the microcrystals or microsand of calcium carbonate, calcium phosphate and calcium sulfate. To test the efficiency of PAA in scale inhibition, calcium carbonate particles were prepared by Yu *et al* [50] in the presence of PAA, a change in the crystals' shape, size and morphology was noticed because the carboxylic group interact with calcium carbonate resulting in inhibition of growth.

3.1.3.1.2 Polyphosphinocarboxylic acid (PPCA)

The industry standard polymeric scale inhibitors widely applied in the field to prevent both carbonate and sulphate scales is the PPCA inhibitor [125]. PPCA is a Polyacrylic acid with imbedded phosphino- groups. H-(CH2CHCOOH)x-POOH-(CH$_2$CHCOOH)y-H.

It is widely used in oil fields as a scale inhibitor because of its good quality, low cost and environmental acceptability [124]. Research also implied that PPCA or its derivatives have potential to be multifunctional inhibitors in boilers, cooling water formulations and oil wells [124].
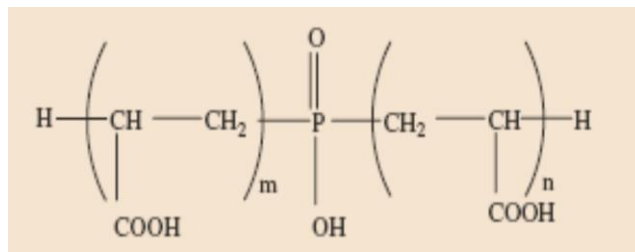
Figure 3-3: PPCA molecular structure [73]

PPCA is commonly referred to as nucleation inhibitor, it can partially inhibit the calcium carbonate nucleation by decreasing the number of nuclei and also the number of active sites on metal surfaces (stainless steel) [126]. It is known to inhibit both bulk precipitation and surface deposition to a different degree. Chen *et al* [127] reported that at 4 ppm PPCA, the inhibition efficiency of surface deposition is greater than the inhibition efficiency of bulk precipitation. It is assumed that the inhibitor film formed on the metal surface at the highest concentration of PPCA (4 ppm) prevent the adsorption of scale crystals on the metal surface.

PPCA can act on the calcium carbonate crystals morphology suppressing aragonite and calcite crystal formation which makes the least stable vaterite crystal to dominate the scale [19, 127]. PPCA inhibitor is water soluble, has a large molecule (atomic mass is about 3600 g/mol), which potentially allows high inhibition efficiency because of its numerous active sites [73]. PPCA,

though an excellent CaCO3 inhibitor cannot remain in solution at high pH or in waters with high calcium [128].

3.1.3.1.3 Phosphonates

The term phosphonate is used for substances comprising of one or more group $CPO(OH)_2$. One of the most widely used to prevent carbonate scale formation is the diethylenetriamine penta methylphosphonic acid (DETPMP). They are very stable at high temperature [55] and are usually referred to as a growth inhibitor [129] as they have been observed to adsorb onto the crystal, limiting their growth [55].
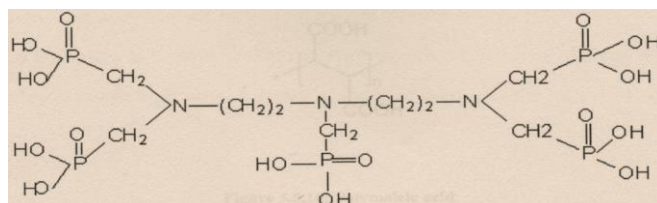
Figure 3-4: DETPMP-Diethylenetriamine penta methylenephosphonic acid [55]

3.1.3.2   Green scale inhibitors

Many of the commercial scale inhibitors contain phosphorus and nitrogen which are toxic to the environment especially having a negative environmental impact on the marine ecosystem. Thus, new environmental-friendly chemicals are formulated to prevent any risk and reduce the harmful impact of inhibitors on marine water ecosystems [130]. Examples of common green scale inhibitors are Polymaleic acid (PMA), Polyaspartate (PASP) and Carboxymethyl insulin (CMI).

3.1.3.2.1 Polymaleic acid (PMA)

Polymaleic acid efficiency at inhibiting calcite deposition has been demonstrated. It is a carboxylic acid usually used to prevent scale formation on boilers and can be efficient even at low concentration [126]. PMA has been

shown to act on both nucleation and growth steps of calcium carbonate scale formation [126].
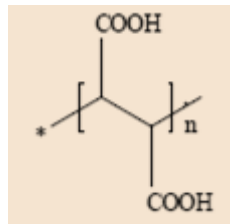
Figure 3-5 : Polymaleic acid (PMA)

Calcite formation inhibition effect of PMA in real time and in-situ has been studied and the PMA was shown to cause a decrease in growth rate. A decrease in the growth rate at weak supersaturation of calcite deposition was also observed with PMA [131].

3.1.3.2.2 Polyaspartate (PASP)

Polyaspartate, is a highly biodegradable molecule derived from aspartic acid, a natural amino acid. It is environmentally friendly with CO_2 and water being the potential secondary products which can be obtained [132].
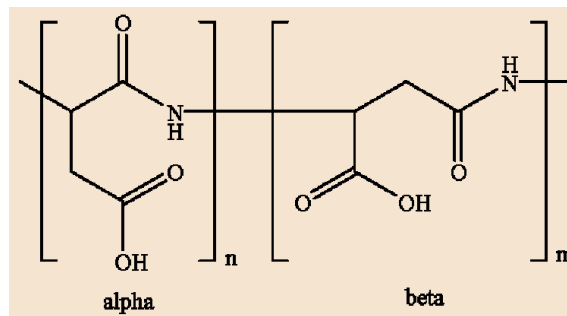
Figure 3-6: Polyaspartate (PASP)

The scale inhibition efficiency is a function of the number of carboxylates groups in its structure and invariably on its molecular weight [133].

3.1.3.2.3 CarboxyMethyl Inulin (CMI)

The growing demand for environmentally-friendly alternatives for phosphonate-based crystal growth inhibitors has also led to the formulation of a nontoxic, biodegradable, and phosphorus free CMI.
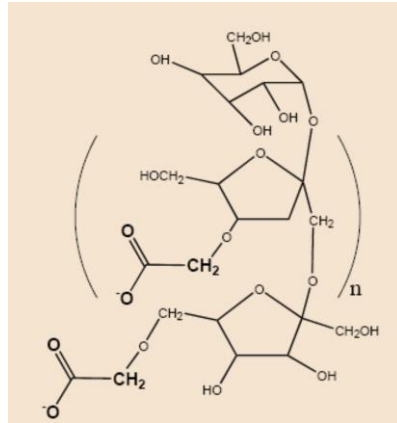
Figure 3-7: CarboxyMethyl Inulin (CMI)

It is an efficient inhibitor synthesised from inulin, a polysaccharide that can be found in various plants such as the cichorium intybus (Chicory) [134, 135]. The effectiveness in inhibiting calcium carbonate crystallization ($CaCO_3$) is based on the ability of the anionic carboxylate groups to adsorb on crystal surfaces by electrical interactions [135]. The inhibitor delays nucleation time, limit seed growth rate as well as act on the crystal morphology [134].

PPCA inhibitor is used for this study and it has been shown to be very effective with respect to reducing the weight of calcareous deposit on stainless steel surface (Figure 3-8) [136].
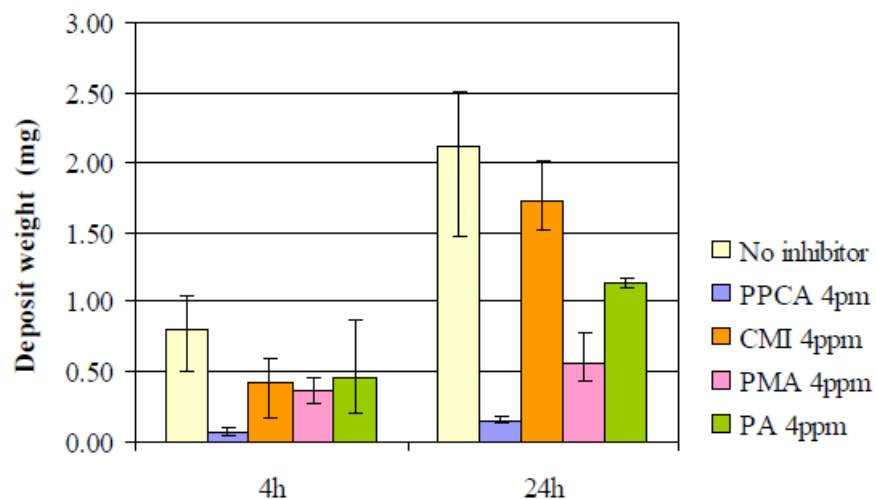
Figure 3-8: Variation of the weight of the calcareous deposit after 24 hours in presence of scale inhibitors at different concentrations [136]

The inhibiting tendency of different inhibitors were also demonstrated by setta *et al* [137]. The results in Figure 3-9 showed their ability to influence the induction time and turbidity rate of $CaCO_3$ scale to varying degree with PPCA having the best performance after 60 minutes.
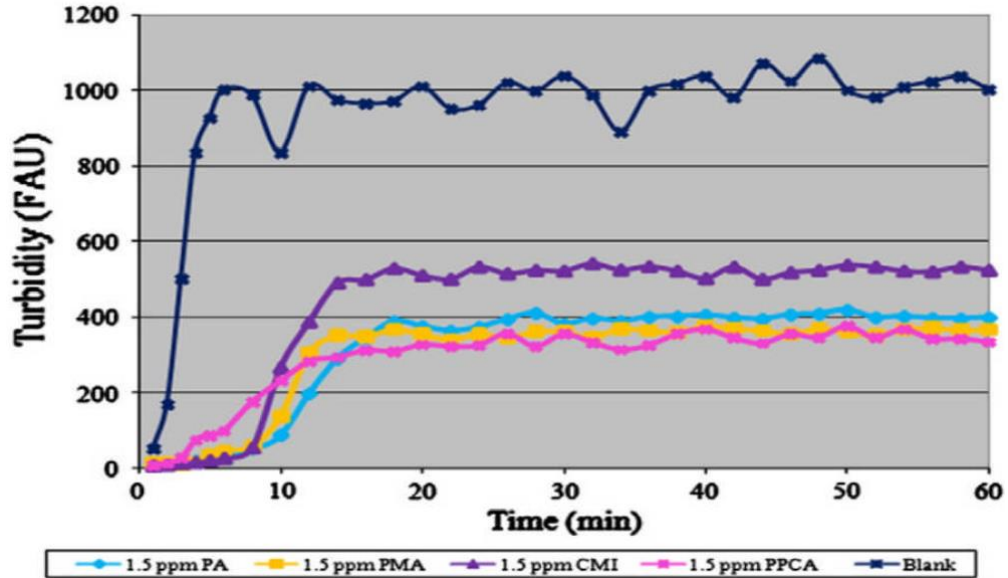
Figure 3-9: CaCO3 turbidity measurements over 1hr at SI=2.1 and 70°C [137]Antifouling surfaces

The field of biofouling has seen major advancement being made towards developing substrates to prevent adhesion or attachment of deposits on surfaces. Surfaces with low surface energy (i.e. hydrophobic surfaces) have shown great efficiency terms of reducing biofouling. Non-stick, fouling release coatings are an attempt to prevent the adhesion of fouling organisms by surface modification to provide a low surface energy on which organisms have great difficulties in settling [138]. However, there are a number of contrary reports on the effects of surface energy on solid deposition behaviour [139]. Studies have shown that the efficiency of a surface varies according to the type of fouling [140], some reports show that organisms attached preferentially to high surface energy surfaces, while others purport to show that deposits attach preferentially to surfaces with low surface energy [141].

Research to the scale deposition process has been focussed on reducing the surface energy because of the perceived similarity to the biofouling process

where particles from the bulk move and adhere on the surface but inorganic fouling has been shown to have different mechanisms to biofouling [20, 30].

The influence of the nature and state of the substrate on the deposition kinetics as well as the morphology of crystal was demonstrated by Jahouari *et al* [76] by an electrochemical technique based on oxygen reduction to deposit calcium carbonate onto different surfaces: stainless steel, bronze and gold. Gold being the less oxidizable appeared to be the fastest to scale followed by bronze and finally stainless steel. It was observed that the presence of oxides on the surface slowed down oxygen and hindered precipitation of scale. The substrate influenced the nucleation rate and consequently the polymorphs formed on it.

Eroini *et al* [142] tested seven different surfaces (stainless steel, stainless steel pre-treated with Polyphosphinocarboxilic Acid (PPCA), Polytetrafluoroethylene (PTFE), Diamond-Like Carbon (DLC), ceramic and polymer coated stainless steels and an isotropic superfinished stainless steel surface (ISF) (Figure 3-10). A subset of these surfaces was eroded to assess the possible effect of in-service performance.
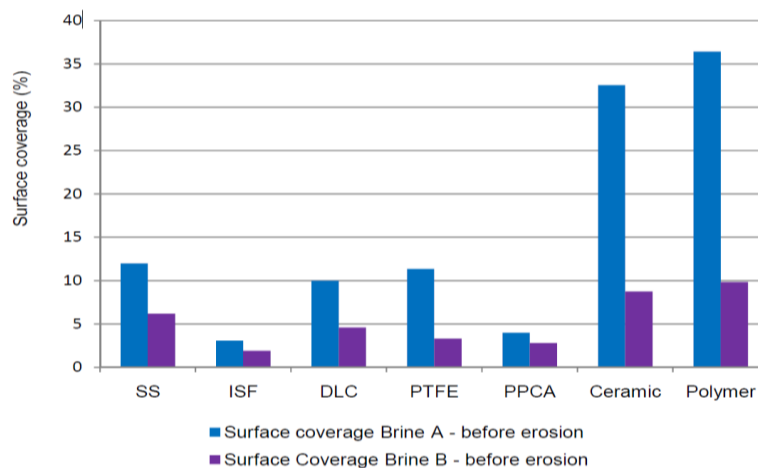
Figure 3-10: Surface coverage of calcium carbonate formed from brine A and brine B on the different surfaces [142].

It was shown that the characteristics which make a surface efficient in terms of scaling appear to be a combination of surface chemistry, water/surface

interaction, roughness and perhaps the shape of the asperities. Both ceramic and polymer coatings show poor performance while the superfinished stainless steel (ISF) and stainless steel treated with PPCA were very efficient in reducing scaling. Amor *et al* [86] also noticed that scale is more likely to deposit on a plastic surface than on a metallic surface.

The state of the surface in terms of surface roughness, surface energy or the presence of impurities has great influence on the kinetics and characteristics of the deposits. Rankin and Adamson [111] showed that adhesion strength is dependent on not just the nature but also on roughness of the surface. It was observed that scale adhesion was greater on rough material because of high surface energy which resulted from increase in surface area. A shorter induction time, large scale deposit and very strong adhesion were all the characteristics shown by rough stainless steel [143].

Recently, potentially permanent low-fouling stainless steel surfaces have been developed through coating the surfaces with carbon that forms a diamond-like structure on the surface [144]. Diamond-like carbon coatings, Figure 3-11, with their chemical inertness, high wear and corrosion resistance, good thermal conductivity and adhesion to metal substrate have been successfully applied in many industries.
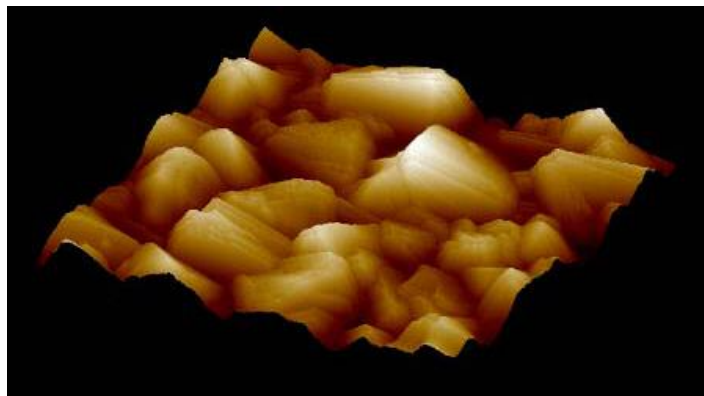
Figure 3-11: AFM image of a vapour deposited diamond-like surface[144].

A very thin and low adherence deposit of calcium sulphate was observed on fluorinated DLC coatings as a result of its low energy whereas the thickness increases on ordinary DLC surfaces with untreated stainless steel surfaces having the thickest deposit formed on it [145].

The effect of surface finish on calcium sulphate fouling as shown in Figure 3-12 was reported by Förster *et al* [117]. The induction period for copper was significantly shorter than stainless steel which reflects the surface free energies of each material. Diamond-like carbon (DLC), produced by a chemical vapour deposition process, was the lowest fouling material despite not having the lowest surface free energy.
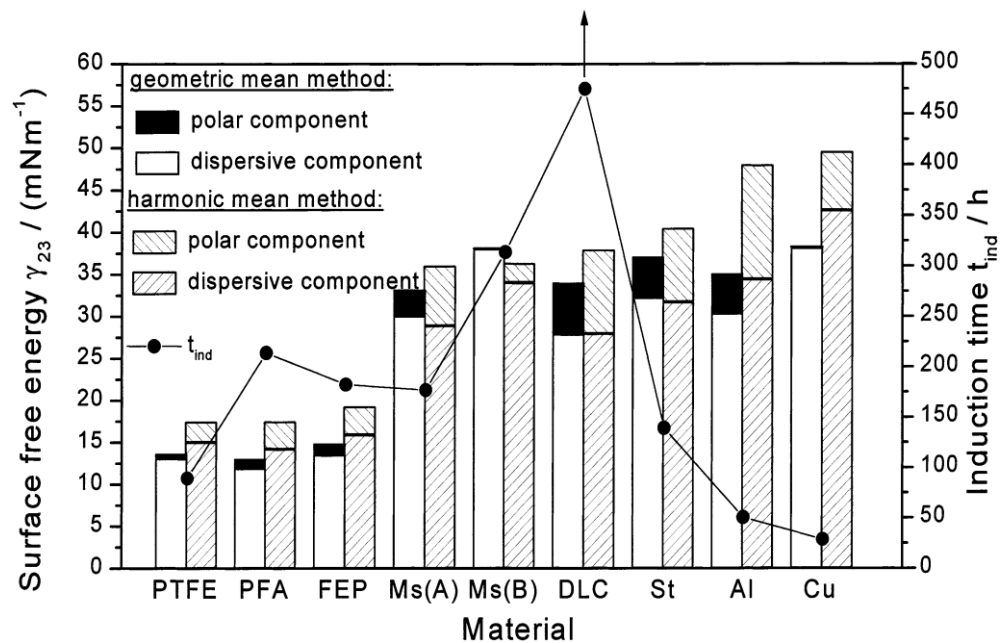
Figure 3-12: Induction time and surface energy characteristics of various surface materials [117].

PTFE- Polytetrafluoroethylene; PFA- Perfluoroalkoxy copolymer- FEP- Fluorinate ethylene propylene; Ms(A)- Brass Ms(B)- Brass; DLC- Diamond like carbon; St-Stainless steel; Al- Aluminium; Cu- Copper.

Further analysis of the PTFE coating showed them to be significantly rougher than both the metal and DLC and this outweighed any benefit of low surface energy. For all the surfaces, once scale had formed the effect surface finish

played was diminished. MacAdam and Parsons [146] observed a scaling reduction of 60% with DLC as compared to PTFE even though it has lower surface energy, Figure 3-13.
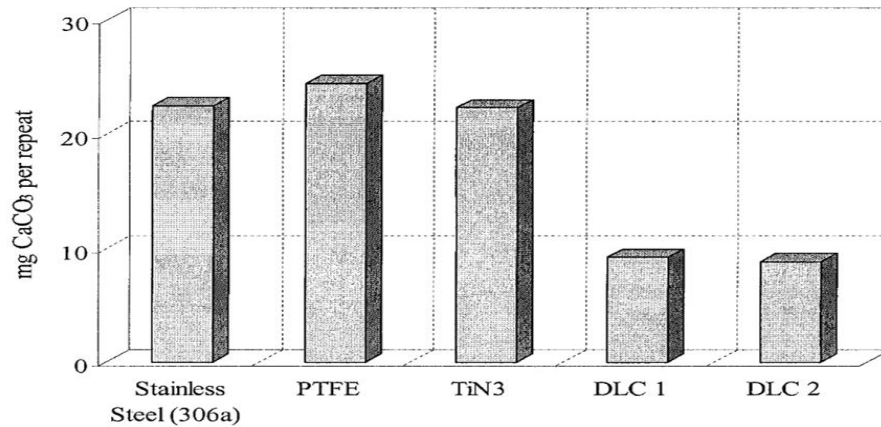
Figure 3-13: The effect of different coatings on CaCO$_3$ scaling rate (300mg L~ CaCO$_3$, 70°C) [146].

Other surfaces shown to have low surface energy include electrodeless plating surface (ELP) where scaling rate was significantly reduced compared to copper [147].

The effect of coating on scaling was studied by Yang *et al* [148] using modified copper surfaces, scale on Cu-DSA (Copperdocosanoic Acid) and Ni-P-PTFE (PTFE co-deposited in electroless nickel solution) have lower surface energy (measured by water contact angle) and were more porous, the induction time was longer and the crystals were smaller than on the unmodified surface. The fouling process is enhanced by the presence of desorbed air bubbles on the modified surfaces (Figure 3-14). Air bubbles are easier to attach on the Cu surface than on the modified surface. It was also shown that the CaCO$_3$ fouling formed on the copper surface is tenacious, while the fouling on the modified surfaces is loose and porous [148].
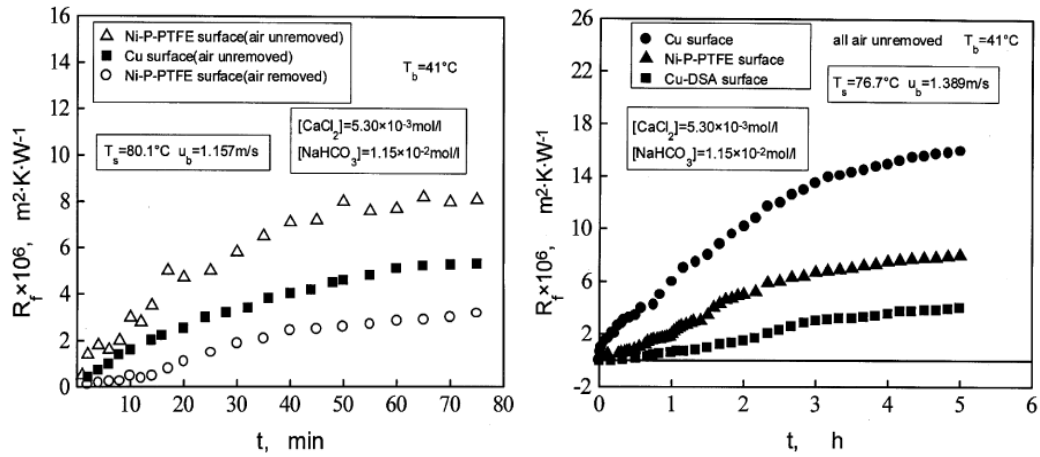
Figure 3-14: Fouling resistance against time for modified, Ni-P-PTFE, Cu-DSA and Cu surfaces [148].

Neville and Morizot [149] investigated scale formation on a stainless steel surface coated with polycarboxylic acid and showed that the coating was very effective in reducing scale formation.

Coating surfaces with PTFE due to its non-stick property to reduce fouling has been attempted in many studies but the poor thermal conductivity, poor abrasion resistance and poor adhesion to metal substrate of PTFE coatings currently inhibit their commercial use [118].

Surface modification to reduce the surface energy or increase hydrophobicity is of great interest in inorganic fouling. Surface energy can be lowered by electroless plating surfaces and self-assembled monolayers (SAMS), where for an initial surface temperature of 79°C, induction time was observed to be about 1hr while there was no induction period observed under the same experimental conditions for Cu [99].
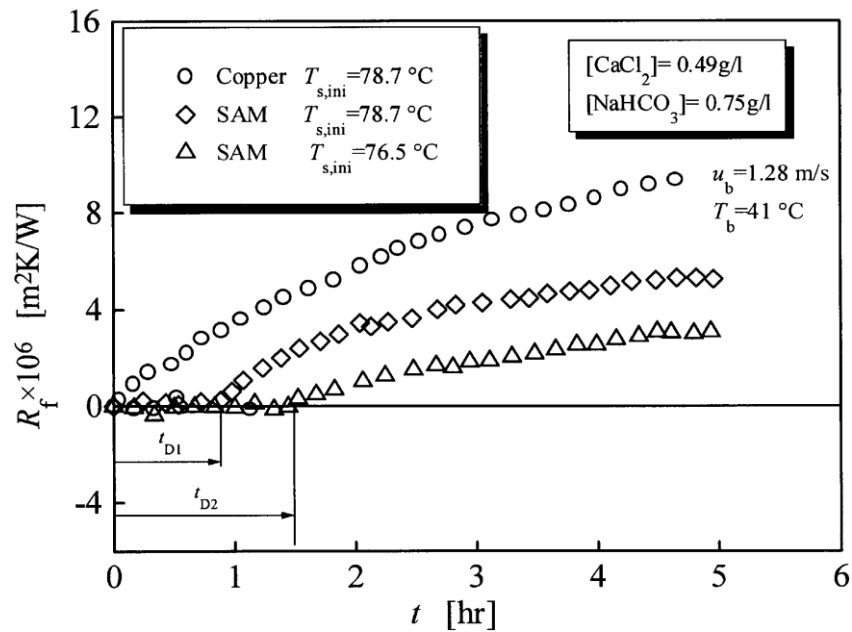
Figure 3-15: Effects of low energy and initial surface temperature on induction period [99]

Other methods are ion sputtering and ion implantation whereby elements with weak metal properties such as F, C, H, Si, are implanted onto metal surfaces causing the number of free electrons on the surface to decrease and hence its surface energy will be reduced. Ion implantation introduce atoms into a solid substrate by bombardment with ions whereas the ion sputtering technique consist in ejected atom from a solid and used them to deposit a coating on the surface. [116, 117, 147, 148].

The application of ion beam implantation, ion sputtering, carbo-nitriding, oxidizing, and Ni-PPTFE coating surface treatment technologies on heat exchanger plates generally showed that with reduced surface energy levels, less deposit were formed. Likewise there was an increase in the amount of deposit with surface roughness [150]. Müller Steinhagen and Zhao [118] used the ion implantation technique to study calcium sulphate deposition on stainless steel surfaces and reported that the microstructure of the $CaSO_4$ deposit formed on the stainless steel surface has a packed structure compared to the loose and porous crystal structure on the Ni-Cu-P-PTFE coated surface .

57

Surfaces possessing almost the same surface energy may have various ranges of performance. Nonetheless, studies found that coated surfaces showed less fouling tendency relative to uncoated surfaces. This is significant as the modified surfaces influence the initial crystallization steps and subsequently lead to different growth behaviour of the overlaying crystals.

3.2 Scale study and investigation techniques

Several methods can be used to study calcium carbonate scale formation using different experimental conditions and set up. Most of the studies focused on precipitation in bulk while few studies were carried out on surface deposition. Some of the different methodologies used to study scale formation in the bulk as well as on the surface are reviewed in the following sections.

3.2.1 Study of scale precipitation in the bulk

The changes in the supersaturated solution as a result of precipitation are usually assessed by different methods in order to quantify bulk scaling.

3.2.1.1 Measurements of turbidity

Turbidity is a measure of the degree to which the solution becomes cloudy and loses its transparency due to the presence of suspended particulates resulting from the precipitation of calcium carbonate. The cloudiness of the solution can be measured in terms of the amount of light scattered by particles in the solution with a turbidity meter. Generally, a parallel light beam of wavelength λ travel through a solution and the encountering of particles result in a global extinction phenomenon [151].

Turbidity is defined by the following equation:

$$T_\lambda = (I/L) \log(I_0/I_L) \tag{3.8}$$

Where I_0 = Intensity of the incident ray; I_L = Intensity of the transmitted ray after an optical path length L.

Parameters such as the critical supersaturation ratio above which turbidity increases, the particles size distribution, the induction time and the volume of solid formed can be determined by turbidity measurement [46, 151-153].

The growth of calcium carbonate crystals characterized by adding them in a stable supersaturated solution were studied by Nancollas [154]. The inoculated solution was filtered during the growth step and the filtrate was analyzed by Atomic Absorption Spectroscopy. Assessment of the changes in the turbidity of the bulk solution was used by Tantayakom *et al* [152] to study barium sulphate scale inhibition. They determined the critical supersaturation ratio for which barium sulphate precipitates for different experimental conditions. He *et al* [155] studied the induction period of calcium carbonate formation at 25 and 90°C by turbidity measurements. Sohnel *et al* [46] measured the turbidity of the solution to study the effects of magnesium, manganese, chromium and fluorine on the kinetics of scale precipitation

3.2.1.2 Measurements of conductivity

The precipitation of calcium carbonate also lead to a decrease in conductivity because of decrease in concentration of electrically conductive species [156]. Conductivity is measured using a conductivity meter. The time between mixing and conductivity steadiness is used to determine the induction time [46, 156].

3.2.1.3 Measurement of pH

This gives information about the precipitation kinetics in various conditions. As $CaCO_3$ precipitates, the pH will decrease due to the decrease in carbonate ions in the solution. Usually pH measurements are performed using a pH meter and the precipitation is assumed to have ended when no further changes in the pH value are observed. Another way to follow the pH is to use a combined glass/saturated AgCl/Ag electrode [60]. The presence of Impurities such as Mg^{2+}, Fe^{2+} and SO_4^{2-} in the solution have a significant effect on the pH when compared with solutions free of foreign ions [157].

3.2.1.4　　Measurement of calcium ion concentration

The decrease in calcium ion concentration in the solution as a result of the precipitation of calcium carbonate can be used to assess the bulk precipitation process. The concentration of calcium ions in the solution can be measured by using a calcium selective electrode [158]. Titration in which an EDTA solution is used to complex the calcium ions is another method used to determine the concentration [86, 159].

The kinetics of crystallization can be studied by measuring the calcium ion concentration [154] and thee degree of precipitation (α) is defined as

$$\alpha = \frac{([Ca^{2+}]_0 - [Ca^{2+}]_t)}{[Ca^{2+}]_0} \tag{3.9}$$

Where $[Ca^{2+}]_0$ is the calcium concentration at time 0 and $[Ca^{2+}]_t$ is the calcium concentration at time, t [94]. Calcium ion concentration can also be measured using a radiotracer such as 47Ca [159] or 45Ca [154].

3.2.2　Study of scaling at the surface

Various electrochemical and non-electrochemical techniques have been employed to study surface scale formation.

3.2.2.1　　Non-electrochemical techniques

Quartz crystal microbalance (QCM) is an example of non-electrochemical techniques [160]. A thin film deposited on the surface of a quartz crystal disc oscillator plated with gold decreases the frequency in proportion to the mass of the film. The resonant frequency and the mass sensitivity are determined by thickness of the crystals.

The crystallization of a number of sparingly soluble salts on the addition of well characterised seed crystals to stable supersaturated solutions provides a highly reproducible non spontaneous crystallization known as "seeded growth

techniques" [161, 162]. This method allows the growth of crystals to be assessed because inoculation of seed in a saturated solution will results in growth of the existing particles rather than nucleation.

A very common method to study scale deposition is the tube blocking test. Supersaturated solutions flow through a thin tube (of the order of millimetres in diameter) and scale builds up on the surface of the tube will result in results in differential pressure between the inlet and outlet of the tube [10, 163]. Tube blocking test were used by Zhang *et al* [18] to perform bulk measurement at the outlet of the tube and to develop a kinetics model to predict downhole scaling. Dyer and Graham [77] studied the effects of temperature and pressure on barium sulphate and calcium carbonate precipitation. The relative efficiency of two inhibitors (Poly combined with temperature and pressure effects on scale formation was also assessed using the dynamic tube blocking rig [77].

Assessment of the efficiency of scale inhibitors is a vital study in scale precipitation and deposition. A technique known as dynamic bulk jar test was used for the determination of PPCA inhibitor efficiency as well as the kinetics of scale bulk precipitation and surface deposition. The bulk jar test consists of mixing brine in a beaker or a jar and carrying out an assessment of the precipitation process [164].

3.2.2.2   Electrochemical techniques

Analytical methods based on the electrochemical process were developed so as to quantify scaling. This technique is based on the correlation between the diffusional characteristics of oxygen at a surface and the changes in the rate of oxygen reduction once nucleation and growth of $CaCO_3$ occurs [165-167]. The electrochemical reactions that occur on the surface of metallic structures are the reduction of oxygen. A metallic surface is cathodically polarized at a negative potential. Thus, there is a reduction in the oxygen dissolved and the hydroxide ions bringing about a sudden increase in pH. It induces the transformation of bicarbonate ions into carbonates which in turn react with the

calcium ions forming a precipitate of calcium carbonate on the surface of the working electrode

The electrochemical mechanism for the formation of calcareous deposits is as follow [168].

Oxygen reduction

$$O_2 + 4e^- + 2H_2O \rightarrow 4OH^- \tag{3.10}$$

Reduction of water leading to hydrogen-evolution for more negative cathodic potentials.

$$2H_2O + 2e^- \rightarrow 2OH^- + H_2 \uparrow \tag{3.11}$$

OH ions near the surface of metallic structures result in the formation of calcareous deposits on the metal surface.

$$HCO_3^- + OH^- \leftrightarrow H_2O + CO_3^{2-} \tag{3.12}$$

$$Ca^{2+} + CO_3^{2-} \rightarrow CaCO_3 \downarrow \tag{3.13}$$

Neville *et al* [166] demonstrated that the extent of scale deposition on a metallic surface can be accurately estimated using analysis of the oxygen reduction reaction at a rotating disk electrode (RDE) surface under potentiostatic control. The electrode cell in Figure 3-16 comprises of a working electrode, to deposit the scale, a reference electrode to maintain the potential and a counter electrode to allow the current to be carried [166].
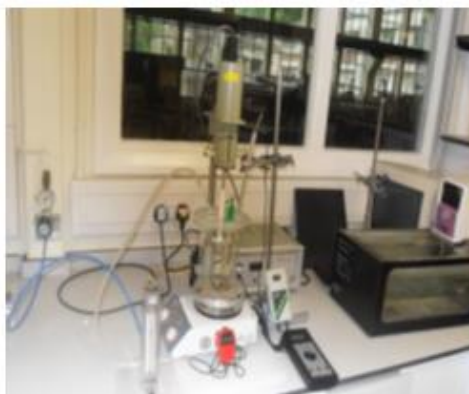
Figure 3-16: RCE for surface scale studies [166]

This technique analyses the diffusion of oxygen to an electrode surface under varying hydrodynamic conditions. The use of the rotating disk ensures that the mass transport to the surface is well defined and may be controlled by changing the disk rotation speed.

A combined bulk chemistry/electrochemical measurement was later employed to study the precipitation, deposition and inhibition of $CaCO_3$ thus enabling the precipitation and deposition kinetics to be compared and contrasted in the absence and presence of a commercial scale-control inhibitor [7].
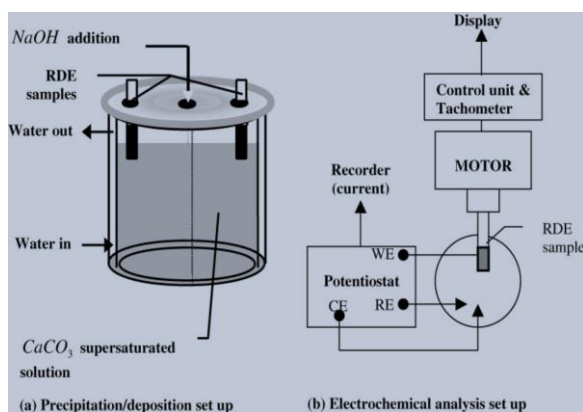
Figure 3-17: Experimental set up for (a) electrochemical analysis and (b) precipitation and deposition of $CaCO_3$ [7]

In order to visualize the crystallization of calcium carbonate scale in real time, a new set up was developed by Euvrard *et al* [17] which composed of an electrochemical cell with availability of an electrode polarization control, that

enable the use of any kind of cathodic surface and a transparent anodic window, connected to a video set-up, an optical assembly monitors and records the surface area of the working electrode during the experiment [17]. The cell as shown in Figure 3-18 comprises of two PMMA plates, one containing the working and reference electrodes and the second including a window coated with tin oxide acting as a counter electrode.

The observation of the surface is made in real time through the counter electrode. The set up gives a better understanding of the calcium carbonate formation and inhibition on a metal surface.
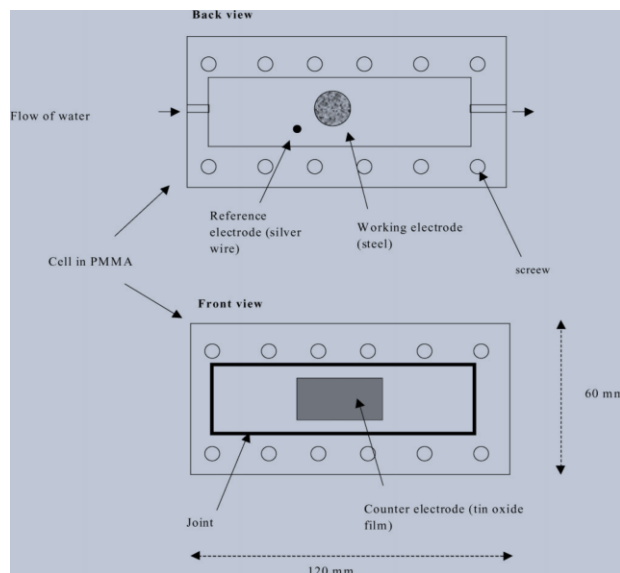
Figure 3-18: Electrochemical cell [17]

In this thesis, a similar *in-situ* visualization cell built into a newly developed flow rig is used to study bulk and surface scaling from a supersaturated solution with control of various experimental parameters. Full details of the rig and of the conditions of the experiments are described in Chapter Four.

3.3   Summary and gap in literature review of scale studies
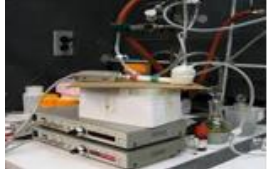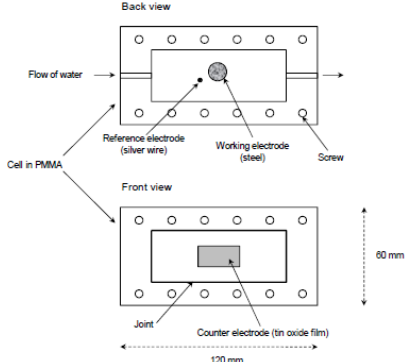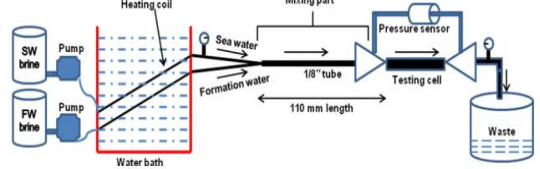
Understanding the kinetics of calcium carbonate formation on surfaces is a real challenge but appears fundamental in order to improve the methods to prevent damage caused by scale. It does appear that the only reliable

prediction for scale formation is based on the supersaturation degree of a solution [169]. However, most supersaturation indices are thermodynamic values and do not inform on the formation rate (kinetics) of a scale layer whereas existing kinetic models use bulk precipitation data to predict the scaling rate on a surface. Indeed existing scaling indices are based on extensive experimentation of bulk scaling parameters [170]. Numerous corrections for temperature, pressure and ionic concentration have been devised to be applied to the indices [7].

Recent studies have shown that more focused knowledge needs to be directed to scaling kinetics at solid surfaces since it has been demonstrated that there are often wide discrepancies between actual surface deposition and rates estimated by predictive models based on scaling indices [23]. Although the effectiveness of scale inhibition depends on the severity of scaling condition such as supersaturation and temperature, studies have also shown that scale inhibition efficiency and the effects on crystal morphology varies between surface and bulk processes [34, 171].

Reliable prediction of $CaCO_3$ scaling for estimating scale production in oilfield production wells and surface facilities requires both thermodynamic models to indicate the tendency for scaling from solution and kinetic models to predict the rate of scaling and thus the time required to cause blockage [7]. Recently, the relationship between bulk and surface scaling has received attention in the literature due to the observation that they are often not sharing the same trends with respect to crystal growth kinetics or inhibition [30, 80, 81, 172]. The growth and inhibition of $CaCO_3$ scale on various surfaces has been examined in many studies. Techniques that have been used include tube blocking tests, quartz crystal microbalance, rotating cylinder electrode, electrochemical methods and modern dynamic techniques such as synchrotron x-ray diffraction. The limitations of some of the techniques are summarised in Table 3-1.

Table 3-1: Limitations of techniques used in surface scale formation studies

RCE, Bulk jar test	• No dynamic flow control • SR decreases as particles grow and settle due to gravity. • Homogeneous and heterogeneous nucleation
Quartz crystal microbalance	• Only suitable for initial stage of crystallization • Very expensive
Electrochemical cell (Electro crystallization)	• Based on electro-crystallization and does not assess deposition from supersaturated solution.
Dynamic/Tube blocking test	• SR decreases as a function of capillary length • Mainly suitable for inhibition efficiency test. (MIC determination). • Difficult to correlate pressure measured with theoretical value

Despite much recent attention on scale formation on surfaces, there is still not a full mechanistic understanding of how scale layers build on component surfaces. This requires a suitable methodology to improve on the understanding of the precipitation/deposition system and build an accurate surface deposition kinetic model.

In this study, a new experimental facility with associated image analysis of scale build-up in real-time is used to assess the formation and inhibition of $CaCO_3$ surface and bulk scaling. Scale precipitation and surface deposition is followed *in-situ* and in real-time in a once-through flow rig that allows control and assessment of various parameters, brine chemistry and scaling indices, temperature, flow rates as well as inhibitor concentrations.

The detailed experimental procedure as well as the planned analysis of data to achieve the set out objectives are presented in Chapter Four.

Chapter 4 Experimental methodology

Improving on the understanding of scale formation requires both thermodynamic and kinetic considerations of bulk and surface scaling with a suitable experimental methodology.

In this chapter, the design, development and the process of the visualization flow rig are presented (section 4.1). The surface image processing and analysis procedure is discussed (section 4.2). Also described are the materials used for the study, brine chemistry, saturation ratio (section 4.3), the kinetic and surface inhibition conditions (section 4.4), and the surface analysis test (section 4.5). The tests were performed with 7 different supersaturated solutions of $CaCO_3$, three different flow rates and two temperatures. Surface images of the scale formed on the sample inserted in the cell were taken at regular intervals and analysed using modified image assessment protocols.

4.1   Set-up for surface deposition and bulk precipitation measurement

Control over scaling parameters is important in order to fully understand the scaling process, therefore in designing the rig, various combinations of scaling parameters such as composition of the feed (i.e. inlet and outlet supersaturation), residence time in the flow cell and temperature of the bulk solution are systematically considered.

The flow rig set up consists of the following:
- An *in-situ* surface visualization cell.
- An *in-situ* fibre optic turbidity probe
- A high performance monochrome digital imaging device with 50FPS (frame per second) and 1 mega pixel resolution.
- A thermocouple (type K)

- A double channel peristaltic digital pump REGLO MS 12 roller used to allow pumping of the brines simultaneously. The tubes are made of 3mm diameter silicone plastic.

- Stainless steel tubing of 3mm internal diameter used to transport the brines from the pump outlets through the thermostatic bath (wound into coils) into the mixing chamber fitting.

- An optima general purpose digital thermostatic circulator bath with pump plastic tank, 15ºC to 99ºC. It circulates ethylene glycol around the stainless steel tubing allowing control of the temperature.

4.1.1 Process

The schematic diagram of the flow rig is shown in Figure 4-1. The brine solutions are pumped through the thermostatic bath from the containers with a two channel peristaltic pump at the same flow rate. The thermostatic bath is used to heat up the brine to the required temperature and a thermocouple (type K) is used to measure the temperature of the fluid at the mixing point. From the thermostatic bath, the brines flow into a mixing chamber where they are mixed together before surface deposition in the cell. At the outlet of the cell, temperature of the fluid can also be monitored in the temperature-pH-conductivity cell that is incorporated into the rig. The thermal loss is minimal or negligible $(-0.2℃)$ and the temperature at the sample is adjusted at the thermostatic bath if necessary. From the cell outlet, the brine flows into a waste container since it is designed to be a once-through rig. The brine is constantly being renewed to keep the saturation ratio at the sample surface and experimental condition constant.
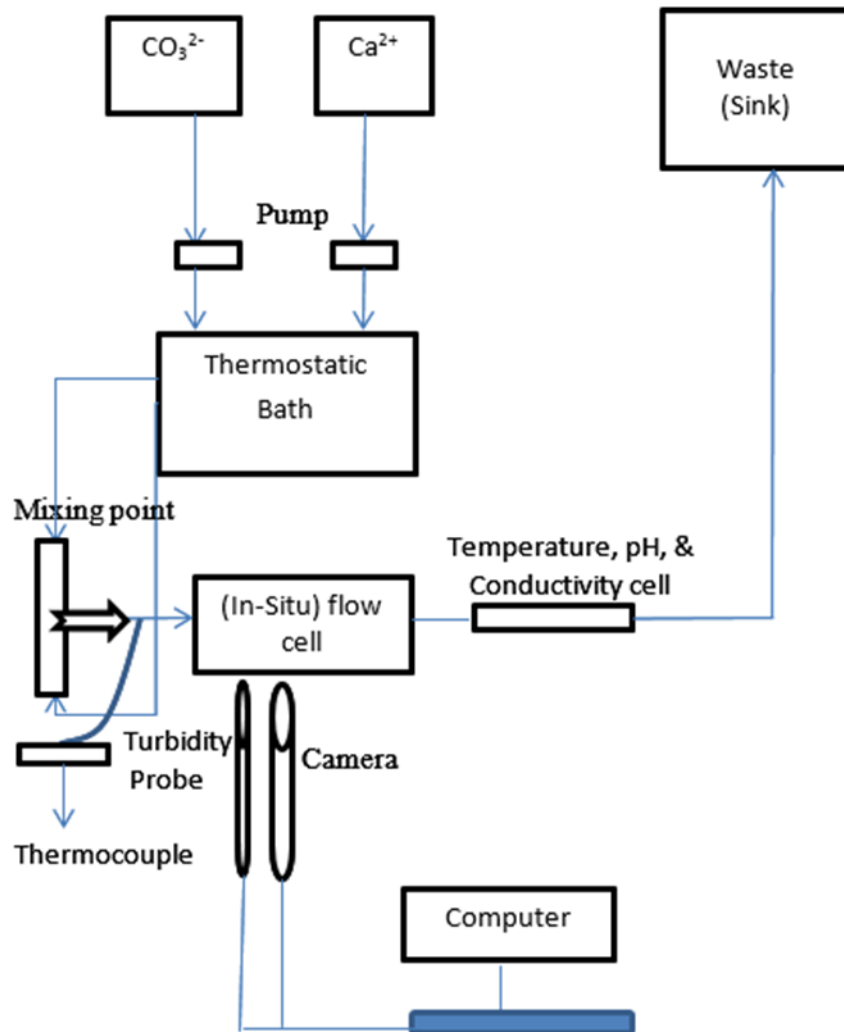
Figure 4-1: Schematic diagram for the experimental flow rig design

The *in-situ* flow cell for surface deposition is made of two poly (methyl methacrylate) PMMA plates Figure 4-2 (a) and (b) separated by chemically inert polytetrafluoroethylene (PTFE) Figure 4-2 (c). The first part is 20mm thick and houses the inlet and outlet of the channel with diameters of 5mm each. The angle at the inlet and the outlet is set at 20^0. It also consists of two separate 20 mm diameter holes made through the plate. The first of the two holes is to allow the removable plug for the surface being studied to be inserted at 75 mm from the outlet. The second hole is for turbidity to be measured directly in the flow cell from a separate photometric glass window made on the third plate. The dimension of the cell channel made by the hole in the middle of the Teflon plate is 160 mm length approximately, 40 mm wide

and 2 mm thick. The thickness enables observation of the surface through the flow by the camera. The third plate (second PMMA) is 5 mm thick and a 30 mm diameter hole is pierced in front of the removable plug covered by a glass window allowing visualisation of the flowing solution and of the surface located on the other plate.
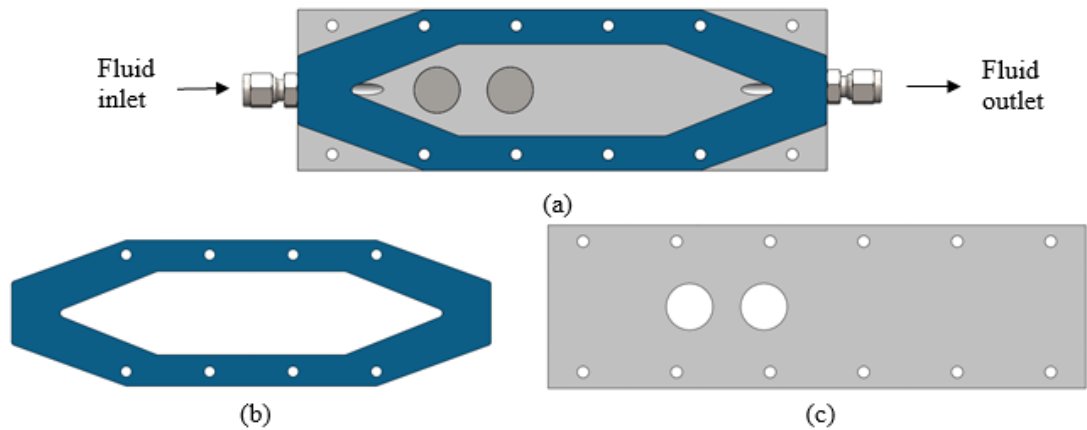
Figure 4-2: Flow cell part

The cell is designed to incorporate turbidity measurement and image capture of the metal surface very close to the point of mixing of the brine.

4.1.2   Turbidity measurement

Turbidity measurement is associated with the cloudiness of the solution. It allows precipitation process in the bulk to be followed and parameters such as the induction time and precipitation kinetics to be assessed.

Turbidity in real time is measured using fibre optic turbidity probe that is focused at an angle 90° to the photometric glass window. The light is transmitted through the glass to measure the turbidity of the solution in the cell and is reflected back by a mirror placed at the back of the cell. The turbidity is measured by light intensity that is reflected back into the sensor of the probe. The optical turbidity probe has a great precision for a range of turbidity between 0 and 400 FTU (Formazin Turbidity Unit) and can be used for temperature up to 140°C.

4.1.3 Surface visualization

The surface scale formation mechanisms and kinetics are followed by a high performance (charged couple device) CCD video camera linked to a computer. The camera will allow real time accurate observations and instantaneous image capture of scale formation on the steel surfaces inserted in the in-situ flow cell. An optic system is adapted onto the camera to magnify the images. A mercury lamp is used to improve the quality of the images. The resolution of the digital camera is 1 mega pixel and has a frame rate of 50FPS. The size of each frame after the lens is adjusted to give a good focus with minimum noise is 1mm x 1mm (Figure 4-3).
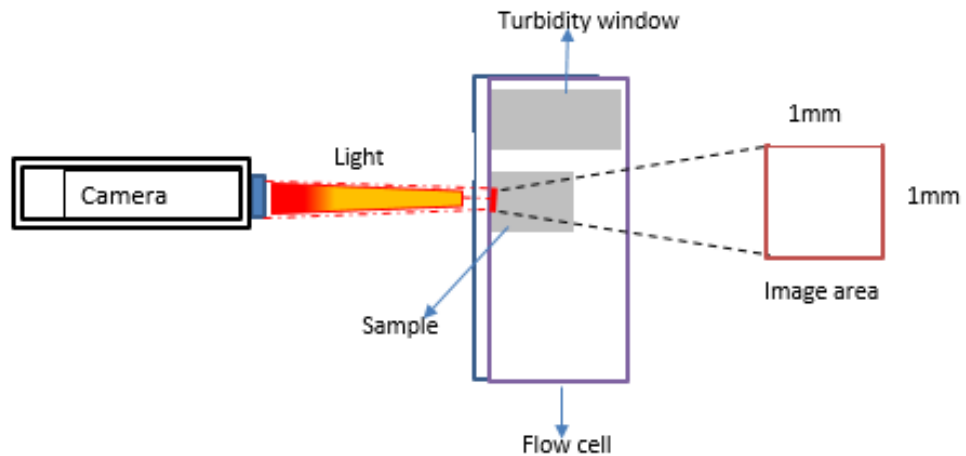
Figure 4-3: Schematic diagram illustrating *in-situ* surface visualization

The images are captured automatically at defined regular time intervals and are saved to file for processing and analysis using a suitable procedure which is discussed in section 4.2. The image analysis procedures allow to determine the surface coverage of scale, number and average size of crystals as well as the particle size distributions.

4.1.4 Fluid dynamics in *in-situ* flow cell

The *in-situ* flow cell has been designed for a laminar flow regime in order to avoid turbulence and recirculation of fluids for a better control of the

experiment as well as to remove the effects of shear stress while scale is being formed. Three different flow rates 10ml/min, 20ml/min and 40ml/min are used in order to verify the effect of increasing flow velocity on scale kinetics. The flow velocity across the cell has been modelled using computational fluid dynamics. The hydrodynamic characteristics of the flow cell which includes flow velocities and Reynolds number shown in Figure 4-4 and Table 4-1 suggest laminar flow regimes (fluids lowing in parallel layers).
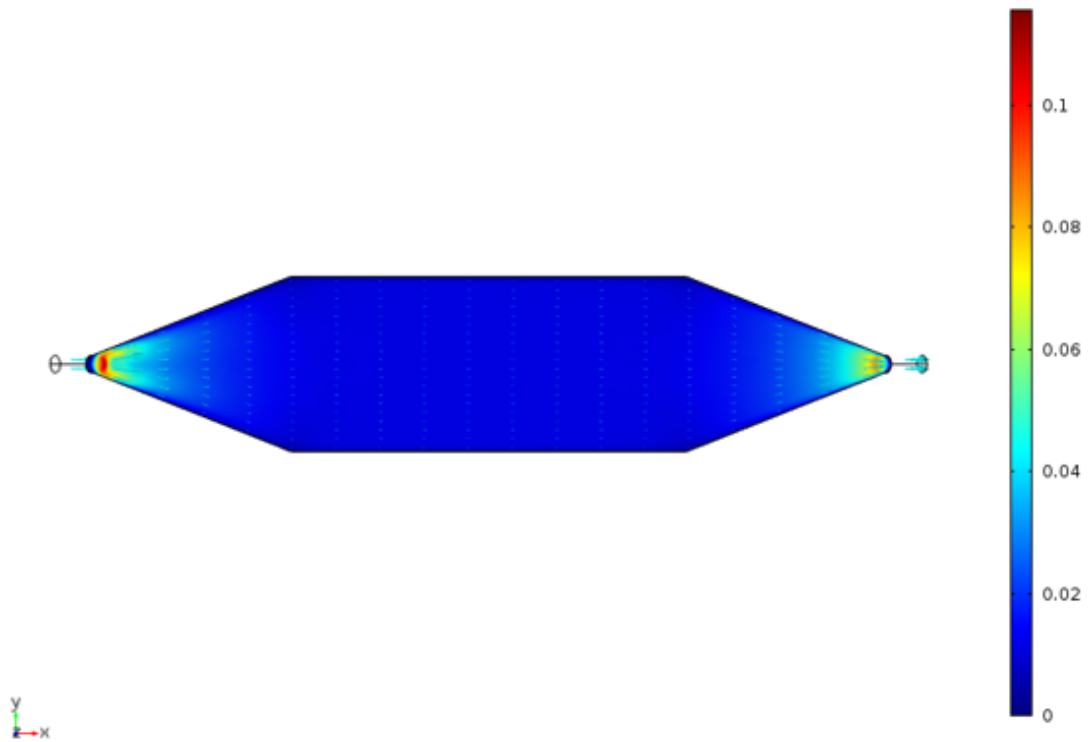
Figure 4-4: Flow characteristic at 20ml/min: velocity magnitude (m/s); Arrow volume indicates velocity field across flow cell

Table 4-1 Hydrodynamic parameters

Flow rate ml/min	m³/s	Average velocity at centre m/s	Max Reynold no	Regime
10	1.67 X 10⁻⁷	0.0032580	4.0187	
20	3.34 X 10⁻⁷	0.0063454	7.6089	Laminar
40	6.67 X 10⁻⁷	0.012770	15.357	

The hydrodynamic analysis of the cell as seen in the flow path in Figure 4-5 shows that there is no recirculation of flow and more importantly, the flow velocity is uniform across the centre of the cell where the images and turbidity measurements are taken.
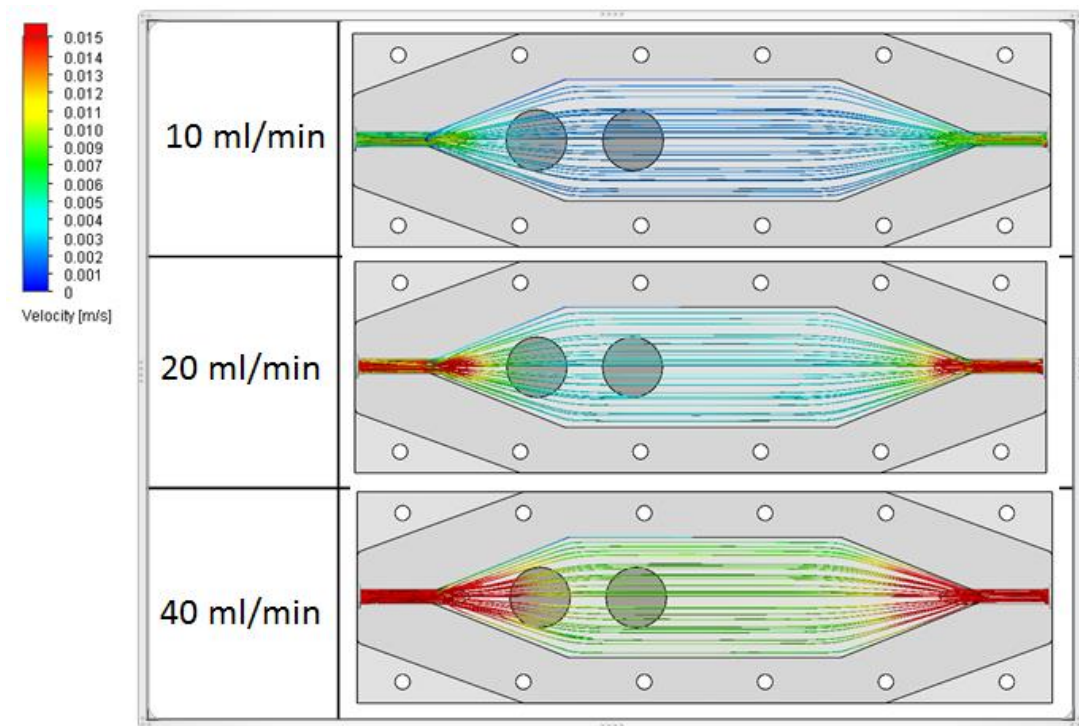
Figure 4-5: Velocity field

The flow path diagrams and characteristics of the *in-situ* cell with the maximum Reynolds number and average velocities for flow rates between 10ml/min - 60ml/min are presented in Appendix A.

4.2 Method for image processing and analysis

The programming language, MATLAB is used to process and analyse the images taken. It consists of a set of algorithms that have been carefully written to suite the operations required. It allows the image to be read as a matrix of pixels that are modifiable in order to improve the quality and extract the information needed, such as the surface coverage, average size and the number of particles.

The operations used to produce a segmented image consists of various steps shown in Figure 4-6. The set of image processing algorithms used for each operation is presented in Appendix B. Segmentation refers to "the identification and isolation of an image into region" to produce a binary version of the image. It is used to obtain a simple matrix composed of 0 (no crystals) and 1 (crystals) only [173].
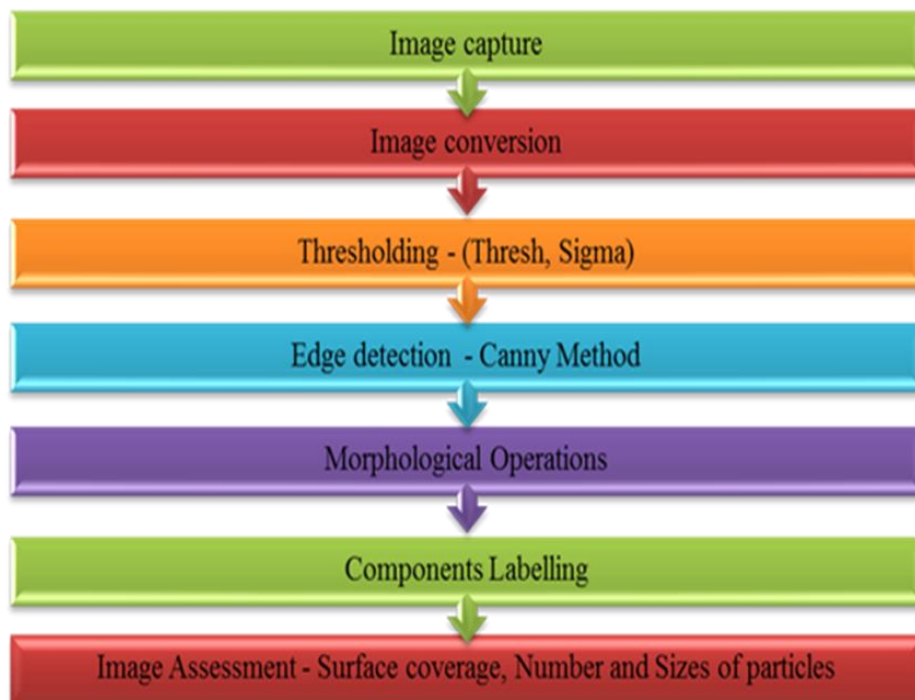
Figure 4-6: Steps for image analysis

In this study, the crystals or clusters forming on the surface are the regions to be isolated. From the binary image created, objects are then labelled and the

surface coverage, average sizes and number of clusters are calculated using a statistical command.

The analysis takes into consideration the image quality or noise and also the details to be detected in choosing the threshold values while the sigma values take into consideration how much the image will be smoothened. A low value threshold will results in lots of edge points while a high threshold will results in few edge points being detected. The edge detection consists of locating significant changes in the intensity corresponding to object boundaries. The edge of object boundaries corresponds to large variation or discontinuity in the image brightness. The image obtained consists of a binary image where pixels are defined as edge or non-edge. The "Canny" filter edge detection algorithm is used for this study because it is the most advanced and it gives optimum result in edge detection [173].

The edge detection is followed by morphological operations ("bridging, closing and opening") to process the shape of the object detected. "Bridging" consists in bridging or connecting unconnected pixel; "Closing" consists of connecting close objects; filling small holes and gaps followed by filling bigger holes; "Opening" consists of removing small objects without affecting the size and shape of the bigger ones [173].

To obtain a very good image analysis output, the procedure and parameters vary depending on quality or the level of image noise. These require having to repeatedly change and adjust processing parameters in MATLAB from image to image. However, a user friendly interface as shown in Figure 4-7 is developed that takes into consideration the adjustments of the various parameters.
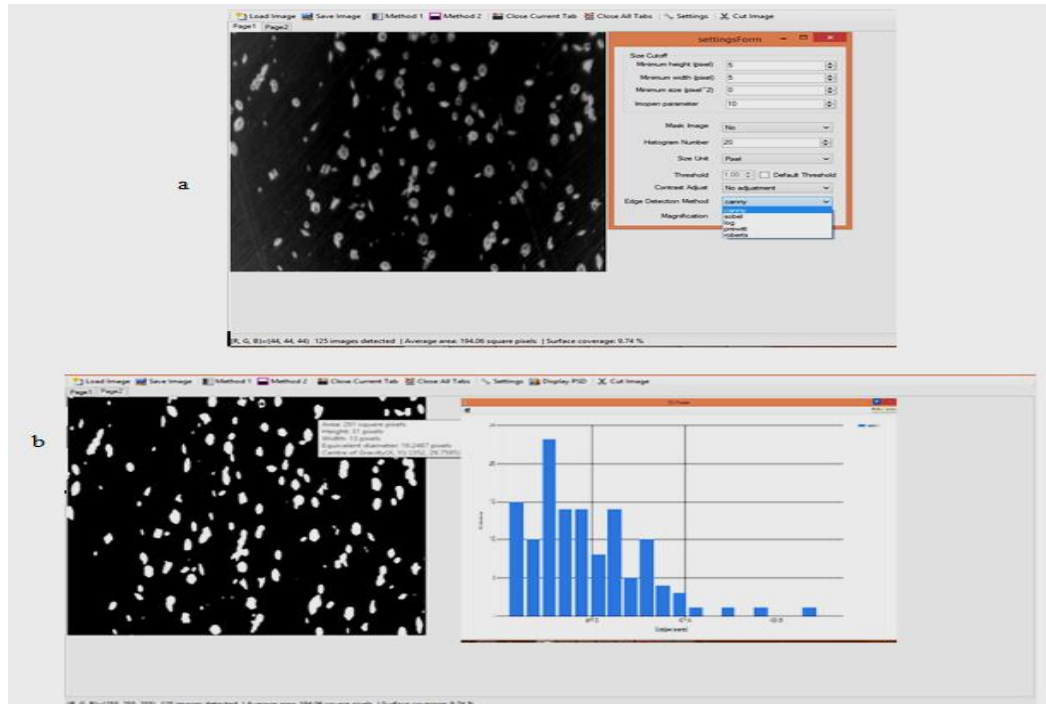
Figure 4-7: User interphase for image analysis (a) Input (b) output

The segmented image produced at the end of morphological operations is labelled and the pixels connected together for assessment. The assessment involves using some statistical code to determine the number of objects and their average size as well as the fractional surface coverage.

Table 4-2: Image assessment parameters

Parameters
Number of objects
Average size
Surface coverage

4.3   Material for deposition and brine chemistry

The material used in this study is a standard austenitic stainless steel UNS S31603. The composition is given in Table 4-3.

Table 4-3: Stainless steel composition used for the study [174]

Elements	Composition (%)
C	0.03
Mn	2.00
Si	1.00
Cr	16.0 - 18.0
Ni	10.0 - 14.0
P	0.045
S	0.03
Mo	2.0 – 3.0
N	0.10

The surface diameter of the sample on which deposition occurs is 1cm. Each sample is a cylindrical piece that can be inserted easily in the cell.

4.3.1 Surface preparation

Each cylindrical stainless steel sample was carefully polished to achieve a surface roughness (R_a) of 0.01µm. The cylindrical stainless steel sample is abraded with silicon carbide P 800 and 1200 followed by 3µm and then 0.25µm diamond paste for the final finish. The surface roughness, R_a, was measured using a Taylor Hobson surface profiler. The sample is inserted vertically into the removable plug with the polished surface facing the glass window of the *in-situ* flow cell. A small recess is made such that there is no interaction between the bulk fluid and the sample. The flow path of fluid on the surface is shown in Figure 4-8.
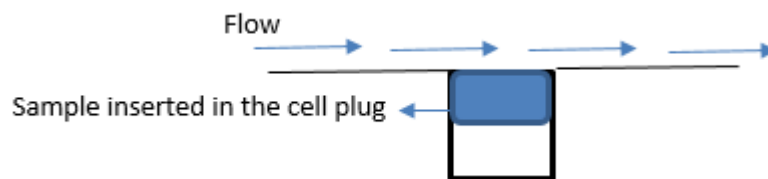
Figure 4-8: Fluid flow on sample surface

4.3.2 Brine chemistry and saturation ratio

Simple $CaCO_3$ brine is used to study the fundamental mechanisms of surface scaling and its relationship to bulk precipitation. The brine is made from mixing two different brine solutions at ratio 1:1. One of the brines (FW) is a simulated

Forties brine (rich in calcium). The second brine (SW) is a synthetic sea water brine (rich in bicarbonate). Using multiscale software, the ion compositions for each brine are adjusted to reach 7 different saturation ratios, SR 10, 15, 25, 45, 60, 70 and 90. These mixtures promote scale formation for calcium carbonate at different saturation ratio with varying temperature. The composition of the simple brines used is given in Table 4-4 (where FW is the formation water and SW is the synthetic seawater brine).

Table 4-4: Composition for simple brine solution (g/L) at 25⁰C

	NaCl		NaHCO$_3$		CaCl$_2$.2H$_2$O	
SR	FW	SW	FW	SW	FW	SW
10	44.05	40.73	0.00	1.91	2.52	0.00
15	44.43	40.55	0.00	2.17	3.00	0.00
25	44.68	40.19	0.00	2.69	3.31	0.00
45	45.52	39.77	0.00	3.28	4.37	0.00
60	46.22	39.56	0.00	3.58	5.26	0.00
70	46.45	39.40	0.00	3.82	5.54	0.00
90	47.01	39.12	0.00	4.22	6.25	0.00

Table 4-5 shows the composition of brines at 40°C. The composition of the ions for each brine are adjusted so as to have the same saturation ratio at the two different temperature considered due to the inverse solubility properties of CaCO$_3$.

Table 4-5: Composition for simple brine solution (g/L) at 40⁰C

	NaCl		NaHCO$_3$		CaCl$_2$.2H$_2$O	
SR	FW	SW	FW	SW	FW	SW
10	43.69	40.85	0.00	1.52	2.06	0.00
15	44.23	40.63	0.00	2.05	2.74	0.00
25	44.23	40.55	0.00	2.16	2.84	0.00
45	44.71	40.15	0.00	2.74	3.34	0.00
60	45.26	39.97	0.00	3.00	4.04	0.00

The compositions of the salts have been determined using the Multiscale^{TM} software. The different saturation ratios A, B, C, D E, F and G were obtained by mixing the corresponding formation and synthetic water (FW and SW respectively) at the ratio 50:50.

4.4 Mechanisms and kinetic study

The study was carried out with supersaturated CaCO$_3$ brine solutions having SR values of 10, 15, 25, 45, 60, 70 and 90 at 25°C and 40°C. The duration for each test is 4hrs. The effects of varying flow rates were tested for brines of SR 10, 15, 25, 45 and 60. The three different flow rates used are 10ml/min, 20ml/min and 40ml/min at 25°C.

An overview of the experiments for the kinetic study is given in Figure 4-9.
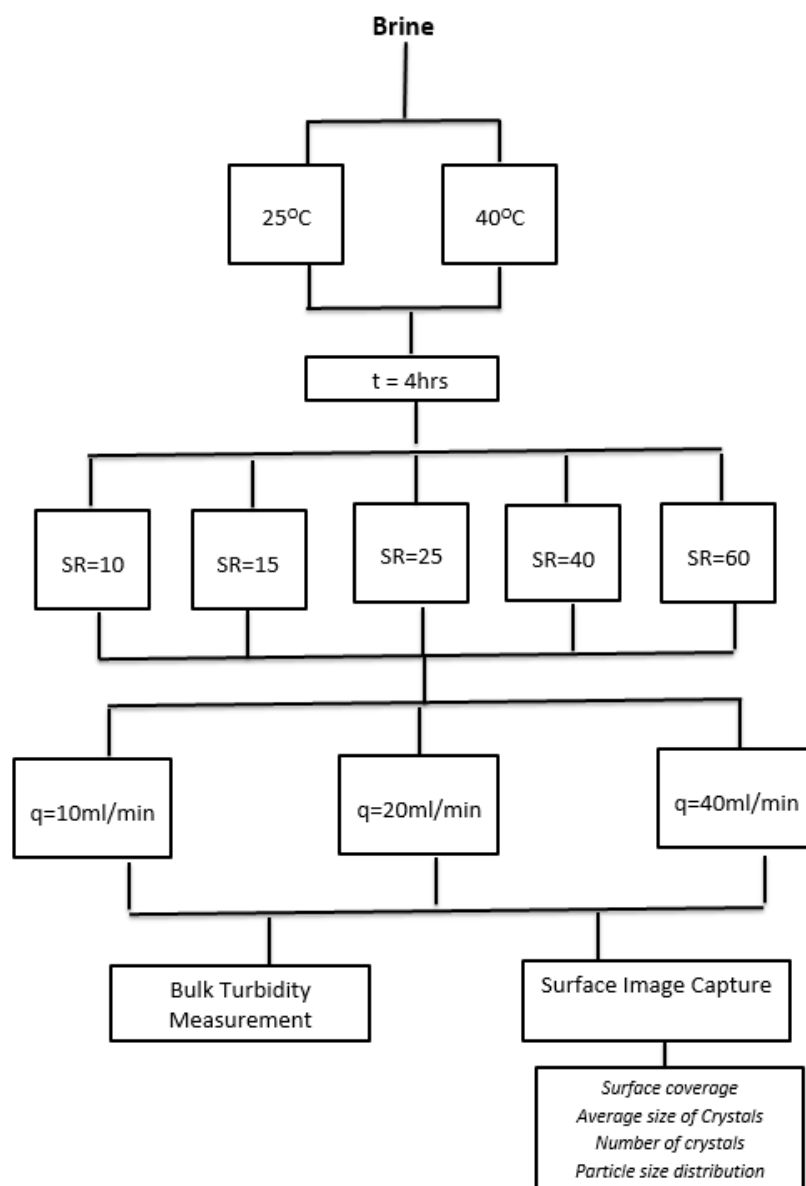
Figure 4-9: Overview of the parameters for the kinetic study

4.4.1 Dynamic Study

The dynamic condition of changing between SR values in a single flow was considered by varying between different SR values while scale is being formed without altering other conditions of the tests. This is to stimulate conditions in the field where SR and inhibitor concentrations may change.

4.4.2 Scale inhibition study

The effect of different saturation ratio on inhibitors injection on the bulk and surface kinetics was assessed using the commercially available Polyphosphinocarboxylic acid (PPCA).

Turbidity measurements and image capture were recorded for all experiments at 5 minutes interval for the duration of each test. From the images, the surface coverage, number and size of the objects are determined leading to the evaluation regarding crystallization process. The surface coverage of scale and particle size distributions were also assessed.

4.4.3 Surface kinetic model

The model originally developed by Beaunier *et al* [42] and subsequently modified by Euvrard *et al* [49] was used as a basis to describe the mechanism of crystallisation and determined if the type of nucleation is either progressive or instantaneous. Instantaneous nucleation describes the situation when, in the initial stages of crystal formation, nuclei are formed and then grow. The nucleation and growth processes are separated, and no further nucleation occurs when the growth is occurring while progressive nucleation describes the process when nucleation occurs and the crystals grow but new nuclei continue to be formed. The model assumes that diffusion controls the crystallization process, that the number of active nucleation sites for a unit area of the substrate is fixed, and that each nucleation event is independent. Therefore, the probability of nucleation at a certain time depends upon the number of free sites.

For instantaneous nucleation:

$$S_{ext}(t) = -\ln(1 - S(t)) = \frac{MK_1 N_o t}{\rho} \qquad (4.1)$$

For Progressive nucleation:

$$S_{ext}(t) = -\ln(1 - S(t)) = \frac{MK_1 N_o A t^2}{\rho} \qquad (4.2)$$

S_{ext} (t) is the extended surface area, S(t); actual covered surface area, A; nucleation rate, k_1; Lateral growth rate (mol/μm/s), M; molar mass of $CaCO_3$(100g/mol), ρ; density of the crystals (ρ =2.71 X 10^{-12}g/μm^3 for calcite), No; number of active nucleation sites (equivalent to detected number of crystals).

Instantaneous nucleation occurs when S_{ext} (t) is proportional to time, whereas progressive nucleation takes place when S_{ext} (t) is proportional to time squared (t^2).

4.5 Surface Analysis

The objective here is to evaluate the surface deposits formed at different SR and temperature. The samples were removed from the flow cell at the end of the test and analysed using the SEM and XRD techniques. XRD was performed to assess the type of polymorphs formed in the rig at different temperature while high magnification SEM was used to assess the morphology of the crystals formed. The surface deposit analysis steps are as shown in Figure 4-10.
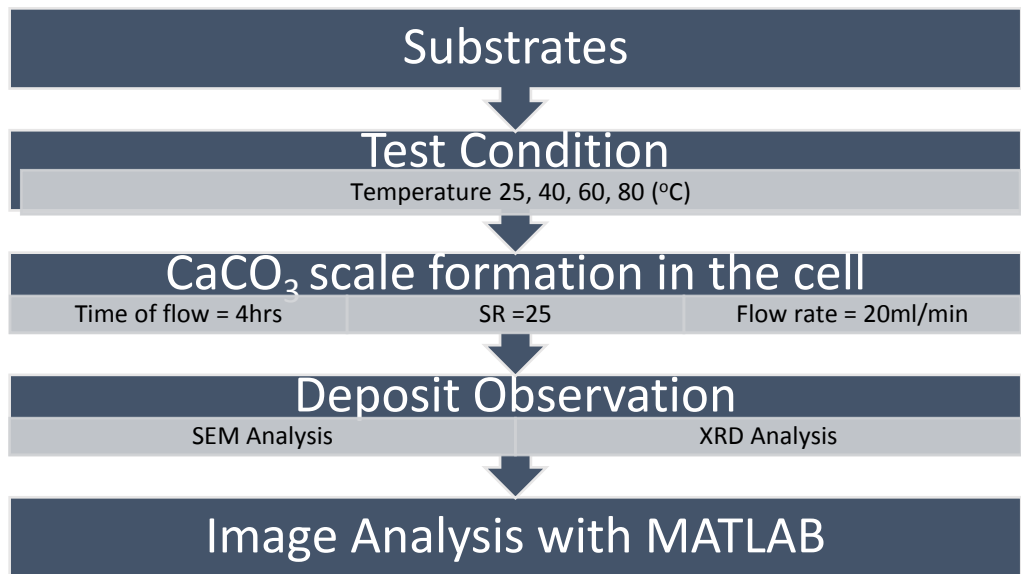
Figure 4-10: Surface analysis steps

Chapter 5 Commissioning of scale-rig

5.1 Once-through flow visualization rig

In previous studies to follow combined bulk precipitation and surface deposition processes, closed or recirculating systems were used [23]. The saturation ratio decreases with time as a result of reduction in ionic species and it is difficult to have a full understanding of the scaling process. Linking the amount of scale to the saturation ratio is impossible because there is reduction in the saturation ratio as time passes. For this study, a once-through *in-situ visualization* flow rig system was built to address this (Figure 5-1). It allows for longer experimental times of assessment as the driving force of scale formation is maintained constant throughout the duration of test.

The digital imaging system allows for the surface scale build up to be followed *in-situ* and recorded in real-time. Turbidity in real time is measured by the turbidity probe incorporated into the *in-situ* cell via a second window made up of quarts glass. The probe has a great precision for a range of turbidity between 0 and 400 FTU (Formazin Turbidity Unit) with heat resistant sensor which can be used for temperature up to 140°C. This allows for brines of different saturation ratio to be used. The thermostatic bath can regulate temperature between the range of $5^{o}C$ – $90^{o}C$. The digital reglo peristaltic pump can be adjusted to vary and control the flow rates. The *in-situ* cell can also be used for electrochemical measurement. In this case, working and reference electrodes can be inserted in the holes on the first part while the window/counter electrode can be inserted in the third part. The electrodes can all be connected to a potentiostat.
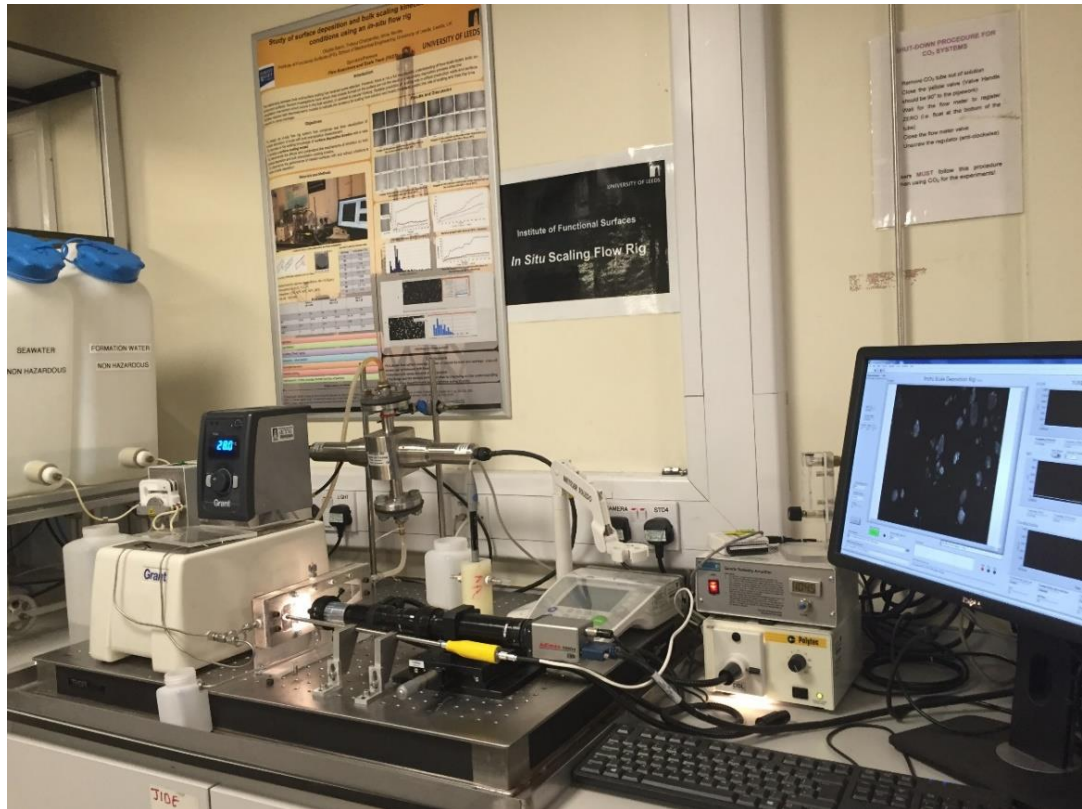
Figure 5-1: Once-through visualization rig for surface and bulk scaling

The procedure for image capture includes a real-time coverage of scale build up process in the *in-situ* cell. The program interface has been synchronised with the turbidity plot that indicates the amount of particles in the bulk solution while scale formation takes place on the surface.

5.2   Scale build–up in flow rig

Initial tests were carried out in order to evaluate the performance of the flow rig. Scale formation on surfaces are followed in real-time and the images presented in Figure 5-2 show real-time surface scale build up for SR = 45 recorded every 15 minutes at T =40°C using a flow rate of 20 ml/min. From the images captured *in-situ*, the changes in the numbers, sizes and surface coverage of crystals as well as the morphology can be observed.
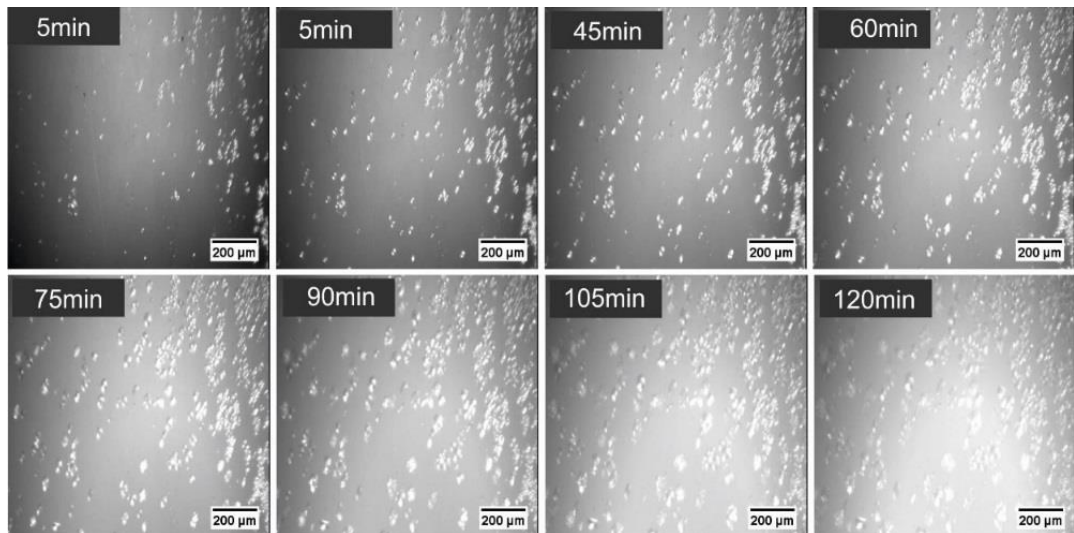
Figure 5-2: Images of the calcium carbonate scale deposited on the surface with SR=45 at 40⁰C

The capability of the flow rig to visualize scale formation in real-time is used to study and improve the understanding of the mechanisms and kinetics of surface scale formation in flowing system at constant saturation ratio.

5.3   Processing and analysis

The image analysis protocol allows quantitative assessment of surface scale to be performed. Figure 5-3 and Figure 5-4 show the suitability and adaptation of the image analysis procedures to process the *in-situ* images of surface scaling captured from the rig at different experimental conditions.
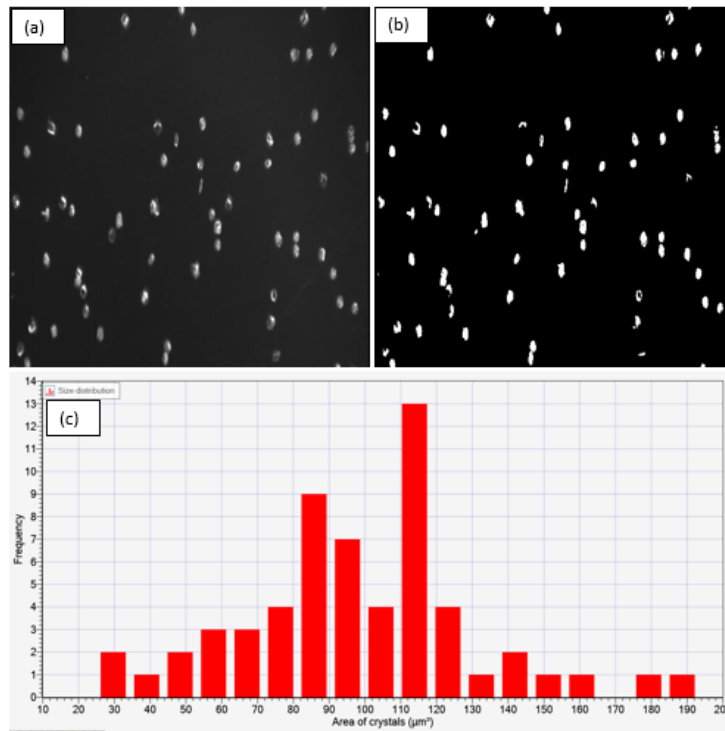
Figure 5-3: Image analysis (a): original image (b): processed image (c): particle size distribution
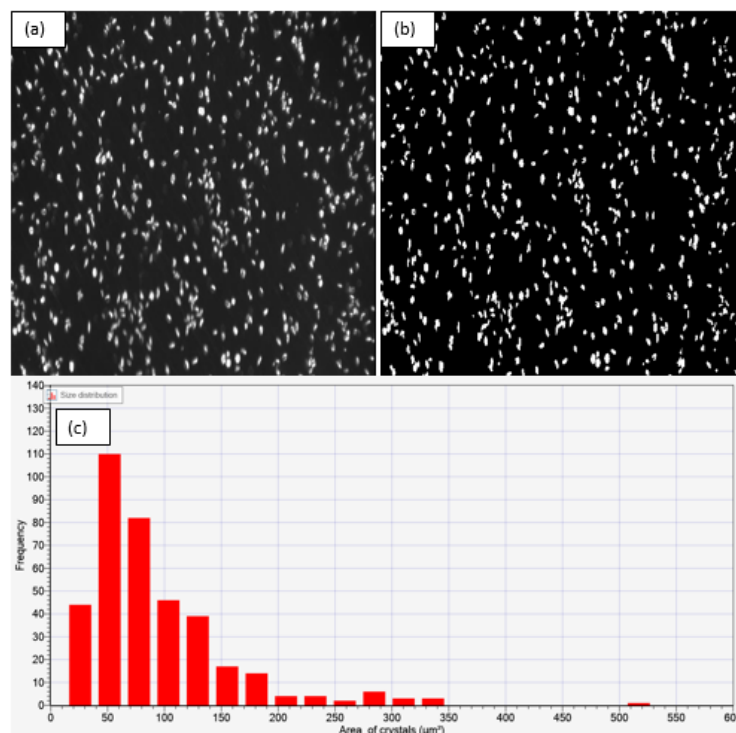
Figure 5-4: Image analysis (a): Original Image (b): Processed image (c): Particle size distribution

The procedure of analysis was used to determine the numbers, sizes, surface coverage and particle size distribution for the images obtained from the tests. The surface coverage gives global information regarding the deposition on the surface. However, it does not permit the nucleation and the growth processes to be differentiated. Therefore, in order to have a better understanding of the whole deposition process, the number of crystals/particles and average sizes of crystals on the surface were assessed. By detecting the number of objects as well as average sizes in the image as a function of time, information regarding the mechanisms and kinetics of nucleation and growth of crystals were collected. The particle size distribution charts shows the evolution of the crystals population with time. Repeatability tests were carried out and presented in the following sections.

5.3.1 Repeatability tests and analysis for surface scale formation

Initial tests were performed to assess the accuracy and repeatability of the procedure as well as the suitability of the analysis procedure. Brine with SR of 45 at 25°C was run through the system at 20ml/min for 4hrs. Polished stainless steel sample with roughness of 0.01µm was used. The process was repeated three times for three different samples (I, II, III) using the same surface conditions. Images were recorded at 5minutes interval and analysed to determine the surface coverage, average sizes and number of crystals with time. Preliminary results show that experimental procedure and analysis are repeatable Figure 5-5 shows the number of crystals, average sizes and surface coverage with time repeated three times (I, II, III) for SR of 45 using the *in-situ* flow rig and analysis protocols.
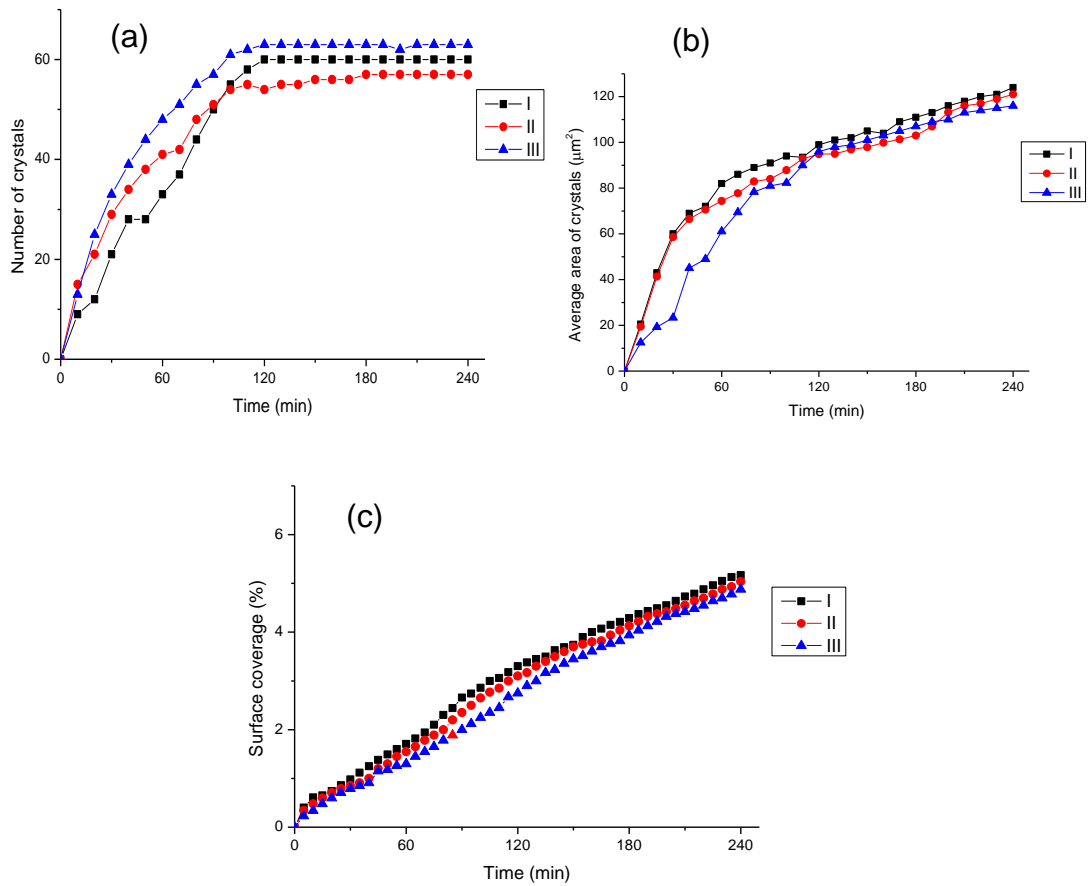
Figure 5-5: Repeatability test for (a): number of crystals detected (b): average size and (c): surface coverage at SR = 45, T =25⁰C

The results of the repeatability tests show that the slopes of the number of crystals, surface coverage and average size with time do not vary by more than 0.8%.

5.3.2 Uniformity of scale formation across the sample surface

Tests were carried out to verify the uniformity of scale formed across samples in the *in-situ* flow rig. 4 samples (A, B, C, D) with the same surface finish (surface roughness= 0.01µm) were subjected to similar test conditions; T=25°C, flow rate = 20ml/min using the $CaCO_3$ brine of SR =45. Each sample was marked at different locations 1,2,3,4 respectively across the surface (Figure 5-6). The camera was focused around the marked location for each sample during individual test.
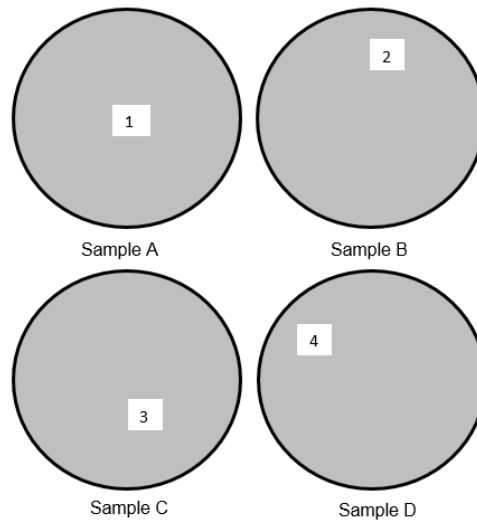
Figure 5-6: Different locations for four samples tested for scale uniformity

The brine was run through the cell and the number of crystals formed on each surface at different points was analysed. Result as presented in Figure 5-7 shows a similar trend in terms of kinetics and number of crystals across the sample locations.
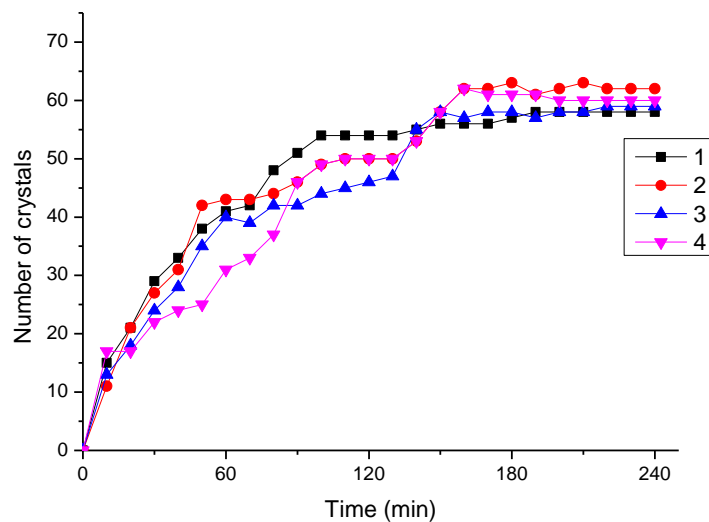
Figure 5-7: Different locations test for 4 samples

A SEM of the final image was taken to detect the scale coverage on a wider surface area and the result (Figure 5-8) shows the uniformity of crystals formed across the surface of a given sample.
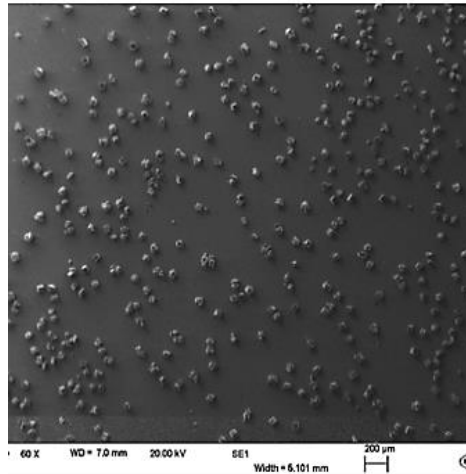
Figure 5-8: SEM image of sample showing uniformity of surface scale

5.4   Summary

A suitable methodology to improve the understanding of the precipitation/deposition system in order to build an accurate surface deposition kinetic model has been developed. Preliminary tests have shown the workability and repeatability of the scale formation process and the image analysis program. It allows for control of various scaling parameters such as the saturation ratio, temperature, flow velocity and inhibitor injection. The rig is used to measure turbidity in the bulk and real-time visualization of scale build up at different conditions. By detecting the number of objects as well as average sizes in the image as a function of time, information regarding the mechanisms and kinetics of nucleation, growth of crystals can be collected. This is used to understand the kinetics and mechanisms of surface scaling and can be useful in predicting and evaluating surface scale especially on topside facilities. The facilities do not discriminate the type of scale and substrates that can be tested, however, for the purpose of this study, the mechanisms and kinetics of $CaCO_3$ scale on polished austenitic stainless steel are considered.

Chapter 6 Bulk precipitation and surface scaling: Influence of saturation ratio

6.1   Introduction

Most studies on scale kinetics and existing scaling indices are based on extensive experimentation of bulk scaling parameters [170]. Nevertheless the surface scaling process has been shown to be different [175, 176]. Eroini [23] in her study showed a non-linear relationship between the rate constants for bulk precipitation and surface deposition. The surface can have a significant effect on the level of scale formation, therefore the solution and the surface as well as other factors must all be considered in holistic manner. This chapter presents the results of bulk and surface scaling tests at different SR values for a $CaCO_3$ brine. As stated earlier, the new *in-situ* visualization rig the thermodynamic driving force to be kept constant through the experiments. The map of the chapter is presented in Figure 6-1.
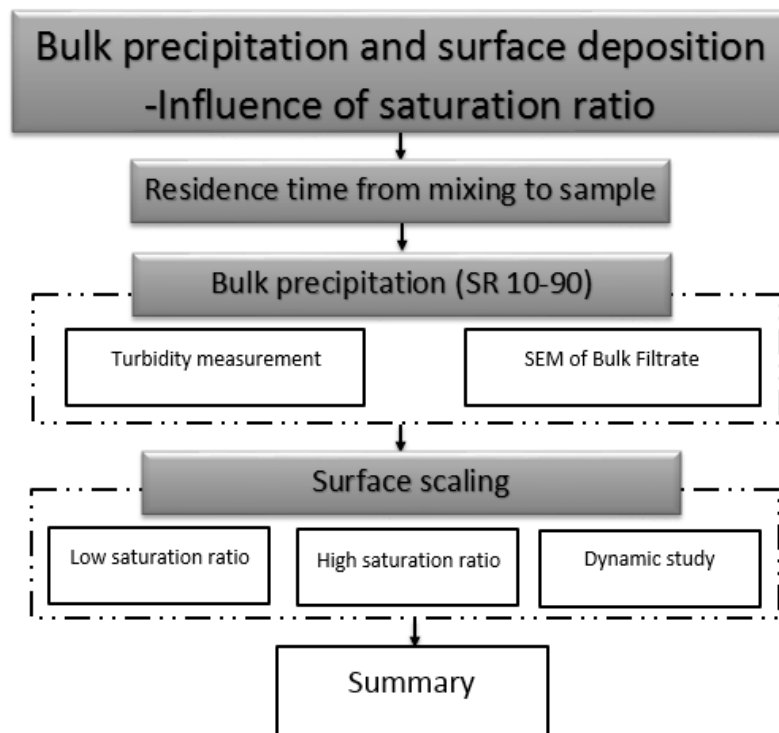
Figure 6-1: Map of Chapter Six

6.2 Residence time from mixing to sample surface

The flow cell incorporates turbidity measurement and surface image visualization of the sample very close to the point of mixing of the brine. This allows for a closer and better comparative study and analysis between the bulk and surface mechanisms. The residence time from mixing point of brine to sample surface in the flow cell as shown in Figure 6-2 was measured for the three flow rates used and are recorded in Table 6-1.
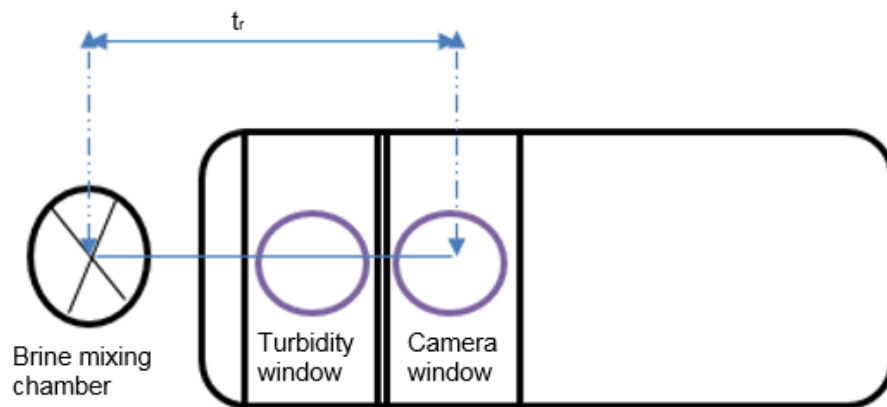
Figure 6-2: Mixing point to sample for bulk and surface measurement

Table 6-1: Residence time from mixing to sample surface

Flow rate (ml/min)	Residence time (t_r) s
10	~5.0
20	~4.0
40	~3.2

6.3 Bulk precipitation

The turbidity probe incorporates into the cell allows bulk turbidity to be followed and recorded automatically with surface visualization. For this test, simple $CaCO_3$ brines of five SR (10, 15, 25, 70 and 90) were tested, quantification of the degree of saturation was performed by calculation of the SR using the multiscale software. The turbidity values were taken at intervals of 5 minutes with the first turbidity measurement recorded immediately after the mixing point at zero minutes.

6.3.1 Turbidity measurement for SR =10, 15, 25, 70 and 90

$CaCO_3$ brine with SR values of 10, 15 and 25 were tested; the corresponding brine solutions containing Ca^{2+} (FW) and CO_3^{2-} (SW) were prepared at 25°C. The brines were pumped with the two channels of the peristaltic pump at the same flow rates of 20ml/min. Mixing of brines takes place at the mixing point just before the inlet of the cell. Turbidity was monitored for 12 hours while fresh brine flows through the cell keeping the ionic concentrations constant and as such the SR is maintained at constant values for each test. From the results recorded in Figure 6-3, the turbidity values of SR 10, 15 and 25 remained at zero for the 12 hours test indicating that there are no particles in the bulk solution for the entire duration of the test.
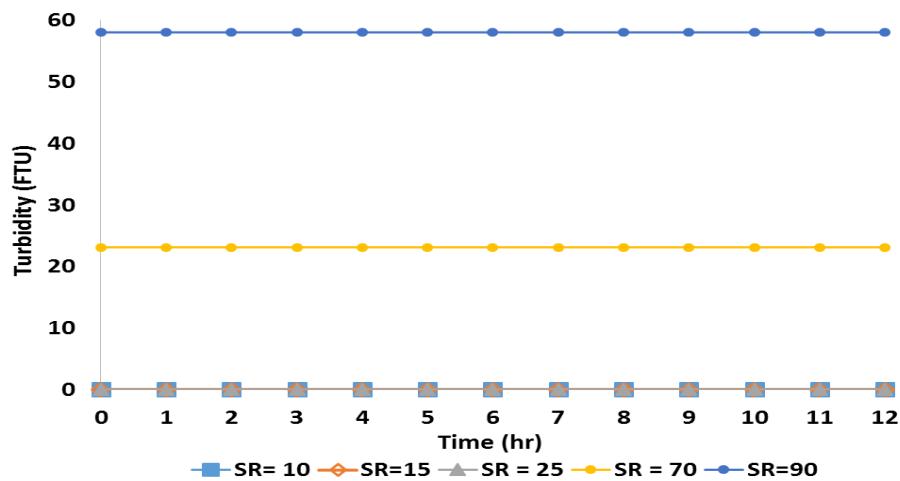
Figure 6-3: Turbidity with time for $CaCO_3$ at T = 25°C, q = 20ml/min

The residence time (~4.0 sec) of the fluids from mixing to sample is shorter than the induction time for bulk precipitation to occur and therefore no crystals were precipitated in the bulk solutions for the entire test even as saturation ratio was kept constant with continuous flow of fresh brine [26, 36]. However, under the same conditions for $CaCO_3$ brine at higher SR values of 70 and 90 the turbidity values are 23.1 and 58.8 FTU respectively. Here, bulk scaling commences immediately as the two brines are mixed due to the high supersaturation i.e. high thermodynamic driving force. In these cases, crystals

94

precipitated from the bulk solution as the induction time is shorter than the residence time (~4.0 sec) from mixing point of fluid to the sample surface.

The turbidity graph at the probe which is a constant distance from the mixing point is in sharp contrast to the typical turbidity curve [28] for a closed system where SR decreases as a result of reduction in ionic species as scale deposition takes place.

6.3.2 Bulk filtrate

Further investigation of the bulk solution was carried out to verify the turbidity measurements in both cases. Each brine solution was collected and vacuum filtered on a 0.2µm membrane after the mixing point and observed with scanning electron microscope (SEM). The SEM images of the bulk filtrate samples for SR values of 10, 15, 25 and 70 are presented in Figure 6-4. There are no scale crystals formed on the membrane for SR values of 10, 15 and 25 when observed with SEM. However crystals readily formed for SR value of 70 as a result of the high SR and very short induction time.
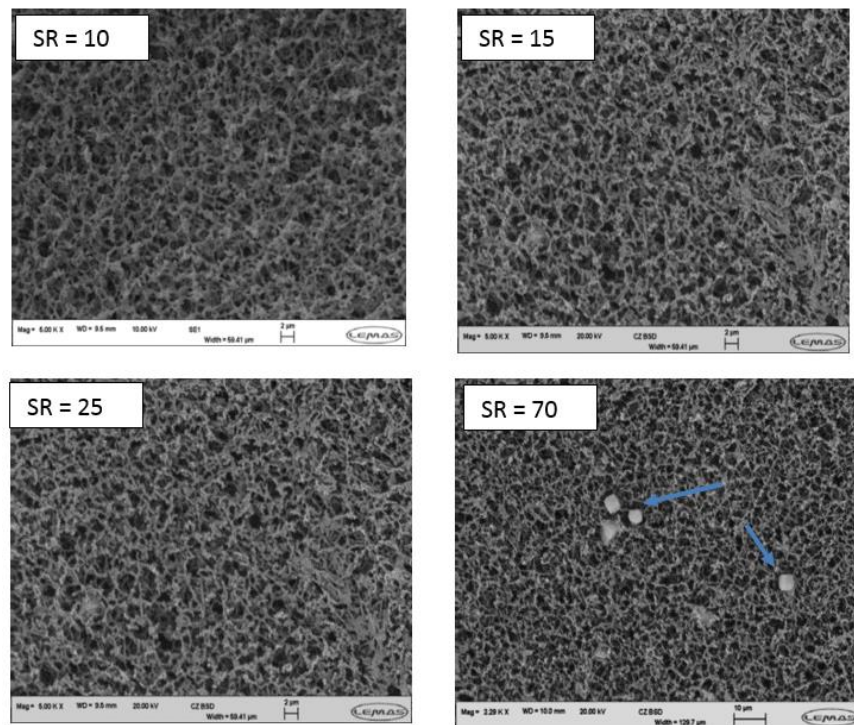
Figure 6-4: Images of the filtrate as observed with SEM

Thus, for low SR values of 10, 15 and 25 tested in the flow rig, no precipitation occurs in the bulk solution while there is precipitation in the bulk for SR values of 70 and 90 considered.

6.4 Surface scaling

The high performance digital camera connected to the computer was used to follow the surface scale build up *in-situ* and in real-time for the tests. The images were captured automatically at 5 minutes intervals at the same time when turbidity measurements were being recorded by the turbidity probe. Stainless steel surfaces were used with surface roughness of 0.01µm. As observed from the turbidity measurements (Figure 6-3), the three brines with saturation ratios of 10, 15, 25 have no precipitated crystals in the bulk solution. However, in all cases surface crystallization was observed. The images captured at different time intervals show crystals being formed on the surface. Figure 6-5, Figure 6-6 and Figure 6-7 show the *in-situ* images for SR 10, 15 and 25 obtained at the beginning of the experiment, time t = 0, prior to mixing of the brine as well as images at time, t = 12 hrs.
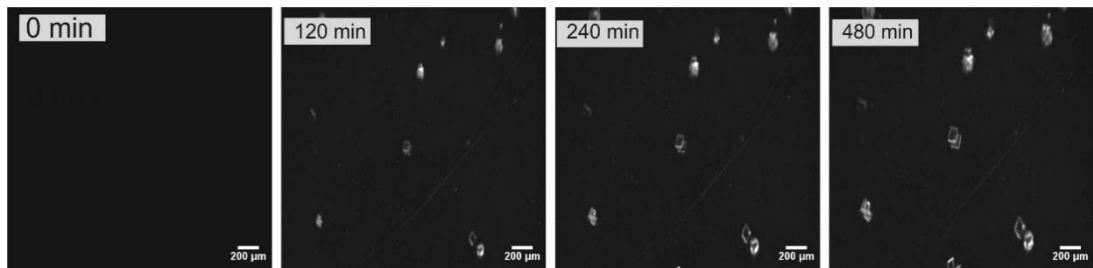
Figure 6-5. Surface scale deposition for SR=10
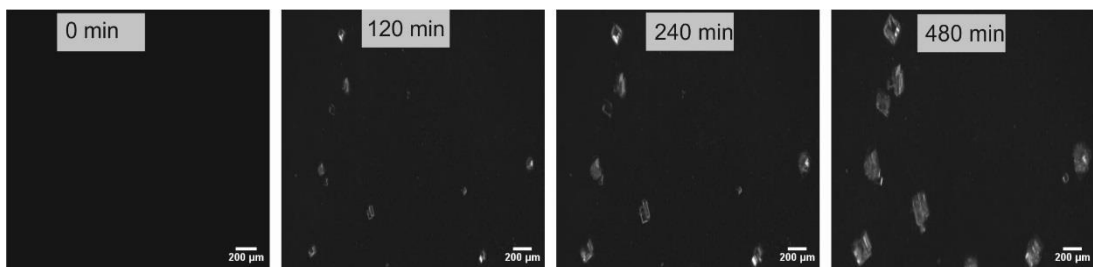
Figure 6-6: Surface scale deposition for SR=15
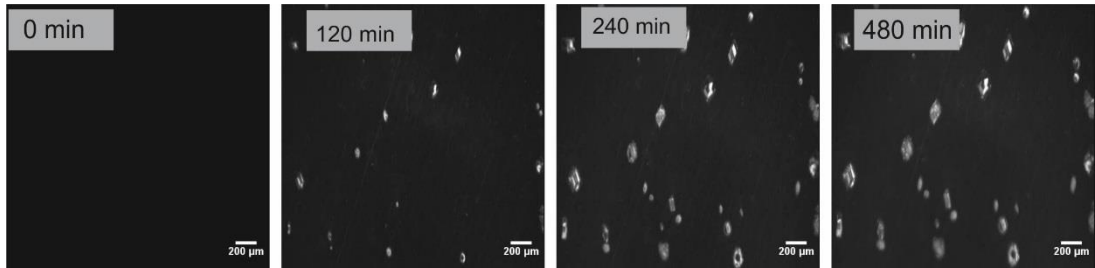
Figure 6-7: Surface scale deposition for SR=25

The samples were removed from the cell at the end of the deposition tests and further viewed with SEM. The SEM images (Figure 6-8) further confirmed crystallization on the surfaces while there are no pre-precipitated crystals in the bulk solution. This suggested a surface crystallization mechanism dominates which is further discussed in chapter 8.
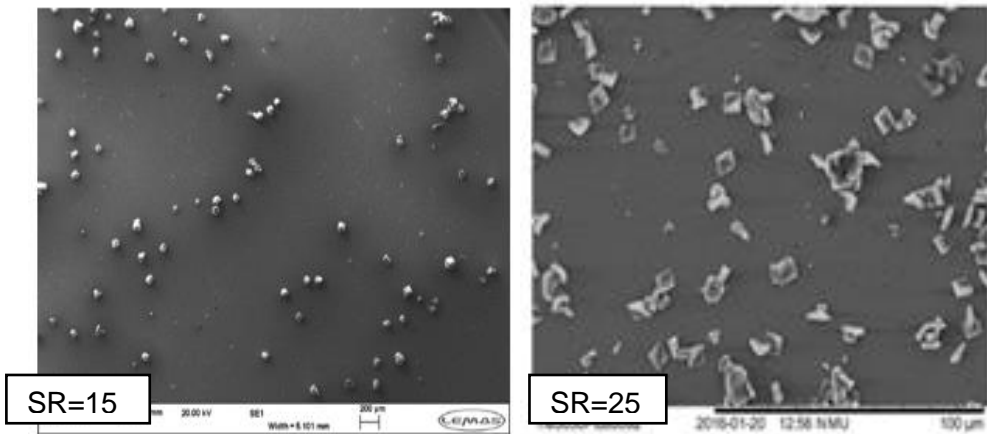
Figure 6-8: SEM images of surface scale with no bulk precipitation at different saturation ratio

This also agrees with investigations such as those carried out by Morizot and Neville [172] and Cheong *et al* [80], stating that crystals formed on the surface can be as a result of a crystallization process rather than a secondary deposition process after the precipitation mechanism which occurred in the bulk.

6.4.1   Surface scaling at SR =10, 15, 25.

With zero turbidity indicating no precipitated crystals in the bulk solution, the corresponding surface images were processed using image analysis procedures. Figure 6-9 shows the number of crystals while Figure 6-10 shows

the average size of crystals as a function of time indicating nucleation and growth of crystals on the surface. The increase in average size shows that there is continuous growth of the crystals as fresh brine flows on the sample inserted into the cell.
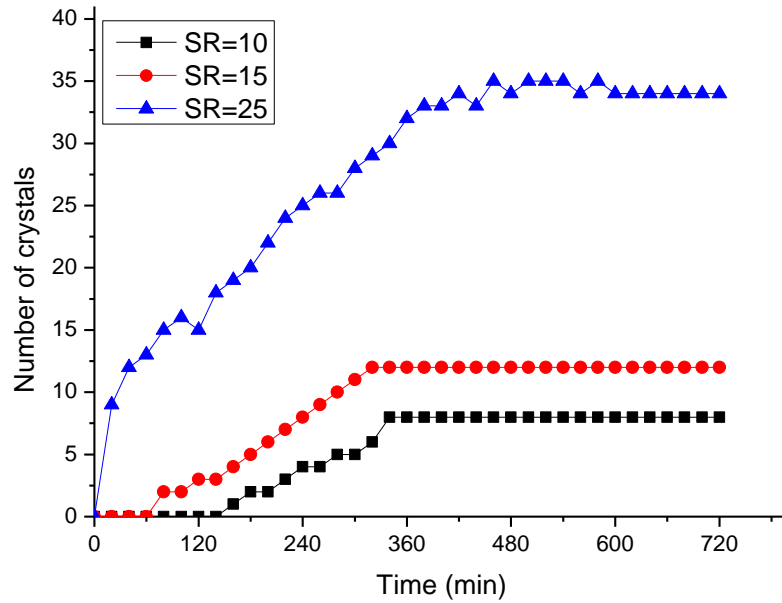
Figure 6-9: Number of crystals at T = 25℃, t =24hrs and 20ml/min
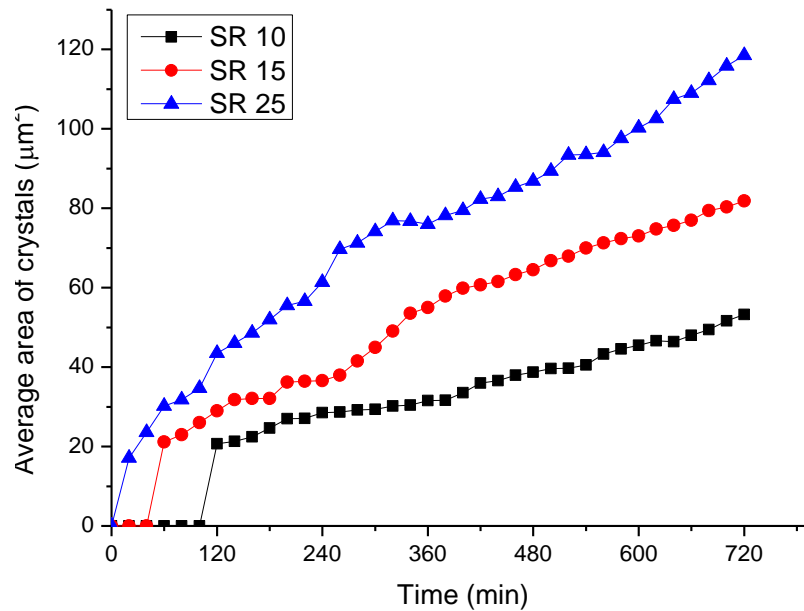
Figure 6-10: Average size crystals at T =25ºC, t = 24hrs and 20ml/min

Surface fouling at these low SR values is driven by crystallisation taking place at the solid/liquid interface rather than the adhesion of crystals that have precipitated in the bulk solution. The supersaturated solution was responsible for forming crystals directly on the surface via true surface heterogeneous nucleation [177].

6.5   Effects of SR on CaCO$_3$ surface scale formation

The scaling tendency for a given solution can be quantified by its saturation ratio (SR) which is the excess of the actual concentration of dissolved ions over the solubility product. It has been mentioned that surface deposition mechanisms are little understood and knowledge in terms of kinetics is sparse compared to bulk precipitation processes [20, 30]. The results of the surface images analysed are presented in the following sections.

6.5.1   Scaling at low saturation ratio

Results of experiments at 20ml/min and 25°C for CaCO$_3$ brine with five different SR values at 10, 15, 25 45 and 60 are presented. As observed from the turbidity measurements in Figure 6-3, in all cases of SR (10, 15, 25 45 and 60), the induction time for bulk precipitation is longer than the residence time from the mixing point to sample surface and as such the five brines had no precipitated crystals in the bulk. The solution was clear all through and the turbidity reading remained at zero for the entire test.

The surface *in-situ* and real time images in Figure 6-11 show progression in the formation of surface crystals while precipitation in the bulk solution did not take place.
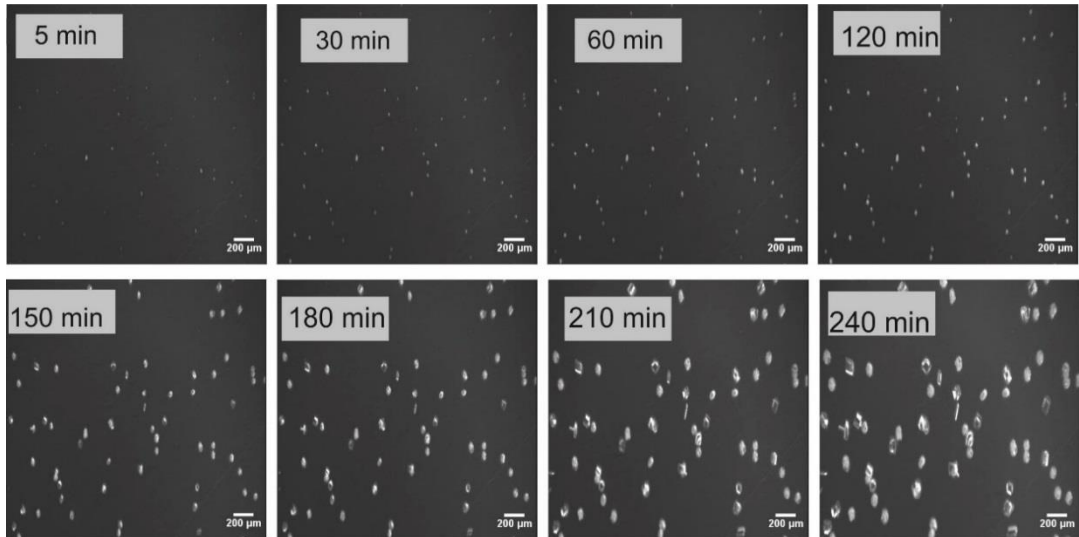
Figure 6-11: *In-situ* surface images for SR = 45, T = 25℃

6.5.1.1 Number of crystals

Figure 6-12 shows the number of crystals with time for SR 10, 15, 25, 45 and 60. Crystals are nucleated on the surface and as expected the numbers vary according to the saturation ratio with surface induction periods being observed for SR values of 10, 15 and 25. Owing to the ionic concentrations, SR value of 10 has an induction period of about 110 minutes and SR value of 15 has an induction period of 50 minutes while it takes about 20 minutes for SR value of 25 before the appearance of the first crystals. Surface nucleation for SR values of 45 and 60 occur immediately after mixing with no induction time observed before the first images were recorded. As expected, higher numbers of crystals are observed as SR increases.

However, in all cases, it is observed that nucleation did not proceed for the entire duration of the experiment as the number of crystals for each brine reaches a maximum value. At this point, even though there is fresh brine flowing through the samples, the number of crystals remains constant as no more new crystals are formed but only growth or agglomeration of existing crystals indicating that a scaling surface consists of a finite number of active nucleation sites [42].
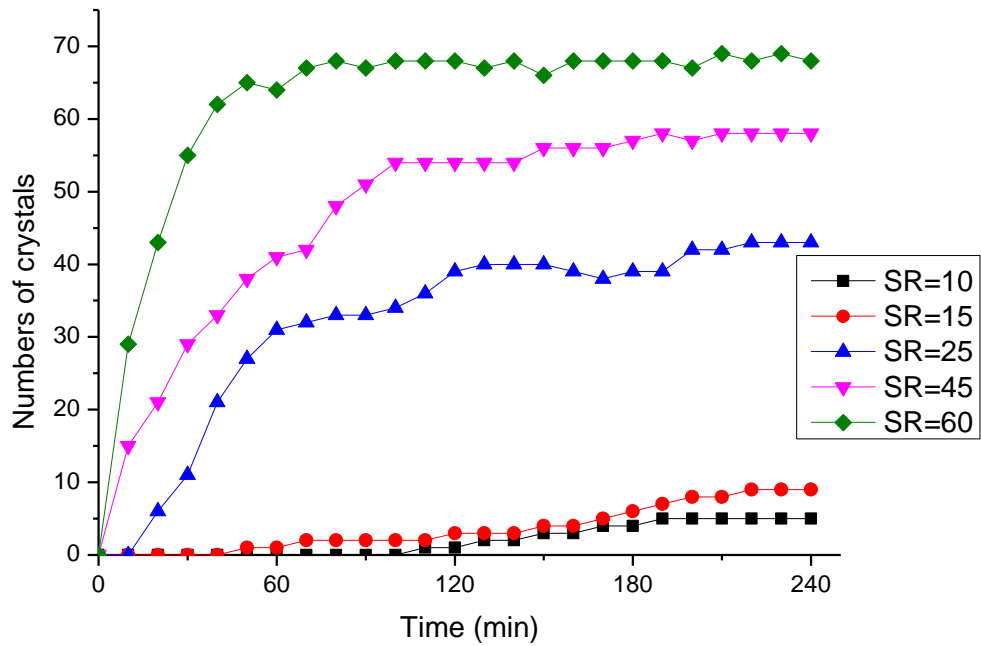
Figure 6-12: Number of crystals as a function of time for low SR at T = 25℃

6.5.1.2   Average size of crystals

The assessment and quantification of the average size with time is presented in Figure 6-13. The average sizes vary with saturation ratio but there is a continuous increase in crystal size for all the SR values which are maintained at constant values while scale is being formed. Consequently, the Ca^{2+} and CO_3^{2-} ions are replaced as much as they are consumed on the surface as fresh brines flow past the samples. The early stages of the curve is non- linear due to the period of induction for the lower SR as well as the dominance of the crystal nucleation process in the early stages. In most cases, as can be observed in Figure 6-12 and Figure 6-13, nucleation and growth of the crystals are taking place while in the latter stages, the growth progresses linearly as no more new crystals are formed. This suggests that nucleation of crystals on the surface of the samples can either be instantaneous or progressive.
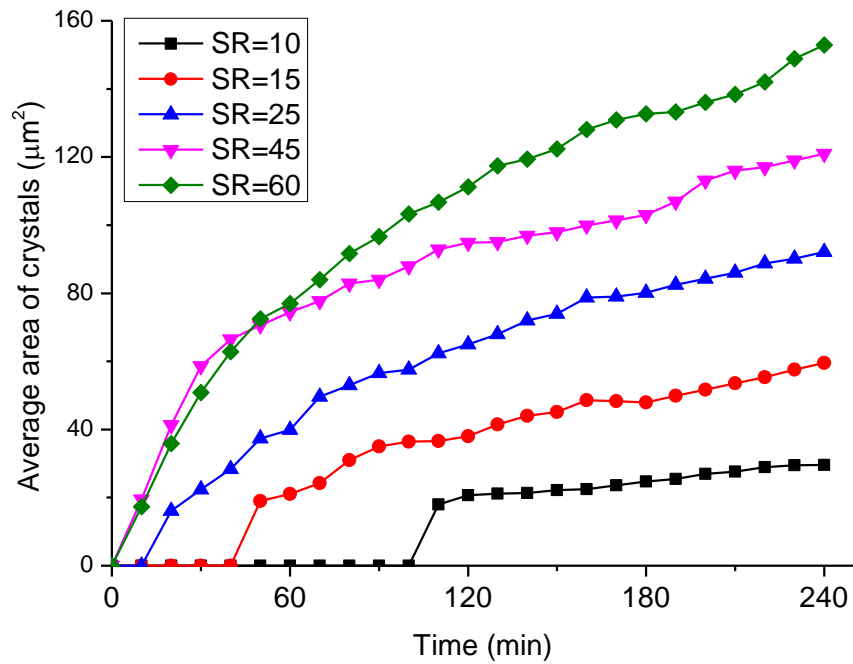
Figure 6-13: Average size of crystals as a function of time for low SR, T = 25°C

6.5.1.3 Surface coverage of crystals for SR = 10, 15, 25, 45 and 60

From Figure 6-14, it is shown that the brine solutions all have different scaling tendencies in terms of the amount of scale formed. The percentage scale coverage on the stainless steel surface is observed to be greater for high saturation ratio than for low saturation ratio as expected. The percentage surface coverage values for SR = 10, 15, 25, 45, 60 at 25°C and 20ml/min for 4hrs tests are approximately 0.9, 1.4, 3.7, 5.1 and 9.0% respectively. The trend of the graph for each brine shows a continuous linear increase once deposition has begun. When compared to the plots obtained for the average size of crystals and number of crystals, the surface coverage plot is more linear especially at the later period of crystallization. The early stages are dominated by surface nucleation while increase in average sizes dominates at the later stages.
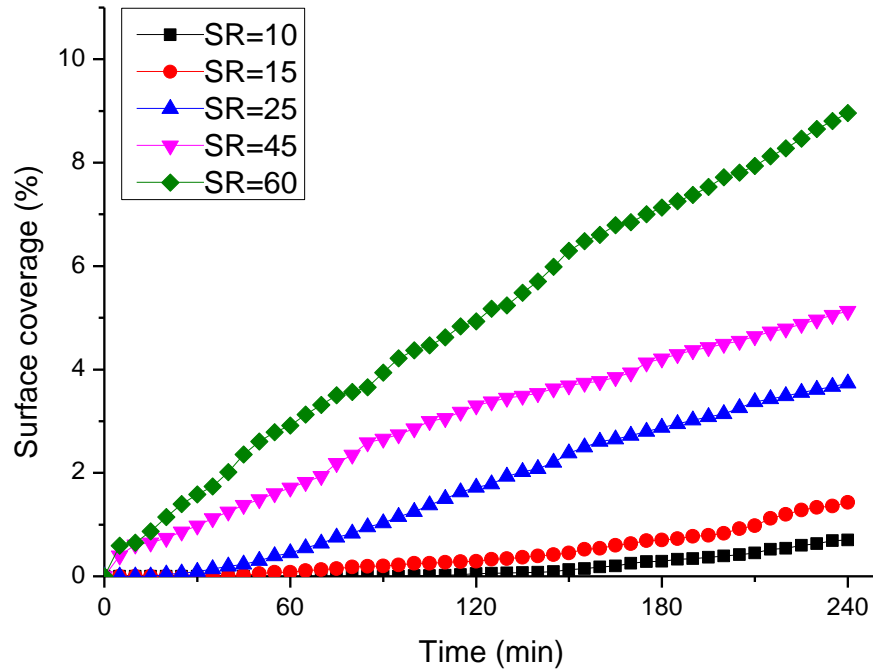
Figure 6-14: Surface coverage of crystals as a function of time for low SR, T = 25℃.

6.5.1.4 Particle size distributions for SR = 60

The particle size distribution generated from the image analysis procedure gives the evolution of crystals size over time. Figure 6-15, Figure 6-16 and Figure 6-17 show the distribution of crystals at 1hr, 2hrs and 4hrs respectively for $CaCO_3$ surface deposition at SR = 60. The average size of crystals increases over time. From 1 hour to 2 hours of experiment, the number of crystals increases from 61 to 69 while their average sizes increase from 39µm² to 106µm² within the same hour. However, the total number of crystals remained the same (n = 69) from 2 hours to the end while the crystals already formed continue to increase in size to an average size of 153 µm².
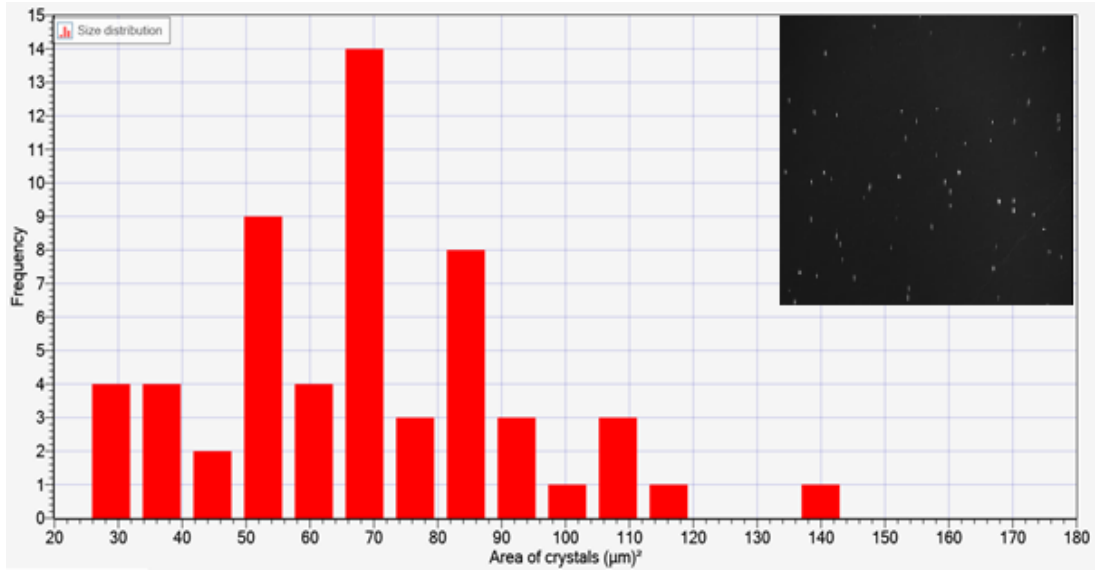
Figure 6-15: Particle size distribution at 1hr for SR = 60 (number of crystals = 62, average size = 77 μm²)
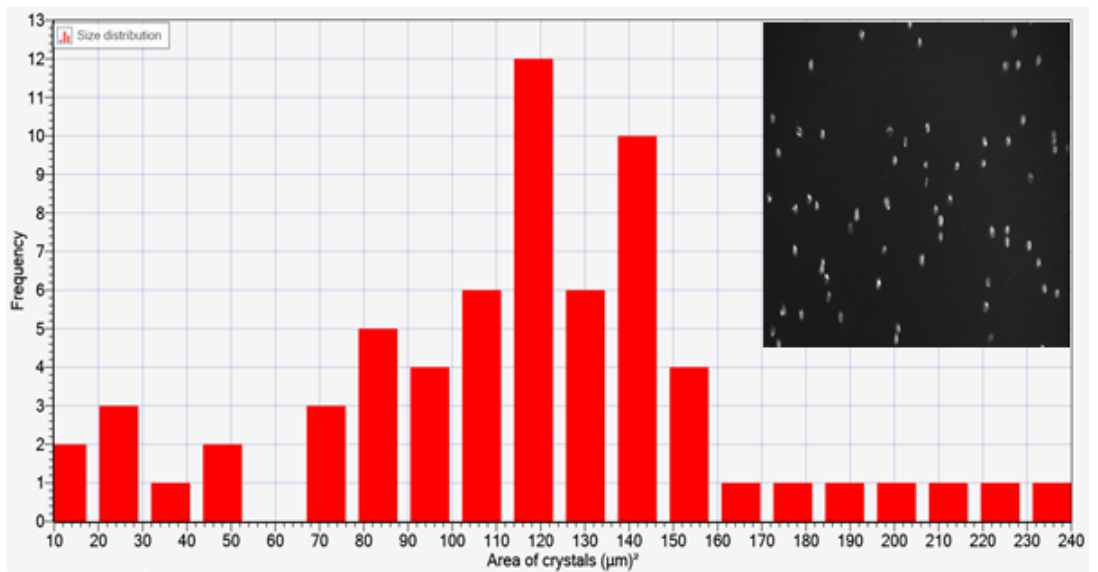
Figure 6-16: Particle size distribution at 2hrs for SR = 60 (number of crystals = 69, average size = 111μm²)
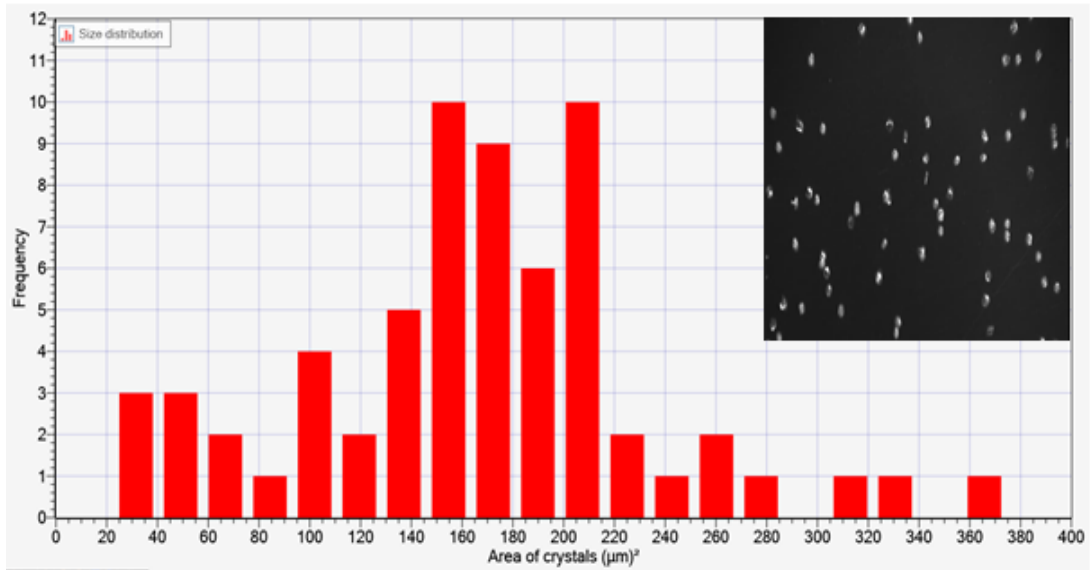
Figure 6-17: Particle size distribution at 4hrs for SR = 60 (number of crystals = 69, average size = 153 μm²)

6.5.2 Scaling at higher saturation ratio, SR values of 70 and 90

Here, results of $CaCO_3$ surface scaling at two SR values of 70 and 90 are presented. Recall from Figure 6-3 that for SR 70 and 90, crystals had already started to precipitate in the bulk solution as the solution reached the sample surface. The induction time for the bulk precipitation for both SR of 70 and 90 is shorter than the residence time from mixing to sample (~4.0 sec). As such, the surface scale formation in this case can be driven by either adhesion of pre-precipitated crystals from the bulk and/or surface crystallisation. The number, average size and surface coverage are presented in the following sections.
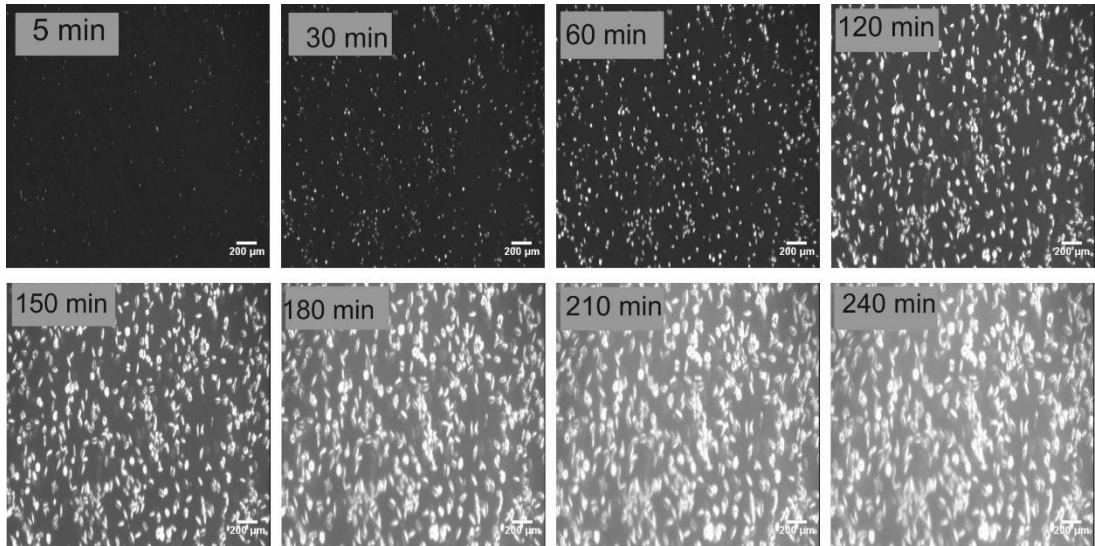
Figure 6-18: Surface scale build up for SR = 90 at 25⁰C

6.5.2.1   Number of crystals at SR = 70 and 90

A spontaneous and rapid increase in the number of crystals was observed at the early stages with no induction period. It is more pronounced at SR 90 as shown in Figure 6-19. This could be attributed to combination of adhesion of pre-precipitated crystals from the bulk and direct surface nucleation. The concepts of homogeneous and heterogeneous nucleation are discussed in chapter 8. The first stage is followed by a second stage where there is steady increase in the number of crystals. This suggests that the growth of already nucleated crystals is becoming increasingly dominant at this stage. The ions would easily facilitate the growth of existing crystals rather than the creation of new crystals which would require higher energy. Also, the number of available active nucleation sites could be reducing. The graph shows that in the later stages, there is reduction in the number of crystals as they get bigger as a consequence of growth. The crystals tend to come together and grow (Figure 6-19). This is in agreement with observations by Beaunier *et al* [42] where the maximum number of crystals at high concentrations of Ca^{2+} is limited by coalescence. For SR value of 90, the agglomeration of crystals and consequently the reduction in numbers is more pronounced due to the higher number of crystals at the early stage of surface scaling.
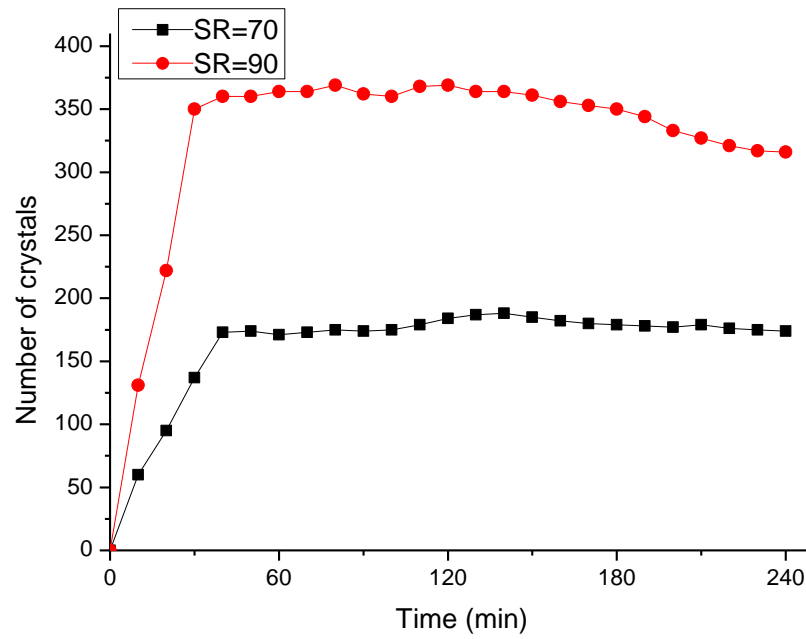
Figure 6-19: Number of crystals as a function of time for high SR brines at T = 25ºC

6.5.2.2 Average size of crystals at SR = 70 and 90

Figure 6-20 shows that the average size of crystals is bigger for SR 70 in comparison to SR 90 owing to the fewer number of crystals.
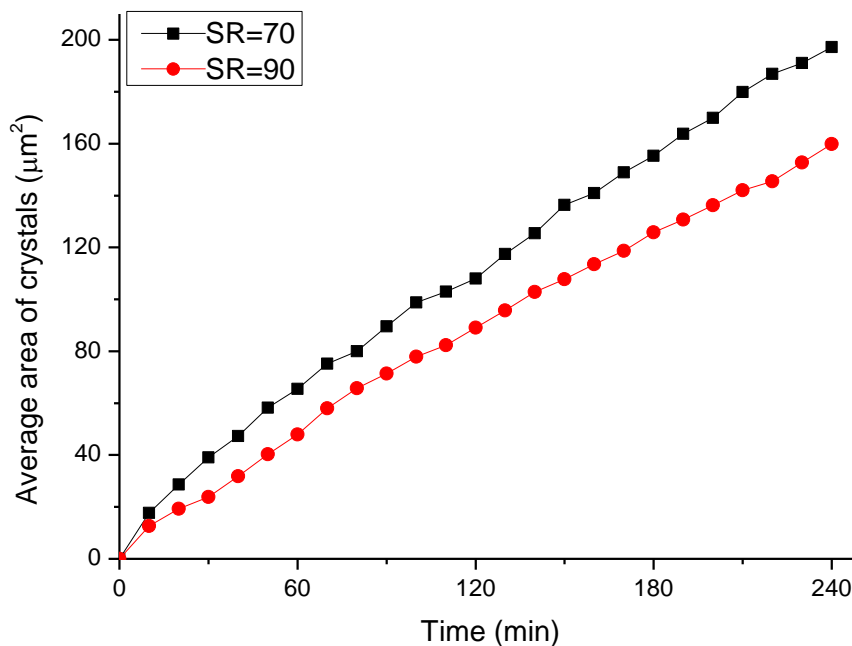
Figure 6-20: Average size of crystals with time for high SR at T = 25°C

At the end of 4hrs CaCO$_3$ brine with SR 70 has an average size of 197 µm²
while the average size reached for SR 90 is 160 µm². However in both cases,
increase in size of crystals takes place and continues linearly through the
experiment.

6.5.2.3 Surface coverage of crystals at SR = 70 and 90

The surface coverage result for SR values of 70 and 90 is presented in Figure
6-21. In contrast to the average size, the total amount of scale deposited in
terms of the surface coverage of the sample is higher for SR value of 90 at
18.9% than for SR value of 70 at 13.5%. Figure 6-21 shows that scale
formation on the surface continues for the entire 4hrs of experiment with the
turbidity at constant values.
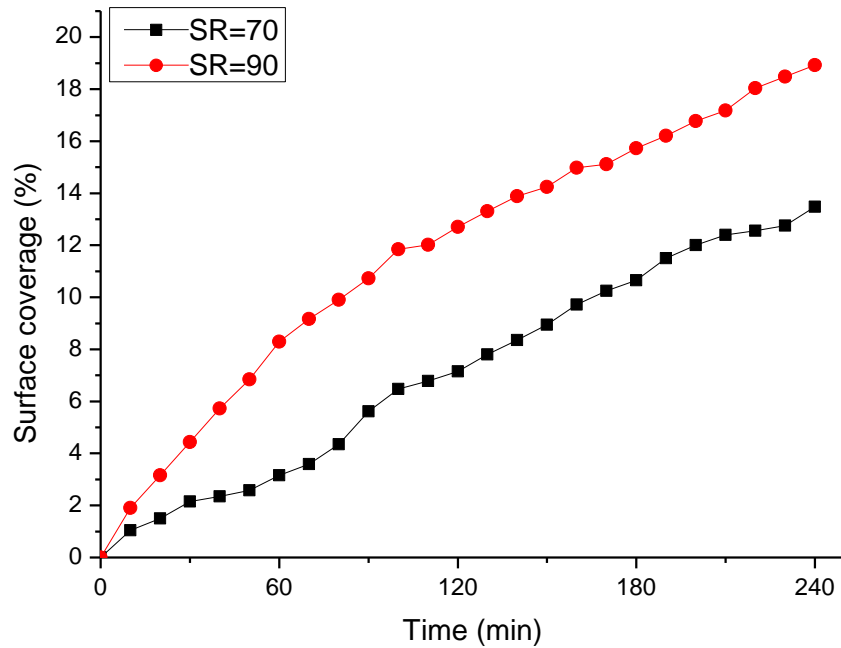
Figure 6-21: Surface coverage of crystals with time for high SR at T = 25ºC

6.5.2.4   Particle size distribution

The particle size distribution graphs, Figure 6-22, Figure 6-23 and Figure 6-24 show the evolution of crystals at 1hr, 2hrs and 4hrs respectively for $CaCO_3$ surface deposition at SR value of 90. At the end of the first hour, there were 365 crystals detected with average size of 25 µm². However, at the end of 2hrs, the number of crystals remain the same at 365, while the crystals already formed continue to increase in size resulting in bigger crystals with an average size of 89µm². At 4hrs, there is clustering of crystals leading to reduction in numbers from 365 to 316 while the average size increases to 160µm².
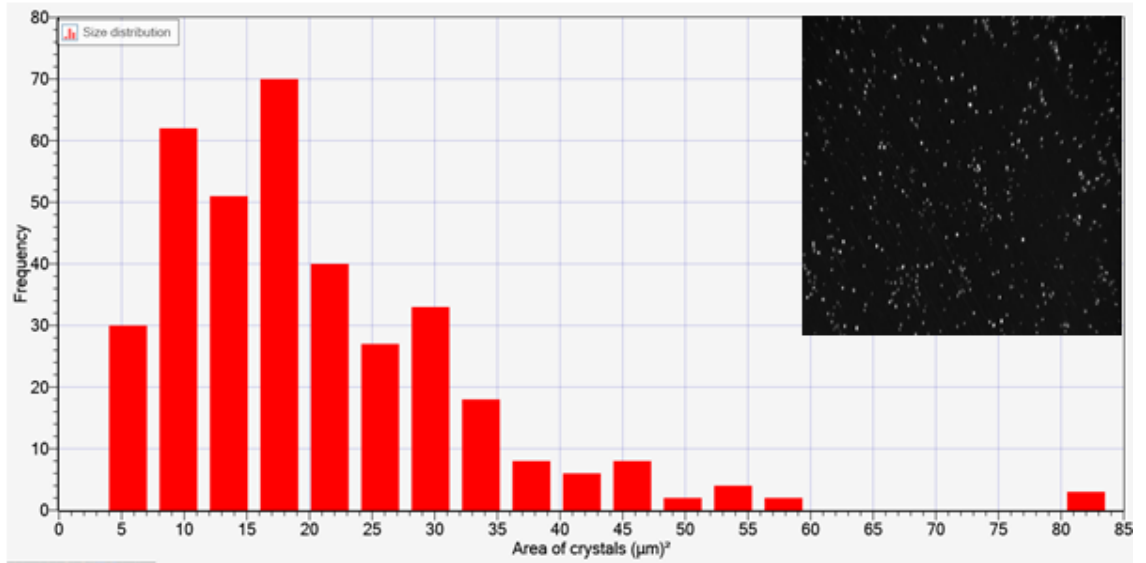
Figure 6-22: Particle size distribution at 1hr for SR 90 (number of crystals = 365, average size = 25µm²)
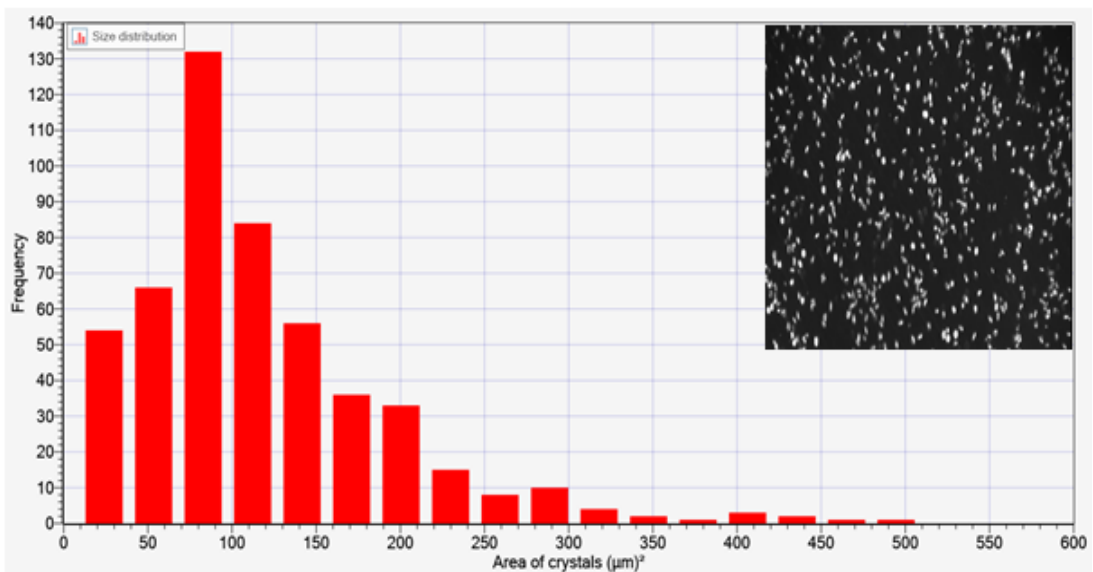
Figure 6-23: Particle size distribution at 2hrs for SR 90 (number of crystals = 365, average size = 89µm²)
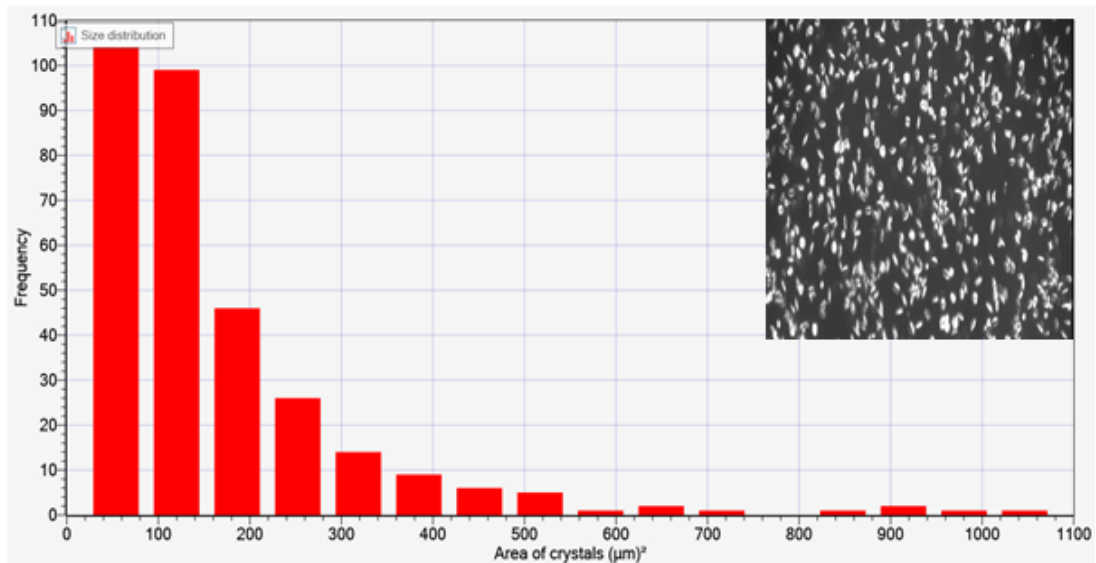
Figure 6-24: Particle size distribution at 4hrs for SR = 90 (number of crystals = 316, average size = 159.86µm²)

6.5.3 Changing between different values of saturation ratio (25-45-70)

The effect of changing SR over time was tested to simulate conditions in oil field where thermodynamic conditions are not constant over time. Figure 6-25. Illustrates 2 possible effects of dynamic change in SR on surface nucleation sites. N_1, N_2 and N_3 are the number of crystals in region 1 2 and 3 with change in SR from 25, 45 and back to 25 respectively after 4hrs.
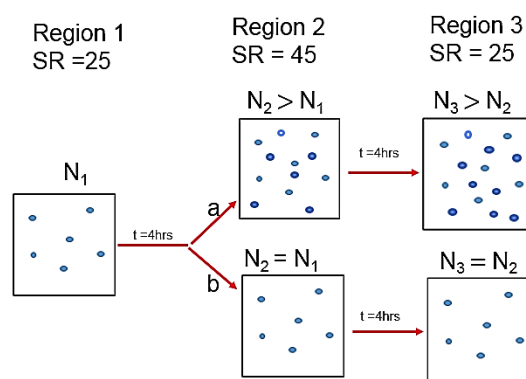
Figure 6-25: Hypothetical diagram of the effect of change in SR on nucleation sites

CaCO$_3$ scale followed *in-situ* for 4 hours with SR 25. The SR was then increased to SR 45 for another 4 hours and later returned to SR 25 for the last 4hrs (25-45-25) in a single test. This was also repeated for SR 25-70- 25. **Figure** 6-26 shows the surface scale build up on a sample where there are changes in the saturation ratio. Surface nucleation stopped after 2hrs while only growth continues at SR 25 for another 2hrs. After 2hrs of no nucleation, more crystals were nucleated and grew on the surface when the saturation ratio was increased to SR = 45 and 70 for the different tests.
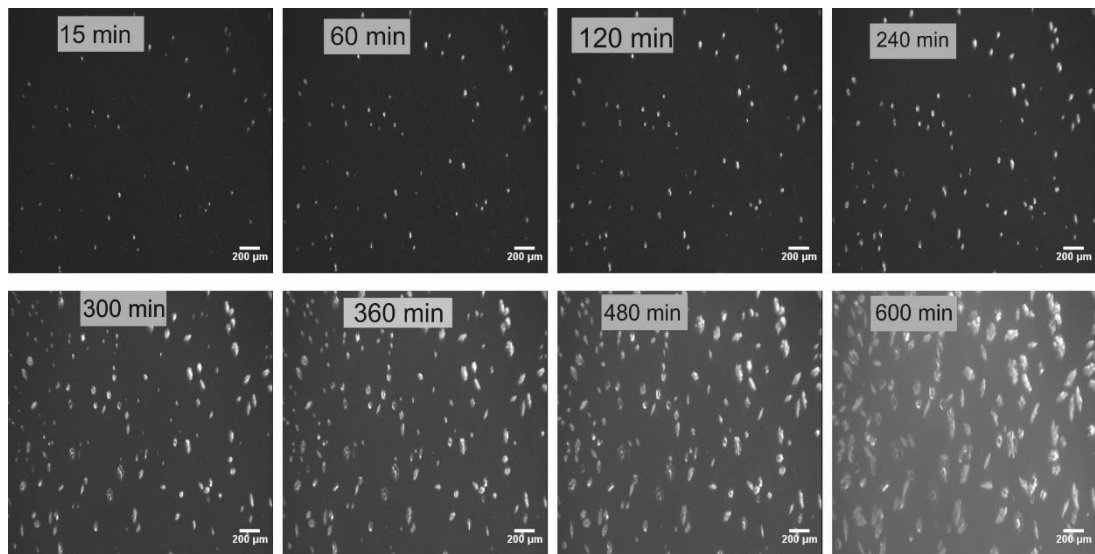
Figure 6-26: Surface scale build up, changing between SR (25 - 70 - 25), T= 25⁰C. q = 20ml/min

As observed in Figure 6-27 increasing the SR from 25 to 45 resulted in more surface crystals being nucleated. Also, a change in SR from 25 to 70 after 4hrs resulted in greater increase in the number of crystals where there were initially no more nucleation for a period of 2hrs at SR 25. This is also connected with the particles in the bulk solution for SR 70. Figure 6-28 shows a more significant increase in the size of crystals with an increase to higher SR. However, no further increase in the number of crystals was observed with the return of SR to 25. Thus, the increase in surface coverage in the later stage of the experiment as observed in Figure 6-29 is due to increase in the size of the crystals only. This suggests that surface nucleation is dependent on the number of active nucleation sites [42] and also a function of SR.
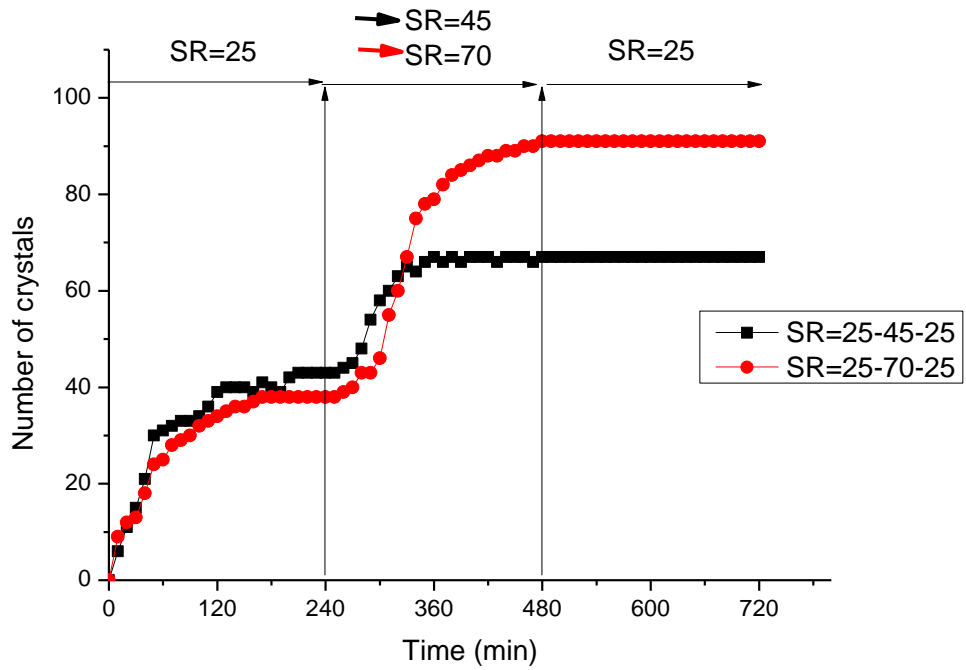
Figure 6-27: Number of crystals for dynamic test, SR (25 - 70 - 25), T= 25ºC. q = 20ml/min
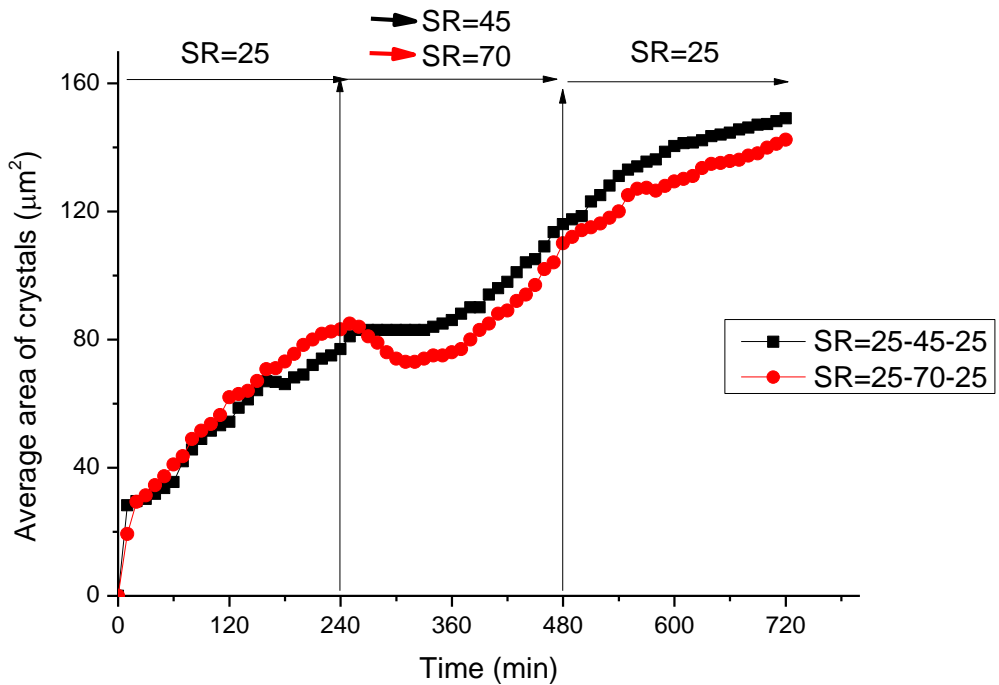
Figure 6-28: Average size of crystals for dynamic test, SR (25 - 70 - 25), T= 25ºC. q = 20ml/min
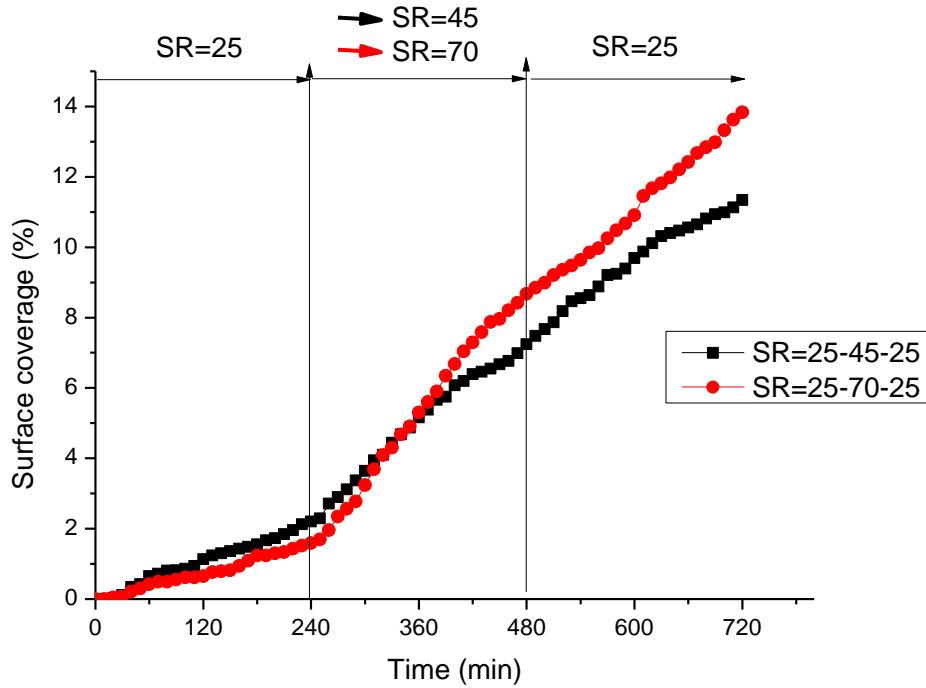
Figure 6-29: Surface coverage of crystals for dynamic test, SR (25 - 70 - 25), T= 25ºC. q = 20ml/min

The SEM image Figure 6-30 shows the new crystals that are nucleated by increasing the SR. The growth of crystals that were initially nucleated continues while new crystals are formed with the introduction of higher SR, resulting in significant difference in crystal sizes.
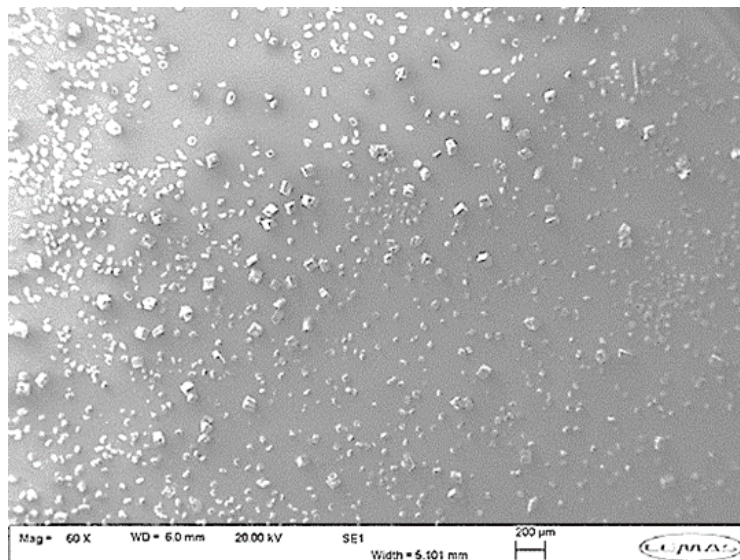
Figure 6-30: SEM image for dynamic test, SR (25-70-25)

6.6   Summary

The effects of SR on CaCO$_3$ scale formation with respect to bulk precipitation and surface crystallization have been studied and results presented showed a significant influence on the nucleation, growth and overall scaling in both processes.

- Surface scale formation was observed in all the SR values (10, 15, 25, 40, 60, 70 and 90) considered while bulk precipitation only takes place at high SR (70 and 90). A summary of the final values for bulk turbidity, number of crystals, average size of crystals and surface coverage obtained after 4 hours of test for each SR is presented in Table 6-2

Table 6-2: Final values of bulk and surface analysis at T=25⁰C and flow rate of 20ml/min

SR	Bulk Turbidity (FTU)	Number of crystals	Average sizes (µm²)	Surface coverage (%)	Surface induction time (t$_s$)
10	0	5	30	0.9	110
15	0	11	60	1.4	50
25	0	43	92	3.7	20
45	0	58	121	5.1	0
60	0	69	153	9.0	0
70	23	182	197	13.5	0
90	59	316	160	19.9	0

- All the brines showed a continuous increase in the average size of crystals on the surface once nucleation had taken place. A relatively linear trend was observed for surface coverage with the most saturated brine showing the highest percentage of surface scaling in terms of surface coverage during the time of testing.

- For all SR values considered, the increase in the number of crystals did not continue all through the time of test as a maximum was reached. The average size of crystals progressed throughout. This is further analyzed and discussed in Chapter 8 using the Beaunier model [42] as a basis and with a view to develop a more suitable surface scaling mechanisms based on constant SR and longer time of test.

- The results would also allow to quantify surface induction and growth kinetics as well as the overall mechanisms of surface scaling at different SR (Chapter 8).

Chapter 7 CaCO₃ scaling kinetics: Effects of temperature, flow rates and injection of chemical inhibitor

7.1 Introduction

The new system design to study surface scale deposition mechanisms and kinetics as described in chapter 5 is used to assess the kinetics of scale deposited in flowing conditions at different temperatures, flow rates and inhibitor concentrations. The three factors and their effects on surface crystallization kinetics are considered in this chapter and are presented in the following sections. The map of the chapter is presented in Figure 7-1.
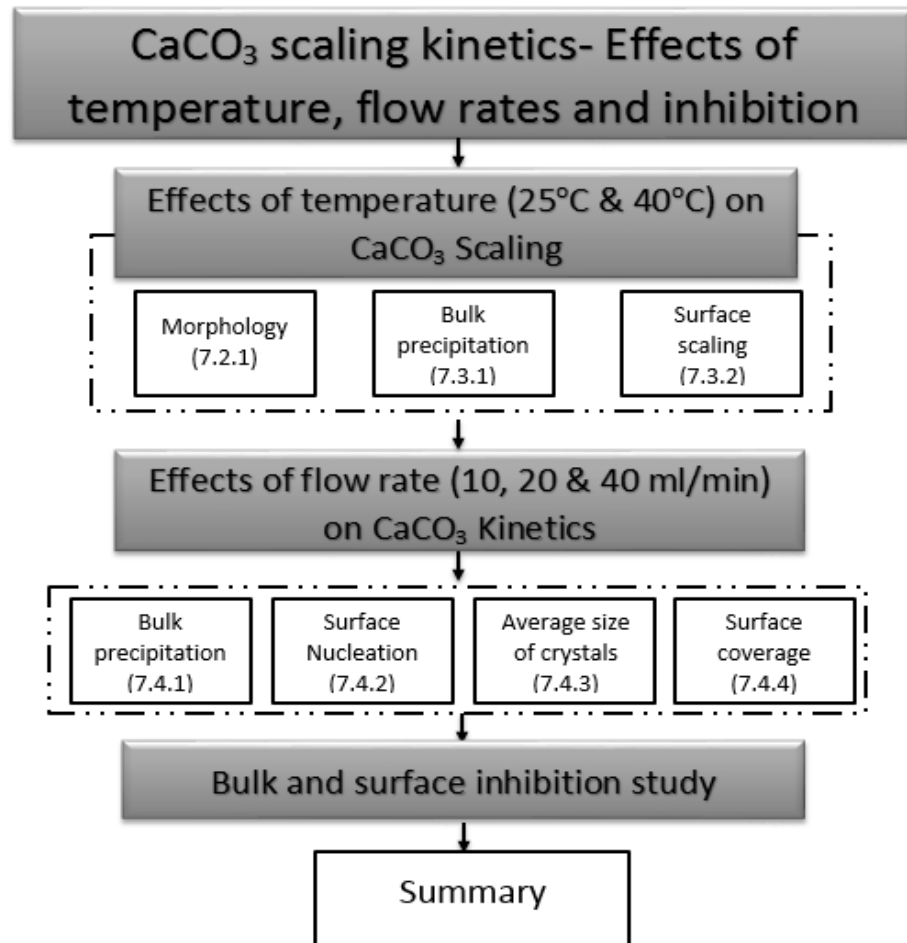
Figure 7-1: Map of chapter seven

7.2 Effects of temperature on scale formation.

Various works on the effects of temperature on scale formation especially in the bulk solution have been reported in the literature review section. It is therefore essential to study the effects of temperature on surface scaling kinetics and mechanisms. The study here is focussed on the effects of temperature on surface scaling kinetics and mechanisms at constant SR.

7.2.1 Effects of temperature on morphology

The morphology of the scale formed at different temperatures of 25ºC, 40ºC, 60ºC and 80ºC in the *in-situ* flow cell were observed using the scanning electron microscope (SEM). The SEM images were taken for $CaCO_3$ scale deposited from brine with SR value of 45 for 4hrs at a flow rate of 20ml/min. The ionic concentrations of the two brine solutions containing Ca^{2+} and CO_3^{2-} were adjusted using the Multiscale^{TM} software so as to take into consideration the effects of inverse solubility characteristics of $CaCO_3$ scale. The samples were removed at the end of the 4hrs of the surface deposition experiment. The SEM images of the surface scale at 25ºC, 40ºC, 60ºC and 80ºC are presented in Figure 7-2 As expected, calcite predominates at low temperature, especially at 25°C, vaterite is more stable at 40ºC while the aragonite structure is dominant at the high temperature of 80°C. This is in agreement with previous studies for bulk precipitation [67, 70, 85]. The observations are verified using X-ray diffraction technique.
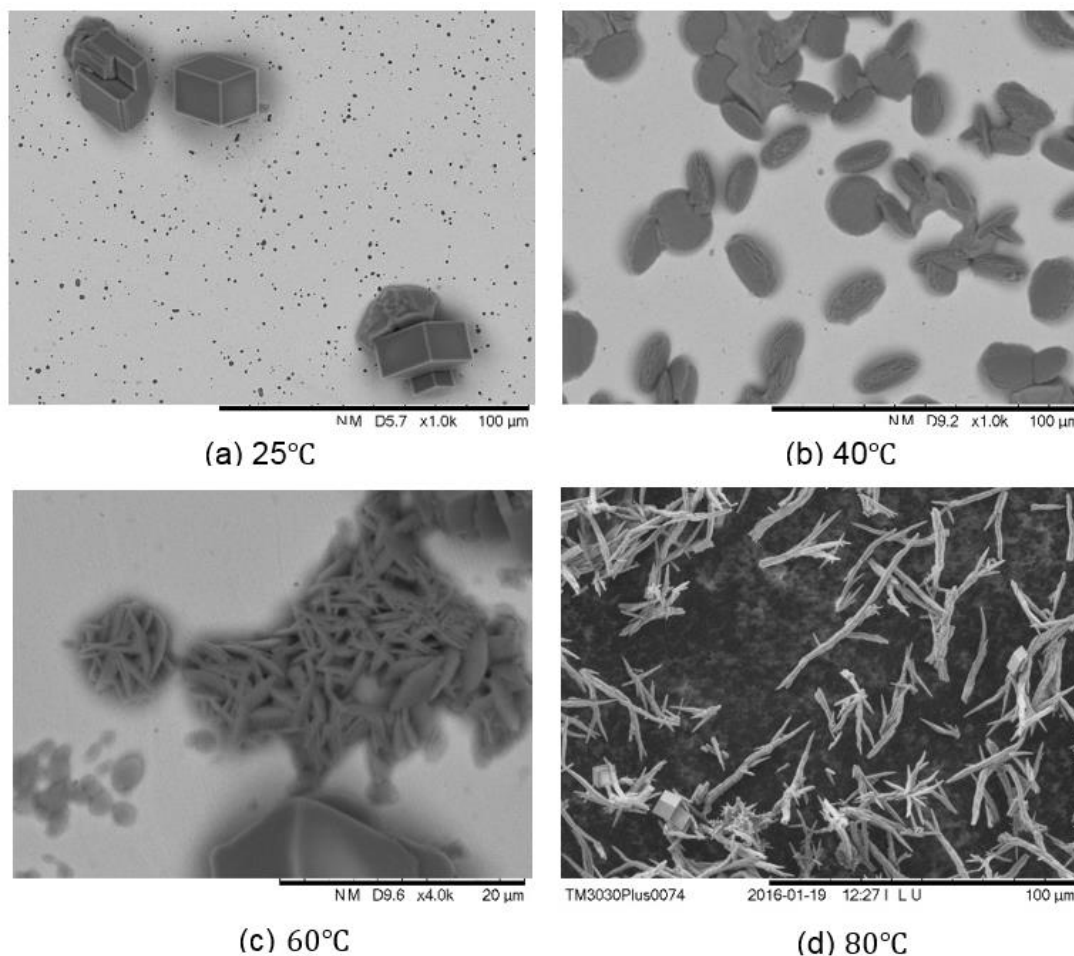
Figure 7-2: SEM of CaCO$_3$ Morphology at SR = 45 for (a) 25ºC (b) 40ºC (c) 60ºC and (d) 80ºC

The corresponding XRD patterns of the crystalline polymorphs for CaCO$_3$ at SR 45 for 25°C, 40°C, 60°C and 80°C are presented in Figure 7-3. The diffraction peaks corresponding to aragonite are observed only at 80°C while only calcite peaks are observed at 25°C. Calcite intensity is highest at 40°C; the same temperature at which vaterite peaks started to appear. Similar results regarding the morphology of CaCO$_3$ crystals precipitated in the bulk solution have been observed in other studies [17, 178].
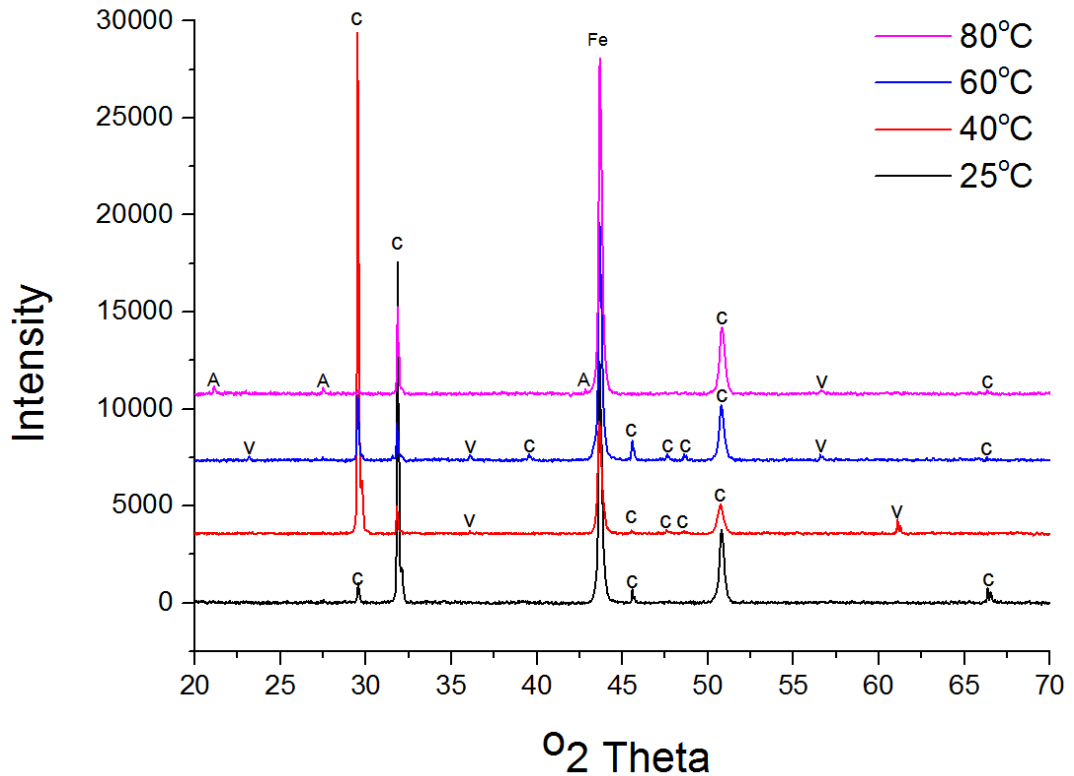
Figure 7-3: Diffraction spectra of CaCO₃ scale for different temperature at SR = 25

7.3 Effect of temperature on calcium carbonate kinetics

The effect of increasing temperature from 25°C to 40°C on the scaling kinetics of $CaCO_3$ was assessed at 20ml/min for SR of 10, 15, 25, 45 and 60. It is known that the solubility of $CaCO_3$ decreases with increasing temperature [83], therefore, SR values were maintained by reducing the ionic concentrations using the Multiscale™ software. The effects of increase in temperature on the turbidity, number of crystals, average size and surface coverage increase are presented as follows.

7.3.1 Effects of temperature on bulk precipitation

The turbidity measurements were followed and recorded *in-situ* for each brine tested at 40°C (Figure 7-4). Similar to turbidity measured at 25°C (Figure 6-3), brine with SR = 10, 15, 25 and 45 have zero turbidity as there was also no

precipitation in their bulk solutions with an increase in temperature to 40°C. The induction time for each brine at 40°C is longer than the residence time from the mixing chamber to sample surface. However, for SR of 60, precipitation in the bulk was observed in contrast to the same SR of 60 at 25°C, where there are no precipitated crystals in the bulk solution. An increase in temperature from 25°C to 40°C resulted in a faster kinetics in the bulk as the induction time becomes shorter than the residence time from mixing to sample surface. The bulk turbidity recorded is constant throughout the duration of experiment and the value is 28 FNU.
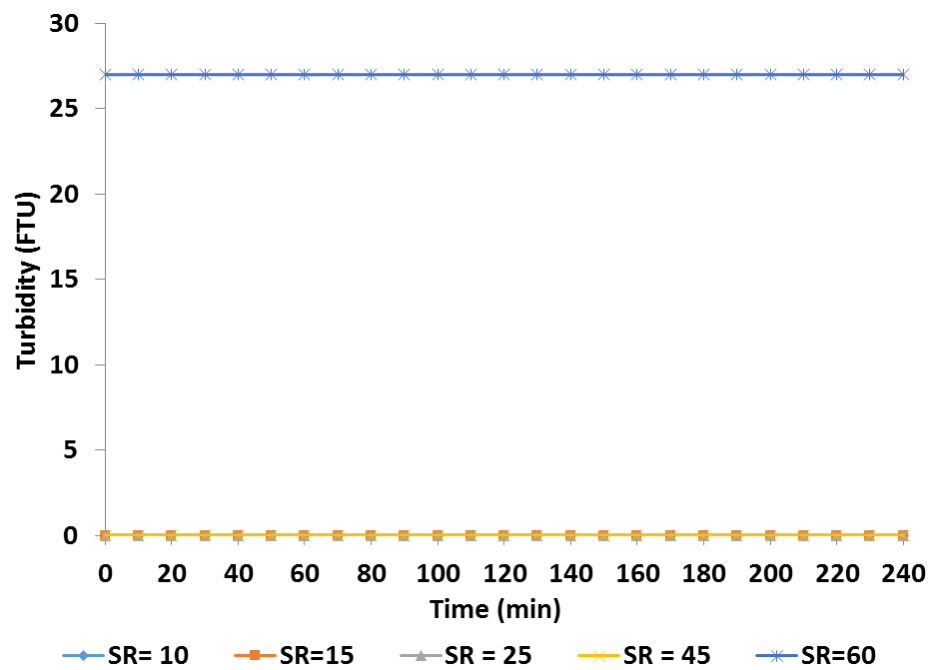
Figure 7-4: Turbidity measurement at 40ºC

7.3.2 Surface scaling at 25ºC and 40ºC

The quantity of scale formed on the stainless steel samples at each temperature, 25°C and 40°C and at flow rate of 20ml/min are compared to assess the effects of increase in temperature on surface scaling viz-a-viz the number of crystals, average sizes and surface coverage of crystals.

121

7.3.3 Effects of temperature on nucleation

The effects of temperature on numbers of crystals are presented in Figure 7-5 (a – e). A similar trend is observed for brines at SR 10 and SR 15 because for each of the low SR considered, the time taken before the appearance of the first crystal (surface induction time) decreases with increase in temperature from 25°C to 40°C. For SR 10, surface induction time is 110 minutes at 25°C and 50 minutes at 40°C while for SR 15, it takes 50 minutes at 25°C and 10 minutes at 40°C before the first particles are detected, the number of crystals detected did not vary significantly with temperature for the two SR. No surface induction period was observed for SR 25 at 40°C in contrast to the 20 minutes surface induction period observed at 25°C for the same SR. The trends for the curves at SR 25 and SR 45 show that a maximum number of crystals is reached faster at 40°C compared to the steady increase in number of crystals to the maximum as observed at 25°C. The curve for SR 60 at 40°C shows three stages; first, a rapid increase in the number of crystals; secondly, a short period of constant numbers followed by a third stage where the number of crystals decreases gradually. This may be due to clustering/agglomeration of crystals. It is to be noted that the turbidity also changes for SR 60 from 0 FTU with no particles in the bulk at 25°C to 28 FTU at 40°C (Figure 7-4). For each brine, a maximum number is reached at which the number of particles detected stays more or less constant.
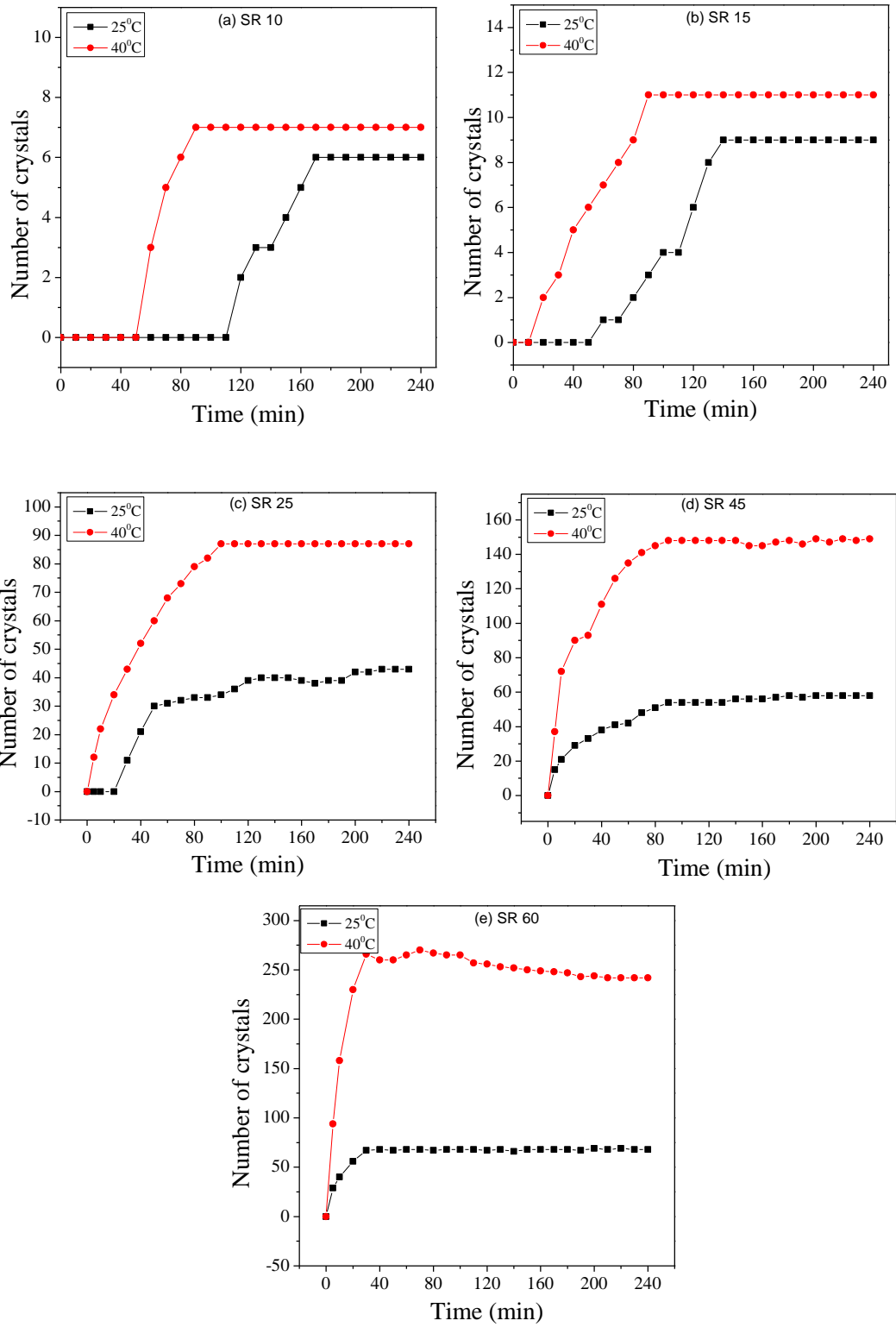
Figure 7-5: Number of crystals on surface as a function of time at T =25⁰C and 40⁰C(a) SR 10 (b) SR 15 (c) SR 25 (d) SR 45 (e) SR 60

The total number of surface crystals detected at the different SR values and temperatures after 4hrs of surface deposition are presented in Figure 7-6. SR 60, shows a very significant increase from 182 crystals detected after 4 hours at 25°C when there is no pre-precipitated crystals in the bulk solution to 312 crystals at 40°C with bulk precipitation. The number of crystals also increases significantly for SR 25 from 43 to 117 crystals and SR 45 from 58 to 149 crystals with increase in temperature. Thus, temperature is seen to have great effects on surface induction and number of crystals formed.
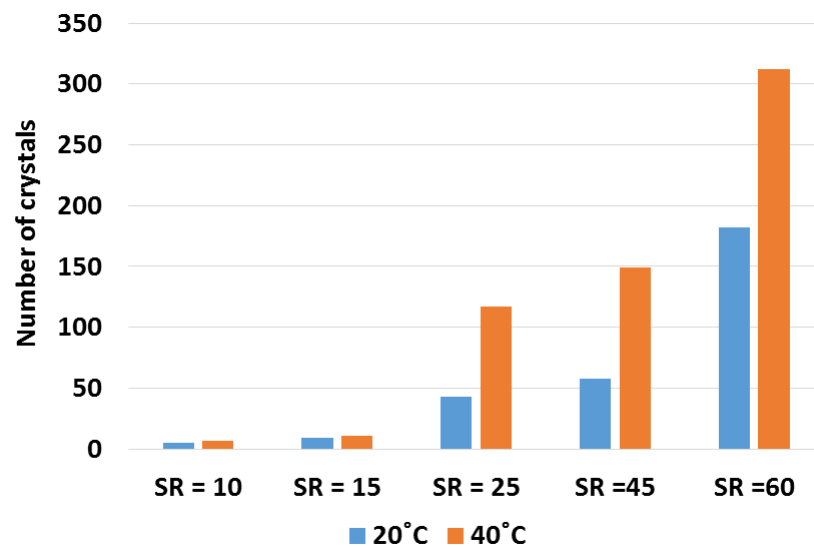
Figure 7-6: Number of crystals after 4hrs at 20⁰Cand 40⁰C

7.3.4 Effects of temperature on average size of crystals

The average area of crystals detected on the surface of the stainless samples for the different SR at 25°C and 40°C steel were quantified so as to assess the growth of crystals with time. The results are presented in Figure 7-7(a– e). At 25°C the increase in average size proceeds steadily but slowly for all the brines except for brine with SR 60. A faster growth with respect to increase in average size of the crystals can be observed at higher temperature, 40°C. Regarding SR 25, where no induction period is observed at 40°C, the crystals are much bigger than when compared to the size of crystals detected at 25°C with surface induction time of 20 minutes.
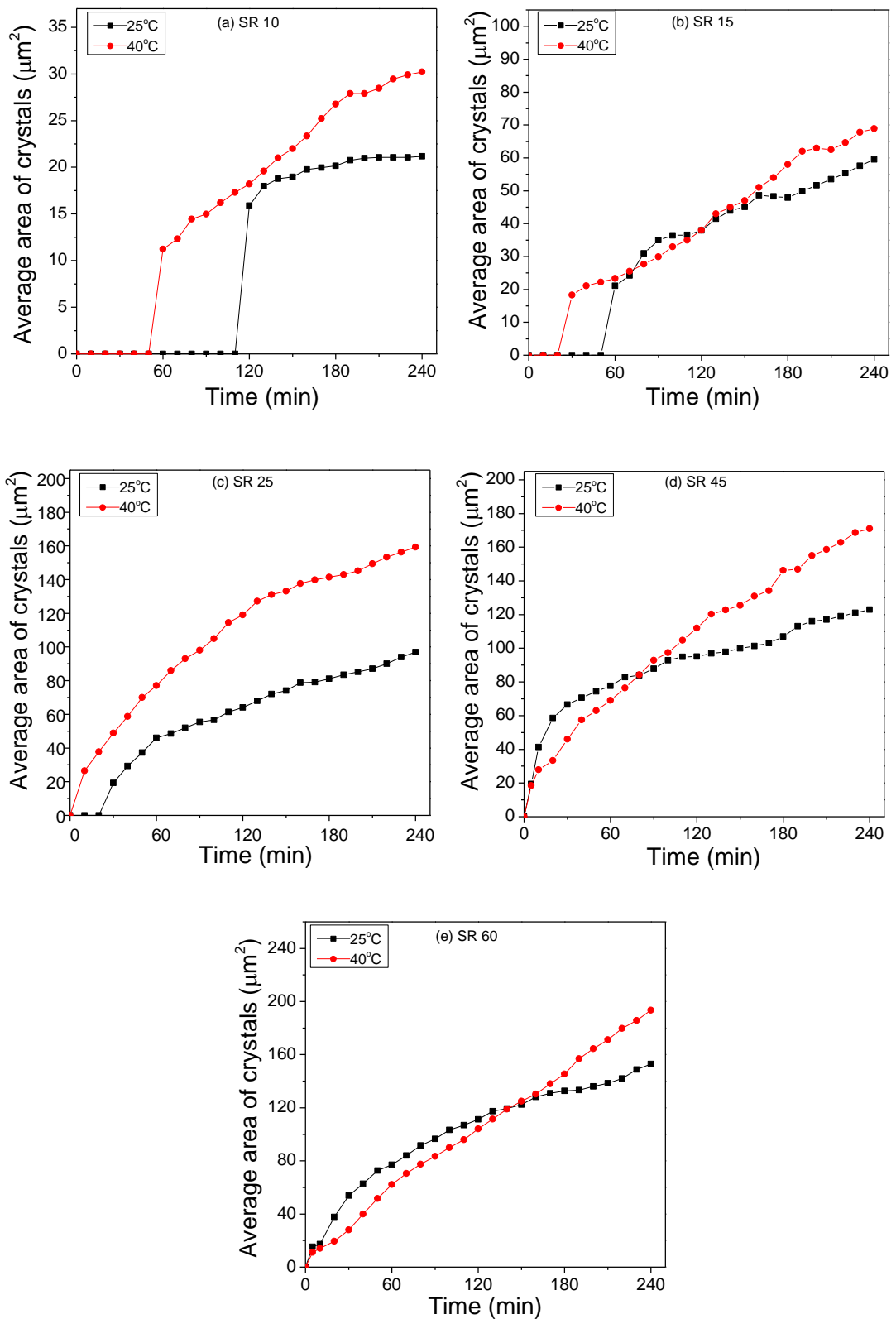
Figure 7-7: Average size of crystals as a function of time at T =25⁰C and 40⁰C (a) SR 10 (b) SR 15 (c) SR 25 (d) SR 45 (e) SR 60

For SR 60 at 40°C, the average size of crystals detected at the initial stage up to 120 minutes is smaller compared to the average size of crystals detected at 25°C. When compared to the large number of crystals observed, it appears that the increase in the number of crystals at 40°C is the dominant process at early stages until the number of crystals reaches a maximum after which increase in average size of crystals becomes the dominant process for surface coverage.

With regards to the curves, there is a continuous increase in average size of crystals for all the SR values considered as fresh brines pass the surface and ion concentrations are kept constant. As such, no plateau was observed, this is in contrast to the number of crystals, where a maximum number was reached for all the SR values. However, as expected, the variations in the shapes and slopes of the curves imply variations in the kinetics and mechanisms of surface crystal growth as a function of temperature and SR.

The final average size data of crystals for all the brine solutions at 25°C and 40°C after 4hrs are presented in Figure 7-8. For all the brines, the final crystals sizes after 4hrs are smaller at 25°C. Final crystal size for SR 10 at 25ºC is 21µm^2 and at 40°C is 35µm^2. The effect of temperature on crystal size is observed to be greatest for SR 25 with an increase in average crystals size from 97µm^2 at 25°C to 168µm^2 at 40°C after 4 hours. Owing to the large number of crystals detected for SR 45 and SR 60 at 45°C, the increase in the average crystal size is smaller with respect to SR 25.
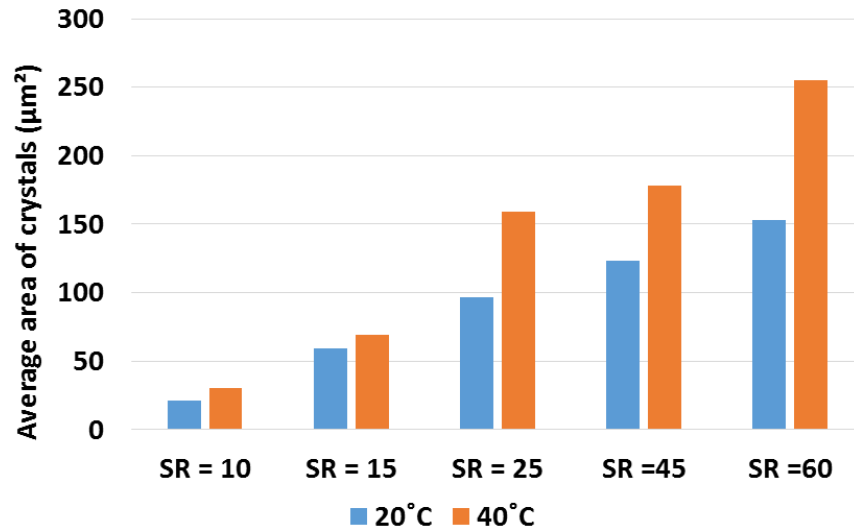
Figure 7-8: Average crystal size of crystals after 4hrs at 20⁰C and 40⁰C

7.3.5 Effects of temperature on surface coverage of crystals

Results of percentage surface coverage measured with time at 25°C and 40°C are presented in Figure 7-9. In relation to the numbers and average sizes of crystals, the percentage surface coverages measured for all brines increase with increase in temperature from 25°C to 40°C. The curves which represent the overall surface scaling show that scale formation continue to increase for all brines once induction has taken place. Similar to the increase in average size, growth of crystals takes place with fresh brines once number of crystals has reached a maximum value. Thus the initial surface coverage may be due to both nucleation and/or growth of crystals. Also, the curves tend to become more linear with increase in temperature and SR. All of these observations could be attributed to change in mechanisms and kinetics which are further discussed in the chapter 8.
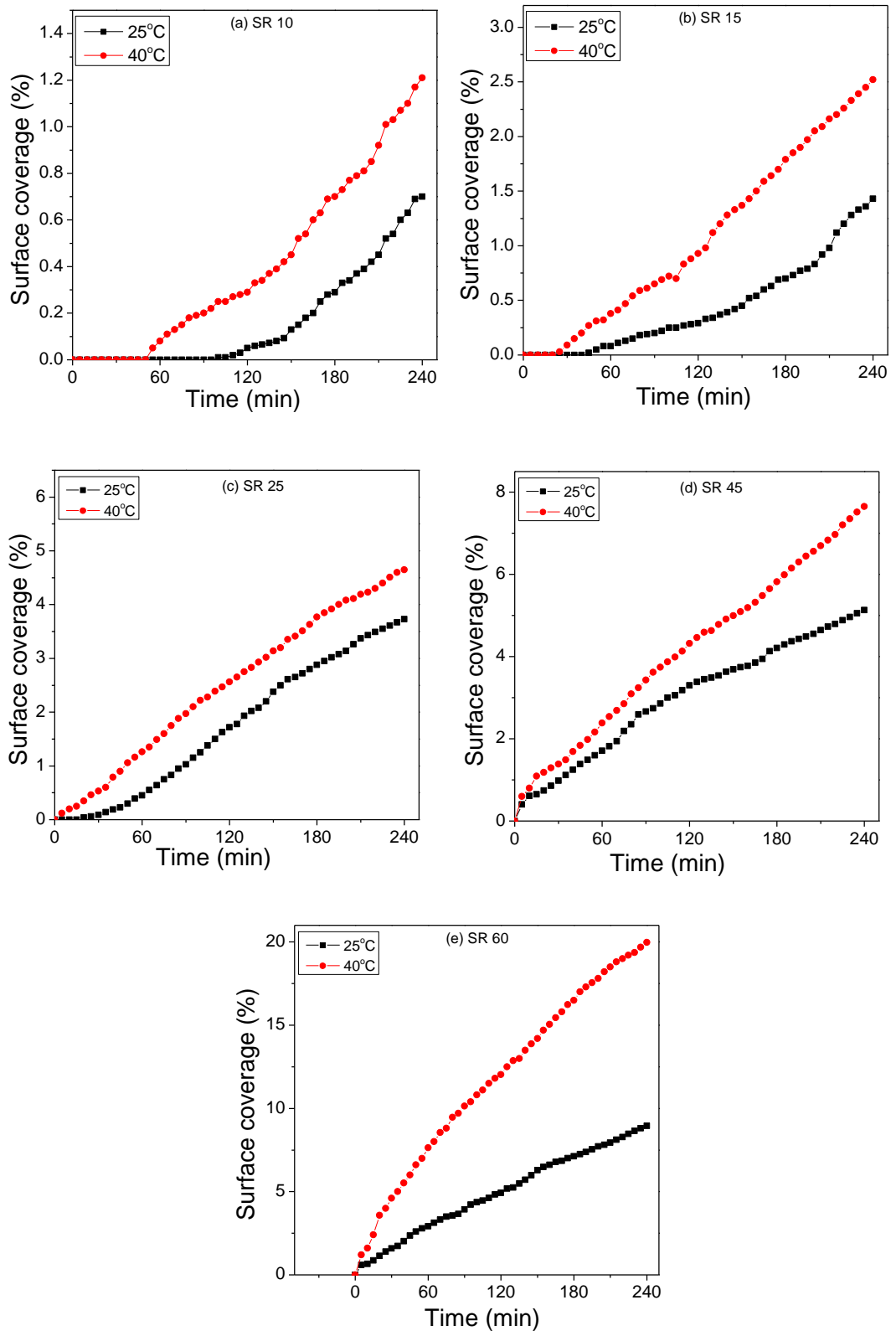
Figure 7-9: Surface coverage of crystals as a function of time at T =25⁰C and 40⁰C (a) SR 10 (b) SR 15 (c) SR 25 (d) SR 45 (e) SR 60

The overall percentage coverage for each brine at 25°C and 40°C after 4hrs of deposition in the cell is presented in Figure 7-10 An increase in surface scale coverage from at 25°C to at 40°C is observed for the lowest SR while an increase in surface scale coverage from at 25°C to at 40°C (SR 25) is observed for the lowest SR after 4 hours.
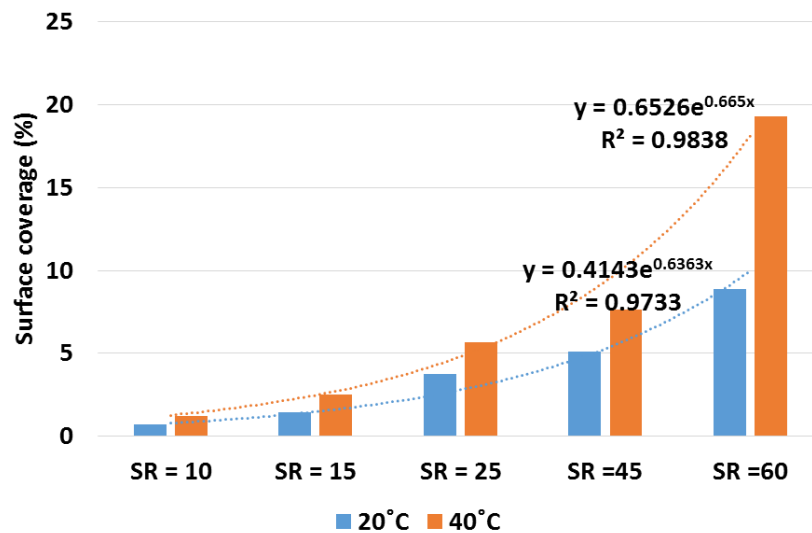
Figure 7-10: Surface coverage of crystals after 4hrs at 20⁰C and 40⁰C

Temperature, especially when high, shows to influence the kinetics more than the SR, in some cases, for both bulk precipitation and surface deposition

7.4   Effect of flow rate on calcium carbonate scaling

The scale deposition was investigated for different flow rates of 10ml/min, 20ml/min and 40ml/min at 25°C for 4 hour test. The flow cell configuration, the hydrodynamic analysis as well as the calculated Reynolds numbers for each flow velocity earlier discussed in chapter 4 show a laminar regime at all flow rates used. The flow rates were varied for each value of saturation ratio. The effects on bulk turbidity and surface scaling are presented in the following sections.

7.4.1 Effects on bulk precipitation

The bulk turbidity observed and recorded for all the SR (10, 15, 25, 45, and 60) at flow rates of 10ml/min, 20ml/min and 40ml/min remain zero for the 4 hour deposition test. The increase in flow rates has no effects on the bulk kinetics for all the SR tested because the induction time for bulk precipitation to occur at each of the flow rates and SR is longer than the residence time from mixing to the surface in the cell.

7.4.2 Number of crystals at different flow rates

Figure 7-11(a–e) shows that the induction time before the appearance of the first crystal varies with flow rate for the low SR values of 10, 15 and 25. It is observed to decrease for all brine tested with increase in flow rates from 10ml/min to 40ml/min. However, no crystal is detected for SR 10 at 10ml/min suggesting that the surface induction time is longer than 240 minutes. There are no effects on the surface induction time for the brine at high saturation ratio as the induction time remain zero for SR 45 and 60 at 10ml/min, 20ml/min and 40ml/min as such, crystals are detected immediately while the number of crystals is observed to be increasing with flow rates and SR.
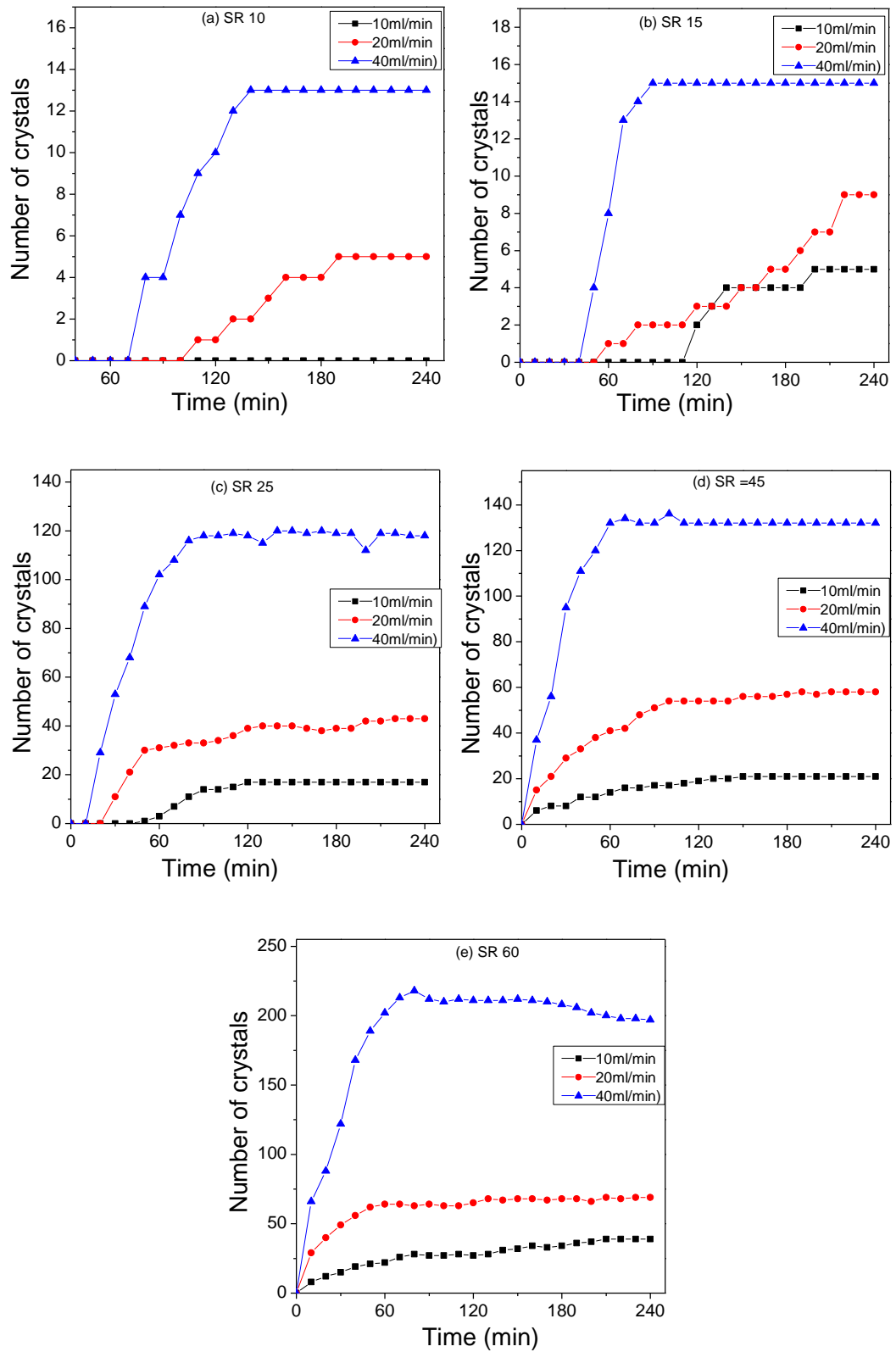
Figure 7-11: Number of crystals at 10ml/min, 20ml/min and 40ml/min

The appearance of crystals are very rapid at 40ml/min while a steady increase is observed at 10ml/min and 20ml/min. For all the flow rates and SR, the number of crystals reaches a maximum at which there is a constant number detected and no more new crystals are formed. The time taken to reach a maximum is shortest at 40ml/min for all the brines indicating a faster kinetics at high flow rates.

7.4.3 Average size of crystals at different flow rates

The results of increase in the size of surface crystals with time as a function of flow rates for all the brines tested are presented in Figure 7-12(a–e). As earlier stated, crystals are not precipitated in the bulk solution at all flow rates considered while there is induction and subsequent nucleation of crystals on the surface of the sample in the *in-situ* flow cell except at 10ml/min for SR =10. For SR 10, 15 and 25, the surface crystals grow faster with increase in flow rate as the increase in size of crystals is observed to be fastest at 40ml/min and steady at the lower flow rates. This account for the larger crystals sizes detected and captured at SR 10, 15 and 25 for 40ml/min which are 58μm², 76μm², and 109μm² compared to crystals sizes of 21μm², 60μm², 92μm² at 20ml/min respectively after 4hours. However for higher SR 45 and 60, the size of crystals are affected by the high number of crystals on the surface, therefore, crystals sizes are smaller at 40ml/min when compared to the sizes of crystals at 20ml/min after 4 hours
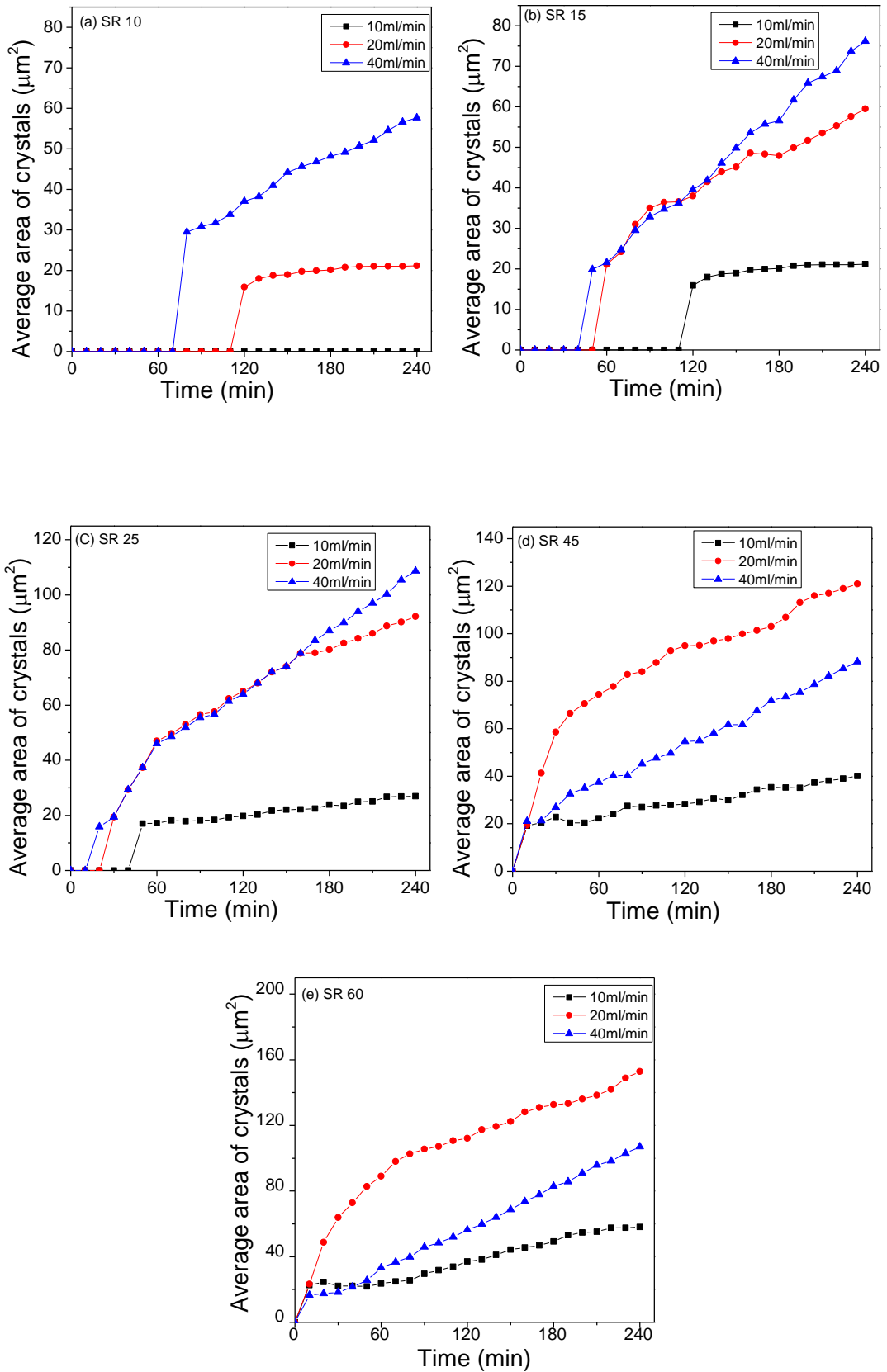
Figure 7-12: Average size of crystal at 10ml/min, 20ml/min and 40ml/min

7.4.4 Surface coverage of crystals at different flow rates

The overall surface scaling process measured in terms of percentage surface scale coverage shows that scale formed continuously at different rates on the surface of the sample at constant saturation ratio and no pre-precipitated crystals in the bulk solution. With formation of new crystals reaching a maximum, the later stages of the curves could be due to crystals increasing in size.

As seen in Figure 7-13(a-e), high flow rates resulted in high surface deposition as illustrated with an increase in percentage surface coverage for SR 60 from 3.9% to 5.1% and finally 11.2% for 10ml/min, 20ml/min and 40ml/min respectively. The same trend is observed for all other brines when the flow rate was increased. The flow velocity is in the laminar regime, thus, the probability of shear stress causing removal of scale from the surface is low or unlikely.
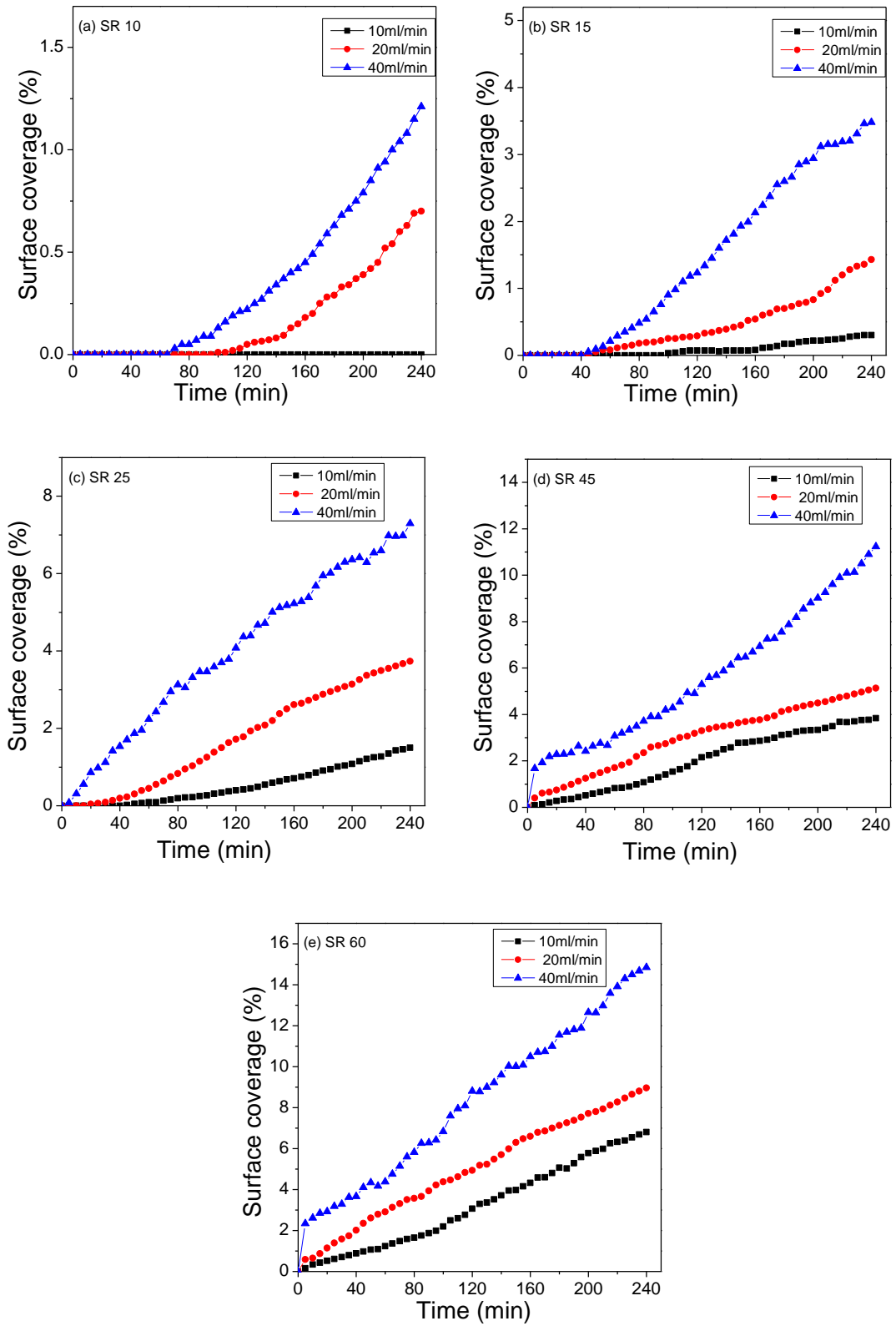
Figure 7-13: Surface coverage at 10ml/min, 20ml/min and 40ml/min.

7.5   Bulk and surface inhibition study at different SR values

CaCO$_3$ scale inhibition tests are carried out in the flow rig with three SR values of 25, 45 and 70 at 25°C using Polphosphinocarboxylic acid (PPCA) at 2ppm. The 2ppm concentration is the bulk minimum inhibitor concentration (MIC) determined by bulk jar test for SR value of 45 at 25°C. The inhibitor was prepared and added after 1 hour of scale formation into the seawater (SW) solution, containing CO$_3^{2-}$, prior to mixing. The flow rate used for the study is 20ml/min and the total time of study is 4hours. The inhibitive effects and mechanisms at different SR on both turbidity and surface scaling were assessed *in-situ* and in real time. The results are presented in the following sections. The hypothetical graph shown in Figure 7-14 summarises the possible effects of inhibitors addition after 60 minutes.
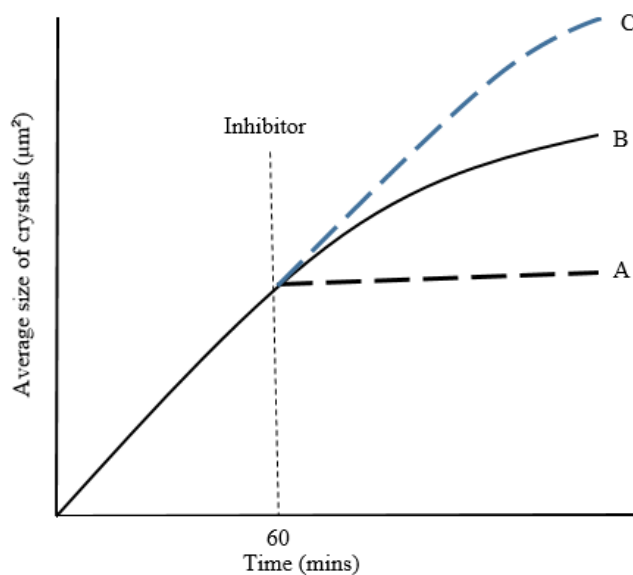
Figure 7-14: Schematic graph (hypothetical) showing the possible effects of inhibitors on surface growth of crystals. A = Stop growth; B= Steady growth; No effects; C= Increase in growth

7.5.1   Efects of 2ppm PPCA inhibitor on bulk solution

The addition of 2ppm of PPCA inhibitor after 1 hour has no effect on brines with SR values of 25 and 45. No bulk precipitation occurs before and after the inhibition as the residence time from mixing to sample is shorter than the

induction time for precipitation. However, for SR 70, there was precipitation in the bulk but the bulk turbidity was reduced from 30 FTU to 4 FTU with the injection of inhibitor into the solution after 1 hour. This suggests that the inhibitor does not completely inhibit the precipitation of bulk scale as it is below the minimum inhibitor concentration (MIC). The time of about 10 minutes taken for the inhibitor to become effective in reducing the bulk turbidity is a reflection of the kinetics of adsorption of the inhibitor on the bulk particles.
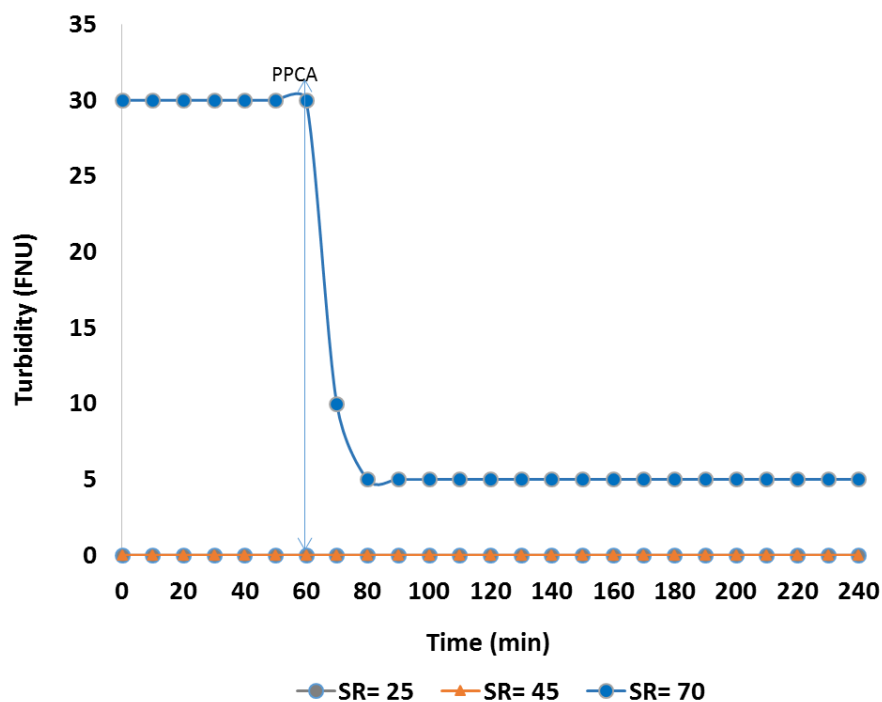
Figure 7-15: Turbidity measurement for inhibitor addition (PPCA -2ppm) after 1hr for SR =25, 45 and 70 at T = 25°C, q = 20ml/min

7.5.2 Effects of PPCA inhibitor on $CaCO_3$ surface scaling at SR = 25

The 2ppm of PPCA inhibitor injected after 1 hour is observed to stop the nucleation, growth of crystals and consequently the surface coverage for SR 25 (Figure 7-16). The surface scaling at the end of 4 hours for the blank solution without injection of inhibitor is quantified as follows: number of crystals detected is 43, average size of crystals is 122 μm^2 and surface coverage is 3.7%. With the addition of inhibitor at 60 minutes, no new crystals are detected beyond 65 minutes while there was also no further increase in crystal size.

This resulted in the quantified numbers, average sizes and surface coverage of crystals as 38, 65.5 μm^2 and 0.9% respectively. Thus, the 2ppm PPCA inhibitor was effective in stopping further surface scaling at SR 25.
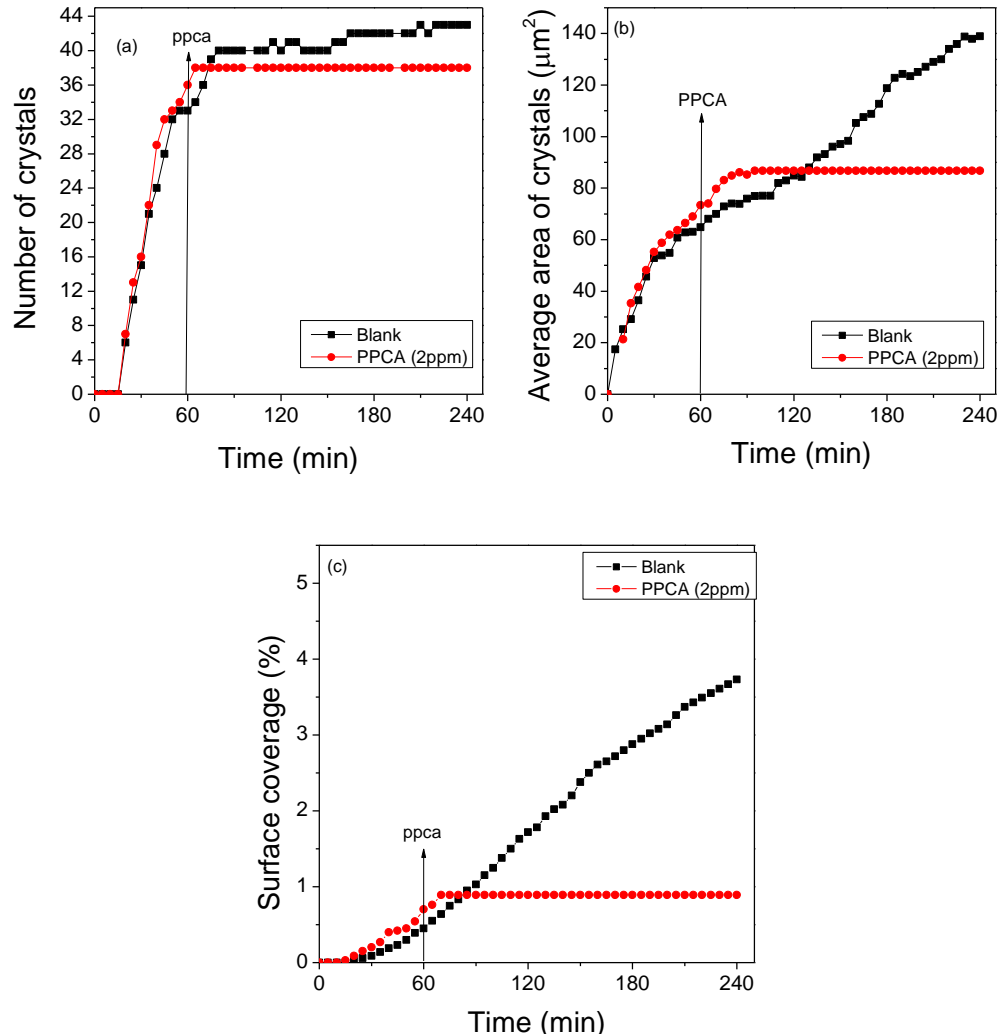
Figure 7-16: Inhibitor addition (PPCA -2ppm) after 1 hour for SR 25, T = 25°C, q = 20ml/min

7.5.3 Effects of PPCA inhibitor on CaCO₃ surface scaling at SR = 45

In Figure 7-17, a similar trend to SR 25 is observed for SR 45 when the same inhibitor concentration (2pppm) was injected into the seawater solution following surface scaling for 1 hour in the flow rig as further scaling was eventually inhibited. No new crystals are observed after 10 minutes while the average size as well as the surface coverage of crystals was observed to stop

after 15 minutes of injecting the inhibitor which, represents a further 10 minutes of surface scaling when compared to SR 25. This suggests that the inhibitor at the same concentration becomes fully effective to inhibit further scaling at different time depending on the SR and/or percentage surface coverage.
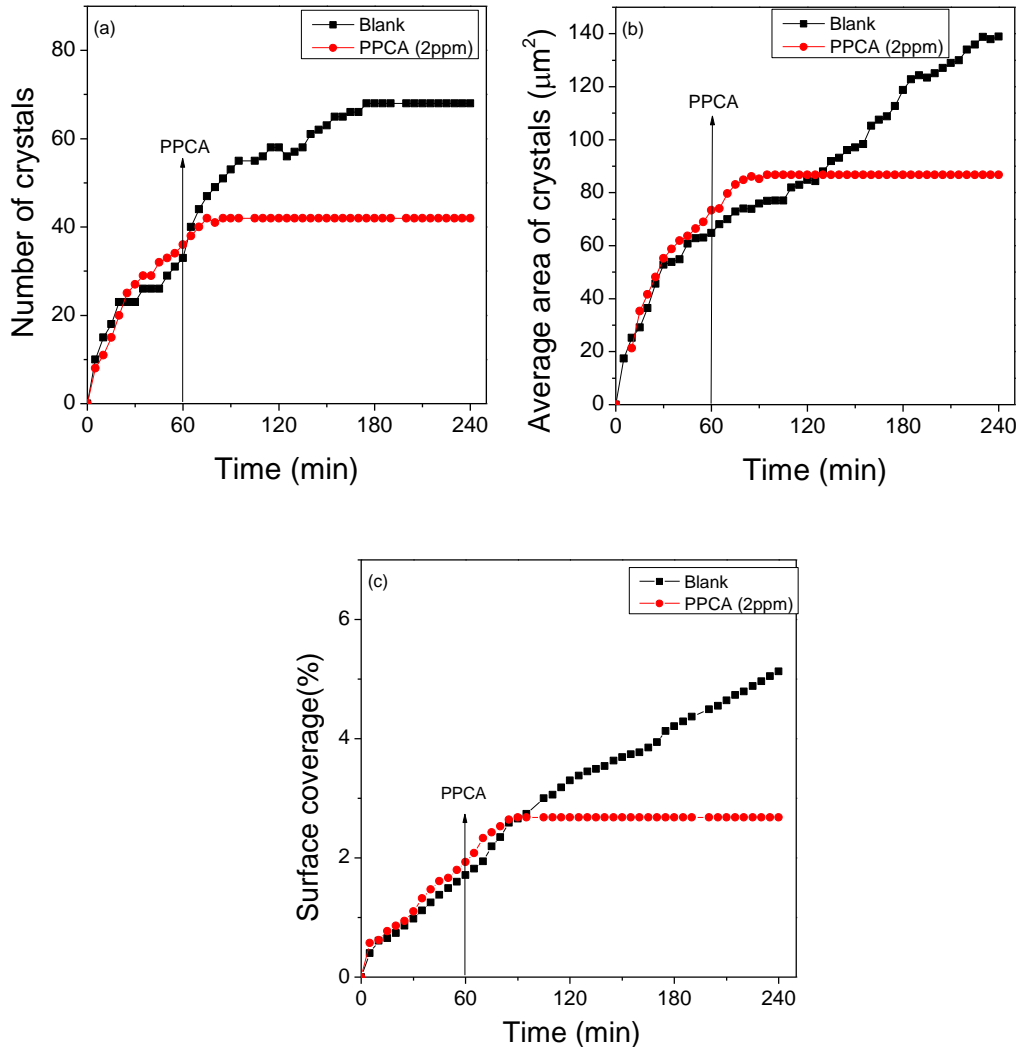
Figure 7-17: Inhibitor addition (PPCA -2ppm) after 1hr for SR 45, T = 25°C, q = 20ml/min

7.5.4 Effects of PPCA inhibitor on CaCO$_3$ surface scaling at SR = 70

The addition of 2ppm inhibitor to the brine with SR = 70 after 1hr results into more surface scale as observed with an increase in the surface growth and surface coverage (Figure 7-18) in spite of the reduction in its bulk scaling

tendency (Figure 7-15). At the end of the 4 hour test, more new crystals were detected for a further 35 minutes after the inhibitor was added, thereby, increasing the numbers from 154 to 179. Surface growth of crystals increases from 72µm² after 1hour to 242µm² while the percentage surface coverage increases from 6.15% to 22.3% with the addition of inhibitor. This is similar to observations by Graham *et al* [179] and Chen *et al* [180]. The unavailability of active sites means that no new crystals are formed at the later stages for both the uninhibited and the inhibited tests. This could be attributed to rapid increase in the number of crystals at the early stage of scaling. However, the increase in average sizes of crystals continue in both cases and it is more pronounced in the inhibited tests resulting in more surface coverage after the injection of PPCA inhibitor.
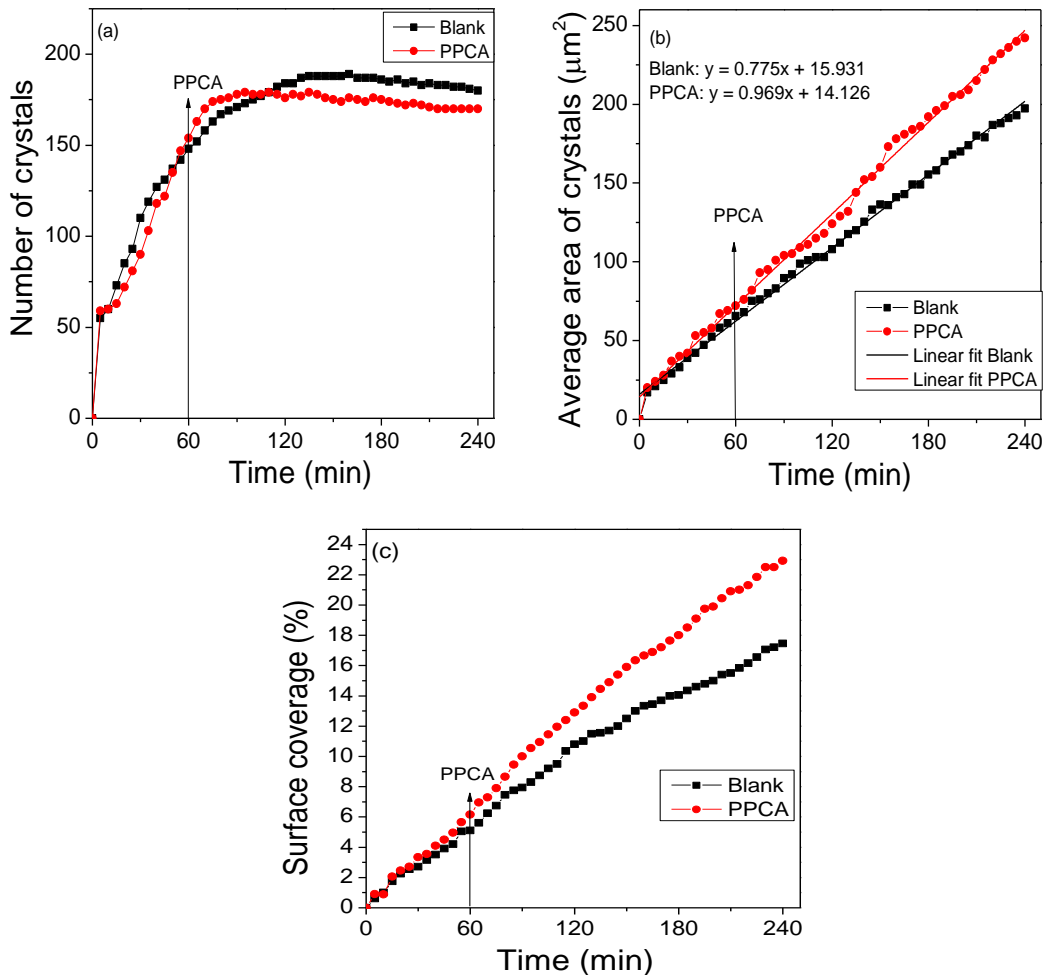
Figure 7-18: Inhibitor addition (PPCA -2ppm) after 1hr for SR =70 at T = 25°C, q = 20ml/min

Figure 7-19 shows the summary of the relative average sizes after 4 hours for all the SR tested in both the inhibited and uninhibited surface scaling. The inhibitor is injected to the brine solutions after 1 hour of surface scaling in the flow rig. An increase in average size is observed for the brine with high SR 70 when inhibitor is injected suggesting that the inhibitor is below the MIC for the surface. The crystals are bigger in uninhibited tests for SR 25 and 45 which shows that no further growth of crystals with continuous injection of 2ppm of PPCA inhibitor.
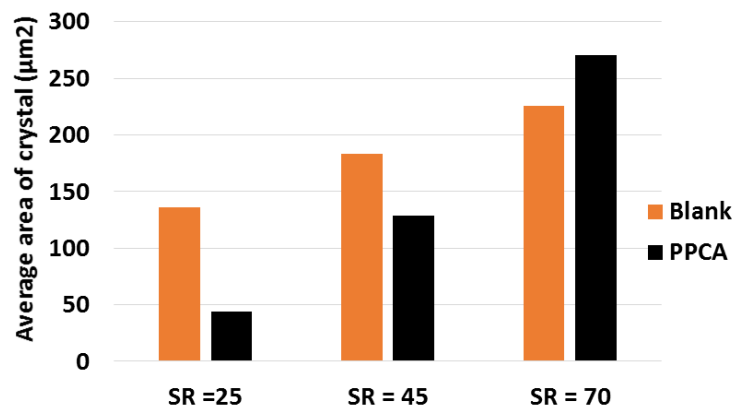
Figure 7-19: Average size of crystals after 4hrs with PPCA, T = 25⁰C

7.5.5 Effects of adding and removing inhibitor on surface scaling

The dynamic test of adding and removing inhibitor in the brine solution was tested to assess its possible influence on surface scaling kinetics. 2ppm of PPCA was added into the seawater solution after an initial two hours of uninhibited scale formation. The brine solution (SR = 45) containing the inhibitor was run for two hours at 20ml/min continuously after which fresh brine (SR = 45) with no inhibitor was re-introduced at the same flow rate for 4 hours to complete the process. The result of a 2 hour interval of inhibitor injection on surface scaling is presented in Figure 7-20. No new crystals are observed on the surface when the injection of inhibitor was stopped. The increase in the average size of crystals was initially stopped after 30 minutes of injecting the inhibitor but was again observed after 40 minutes of running fresh brine to the

already inhibited surface. The increase in average size proceeds steadily when the inhibitor was removed.
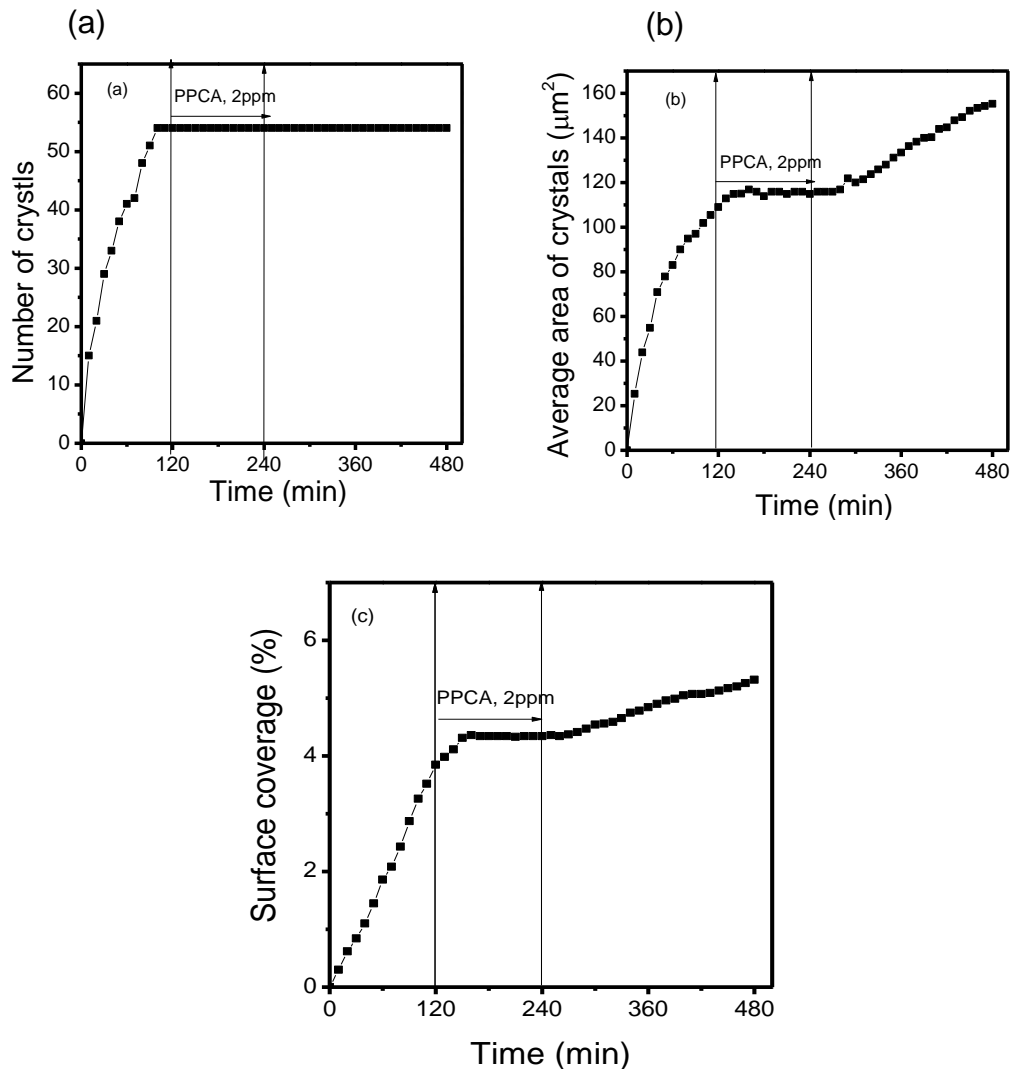
Figure 7-20: Effects of injection and removal of inhibitor on (a)number of crystals (b) average size of crystals (c) surface coverage

7.6   Summary

The results presented in this chapter show the effects of temperature, flow rates as well as inhibitor injection on bulk precipitation and surface scaling at different SR.

- The number of crystals reaches a plateau while the growth and surface coverage proceeds for the 4hrs in the uninhibited test as the solution supersaturation is constant for each test.

- With increase in temperature, there was a transition from no bulk precipitation at 25°C to bulk precipitation at 40°C for brine with SR 60 as the bulk induction time decreases significantly while the turbidity for SR (10, 15, 25) remains at zero even though surface scaling was affected to different degrees. An increase in temperature has a pronounced effect on surface scaling induction time and consequently on the surface scaling kinetics.

- The effects of flow rates on surface scaling is very significant at high SR. Surface scaling at high flow rates resulted in a higher number of crystals which consequently resulted in relatively smaller crystal sizes.

- The effects of 2ppm PPCA inhibitor added after 1 hour into the seawater brine solution before mixing vary from bulk to surface scaling and also between the various saturation ratios. The inhibitor is effective to stop bulk scaling at all the SR values considered but is only effective at SR 25 and 45 for surface. Surface scaling was promoted at SR 70.

Chapter 8 Discussion

The objective for the research work is to develop a once-through flow visualization rig that allows both bulk precipitation and surface scaling mechanisms to be distinctively studied in a single system where the saturation ratio (SR) at the sample can be controlled. Secondly, in order to improve the understanding of surface scaling, the study attempts to examine the factors that influence surface scaling such as SR, flow rate and temperature. are quantified. In addition, the effects of inhibitor are also examined and how these vary between surface and bulk scaling [30].

This chapter is divided into four different sections intending to analyse and discuss the results presented in Chapters Five, Six and Seven. First, the capability of the rig and its advantages are briefly discussed. Also discussed are the formation of surface scale with and without pre-precipitated bulk crystals, the mechanisms of surface scale build up in the system at both low and high SR, the effect of different parameters such as supersaturation ratio, temperature, flow rate and inhibitor injection on surface crystallization kinetics.

The discussion is presented in the following format:

(1) Once-through real-time visualization technique;

(2) Bulk precipitation versus surface deposition;

(3) Crystallization mechanisms and kinetics;

(4) Effects of inhibitor injection on scaling at different SR;

The map of chapter eight is presented in Figure 8-1.

144
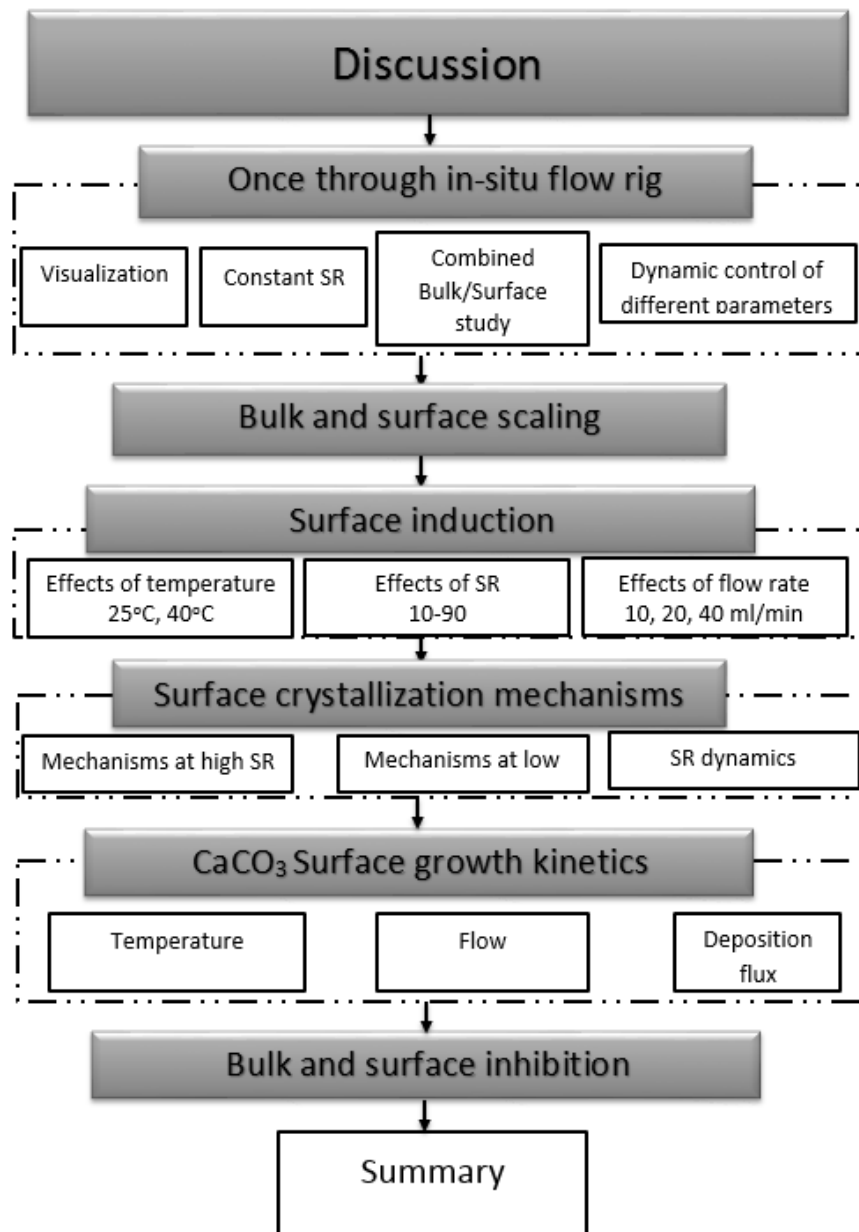
Figure 8-1: Map of chapter eight

8.1   Once-through real-time visualization technique

The $CaCO_3$ deposition and the effect of inhibitor addition have been studied with a range of techniques [7, 17, 18, 34, 160, 165, 172, 181]. The gaps in previous techniques as highlighted in chapter three (3.3) include that the assessment of surface scaling is made from simply bulk thermodynamics and kinetics, no flow control in most techniques, SR is often decreasing through

the test as particles grow and settle due to gravity, and an inability to distinctively assess homogeneous and heterogeneous crystallization as well as non-suitability for later stages of crystallization. Significantly less is known about the $CaCO_3$ crystal formation mechanisms on a solid surface at constant SR. This is important in order to move towards predictions and proper assessment of kinetics. In the field, it is likely that a surface is exposed to the same condition for a fairly long time. The newly developed flow rig for scale formation study offers several new capabilities which are highlighted in the following sections.

8.1.1 *In-situ* Visualization

The new flow rig is an *in-situ* methodology which visualise the surface crystallization of calcium carbonate from a supersaturated solution and quantifies the nucleation and growth processes in real time. Visualization allows the mechanisms of build-up of scale in-situ and in real-time to be followed. It also allows the assessment and quantification of the nucleation and growth processes.

8.1.2 Constant saturation ratio

The study of crystallisation kinetics of calcium carbonate from a supersaturated solution requires that the driving force be maintained constant. Previous methodologies such as bulk jar and RCE tests to study scale formation have seen SR decrease with scale formation as a result of reduction in the ionic species [7, 34]. SR decreases with capillary length in the dynamic tube blocking rig [18, 182].

Scale formation in the bulk solution and on surfaces is affected by changes in initial supersaturation [54, 79-81]. In a recirculating system where the SI was not fixed and only the concentration and the temperature were varied, it appeared difficult to assess the effect of other factors such as temperature on induction time and compare results [81].

146

To maintain a constant driving force, the new rig is designed in such a way as to match the rate at which supersaturation is produced to the rate at which crystals are formed. Continuous processes may operates at steady conditions and if this is the case then the supersaturation and indeed all other parameters will be constant with time [26]. Fresh fluid of controlled supersaturation comes in contact with the sample thereby avoiding the possible recirculation of pre-formed colloidal particles that may influence scale formation and complicate the analysis.

8.1.3 Combined study of bulk and surface scaling

Existing scaling indices are based on extensive experimentation of bulk scaling parameters but combined assessment of bulk and surface scaling seems to be critical for understanding scale formation [183]. Investigations such as one carried out by Morizot and Neville [172], Cheong *et al* [80] showed that crystals formed on the surface are rarely the result of a secondary deposition process after the precipitation mechanism which occur in the bulk. This experimental set-up allows to study both homogeneous crystallization in the bulk and heterogeneous surface crystallization.

8.1.4 Control of different experimental parameters: flow, temperature and inhibitor addition.

The study of nucleation and growth processes requires a suitable methodology to assess the effects of temperature, flow and inhibitor addition in a single system. The once-through real-time visualization flow rig system allows these factors to be considered. The configuration of the cell allows only a laminar flow regime so as to avoid recirculation of fluids in the cell.

8.2 Bulk precipitation and surface scaling

This section intends to discuss some of the results presented in Chapters Five and Six with respect to bulk precipitation and surface scaling for both low SR (10, 15, 25, 45 and 60) and high SR (70 and 90). It is important to determine

whether the calcium carbonate particles are deposited by adhesion or the crystals are formed directly on the surface.

As shown in Figure 6-3, there were no pre-precipitated crystals in the bulk for SR values of 10, 15, 25, 45 and 60 with turbidity of Zero FTU as the induction time for bulk precipitation is longer than the residence time (3 secs) from mixing to sample surface. Higher SR of 70 and 90 with turbidity values of 23 FTU and 58 FTU shows that crystals were precipitated in the bulk. Results of the SEM images of the bulk filtrate on 0.2μm membrane to further verify the turbidity measurements were presented in Figure 6.4. No crystals are formed on the membrane for the low SR values of 10, 15, 25, 45 and 60 while crystals were observed for the high SR values 70 and 90.

Within the range of SR (10-60) surface scaling is driven by surface crystallisation with surface induction, nucleation and growth taking place at solid/liquid interface rather than the adhesion of bulk precipitate. There are no pre-precipitated crystals in the bulk solution to adhere to the surface. Recently, Cheong *et al* [20] showed evidence that regarding crystallisation, the scale layers observed on a surface was directly formed onto the surface. Hao Wang *et al* [184] suggested from SEM analysis of crystals orientaion on stainless steel that there are two types of ways in which crystals arrive on the surface, large crystals with size about 10μm almost the same as those in the bulk solution are deposited directly from bulk solution while the small crystallites are suggested to nucleate and grow at the surface.

The results from this study show that surface scaling is not always the adhesion of pre-precipitated crystals from the bulk solution. Particles are formed directly on a surface via true surface heterogeneous nucleation [177]. The minimal contact points of the polished steel with roughness of 0.01μm used would reduce the contact area between the crystals and surface and makes adhesion difficult [28, 80]. At low SR, deposition is initiated with heterogeneous nucleation on the substrate and subsequent growth of isolated crystals. A supersaturation of 40 fold (SR $\geq$ 40) is necessary to trigger

homogenous nucleation but this value can be strongly lowered by the presence of impurities or in the case of heterogeneous nucleation where the wall lowers the supersaturation [42, 154].

8.3   Comparison between surface and bulk induction

The induction time is the time between supersaturation state and the detection of the first crystal particles [26, 36]. Plots of the induction times as a function of the saturation ratio are defined as the stability diagram used for defining metastability limits of the supersaturated solutions [36]. For the same set of SR values of 10-60, surface scaling induction time from the *in-situ* flow cell was compared with bulk induction time from conventional bulk jar tests at 25°C and 20ml/min as shown in Figure 8-2. SR 10, 15, 25, 45 and 60 all have a distinct induction period for bulk precipitation. However, the same cannot be said of the surface scaling time as no measurable surface induction time existed for SR 45, 60, 70 and 90.
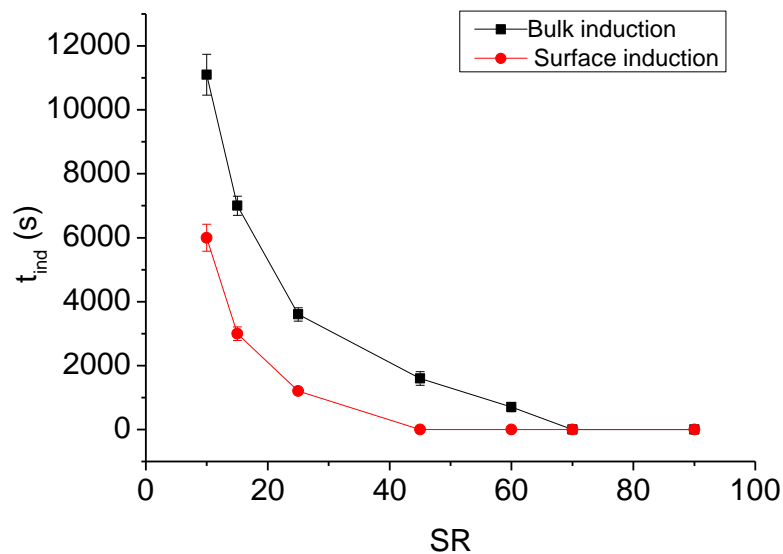
Figure 8-2: Surface and bulk induction

With regards to the trends of the curves, a similar exponential relationship between the induction time and SR are observed for both surface and bulk induction. This is comparable to observations that the induction time is

inversely proportional to the degree of saturation [36, 37, 62]. However, the study shows that the induction time varies between bulk and surface scaling. For the same values of SR, the induction period is shorter for the surface which shows that the nuclei attain a stable or critical size faster on the surface than in the bulk.

The variation in the induction time is significant at low SR, (SR $\leq$ 45 at 25ºC) where there is a huge difference in the induction time between the bulk and surface. As such, there is an effect of the surface characteristics which may be attributed to the surface topography on the induction time [28, 142]. At higher SR, the surface effects are less important as the difference in induction time for bulk precipitation and surface scaling tends to decrease or disappear with increasing SR.

At low SR,

$$t_{surf} \ll t_{bulk} \tag{8.1}$$

At high SR,

$$t_{surf} \sim t_{bulk} \tag{8.2}$$

Where, t_{surf} is the induction time for surface scaling and t_{bulk} is the induction time for bulk precipitation.

The differences in induction time especially at lower SR highlight the importance of incorporating surface induction in scale formation and inhibition treatments [80]. The large difference in induction time at low SR potentially means that in a flowing system, close to the mixing point, more scale will be formed on the surface with little or no scale formation in the bulk solution. However, the little or no difference between bulk and surface scaling induction time at high SR means that the amount of scale formed on the surface compared to the bulk solution will be reduced depending on the ratio of

surface area to the bulk volume. The surface and bulk scaling with increase in SR is illustrated schematically in Figure 8-3.
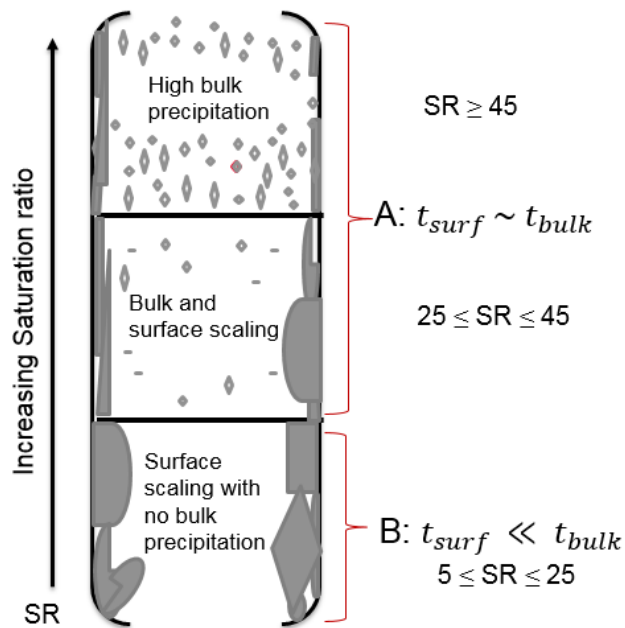
Figure 8-3: Region of surface and bulk scaling with increase in SR

Bulk induction time and crystallization rate could not be accurately used to predict surface scaling. The variation between induction times and crystallization kinetics means that the Minimum Inhibitor Concentration (MIC) for bulk precipitation will not be accurate and effective to inhibit surface scaling. Setta *et al* [137] showed that the MIC for surface is different from the MIC for bulk precipitation.

Figure 8-4 shows bulk and surface induction ratio, T_{ind} as a function of SR. Where,

$$T_{ind} = \frac{Bulk\ induction\ time, t_b}{Surface\ induction\ time\ t_s}$$

$$y = 0.0041x^2 - 0.0394x + 1.6667$$
$$R^2 = 1$$
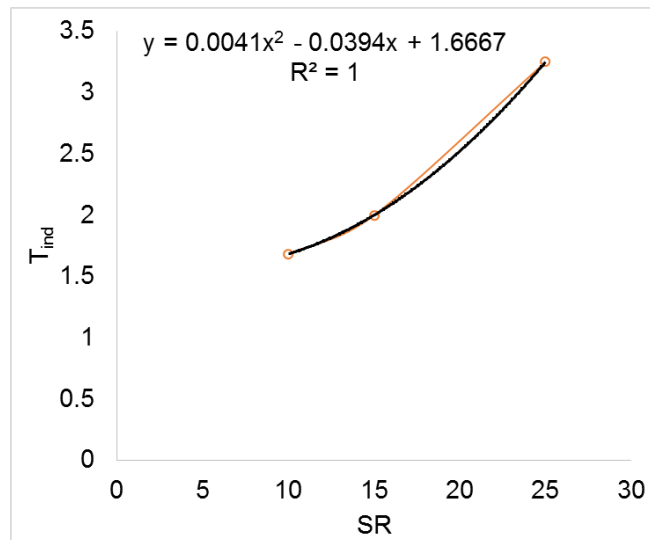
Figure 8-4: Bulk and surface induction as a function of SR

The relationship between bulk and surface induction as a function of SR does not show a linear correlation but a polynomial of second order. This indicates a different kinetics for both processes and therefore different rates of crystallization.

The surface induction time could be affected by factors such as SR, temperature, flow rates and surface topography. For this study, a very smooth surface, polished austenitic stainless steel sample with surface roughness (R_a) of 0.01µm is used. However, in realistic industrial scaling conditions, very rough surfaces are encountered. The significant difference between the surface induction time and bulk induction time at low SR as shown in Figure 8-2 makes it essential to study the effects of surface roughness on the induction time especially the heterogeneous nucleation at low SR. It is expected that the surface induction time and consequently crystallization rate will vary with change in surface roughness and substrates. Generally, low surface energy and surface roughness is associated with low scale formation [28, 111].

8.3.1 Surface scaling induction time as a function of saturation ratio

The surface scaling induction time which is taken as the time for the first crystal to be detected on the surface plotted against the SR is presented in Figure 8-5. In all cases, the crystals could be quantified as soon as their sizes reached 1µm. For the range of low SR 10-45 with low ion concentrations, the surface induction period observed in the scale growth process tends to decrease exponentially with increasing SR. It is a direct consequence that only heterogeneous surface nucleation is taking place at relatively small rates and is in contrast to the homogenous nucleation in static conditions assumed by most models [36]. At low SR, the surface induction time resulted from the time taken for the distribution of molecular clusters for the system to reach a quasi-steady-state and form a stable nucleus and for the nucleus to attain a visible size [35].
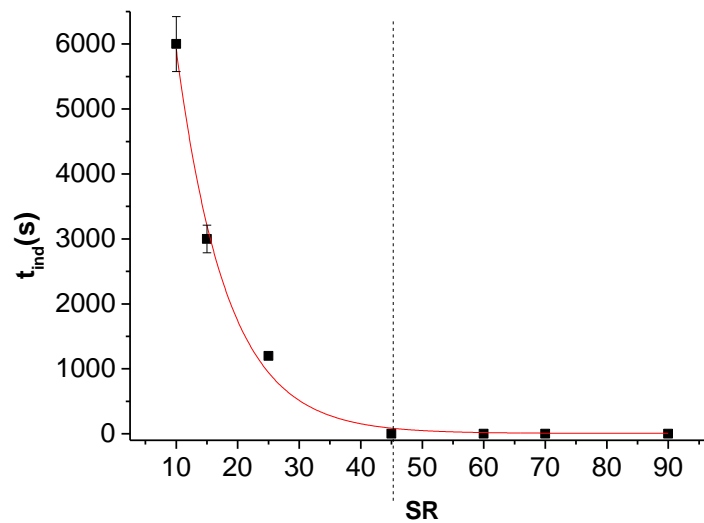
Figure 8-5: Surface scaling induction time as a function of SR

In the SR range 60-90, the rate of nucleation is fairly large compared to SR values of 10-45, and the substrate is rapidly covered by scale. Thus, there is no measurable induction time. This is comparable to observations at high SR by Anastsios [185] and Stamatakis *et al* [36]. In addition, homogeneous bulk precipitation and subsequent adhesion of crystals to the surface appear to

take place in this higher SR. There is a weak adherence with regards to crystals migrating from the bulk to stick onto the surface. The adhesion being the resultant force between attractive Van der Waals forces and the repulsion from adsorbed double layer forces [28]. When the particulate material that adheres to the surface is about 1µm, the net interaction between particulates in a liquid medium and the surface can be described by the classical Derjaguin-Landau-Verwey-Overbeek (DLVO) theory which describes the chemical interactions where the force of adhesion is the sum of the electrostatic forces and the Van der Waals forces. However, when nucleation proceeds in a heterogeneous manner, there is expected to be a strong interaction between the nucleating phase and the substrate. Thus, a compact and tough structure is formed due to strong adherence of the crystals to the surface [20, 80].

Based on the classical nucleation theory, the induction time of CaCO$_3$ will obey the relationship [35]

$$\log t_{ind} = BT^3 (SI)^{-2} + C \qquad \textbf{(8.3)}$$

Where SI denotes the saturation index (log SR), C is a constant, and B is a function of interfacial tension, γ.

From Figure 8-5, which shows the surface induction as a function of SR at 25°C, two cases can be observed as follows:

Case 1: For $10 \leq$ SR ≤ 25, $t_{ind} \neq 0$.

Therefore, plot of $\log t_{ind}$ against $1/(\log SR)^2$ at this condition yields a linear fit as shown in Figure 8-6.

Case 2: For $40 \leq$ SR ≤ 90, $t_{ind} \sim 0$, $\log t_{ind} = 0$, Thus, $\log t_{ind}$ against $1/(\log SR)^2$ is invalid

Fitting the relation with the results obtained for surface and bulk scaling induction time at 25°C at a constant flow rate of 20ml/min.
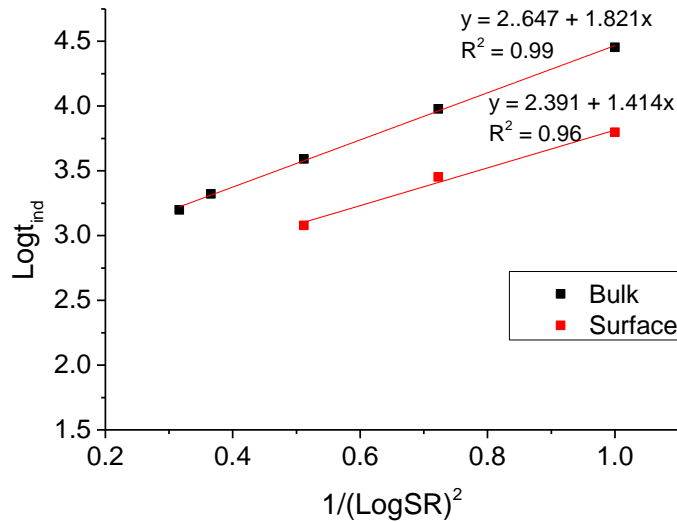
Figure 8-6: SI dependence of the induction time at 25°C

The relationship allows surface scaling time of very smooth surfaces for SR values 10-25 at 25°C and flow rate of 20ml/min to be estimated as follows.

From equation (8.3), $BT^3 = 1.414$, the slope of the plot of $\log t_{ind}$ against $1/(\log SR)^2$ is a function of temperature and interfacial energy. Therefore for surface scaling at 25°C and 20ml/min, equation 8.3 becomes

$$\log t_{ind} = 3.71 \; X \; 10^{-7}(SI)^{-2} + 2.391 \tag{8.4}$$

While for bulk scaling at 25°C

$$\log t_{ind} = 4.82 \; X \; 10^{-7}(SI)^{-2} + 2.647 \tag{8.5}$$

This could be useful as a design tool for predicting t_{ind} before scaling starts. The interfacial energy can be calculated from the relationship described in equation 2.10 which is given as:

$$B = \frac{\beta \gamma^3 V_m^2 N_A^2 f(\theta)}{(1.3R)^3}$$

The calculated values of interfacial energy are given in Table 8-1

Table 8-1: Values of calculated interfacial tension

	Temperature	Flow rate (ml/min)	γ (mJ/m^2)
Surface scaling	25°C	20	0.012
Bulk precipitation	25°C	20	1.321

Larger values of interfacial tension reported in other studies are due to consideration of induction measurements simply during homogeneous nucleation [46, 186]. However, the low value for interfacial energy obtained in this study indicates the effects of heterogeneous nucleation at low supersaturation. It also could be a result of the techniques and the experimental conditions used for this study.[80]

The effects of temperature and flow rates on the surface induction at the range of SR 10-60 are discussed in the following sections.

8.3.2 Effects of temperature on surface induction

Previous works found a linear correlation between the induction time and SR for a given temperature [38, 152, 156]. Most of these methods to assess the effects of temperature are based on initial supersaturation ratio in the bulk as the composition of ions varied with scale formation. In this study, the assessment is made with the SR maintained constant in the flow rig and the induction is compared for both 25°C and 40°C. Figure 8-7 shows the variation of the induction time at the two temperature tested in this study to determine the influence of temperature. The induction time is shown to decrease with increase in temperature from 25°C to 40°C for the same degree of SR which is comparable with observations by Stamatakis [36]. The effect of temperature on induction time is greater at low SR while it becomes less significant at high SR. At low SR, where heterogeneous surface crystallization occurs, the surface integration or reaction of the ions at the surface is promoted at higher temperature resulting in rapid formation of stable nuclei on the surface.
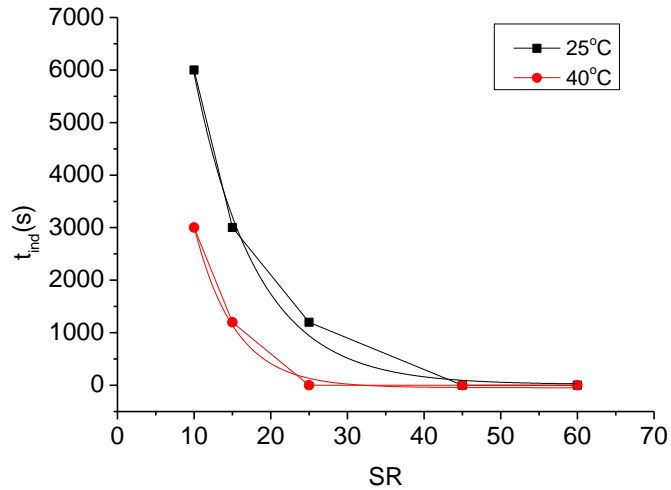
Figure 8-7: Influence of temperature on surface induction time at constant saturation.

Yang *et al* [187] also observed that an increase in surface temperature will lead to a corresponding increase in the reaction rate.

Considering the classical nucleation theory expressed in equation 8.3. At 40°C, $t_{ind} \sim 0$ for SR $\geq$ 25, therefore,

$$\log t_{ind \sim 0} \text{ (For SR} \geq 25 \text{ at } 40^{\circ}\text{C)}$$

As such, the linear relationship between the $\log t_{ind}$ and $1/(\log SR)^2$ is only valid at 40°C for the SR values of 10 and 15.

8.3.3 Effects of flow rates on induction

Figure 8-8 shows the plot of surface induction for different flow rates for SR 10, 15, 25, 45, 60. At low SR value of 10, no scaling takes place in the rig at the flow rate of 10ml/min within the 4 hour test. This is the combined effect of the low ionic concentration and low rate of transport of the molecules to the surface for reaction to take place. There is no sufficient concentration of ions at every time to form stable nuclei greater than the critical size for nucleation and growth to take place before dissolution. At low SR values of 15 and 25, an induction period is observed in the scale growth process. However, at the fixed temperature of 25ºC, the surface induction period decreases with

increasing fluid velocity as the movement of solvated ions to the surface is faster at higher flow rates.

Yang *et al* [99] observed the induction time to be decreasing with increasing flow rate, and consequently resulted in an increase in the growth rate. The velocity at which the ions reach the surface has a pronounced effect on the time required for the nuclei to reach a critical size and subsequently for the crystal to grow to a measurable size which tends to be inversely proportional to ion concentration. At high SR values of 45 and 60, there is no measurable surface induction period at the different flow rates.
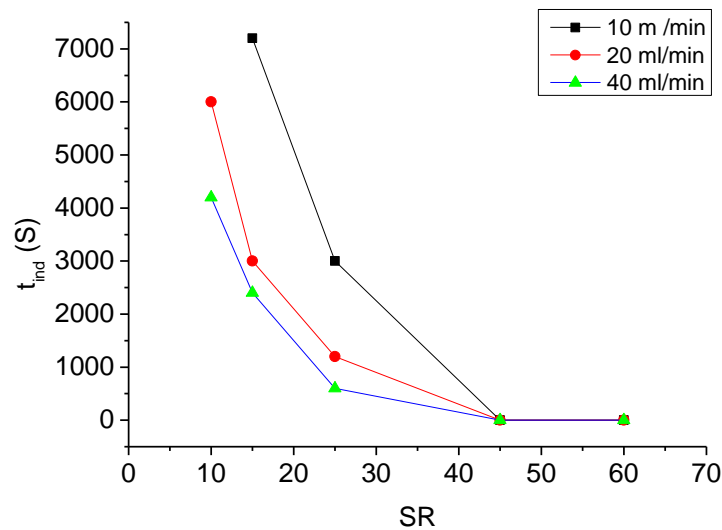
Figure 8-8: Influence of flow rate on surface induction time at constant saturation.

In relation to the classical nucleation theory expressed in equation 8.7,

For surface induction, $t_{ind} \to \infty$ for SR = 10 at Q = 10ml/min, t_{ind} = 0 for Q = 40ml/min.

Therefore, $\log t_{ind \to 0}$ at 40 ml/min and SR = 10 at 10ml/min.

The linear relationship between the $\log t_{ind}$ and $1/(\log SR)^2$ is limited to flow rate of 20ml/min at a fixed temperature of 25°C.

8.4 Surface crystallization mechanisms

Scale management strategies require the understanding and being able to predict the characteristics of scale formation [185]. Significantly less information exists for the mechanism of scale formation on a solid surface [21]. In most experiments, it is not possible to determine whether nucleation and crystal growth occur simultaneously or consecutively. Also, there is a strong likelihood of complications caused by heterogeneous nucleation [49, 103].

The analytical data in this study were exploited using the model proposed by Beaunier *et al* [42] and modified by Euvrard *et al* [49] as described in chapter four (4.4.3) to develop a mechanistic understanding of surface crystallization. The model assumes that the number of active nucleation site for a unit area of the substrates is fixed, and that each nucleation event is independent. Therefore, the probability of nucleation at a certain time depends on the number of free sites. However, the models considered only the initial stage of growth ($t < 1000s$) and SR was decreasing with time.

In this present study, SR was kept constant and longer time (4hrs) of scaling was considered. The results obtained experimentally allow the type of nucleation to be assessed. With reference to equation 4.1 and 4.2, for progressive nucleation, actual surface coverage $S_t(\%)$ is proportional to t^2 while for instanteneous nucleation, $S_t(\%)$ is proportional to t. As a result of overlapping crystals, the St (%) differs from extended surface coverage S_{ext} (%) where there is no overlapping crytals.

The actual surface area S (t) is related to the extended surface area S_{ext} (t) as

$$S_{(t)} = 1 - \exp[-S_{ext}(t)] \qquad \textbf{(8.6)}$$

If there is no overlap of crystals or at the early stage of crystallization process

$$S_{ext}(t) = S(t) \qquad \textbf{(8.7)}$$

For instantaneous nucleation, all sites are assumed to be converted into nuclei at the very early stages. The fractional area covered by scale increases linearly for quasi-instantaneous nucleation and quadratically for progressive nucleation. This is also strong support for the assumption of the linear increase in the area of the individual nuclei during the process of growth [42].

8.4.1 Mechanisms of surface crystallization at low SR

The plots for the extended surface coverage as a function of time, t^2 at SR = 10, 15 and 25 are presented inFigure 8-9. A linear relationship was observed with the extended surface coverage $S_{ext}(t)$ againt t^2 at SR values of 10, 15 and 25. This shows a progressive nucleation mechanisms as defined by the model below.

$$S_{ext}(t) = \frac{MK_1N_oAt^2}{\rho} \qquad (8.8)$$
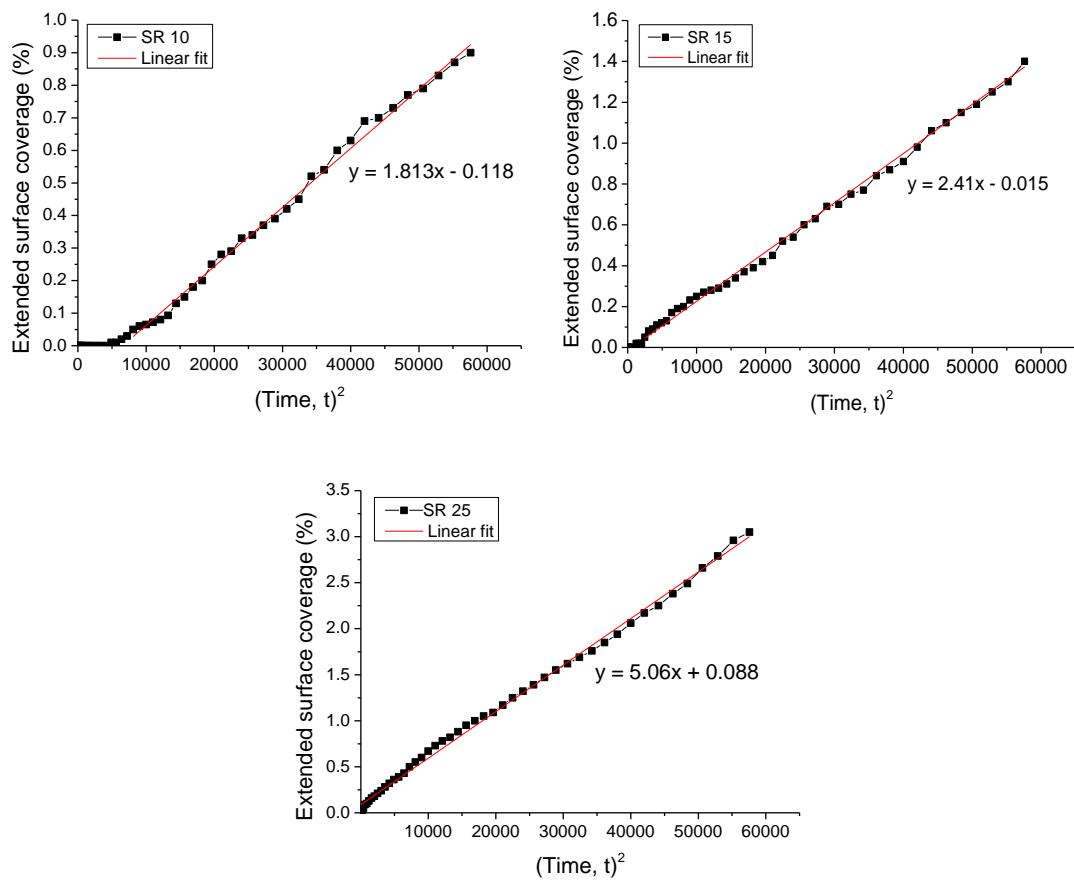
Figure 8-9: Extended surface coverage as a function of t² at low SR

Deposition is initiated by heterogeneous nucleation on the surface and subsequent growth of isolated crystals. The mechanisms here is solely surface crystallization with no pre-precipitated crystals in the bulk. In a comparable result, Karabelas [185] showed that at small supersaturations the deposition rate is quite small and tends to increase with supersaturation. Nucleation continues rather slowly and progressively while growth of already stable nuclei occurs simultaneously. In relation to the curve for surface induction time as a function of SR as shown in Figure 8-5, heterogeneous nucleation takes place in this range.

Plotting the the extended surface coverage $S_{ext}(t)$ againt t, for the same set of low SR values shows that the crystallization mechanism is not entirely progressive especially at longer experimental time towards the end of the process. Figure 8-10 shows that the initial stage of crystallization is progressive as illustrated with the exponential part of the curve while the latter stage is linear indicating no further nucleation of crystals but increase in average sizes only.
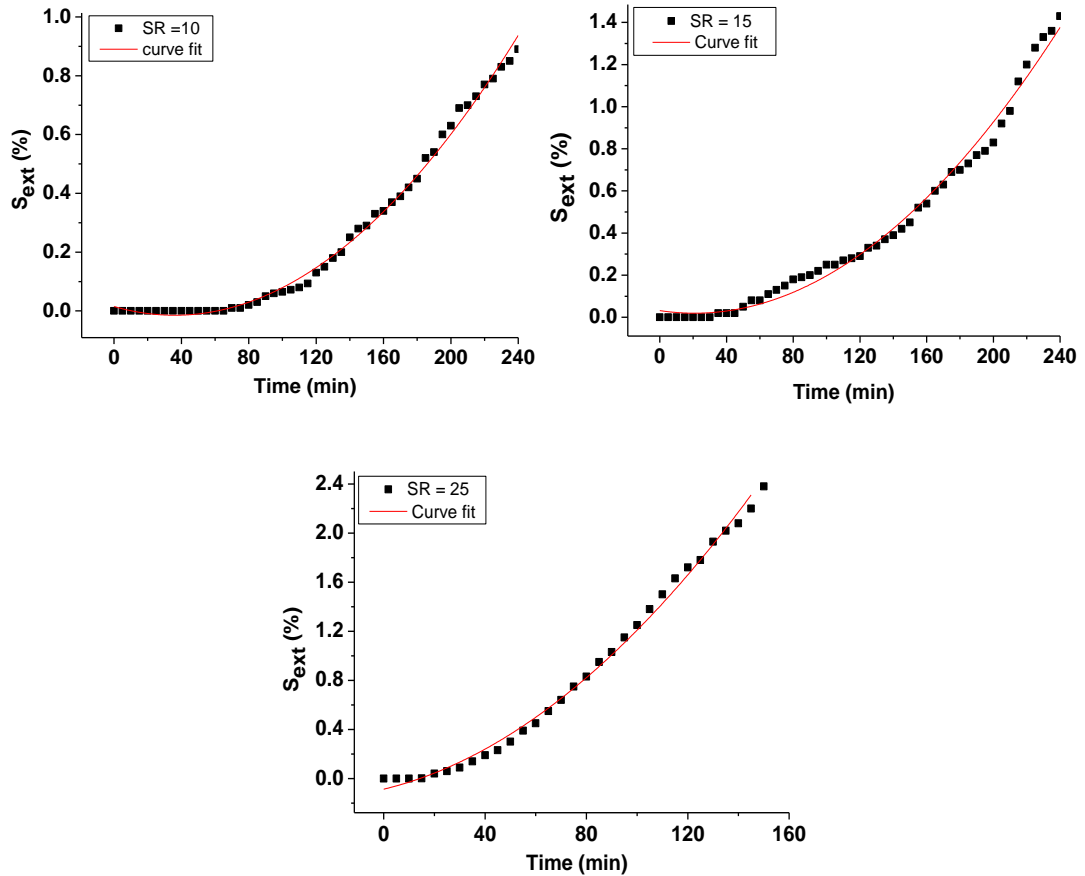
Figure 8-10: Extended surface coverage as a function of time

From the curve fittings and empirical model, two stages, exponential and linear can be observed (

Figure 8-11). The exponential part at the early stage of the curve indicates the initial stage of progressive nucleation where both nucleation and growth proceeds simultaneously, the surface coverage on the surface in the later stages is driven by crystals growing with increase in the concentration of ions on the surface without further increase in the number of crystals.
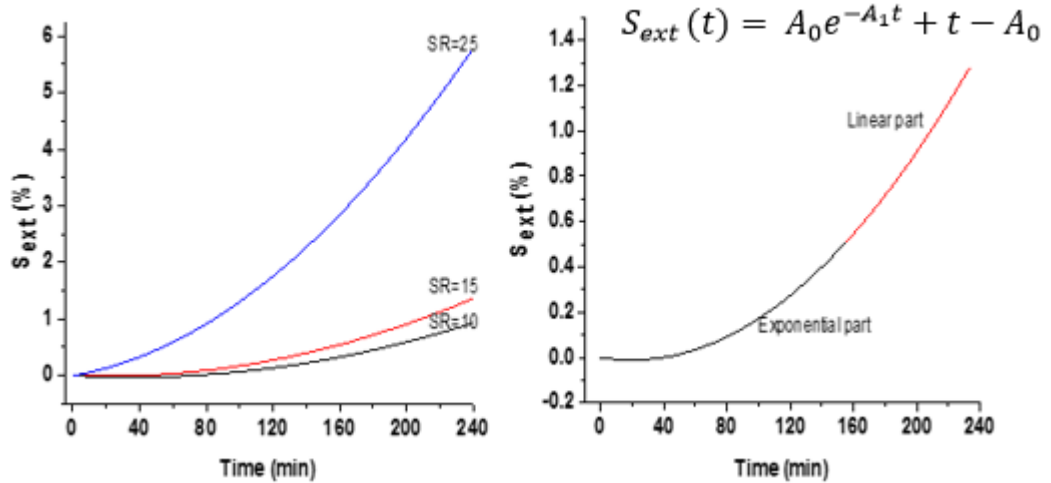
Figure 8-11: Surface scaling mechanisms at low SR

With this mechanisms, for the range of SR 10 -25, during the first instant, the curve has a parabolic shape, however, it becomes linear towards the later stage resulting in an empirical model given below:

$$S_{ext}(t) = A_0 e^{-A_1 t} + t - A_0 \qquad (8.9)$$

A_0 = constant, A_1 is a function of SR, t is scaling time and S_{ext} is the extended surface coverage without overlap of crystals.

A schematic illustration of early stage progressive nucleation is given in Figure 8-12. Active sites are progressively generating nuclei while growth of nuclei that have reached a stable size continues simultaneously. For the crystals to nucleate there is need for a high concentration of ions on the surface to cause nucleation and because it is at low SR, it takes some time to reach a point of nucleation whereas it is easier for crystals to grow once they are formed or nucleated. As the concentration is gradually increasing on the surface, more crystals will nucleate until there are no more active sites for the SR to generate more nuclei, growth continues as the supersaturation is maintained constant.

Stage 1	Stage 2

Stage 3	Stage 4
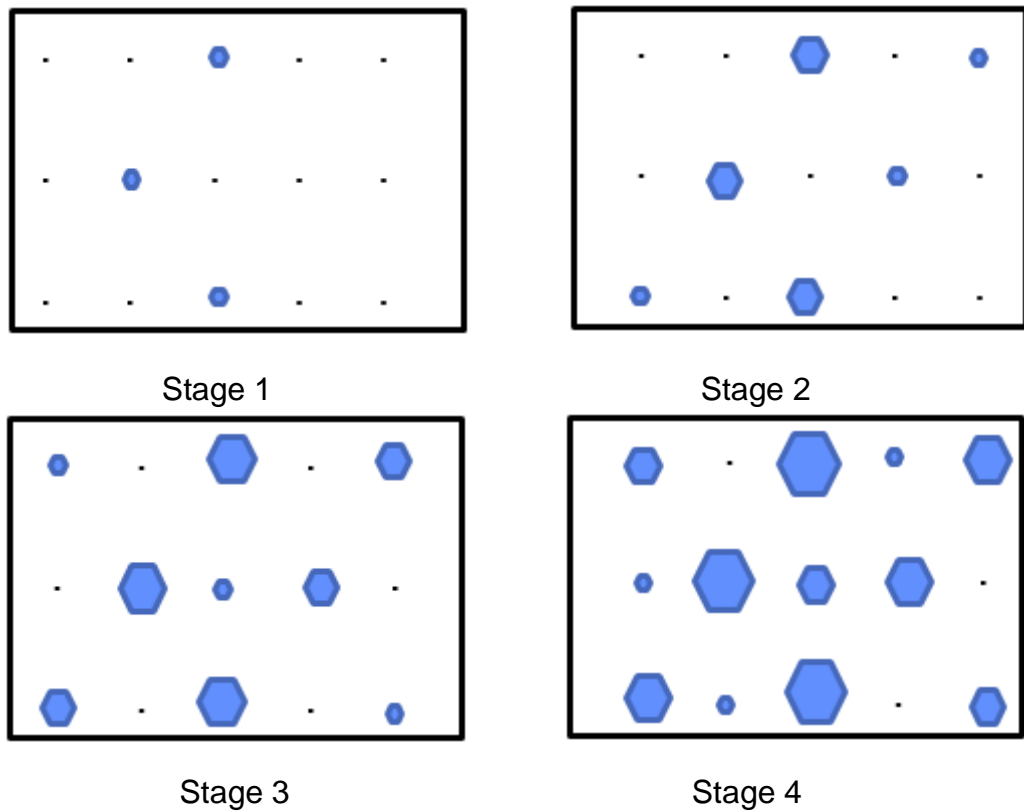
Figure 8-12: Mechanisms of crystallization at low SR

8.4.2 Mechanisms of surface crystallization at high SR

Figure 8-13 shows the mechanisms at higher SR > 45. The mechanism is solely instantaneous as indicated by the plots for SR of 60 and 70.

For instantaneous nucleation:

$$S(t) = \frac{MK_1N_o t}{\rho} \tag{8.10}$$

Therefore, plotting the actual surface coverage, $S(t)$ against time, t for SR values of 60 and 70 gives a linear relationship as shown in Figure 8-13.
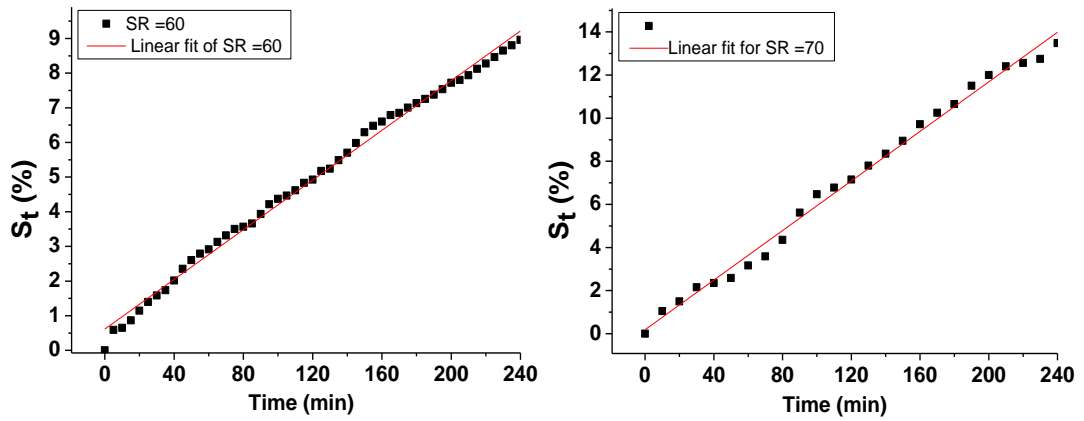
Figure 8-13: Actual surface coverage as a function of time

A linear fit generated by the fast and instantaneous nucleation can be observed in Figure 8-14. At high concentration of ions, there is a faster kinetics and more ions are rapidly nucleated. The nucleation is instantaneous and growth dominated at the later stage once there are no more active sites. Gabrielli *et al* [165] showed diffusion process control the growth of electro-crystallised calcium carbonate on a substrate of gold and the surface coverage S(t) to be a linear function of time.
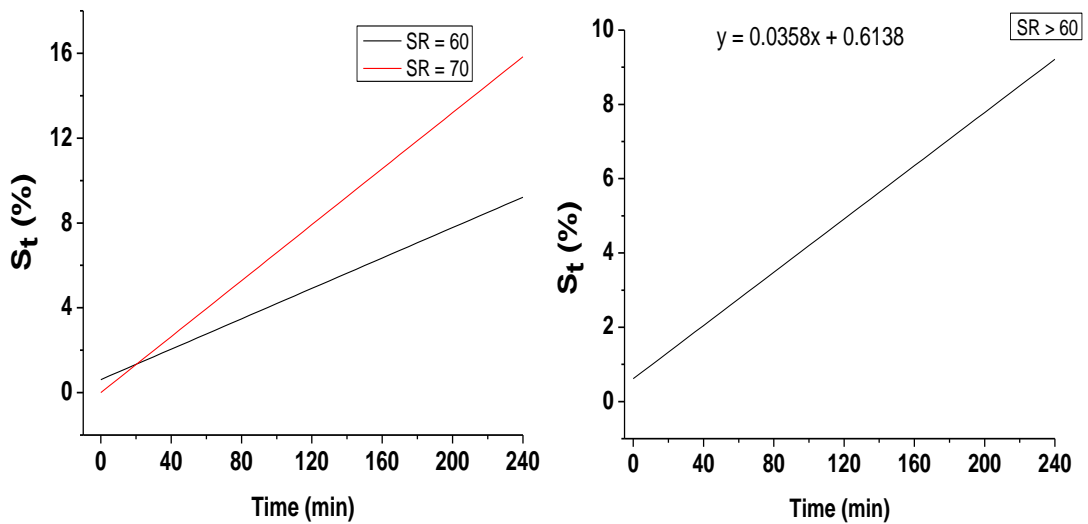
Figure 8-14: Surface scaling mechanisms at high SR

Figure 8-15 illustrates the instantaneous nucleation mechanisms. The early stage of crystallization is dominated by rapid nucleation with all available active sites generating nuclei in a relatively short period. The growth of the

165

crystals takes place after the nucleation stage. This is similar to the observations by Beaunier *et al* [42] for high concentrations of calcium ions where it was assumed that difusion controls the process. Also in this range of SR, the rate of nucleation is fairly large and the substrate is rapidly covered by deposited mass, thus there is no measurable induction period [185]. It will be added that homogeneous bulk precipitation and adhesion onto the surface takes place in this range of SR (Figure 8-5) along the flow and this is intesified with incerease in supersaturation. The $CaCO_3$ crystals are formed in a shorter time and grow progressively as a result of constant supersaturation.

| Stage 1 | Stage 2 |

| Stage 3 | Stage 4 |
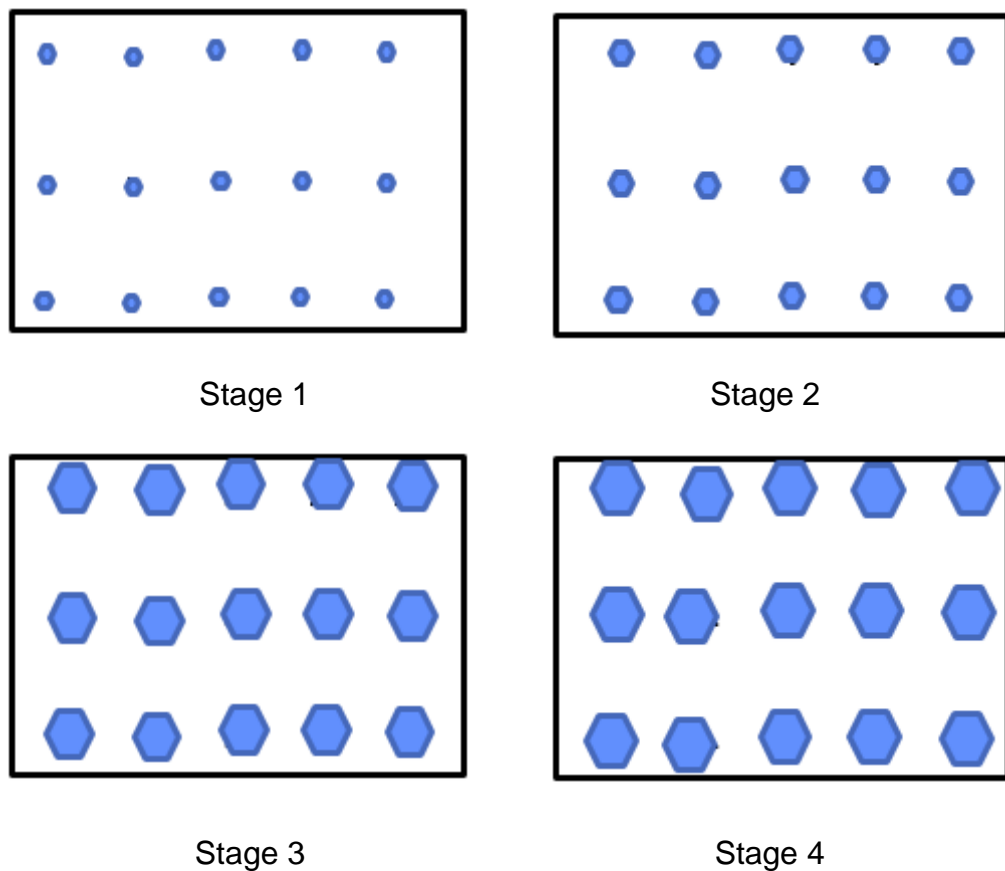
Figure 8-15: Schematic illustration of crystallization at high SR

The model makes it possible to determine whether nucleation and crystal growth occur simultaneously or consecutively at low and high SR. It is shown that progressive nucleation does not exist at high SR as shown in Figure 8-16.

(a) low SR	(b) high SR
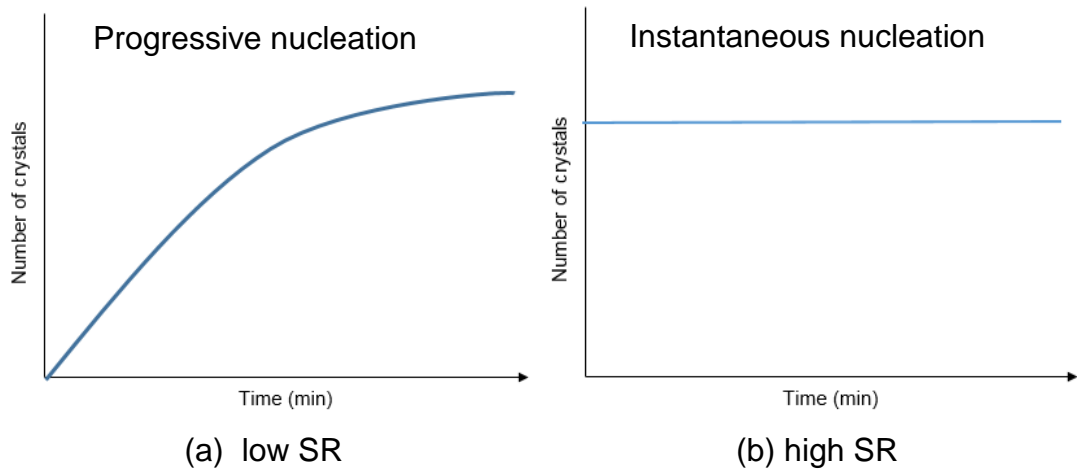
Figure 8-16: Progressive and instantaneous nucleation

Progressive nucleation occurs at low SR values of 10-45 and instantaneous nucleation takes place at high SR values of 60-90. A more precise imaging techniques such as the synchrotron x-rays imaging would probably be able to detect more nuclei earlier than observed. As such, there is a likelihood of progressive nucleation even at high SR. In both cases, the surface coverage in the later stage is driven by crystals growing without further increase in the number of crystals. This shows that there is a finite nucleation period. The period of nucleation illustrated with a schematic diagram in Figure 8-17 is the length of time the number of crystals is increasing. This is taken as the time of detecting the first crystals on the surface to the time where no new crystals are formed.

The overall surface crystallization consists of two regions which are illustrated in Figure 8-17.

(a) Region of progressive/instantaneous nucleation, equivalent to the period of nucleation
(b) Region of no further nucleation, dominated by growth of crystals
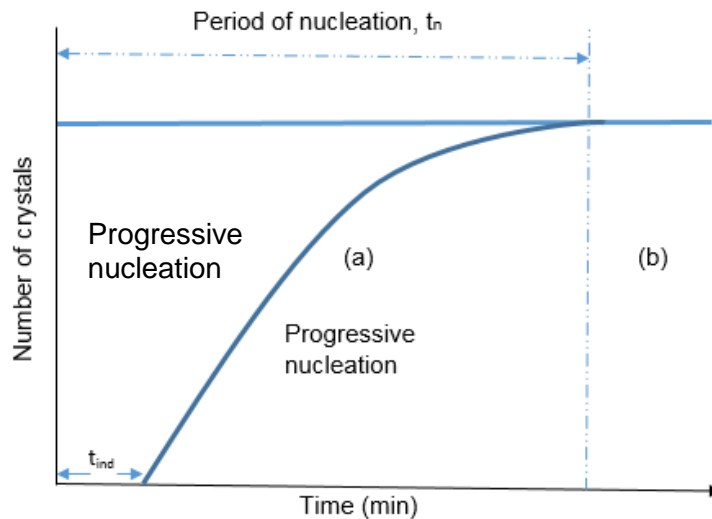
Figure 8-17: Period of nucleation

In the model, region a, for the progressive nucleation will be very essential when trying to look at the interference between nucleation inhibitors and how scale layer grows. The period of nucleation, t_n in relation to the time taken for the inhibitor to interact with the nuclei may be longer for progressive or shorter for instantaneous nucleation. Region (a) is therefore valid in order to study the efficiency of inhibitor in terms of the rate of adsorption. The linear part, region (b) is very important when trying to model a well, for a long time scaling in order to stimulate crystal growth layer.

A hypothetical diagram, Figure 8-18 is generated based on the mechanistic model for low and high SR by plotting the SR against the period of nucleation. It illustrates the mechanisms of $CaCO_3$ scale formation system at 25°C within the range of SR 10-90. Across the diagram from left to right shows the period of nucleation and indicate the region of instantaneous and progressive nucleation. In this range, SR value of 45 coincides with the transition from instantaneous to progressive nucleation.
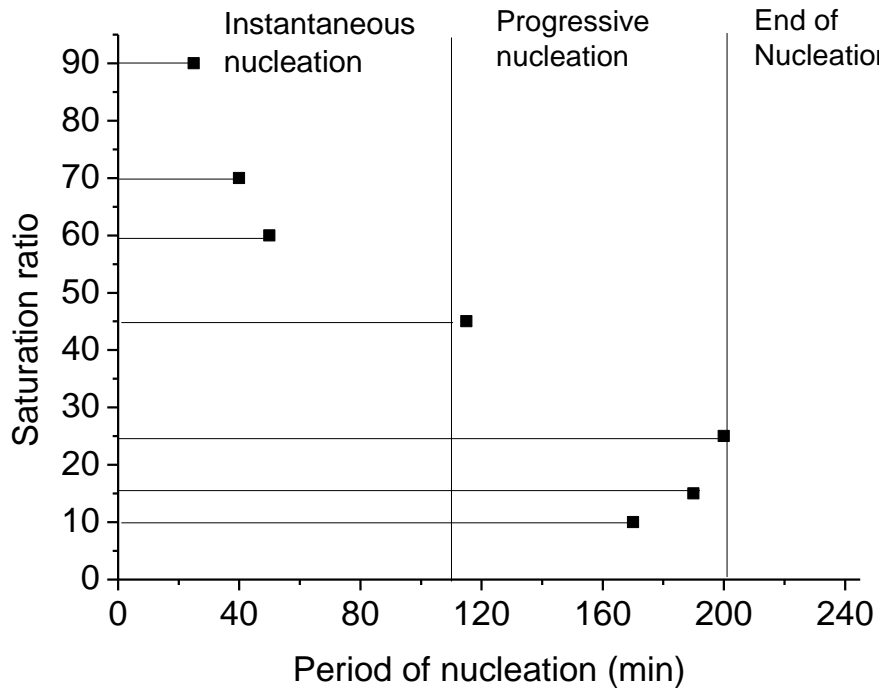
Figure 8-18: Nucleation period of heterogeneous crystallization at different saturation ratio, T = 25°C, Q = 20ml/min.

It can be observed that in the range of instantaneous nucleation, the nucleation period decreases with increasing SR or ionic concentrations. It takes a lesser time for the active nucleation sites to completely generate nuclei due to higher concentrations of ions aided with diffusion from the bulk solutions. In addition to homogenous bulk crystallization, there is possibility that crystallization may also occur by heterogeneous nucleation. At low SR, within the progressive nucleation range, the nucleation period increases with increasing SR. Also in this range, only heterogeneous surface crystallization occur as the bulk induction time is longer than the residence time. Heterogeneous nucleation is energetically more favourable on the surface according to the classical nucleation theory due to the lowering of surface energy of the nucleus and the substrates upon interfacial contact [35]. Conditions favourable for the heterogeneous nucleation of calcium carbonate are mainly determined by the electrostatic interaction between the hydrated calcium ion and the substrate [53].

Across the SR values 10-90, no nucleation process takes place in the later stage as all available sites have generated nuclei. The model can be potentially exploited to predict the types of nucleation and the mechanisms of CaCO$_3$ surface scaling in the range of SR 10 – 90 at 25°C.

At low SR values 10-15 and high SR values 45-90, the mechanistic model in terms of the relationship between the extended surface coverage and time is unaffected by an increase in temperature from 25°C to 40°C. However, the mechanisms changes with increase in temperature from 25°C to 40°C at SR value of 25. Increase in temperature increases the rate of formation of stable nuclei leading to faster rate of surface coverage. Thus, there is a change from progressive to instantaneous nucleation mechanisms (see Figure 8-19)
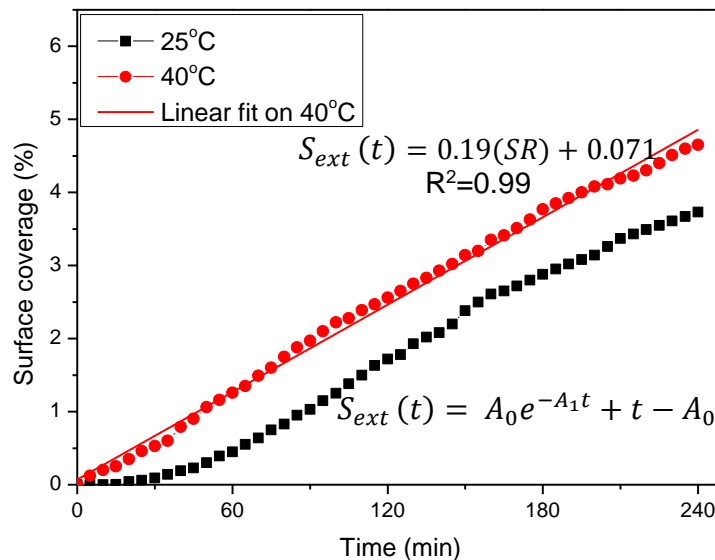
Figure 8-19: Nucleation mechanism as a function of temperature.

The number of nuclei formed per unit time and volume occurs more rapidly at higher temperature according to the Arrhenius relation described in equation 2.15 and 2.16. The molecules possess more energy for a faster reaction. As T increases, $\exp(\frac{-\Delta G_c}{KT})$ increases, therefore the nucleation rate, J increases[35].

8.4.3 Saturation ratio; dynamic values

Results from the dynamic study of changing between SR values of 25, 45 and 70 presented in Chapter Six (6.5.3) are further discussed with respect to the crystallization mechanism. The model is valid when all factors are constant. In the field, there could be an upset to the conditions in a continuous process and the supersaturation will change with time [46].

The surface coverage presented in Figure 8-20 gives an overall assessment of the effects of change in SR during test. The plot is divided into three regions. Region 1 depicts the initial 4hrs of surface crystallization at SR 25 in two separate experiments. Region 2 represents the surface coverage when the SR were increased from 25 to 45 in one case and from 25 to 70 in the other case. Region 3 represents the return of SR to 25 in both cases. The results of the crystallization rate determined from the linear fit for each region are presented in Table 8-2.
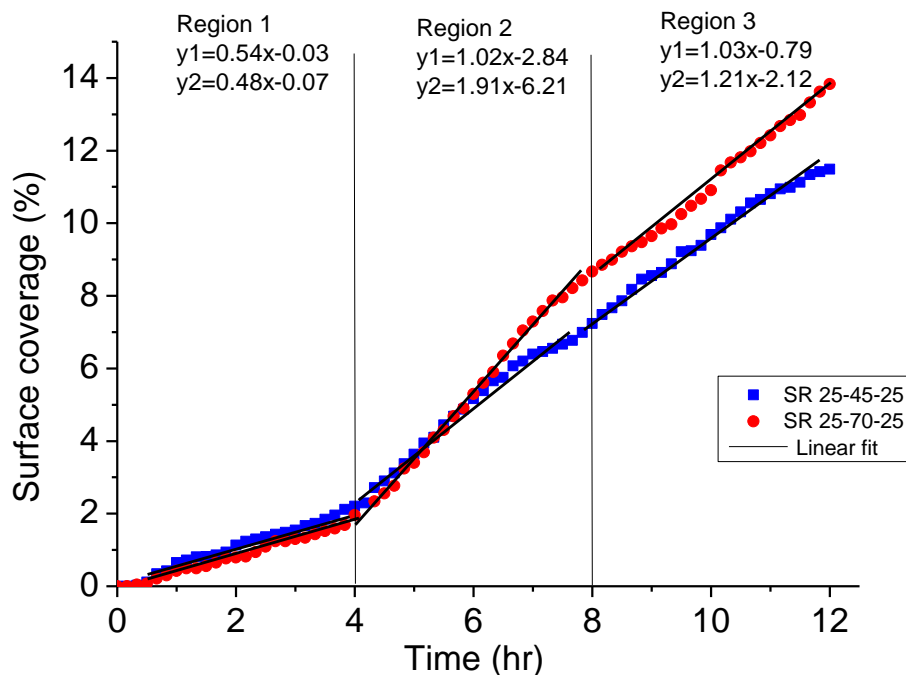
Figure 8-20: Surface coverage for dynamic test as a function of SR

Table 8-2: Crystallization rates for different regions.

SR	Crystal	Linear Equation	Rate (µm²/s)
25-45-25	Region 1	$y_1 = 0.54x - 0.03$	0.54
	Region 2	$y_1 = 1.02x - 2.84$	1.02
	Region 3	$y_1 = 1.03x - 0.79$	1.03
25-70-25	Region 1	$y_2 = 0.48x - 0.07$	0.48
	Region 2	$y_2 = 1.91x - 6.21$	1.91
	Region 3	$y_2 = 1.31x - 2.12$	1.31

With reference to results of dynamic experiments already presented in the result section in chapter six (6.5.3). In region 1, the surface coverage is as a result of initial surface nucleation and subsequent growth of crystals while in region 2, more new crystals are nucleated by increasing the SR to 45 and 70 in the respective cases. The surface coverage rate in the third region when SR was reduced back to 25 is only due to crystals getting bigger in size with no further nucleation suggesting that all available active sites at the existing SR have generated nuclei. Growth of crystals continues as the solution supersaturation is maintained constant.

The fastest rate of crystallization in the second region corresponds to new crystals being formed on the surface simultaneously with the growth of existing crystals. This is supported by the results of experiments made in the presence of strongly adsorbed anions. This shows that for a given supersaturation, a sufficient number of growth sites must be provided initially for uncomplicated high-order growth otherwise new sites must be generated by nucleation at higher SR [161].

In the third region, the rate of coverage is slower than in the second region because no more crystals are nucleated and the coverage is only due to crystals getting bigger due to existing supersaturation.

For the same SR value of 25, there is a significant difference in the rate of crystallization in region 3 as compared to region 1. This is due to the variation in events that has taken place in both regions. In region 1, deposition takes place on clean surface simply by progressive nucleation and growth of crystals while in region 3, surface deposition takes place on existing growing crystals. As such, prediction models for surface deposition based on only the SR value will be inaccurate as total deposition would also be affected by the state of the surface onto which the deposition is made.

8.5 Kinetics of CaCO$_3$ surface growth

The *in-situ* image analysis procedure employed allows the increase in size of individual crystal to be followed with time and assessed from the surface images. Figure 8-21 shows three different crystals designated as A, B and C at 60 minutes and 240 minutes for SR 25.
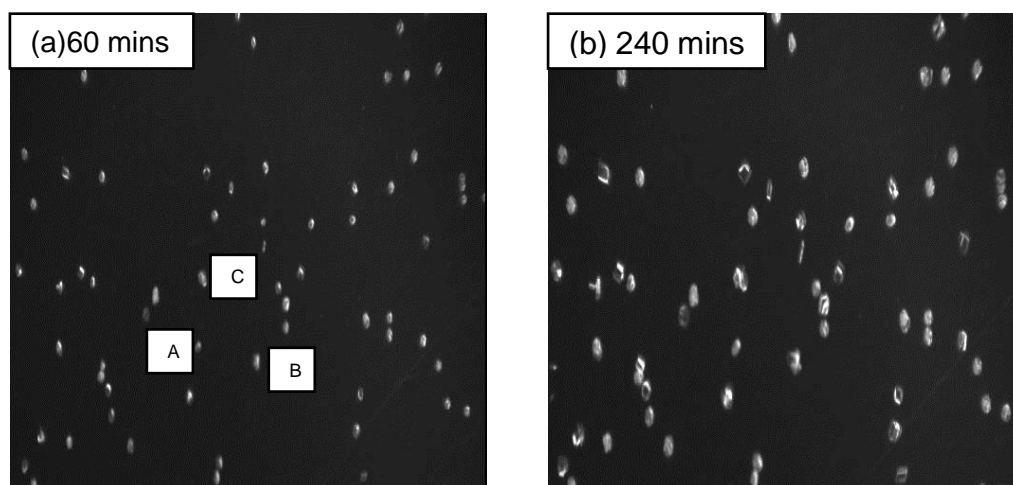
Figure 8-21: Three designated crystals (a) 60minutes and (b) 240 minutes.

The plot of growth as function of time for three single crystals (a) SR = 25 and (b) SR = 60 are presented in Figure 8-22

The nuclei reached stability or the critical size at different times; the first crystals at SR 25 appear at 20 minutes indicating an induction period. More

crystals continue to nucleate in the process while growth of stable nuclei progresses.

A linear increase in size with time is observed for individual crystals with crystals reaching different sizes after 4hrs. The growth rate of individual crystals is determined from the slope of the linear fit and are presented in Table 8-3.
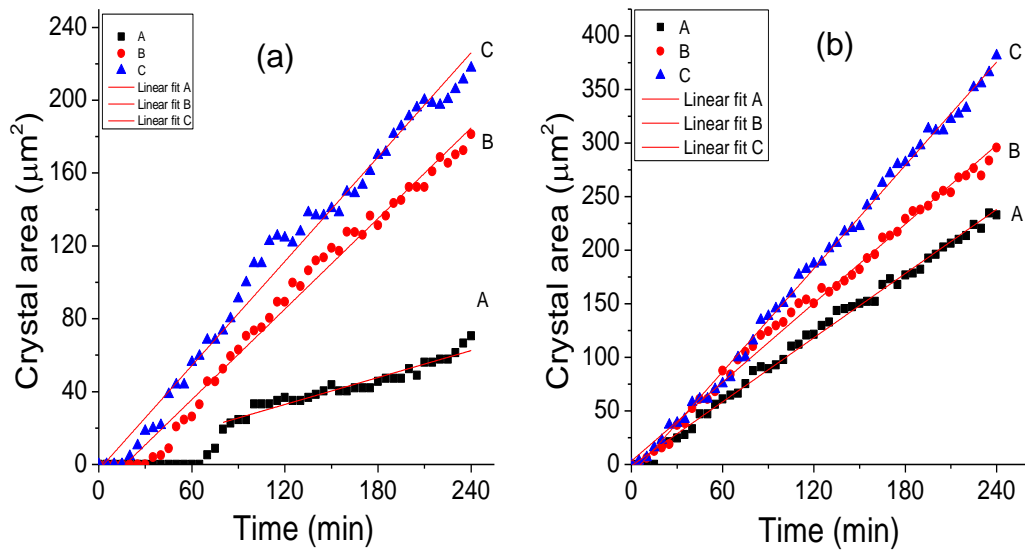
Figure 8-22: Area of single crystals as a function of time (a) SR 25 (b) SR 60

Table 8-3. Growth rate for individual crystal

SR	Individual crystal	Linear equation	Rate (μm^2/s)
25	**A**	y = 0.24x 3.35	0.24
	B	y = 0.83x -14.41	0.83
	C	y = 0.96x -3.48	0.96
60	**A**	y = 1.00x -1.30	1.00
	B	y= 1.23x + 3.20	1.23
	C	y = 1.61x -9.67	1.61

Growth rates of small crystals formed at the later stage of scaling are affected by the presence of large adjacent crystals formed earlier. The Ostwald ripening process describes the growth rate of a second-phase particle with respect to another. When two crystals of different sizes compete for dissolved mineral ions, the larger crystal attracts the ions much more efficiently than the smaller crystal and therefore the larger crystal grows at a much faster rate than the smaller one [188]. However, according to the Ostwald ripening process the smaller crystal would eventually grow to the equivalent size of the larger crystal, as the growth rate of the larger crystal would have reached an asymptotic value. The Lifshitz and Slyozov [189, 190] (LS) modern theory of Ostwald ripening assumes that the mechanism responsible for the process is the diffusion of ions from the bulk to the growing crystals. If the crystals incorporates every ion arriving on it, the concentration of ions in the vicinity of the growing crystals decrease. Therefore a concentration gradient developed within the system.

The theory used the hydrodynamic continuity equation to describe the particle radii distribution: at long times the cube of the average particle radius should vary linearly with time.

$$R^3(t) - R^3(o) \ = \ K(Q)t \qquad \textbf{(8.11)}$$

Where $R(t)$ is the average radius at time t, $R(0)$ is the average particle radius at time $t = 0$, K is the rate constant given as

$$K = \frac{8\gamma c_\infty v^2 D}{9R_g T} t \qquad \textbf{(8.12)}$$

γ is particle surface tension or surface energy, c_∞ is solubility of the crystals, v is molar volume, D is the diffusion coefficient, R_g is the ideal gas constant and T is absolute temperature.

Thus, the rate of change of the average sized particles is proportional to $t^{1/3}$. Regarding nucleation, a precipitate must have a certain critical size r_c

before it can start to grow in an environment where there is some supersaturation of some atomically dissolved constituents.

$$r_c = \frac{-2\gamma}{\Delta G \upsilon} \tag{8.13}$$

ΔG_υ = volume excess free energy particle of solute (a negative quantity proportional to r^3), γ = interfacial tension (mJ/m^2). The maximum value of ΔG_υ, ΔG_C corresponds to the critical nucleus, r_c

The experimental and analysis methods allow to study the possibility of Ostwald ripening during the crystals growth process. From the image analysis procedure, the height, width and equivalent diameter of each crystal can be followed with time. Therefore, the radius of a crystal is calculated as

$$R = \frac{equivalent\ diameter}{2}\ (\mu m) \tag{8.14}$$

The plots of radius as function of cube root of time for three single crystals (a) SR = 25 and (b) SR = 60 are presented in Figure 8-22 Figure 8-23 and Figure 8-23
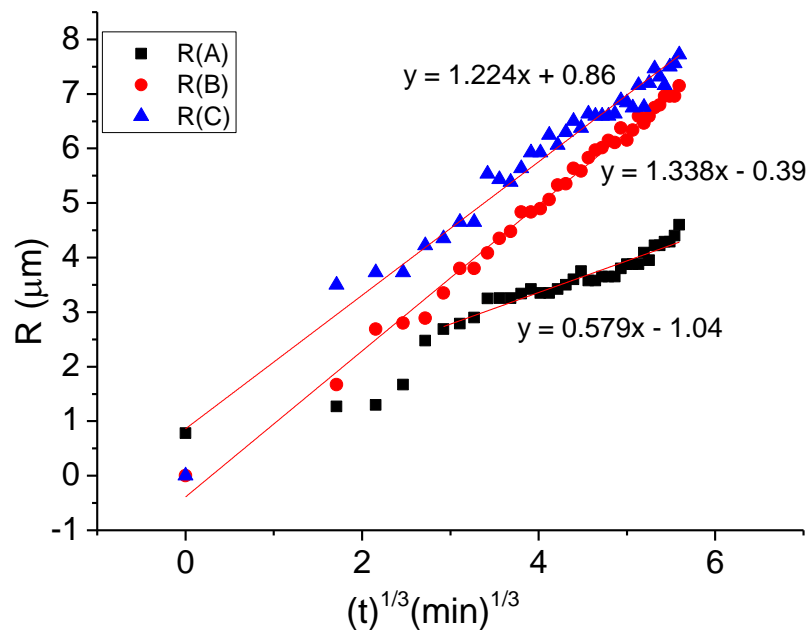
Figure 8-23 : Equivalent radius of single crystal as a function of time at SR = 25
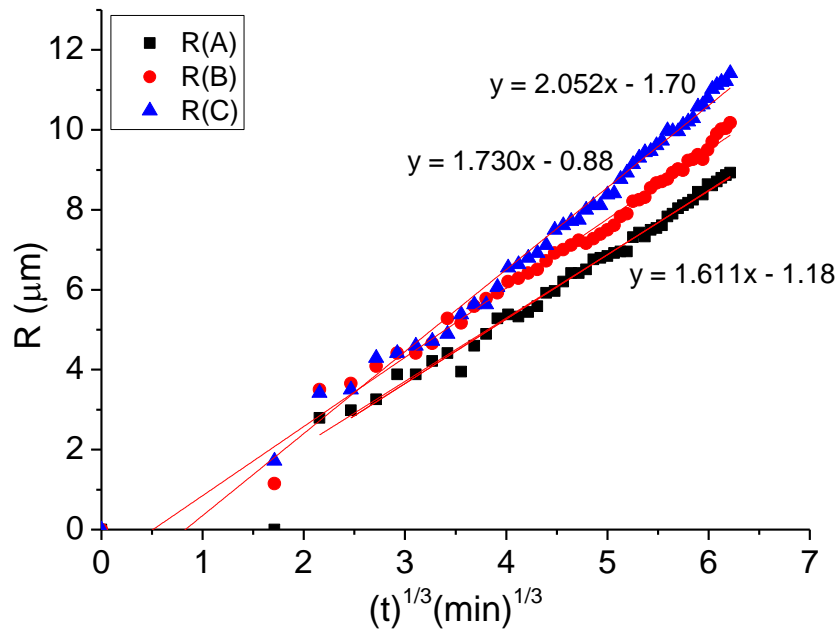
Figure 8-24: Equivalent radius of single crystal as a function of time at SR = 60

Competitive growth takes place when particles with various sizes are dispersed in a matrix. In a polynuclear system brought about by nucleation due to difference in induction time, the growth rate of individual crystal is size dependent. While the formation of many small crystals is kinetically favored, (i.e. they nucleate more easily) large crystals are thermodynamically favored. The driving force is the difference in solubility between the polydisperse particles of the precipitate. This solubility difference establishes a concentration gradient between the smaller and the larger particles, which leads to the growth of the larger particles at the expense of the smaller ones. The rate of this growth process will thus be determined by the size distribution of the precipitate, its growth kinetics and the transport properties of the parent phase [188, 191].

The effect at lower SR is a fewer number of crystals due to a combination of factors such as low concentration of ions on the surface and the progressive nature of nucleation. The growth of already stable crystals that are formed at the early stage of crystallization are favoured over nucleation of new crystals resulting in bigger crystals and dissolution of unstable nuclei before they reach

177

the critical radius, r_c. At higher SR with a higher concentration of ions and instantaneous nucleation, more crystals are rapidly formed and the growth rate of each crystal depends on the radius. The dissolution of smaller crystals would not occur because the concentration of ions on the surface is maintained by the diffusion of solvated ions from the bulk to the surface.

8.5.1 Surface growth rate as a function of saturation ratio

The rate of the scale formation process is normally a function of the level of supersaturation in the brine. The surface growth rates for SR 10, 15, 25, 45 and 60 were determined by a linear fit after the induction period of the average size of crystals versus time plot (Figure 8-25). Hasson *et al* [61] stated that the rate of scale growth is best accurately measured under the condition such that the scale layers grows linearly with time. The plot of crystal size against time gives a straight line and the calcite layer growth rate can be determined from the slope of this straight line [5].
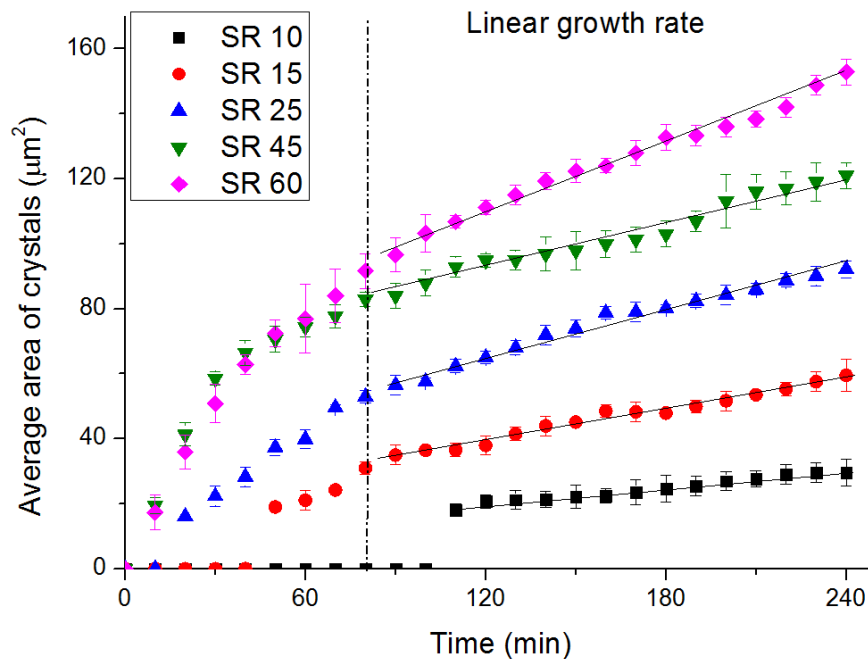
Figure 8-25: Linear fit on the average size of crystals with time

The linear equation and the rates for each SR are presented in Table 8-4.

Table 8-4: Growth rate at different SR

SR	R^2	Linear Equation	Rate ($\mu m^2/s$)
10	0.978	y = 0.08x + 9.23	0.08
15	0.979	y = 0.16x + 20.18	0.16
25	0.990	y = 0.28x + 30.48	0.28
45	0.937	y = 0.31x + 72.98	0.31
60	0.990	y= 0.37x + 77.45	0.37

In previous assessment of deposition rate [62, 81, 185, 186], initial rate constant and initial SR were used because of the decrease in concentration of ions with time. Euvrard *et al* [49] observed the lateral growth rate of $CaCO_3$ decreases as the degree of supersaturation ratio decreases during an electrodeposition test. The plot of growth rate versus saturation ratio at 25°C presented in Figure 8-26a gives a logarithmic relationship as the growth rate becomes slower in proportion to the growing total number of crystals. Figure 8-26b shows the predicted linear correlation between SR and bulk precipitation rate in g/min calculated using the multiscale software at 25°C, 20ml/min.
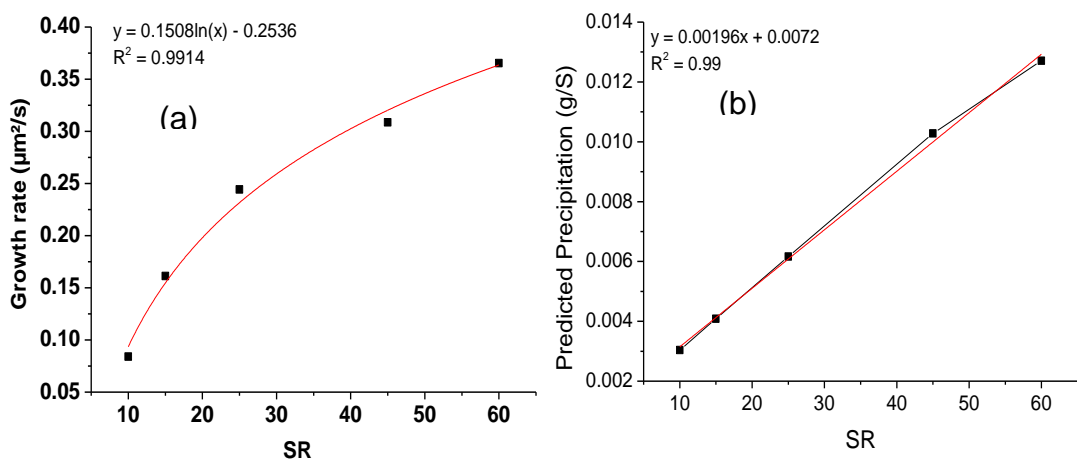
Figure 8-26: Surface growth rate as a function of saturation ratio

Surface growth rate cannot be predicted by the software as the calculation of the surface area is not taken into consideration. Thus, the relationship

obtained for surface deposition is compared with the multiscale software prediction for bulk precipitation. The logarithmic expression for the relationship between the surface growth rate and SR as obtained from the curve fit is given as:

$$y = 0.1508 \ln(SR) - 0.2536 \qquad \textbf{(8.15)}$$

This is in variance with the linear relationship for the bulk precipitation rates as a function of SR predicted by multiscale. It shows that the mechanisms and kinetics of surface scaling differ from the bulk precipitation for the SR values of 10-60 at 25°C. It shows that scaling indices and amount of precipitation based on extensive experimentation of bulk scaling parameters [170] would not be accurate for predicting the rate of surface scaling. Thus, the inhibition strategy design based on bulk MIC would also be incorrect for inhibiting surface deposition.

8.5.1.1   Surface growth rate and mechanisms

The relationship between the growth rates and supersaturation is used to indicate the growth mechanisms. The different rate laws and respective growth mechanisms were discussed in the literature review in Chapter Two. sparingly soluble electrolytes mostly grow by either a parabolic or exponential rate law at small or moderate supersaturations, and may change to transport control, linear rate, at larger concentrations[59],

The plot of the rate of growth as a function of the logarithm of the relative supersaturation is shown in Figure 8-27. Over the range of SR 10-60, the model fits the exponential growth rate law which describes a crystallization mechanisms involving a surface nucleation determining step. This is in agreement with the model earlier described that surface crystallization (induction and nucleation) takes place without bulk precipitation within this range or SR. When fouling rate increases exponentially with temperature, it illustrates that the fouling is occurring under surface-reaction controlled mechanisms [59].

$$Growth\ rate = A_1 e^{-x/A_1} + y_0$$

$R^2 = 0.97$
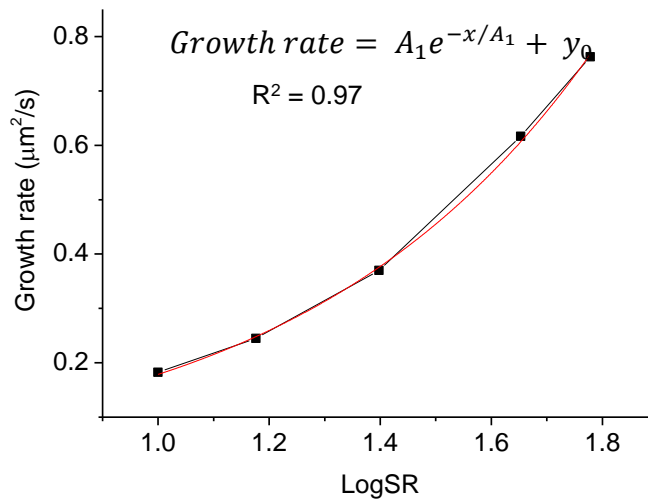
Figure 8-27: Exponential relationship between growth rate and SI

Previous results for the growth of vaterite in the literature have shown that the particles grow by surface reaction controlled mechanisms characterised by a parabolic rate law [58]. However, in this study, the rates of growth showed a high-order dependence on the supersaturation, indicating a polynuclear growth mechanism [59].

In the model, and in the range of SR (10-60), nuclei are formed and grow progressively from the surface. The surface crystals detected are a direct result of nuclei which are continuously formed on the surface and grow simultaneously during the nucleation period. It also corresponds to the progressive nucleation range in the model described for nucleation mechanism.

8.5.2 Effects of temperature on surface growth rate

The relationship between bulk precipitation and $CaCO_3$ formation on surfaces has received little attention, in particular how temperature affects the $CaCO_3$ deposition mechanism on hard surfaces [184]. The results earlier presented in section 7.3 show that temperature has a great effects on the number and growth of crystals on the surface regardless of what happens in the bulk. In the range of SR 10-45, no precipitation was observed in the bulk with an increase in temperature from 25°C to 40°C. At SR 60, the induction period in

the bulk significantly reduced, as such there was a transition from no bulk precipitation at 25°C to having pre-precipitated crystals at 40°C.

In this section, the results of increasing temperature from 25°C to 40°C on surface crystallization are assessed in terms of its effects on surface growth rate. The growth rate increases as temperature is increased and a linear fit with SR can be observed at 40°C compared to a logarithmic relationship at low temperature.
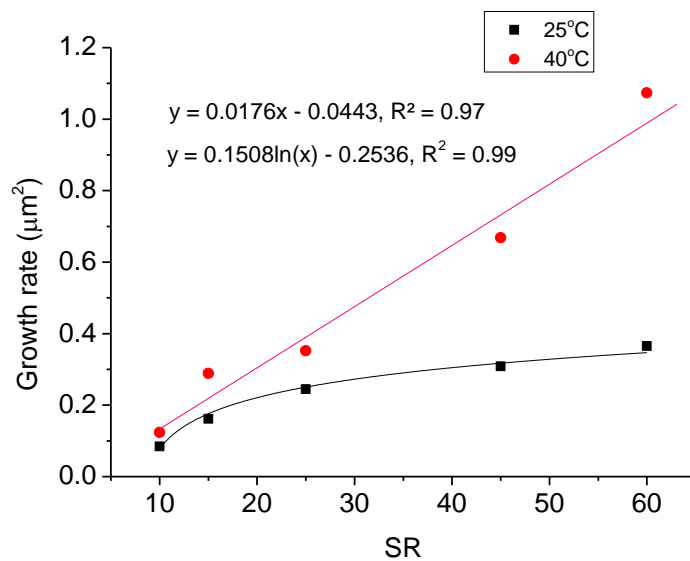
Figure 8-28: Comparison of the effects of temperature on surface growth

Muryanto *et al* [192] found the growth of the scale to increase as temperature was raised from 25°C to 40°C. According to the classical Arrhenius equation [35], higher temperature could bring more energy to the molecules or ions thereby resulting in a faster reaction rate.

Temperature has a very significant and direct effect on the process of calcium carbonate scale formation as well as the morphology of the calcium carbonate formed [68, 82]. It can influence the particle size [50], the induction time, [42]. nucleation mechanisms; where heterogeneous nucleation occurs at low temperature and homogeneous nucleation predominates at high temperature [86] as well as the kinetics of crystallization; as an increase in temperature leads to faster crystallization [56, 81].

8.5.3 Effects of flow velocity on crystallization rate

The effects of flow velocity on surface scaling was investigated over the range of 10ml/min-40ml/min corresponding to laminar flow regime with Reynolds numbers 4.02 – 15.36. The effects of flow rates on surface deposition which are presented in Chapter Seven (7.4) are summarised with a three dimensional plot of surface coverage versus SR and flow rates in Figure 8-29.
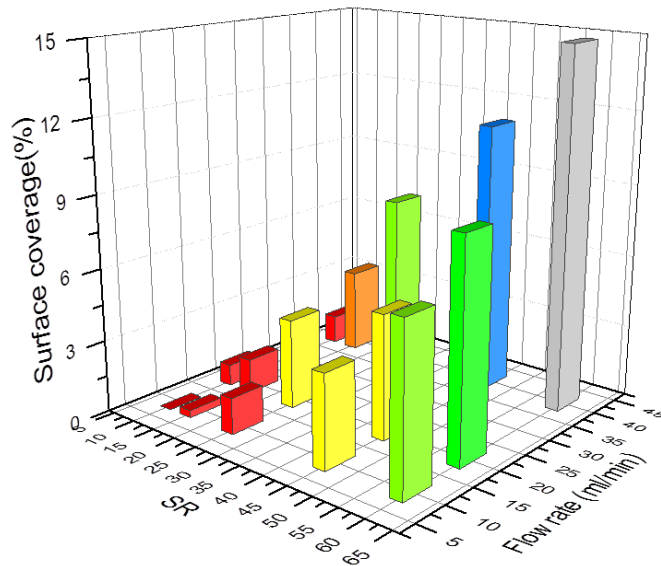
Figure 8-29: Effects of flow rates on surface coverage for different SR

Figure 8-29 shows the effect of fluid velocity on surface coverage for different ion concentrations (SR). For low SR, surface nucleation controls the initial growth of nuclei/crystallites, which are isolated and distributed on the surface. Under these conditions, individual crystal growth, and in particular surface coverage are relatively slow. The controlling process here implies that there is little effect of flow velocity on the deposition rate. However, velocity still affects the surface diffusion of ions. At higher ionic concentration, the surface is rapidly covered by deposited mass and the effect of flow velocity on deposition rate is quite strong as diffusion of ions controls the scale formation [99, 185, 193].

Calcium carbonate surface scaling has a pronounced dependence on velocity. An increase in fluid velocity will cause more solvated ions to diffuse

to the surface resulting in an increase in the fouling growth rate with increasing velocity [99]. Higher velocities can assist in the transportation of ions to the wall and crystallisation at the wall while also the removal rate is increased with increased velocities because of higher shear rate at the liquid-solid interface if the hydrodynamic interactions are greater than the adhesive bond between the particle and the substrate [95]. $CaCO_3$ scale is very tenacious and wall shear stress of 82.5Pa with range of Re 14000-42500 was required to remove scale from the surface. The range of Re in this study is considerably lower and the flow velocity is the laminar regime, therefore no removal of scale from the surface would be possible. The higher the flow rates, the faster the ions become available to replace consumed ions at the surface in the crystallization process therefore increasing the surface concentrations of the active species.

8.5.4 Deposition flux

The composite effects of flow rates and ionic concentration (SR) on surface deposition is represented by Figure 8-30. The parameter Q*SR is referred to as deposition flux and represents the "flux" of ions to the surface. Interestingly the surface coverage varies linearly with the SR*Q parameter. The surface diffusion of ions on active sites is enhanced at high flow rates coupled with the high concentration of ions at higher SR resulting in faster rate of surface crystallization.
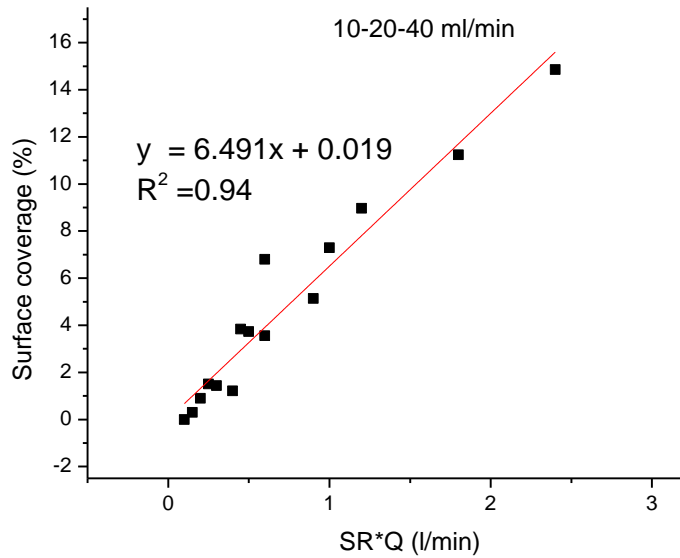
Figure 8-30: Variation of surface coverage with deposition flux

The empirical relationship between total surface coverage, saturation ratio and flow rates at 10-20-40ml/min is given by the equation

$$Surface\ coverage = 6.49(SR * Q) - 0.02 \qquad \textbf{(8.16)}$$

8.6 Inhibition study at different SR- Mechanism and kinetics

The effects of 2ppm of PPCA inhibitor added after 1 hour into the seawater brine before mixing vary from bulk to surface and also between the various saturation ratios. The results already presented in Chapter Seven (7.4) showed that the inhibitor is effective in preventing further nucleation and growth of crystals for SR values of 25 and 45. The longer time require to completely stop further growth at higher SR is a function of percentage surface coverage of crystals and the number of active growth sites. At higher surface coverage, it requires longer time for the inhibitor molecules to be completely adsorbed on the crystals.

When the injection of inhibitor was stopped after 2hrs (Figure 8-31), no new crystals were formed. However, the growth of existing crystals is again

185

observed to continue and this is responsible for the increase in surface coverage in the later stage albeit at a slower rate than the uninhibited stage.
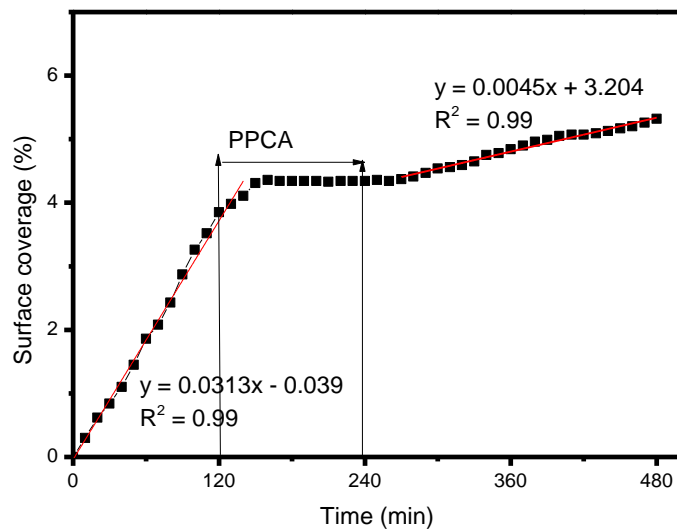
Figure 8-31: Inhibitor injection and removal after 2hrs

For SR 70 an increase in average size is observed for the brine with the injection of inhibitor after 1hr in spite of the reduction in its bulk turbidity. This suggests that the inhibitor is below the MIC for the surface at SR = 70. Growth rates were determined for the uninhibited and inhibited conditions as shown in Figure 8-32. The addition of inhibitor results in formation of bigger crystals at relatively faster rate compared to the uninhibited scaling. At this high SR, further precipitation in the bulk and consequently adhesion of crystals to the surface was inhibited. However, surface growth was enhanced as the inhibitor concentration was not effective at stopping the growth of crystals but otherwise enhances surface growth.
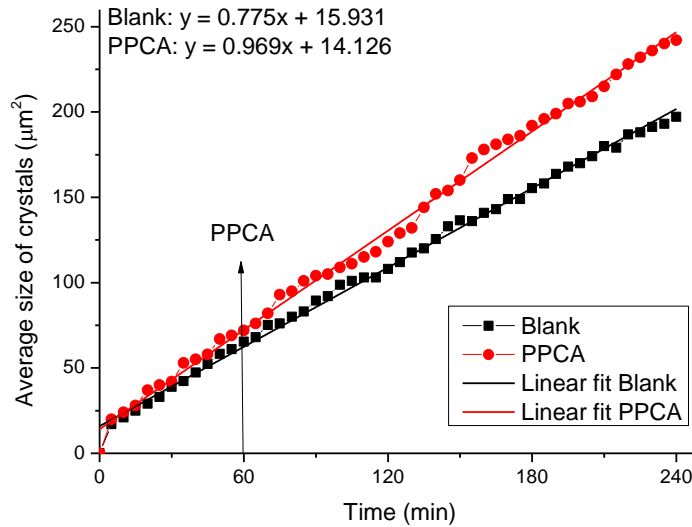
Figure 8-32: Increase in average size in inhibited and uninhibited scaling

Graham *et al* [179] showed that the minimum inhibitor concentration MIC for bulk is different for the MIC for surface scaling. In their study, the surface deposition of barite increased at below the MIC. Chen *et al* [180] also found that inhibition efficiency and the effects on crystal morphology vary between surface and bulk scaling processes.. When 2ppm of inhibitor was injected at low SR 25 and 45, the surface growth of crystals stopped as the inhibitor molecules are well adsorbed and blocked all the active lattice sites to prevent further growth [194, 195]. However, at SR 70, the inhibitor molecules are not completely incorporated onto the crystal lattice to block all active growth sites thereby enhancing the growth of crystals.

Hence, injecting inhibitor at bulk MIC actually aggravates the surface growth tendency and increases surface coverage of crystals.

Chapter 9 Conclusions and future work

9.1   General Summary

The kinetics and mechanisms of surface scaling in terms of surface coverage, number of crystals formed and the average size of crystals have been studied together with bulk precipitation processes in a newly developed rig system under different test conditions. Analysis of the results and further assessment of the kinetics and mechanisms have also been presented. This chapter gives a general summary of the discussion, conclusions of the study and future works.

9.2   Visualization technique

A once-through *in-situ* flow visualization rig with associated image analysis protocols has been developed and used to assess both bulk and surface scale formation. The visualization flow cell in the rig is a modification of the one used in electrochemical deposition of $CaCO_3$ scale [17]. Scale study at constant SR under flow control and *in-situ* visualization is essential to develop a better understanding of the deposition mechanisms [196]. The flow rig was designed to work under atmospheric pressure and can be adjusted to allow experimental conditions (e.g. saturation ratio, inhibitor concentration) to be kept constant at the point where the imaging is done.

It was shown that the kinetics and mechanisms of scaling in terms of surface coverage, number of crystals formed and average sizes of crystals can be studied together with bulk precipitation processes in a dynamic system and under different test conditions. The rig design as well as the image analysis procedures allow for combined studying and improving on the understanding of both surface deposition and bulk precipitation scaling kinetics. It allows for a real-time and *in-situ* visualization and quantitative assessment of surface scale build up while maintaining a constant driving force as fresh brine

continuously flow through the cell. The approach enables to distinctively quantify the nucleation and growth processes at different test conditions.

9.3   Bulk versus surface scaling

Studies of the kinetics of mineral scale formation have primarily focused on determining the processes involved in the bulk solution rather than on solid surfaces. Much information therefore exists on nucleation and growth mechanisms and kinetics in the bulk solution but significantly less information exists relating to scale formation on a solid surface. The present study has shown that surface scale formation are not always a results of the adhesion of pre-precipitated crystals from the bulk solution. There are no pre-precipitated crystals in the bulk solution within the range of SR (10-60). As such, surface scaling is driven by surface crystallisation with surface induction, nucleation and growth taking place at solid/liquid interface rather than the adhesion of bulk precipitate. At low SR, particles are formed directly on a surface via true surface heterogeneous nucleation. Therefore, existing scaling indices for bulk precipitation are not accurate for predicting surface scaling. The differences in induction time between bulk and surface scaling especially at lower SR highlights the importance of incorporating surface induction in scale formation and inhibition treatment.

9.4   Surface scale mechanisms and kinetics

The formation of scale at different ionic concentrations is controlled by different mechanisms which are mainly dependent on saturation ratio. At constant supersaturation, all brines showed a continuous increase in growth and surface coverage once crystallization had begun while surface nucleation depends on the availability of active nucleation sites. The methods developed in this study helps to determine and understand the types of nucleation at different SR.

189

For the crystallization law mechanisms with surface nucleation, the model was used as a basis to determine the types of nucleation. In agreement with Euvrard *et al* [49] and Gabrielli *et al* [165], a linear relation shows that nucleation at high SR is instantaneous. However a further analysis at low SR shows progressive nucleation as observed with the exponential part of the model developed

Two types of nucleation mechanisms are identified.
- (a) Progressive at low SR
- (b) Instantaneous at high SR

At the low SR, nucleation is progressive, the curves show an exponential part; where there is a simultaneous nucleation and growth of crystals and a later stage linear part where the nucleation stops and surface scaling proceeds by growth of crystals only. The nucleation process is instantaneous at high SR. All available active sites generates nuclei at the early stage of the crystallization process. The surface coverage at the later stage is dominated by crystals that are getting bigger rather than new crystals that are forming. It demonstrates that a scaling surface has a finite number of nucleation sites and the number of nucleation sites is a function of saturation ratio.

Increase in flow rates caused faster diffusion of the ions at high SR but the effects of temperature is more significant on the nucleation mechanisms. An increase in temperature to from $25^{o}C$ to $40^{o}C$ changes the mechanisms from progressive nucleation to instantaneous nucleation. A relatively small change in temperature leads to significant change in the kinetics of formation of calcium carbonate scale because its solubility is greatly influenced by temperature.

9.5   Scale inhibition

Scale prevention by inhibition has majorly focussed on the control of bulk precipitation. However the study shows that injecting inhibitor at bulk MIC may

actually aggravate the surface scaling tendency and increase surface coverage of crystals. Determination of surface crystallization mechanisms and kinetics allows for the correct type and dosage of inhibitor to be selected. Inhibition strategy should be able to accommodate the possibility of surface scaling without bulk precipitation and the use of either nucleation or growth inhibitors.

9.6   Summary of contributions and novelty

The rig design as well as the study protocol involving in-situ and post-test surface analysis helps to decouple the surface deposition and bulk precipitation processes and study the scaling kinetics at constant SR.

- The work has shown the uniqueness and suitability of the new methodology to distinctively quantify the nucleation and growth of surface scaling *in-situ* and in real time.
- In contrast to popular thinking, this present study has shown that surface scale formation are not always the adhesion of pre-precipitated particles from the bulk solution.
- There are different mechanisms to control the process of scale formation at different ionic concentrations, usually at very low SR, surface scaling takes place merely by surface crystallization without adhesion of pre-precipitated crystals in the bulk solution.
- Mechanisms at low SR is progressive and at high SR id instantaneous The later stages in both mechanisms of crystallization is merely surface growth with no more nucleation due to a finite number of active nucleation sites.
- The growth mechanisms at low SR 10-60 follow the exponential rate law with surface nucleation as the rate controlling step. This shows that within this range, the nucleation mechanisms is polynuclear with the resultant exponential relationship between SR and induction time.

191

- At high SR 70 -90, a linear relationship suggesting diffusion of ions from the bulk. It could also be seen from the turbidity that bulk precipitation occurs at this range of supersaturations

- The experimental data shows a trend that surface scaling increases as the velocity increases, because the surface diffusion of solvated ions is affected with flow velocity

- Temperature has a greater effects on induction period, the kinetics of crystallization and the mechanisms of crystallization. It results in change of mechanisms from progressive to instantaneous at high temperature.

- Also the suitability of the rig to study both bulk and surface deposition is demonstrated. The minimum inhibitor concentration (MIC) for bulk is different from surface and surface scale is aggravated by working below bulk MIC.

9.7   Relevance of study to the academia and industry

For the control of surface scaling and implementing effective scale management strategy, it is essential to have a clear understanding of how various factors interact and affect materials performance as well as the kinetics of the surface scaling process.

Most predictive indices used in the field to quantify surface deposition are based on bulk scaling parameters. However, results from this study show that the ratio of bulk to surface scaling induction time does not vary linearly SR but is a polynomial of second order which shows that the kinetics and mechanisms are different in relation to SR.

At low SR, there is possibility of surface scaling with no bulk precipitation due to the difference in the induction time. Scale could actually be building up on the surfaces such as the injection valves and topside facilities at low SR with no precipitation in the bulk. Therefore, the possibility of scale formation on

surfaces is one of the criteria to look at before implementing new chemicals in the industry.

The scale inhibition study in the rig shows that the efficiency of scale inhibitor to stop growth on the surface differs to the bulk. This is greatly dependent on SR and the concentration of inhibitor. The minimum inhibitor concentration (MIC) for bulk precipitation will also not be accurate and effective to inhibit surface scaling. Techniques used for the assessment of scale formation needs to incorporate surface study. It is essential to introduce metallic samples into bulk jar test used to study MIC in order to assess the possibility of preventing surface scaling.

The model developed for nucleation mechanism in relation to the period of nucleation and growth can be exploited to develop scale inhibition strategy. It can be used to model the efficiency of inhibitor in terms of the rate of adsorption as well as to model a well for a long time scaling in order to simulate crystal growth layer.

This study has shown that surface crystallization is an important mechanisms to be considered in preventing scaling problems. It is therefore very important that more attention be given to research and application of modified surfaces to prevent scaling in the industry.

The practice of predicting surface scaling using bulk precipitation models is inaccurate. The mechanisms and kinetics are different, therefore bulk precipitation is not always an accurate estimation for surface scaling.

9.8 Future work

9.8.1 Scale Rig

Further improvement and modification to the scale rig is suggested. The study could to be carried out at an extended range of Reynolds number, pressures and temperatures. Therefore, designing the rig to accommodate flow study at

high turbulence to see the effects of removal on growth of scales is suggested. The flow cell can also be used for electrochemical study of scale formation. The removable plug in which the sample is inserted also permits working and reference electrodes to be inserted. All electrodes can then be connected to a potentiostat.

9.8.2 Surface kinetic study

The study has shown the variation between bulk and surface induction time and consequently surface crystallization rate and mechanisms. As such surface characteristics such as surface topography will therefore be a major factor to be considered in surface scaling. The development of surface scale kinetic models requires more rigorous study to include different surface/substrates at various surface roughness and surface energy in the flow rig. This will allow to take into consideration the effect of surfaces on surface crystallization. It is essential to find out a connection between a surface crystallization and surface characteristics [53].

A hypothetical curve is presented in Figure 9-1 based on the exponential relationship between t_{ind} and SR to illustrate how change in surface roughness would impact on the relationship between induction time and SR.
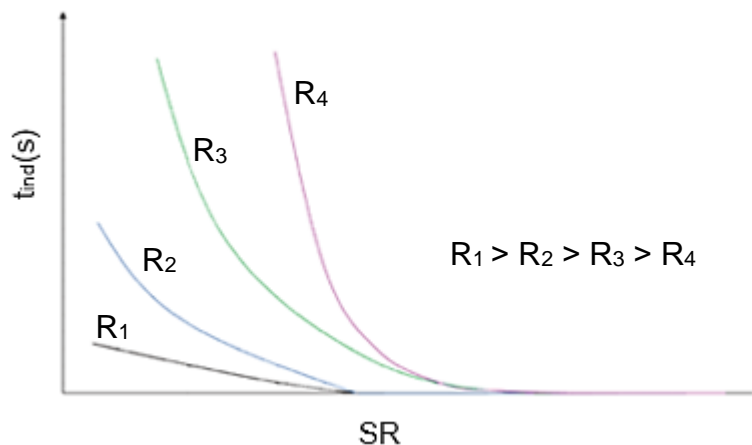
Figure 9-1: Schematic graph (hypothetical) showing the evolution of the induction time at different SR; each colour represents substrate(s) with different surface roughness

R_1, R_2, R_3 and R_4 are different surface roughness.

The hypothesis can be compared to Forster *et al* [115] in which the result of induction time for scaling was found to be dependent on surface roughness with very rough stainless steel surfaces showing a minimum induction time. A high surface roughness will increase the surface area which provides more sites to trigger early stage heterogeneous nucleation and crystal growth.

Naturally, an understanding of surface crystallization will be insufficient just by considering supersaturation of bulk solution. The structure and the dynamics of solute and solvent molecules near the substrates in solution are fundamental in controlling the surface crystallization [54]. AFM studies can also be used to determine the role of surfaces in the growth process of calcium carbonate.

Also, to improve on the developed mechanistic model for surface scaling, it is suggested that a more precise synchrotron x-ray imaging could be used to detect the probability of early stage nucleation and assess the progressive and instantaneous mechanisms.

9.8.3 Inhibition study

The MIC for bulk has been shown to be inaccurate for surface scaling inhibition. The results from this study has shown that inhibition strategy for surface scaling is necessary to complement the inhibition of bulk precipitation. This requires further surface inhibition test and analysis at different inhibitor concentrations and injection time to improve on this aspect. Also, injecting inhibitor at different flow rates should be considered to see the effects of the rate of adsorption of the inhibitor on crystallization. The flow rig offers the capability to vary and control the rates at which different concentration of inhibitor is injected into the scale formation and allows the effects to be quantified in real time.

REFERENCES

[1]   M. A. Kelland, "Production Chemicals for the Oil and Gas Industry," vol. 03, pp. 53 -55, 2009.

[2]   O. J. Vetter, "Oilfield Scale---Can We Handle It?," *Journal of Petroleum Technology,* vol. 28, pp. 1402-1408, 1976.

[3]   Z. Amjad, "The science and Technology of Industrial Water Treatment," 2010.

[4]   E. Protasova, "Reduction of scaling in biological treatment of industrial waste water," 2012.

[5]   R. A. Dawe and Y. Zhang, "Kinetics of calcium carbonate scaling using observations from glass micromodels," *Journal of Petroleum Science and Engineering,* vol. 18, pp. 179-187, 1997.

[6]   M. A. Kelland, "Effect of various cations on the formation of calcium carbonate and barium sulfate scale with and without scale inhibitors," *Industrial and Engineering Chemistry Research,* vol. 50, pp. 5852-5861, 2011.

[7]   A. Neville and A. P. Morizot, "A combined bulk chemistry/electrochemical approach to study the precipitation, deposition and inhibition of $CaCO_3$," *Chemical Engineering Science,* vol. 55, pp. 4737-4743, 2000.

[8]   M. Scheck and G. Ross, "Improvement of Scale Management Using Analytical and Statistical Tools," presented at the SPE International Oilfield Scale Conference, Aberdeen, UK, 2008.

[9]   B. H. Caudle, "Production process and operations: Enhanced secondary recovery technology," *Fundación Universidad de América at Fundación Universidad de América* 2014.

[10]   W. Frenier, M. Ziauddin, "Formation, removal, and inhibition of inorganic scale in the oilfield environment.," *Society of Petroleum Engineers Journal,* 2008.

[11]   M. Crabtree, et al, "Fighting Scale - Removal and prevention," *Oilfield review,* pp. 30-45., 1999.

[12]   B. J.R., "Corrosion and Scale handbook," *PennWell Corp.,* 1998.

[13]   E. A. Graham, "The challenges for Scale Control in Deepwater Production Systems: Chemical Inhibition and Placement," *Presented at the NACE Corrosion, , Denver,* 2002.

[14] A. G. Collins, "Saline Groundwaters Produced with Oil and Gas," *Environ Prot Technol Ser EPA 660/2-74-010,* 1974.

[15] O. J. Vetter and W. A. Farone, "Calcium Carbonate Scale in Oilfield Operations," presented at the SPE Annual Technical Conference and Exhibition, Dallas, Texas, 1987.

[16] J. Moghadasi, et al., "Model study on the kinetics of oil field formation damage due to salt precipitation from injection," *Journal of Petroleum Science and Engineering,* vol. 43, pp. 201-217, 2004.

[17] M. Euvrard, C. Filiatre, and E. Crausaz, "Cell to study in situ electrocrystallization of calcium carbonate," *Journal of Crystal Growth,* vol. 216, pp. 466-474, 2000.

[18] Y. Zhang, H. Shaw, R. Farquhar, and R. Dawe, "The kinetics of carbonate scaling - Application for the prediction of downhole carbonate scaling," *Journal of Petroleum Science and Engineering,* vol. 29, pp. 85-95, 2001.

[19] T. Chen, A. Neville, and M. Yuan, "Influence of Mg^{2+} on $CaCO_3$ formation-bulk precipitation and surface deposition," *Chemical Engineering Science,* vol. 61, pp. 5318-5327, 2006.

[20] W. C. Cheong, "Biomimetic Approach to Anti-Fouling Surfaces," *School of Mechanical Engineering. University of Leeds PhD. Thesis,* 2011.

[21] N. Abdel-Aal, K. Satoh, and K. Sawada, "Study of the adhesion mechanism of CaCO3 using a combined bulk chemistry/QCM technique," *Journal of Crystal Growth,* vol. 245, pp. 87-100, 2002.

[22] T. Chen, A. Neville, and M. Yuan, "Calcium carbonate scale formation - Assessing the initial stages of precipitation and deposition," *Journal of Petroleum Science and Engineering,* vol. 46, pp. 185-194, 2005.

[23] V. Eroini, "Kinetic study of calcium carbonate formation and inhibition by using an in situ flow cell," *University of Leeds PhD Thesis,* 2012.

[24] M. S. H. Bader, "Sulfate removal technologies for oil fields seawater injection operations," *Journal of Petroleum Science and Engineering,* vol. 55, pp. 93-110, 2007.

[25] A. Eseosa and A. J. Atubokiki, "Prediction and monitoring of oilfield carbonate scales using scale check©," 2011, pp. 619-628.

[26] O. Sohnel and J. Garside, "Precipitation: Basic Principles and Industrial Applications," *Butterworth-Heinemann Ltd,* 1992.

[27] R. Fürstner, W. Barthlott, C. Neinhuis, and P. Walzel, "Wetting and self-cleaning properties of artificial superhydrophobic surfaces," *Langmuir,* vol. 21, pp. 956-961, 2005.

[28] R. Oliveira and B. Engenharia, "Understanding Adhesion: A means for preventing Fouling," *J. Expermental Thermal and Fluid Science,* vol. 14, pp. 316-322, 1997.

[29] Pytkowicz, "Rates of inorganic calcium carbonate nucleation," *J. Geol,* vol. 73., pp. 196-199, 1965.

[30] T. Chen, A. Neville, and M. Yuan, "Assessing the effect of Mg^{2+} on $CaCO_3$ scale formation - bulk precipitation and surface deposition," *crystal growth,* vol. 275, pp. 1341-1347, 2004.

[31] Walton, "The Formation and Properties of Precipitates," *Interscience Publishers, New York,* 1967.

[32] Roberge, "Handbook of Corrosion Engineering," *McGraw-Hill,* 2000.

[33] T. E. Larson and A. M. Buswell, "Calcium Carbonate Saturation Index and Alkalinity Interpretations," *The American Water Works Association,* vol. 34, 1942

[34] A. P. Morizot, "Experimental Based Technique study of Mineral scale Formation and Inhibition," *PhD Thesis Heriot Watt University, UK,* 1999.

[35] J. W. Mullin, "Crystallization," *Butterworths, London,* vol. 4th Edition, 2001.

[36] E. Stamatakis, Stubos, A, Palyvos, J., Chatzichristos, C., Muller, J., " An improved predictive correlation for the induction time of calcium carbonate scale formation during flow in porous media," *Journal of Colloid and Interface Science,* vol. Volume 286, pp. 7-13, 2005.

[37] W. A. G., "Nucleation in liquids and solutions. In Nucleation (ed. Zettlemoyer)," *New York: Marcel Dekker Inc,* pp. 225-307, 1969.

[38] O. Söhnel and J. W. Mullin, "Interpretation of crystallization induction periods," *Journal of Colloid and Interface Science,* vol. 123, pp. 43-50, 1988.

[39] L. F. Olsson, "Induction time of precipitation of calcium carbonate," *Journal of Molecular Liquids,* vol. 65-66, pp. 349-352, 1995.

[40] J. Garside, "Industrial crystallization from solution," *Chemical Engineering Science,* vol. 40, pp. 3-26, 1985.

[41] G. Nancollas, "The growth of crystals in solution. Advances in Colloid and Interface Science," vol. 10, pp. 215-252, 1979.

[42] L. Beaunier, C. Gabrielli, G. Poindessous, G. Maurin, and R. Rosset, "Investigation of electrochemical calcareous scaling: Nuclei counting and morphology," *Journal of Electroanalytical Chemistry,* vol. 501, pp. 41-53, 2001.

[43] G. H. Nancollas, "Oilfield scale: Physical and Chemical properties of its formation and prevention," *symposium on 'chemicals in the oil industry',* p. 143, 1985.

[44] S. Keysar, R. Semiat, D. Hasson, and J. Yahalom, "Effect of surface roughness on the morphology of calcite crystallizing on mild steel," *Journal of Colloid and Interface Science,* vol. 162, pp. 311-319, 1994.

[45] J. C. A.E. Nielsen, "The mechanisms of crystal growth and dissolution," *Biological Mineralization and Demineralization,* vol. ed. G. H Nancollas, pp. 37-77, 1982.

[46] O. Söhnel and J. W. Mullin, "Precipitation of calcium carbonate," *Journal of Crystal Growth,* vol. 60, pp. 239-250, 1982.

[47] S. Labille, A. Neville, G. M. Graham, and L. S. Boak, "An Assessment of Adhesion of Scale and Electrochemical Pre-treatment for the Prevention of Scale Deposition on Metal Surfaces," presented at the International Symposium on Oilfield Scale, Aberdeen, United Kingdom, 2002.

[48] P. J. Daudey, G. M. V. Rosmalen, and E. J. d. Jong, "Secondary nucleation kinetics of ammonium sulfate in a CMSMPR crystallizer," *Crystal Growth,* vol. 99 pp. 1076-1081, 1990.

[49] M. Euvrard, F. Membrey, C. Filiatre, C. Pignolet, and A. Foissy, "Kinetic study of the electrocrystallization of calcium carbonate on metallic substrates," *Journal of Crystal Growth,* vol. 291, pp. 428-435, 2006.

[50] J. Yu, et al, "Facile preparation of calcium carbonate particles with unusual morphologies by precipitation reaction," *Crystal Growth,* vol. 261, pp. 566-567, 2004.

[51] G. H. Nancollas and N. Purdie, "The kinetics of crystal growth," *Q. Rev. Chem. Soc,* vol. 28., 1964.

[52] N. F. Mott, "Theory of crystal growth. ," *Nature Publishing Group,* p. 4191., 1950.

.

[53]   N. I. Shinya Yamanaka, Atsuko Shimosaka, Yoshiyuki Shirakawa, Jusuke Hidaka, "AFM Investigation for the Initial Growth Processes of Calcium Carbonate on Hydrophilic and Hydrophobic Substrate," *Crystal Growth & Design,* vol. 9, pp. 3245-3250, 2009.

[54]   S. Yamanaka, N. Ito, K. Akiyama, A. Shimosaka, Y. Shirakawa, and J. Hidaka, "Heterogeneous nucleation and growth mechanism on hydrophilic and hydrophobic surface," *Advanced Powder Technology,* vol. 23, pp. 268-272, 3// 2012.

[55]   M. M. Reddy and G. H. Nancollas, "Calcite crystal growth inhibition by phosphonates," *Desalination* vol. 12 p. 61−73, 1973.

[56]   B. Feng, et al., "Effect of various factors on the particle size of calcium carbonate formed in a precipitation process," *Materials Science and Engineering,* vol. 445-446, pp. 170-171, 2007.

[57]   S. He, A. T. Kan, and M. B. Tomson, "Mathematical Inhibitor Model for Barium Sulfate Scale Control," *Langmuir,* vol. 12, pp. 1901-1905, 1996.

[58]   E. M. Flaten, M. Seiersten, and J.-P. Andreassen, "Growth of the calcium carbonate polymorph vaterite in mixtures of water and ethylene glycol at conditions of gas processing," *Journal of Crystal Growth,* vol. 312, pp. 953-960, 3/15/ 2010.

[59]   A. E. Nielsen, "Electrolyte crystal growth mechanisms," *Journal of Crystal Growth,* vol. 67, pp. 289-310, 1984/07/01 1984.

[60]   N. Andritsos, A.J. Karabelas, and P.G. Koutsoukos, "Morphology and Structure of CaCO3 Scale Layers Formed under Isothermal Flow Conditions," *Langmuir,* vol. 13, pp. 2873-2879, 1997.

[61]   D. Hasson, M. Avriel, W. Resnick, T. Rozenman, and S. Windreich, "Mechanism of calcium carbonate scale deposition on heat-transfer surfaces," *Industrial & Engineering Chemistry Fundamentals,* vol. 7, pp. 59-65, 1968.

[62]   M. G. Lioliou, C. A. Paraskeva, P. G. Koutsoukos, and A. C. Payatakes, "Heterogeneous nucleation and growth of calcium carbonate on calcite and quartz," *Journal of Colloid and Interface Science,* vol. 308, pp. 421-428, 4/15/ 2007.

[63]   Y. Zhang and R. Dawe, "The kinetics of calcite precipitation from a high salinity water," *Applied Geochemistry,* vol. 13, pp. 177-184, 1998

[64]   M. M. Reddy, et al., "Crystal growth of calcite from calcium bicarbonate solutions at constant P (sub cod) 2 and 25 degrees C; a test of a calcite dissolution model," *Geochimica et Cosmochimica Acta,* vol. 45, pp. 1281-1289, 1981.

[65] K. Mitsutaka, K. Haruo, and Y. Atsunuri, "Controling Factors and Mechanisms of Reactive Crystallization of Calcium Carbonate Polymorphs from Calcium Hydroxide Suspensions," *Crystal Growth,* vol. 236, pp. 323-332, 2002.

[66] L. Brecevic and Kralj, "On Calcium Carbonates: from Fundamental Research to Application," *Croatica Chemica Acta,* vol. 80, pp. 467-484., 2007.

[67] M. Kitamura, "Controlling factor of polymorphism in crystallization process," *Crystal Growth,* vol. 237-239, pp. 2205-2214, 2002.

[68] B. Ghiringhelli, "The Solubility Products of Calcium Carbonate in Aqueous Systems from 0' to 50°C.," *Am. Idiol,* vol. 1, 1963.

[69] Boynton, "Chemistry and Technology of Lime and Limestone," *New York: Interscience Publishers* p. 520, 1967.

[70] Y. S. Han, et al, "Factors affecting the phase and morphology of CaCO3 prepared by a bubbling method," *European Ceramic Society,* vol. 26, pp. 843-847, 2006.

[71] Z. Amjad, J. Pugh, and M. M. Reddy, "Kinetic Inhibition of Calcium Carbonate Crystal Growth in the Presence of Natural and Synthetic organic Inhibitors," *Advanced Technology Group,* 2004.

[72] D. Evangelos and P. G. Koutsoukos, "Calcium Carbonate Scale Formation Heated Metal Surfaces," *Geothermics,* vol. 18 1989.

[73] Amjad, "Water Soluble Polymers Solution Properties and Applications," *Springer-Verlag,* 1998.

[74] C. Gabrielli, et al, "Insitu Raman Spectroscopy Applied to Electrochemical Scaling-Determination of the Structure of Vaterite," *J. Raman Spectrosci,* vol. 31, pp. 497-501, 2000.

[75] C. Gabrielli, et al., "An Electrochemical Method for Testing the Scaling Susceptibility of Insulating Materials," *j. Electrochemical Society,* vol. 148, pp. 517-521, 2001.

[76] R. Jaouhari, et al., "Influence of water Composition and Substrate on Electrochemical Scaling," *j. Electrochemical Society,* vol. 147, pp. 2151-2161, 2000.

[77] S. Dyer and G. M. Graham, "The Effect of Temperature and Pressure on Oilfield Scale formation," *Petroleum Science and Technology,* vol. 35, pp. 95-97, 2002.

[78] G. Nancollas and K. Sawada, "Formation of Scales of Calcium Carbonate Polymorphs: The Influence of Magnessium ion and

Inhibitors " *Petroleum Science and Technology,* vol. 34, pp. 645-652, 1982.

[79]   K. Hyllestad, "Scaling of Calcium Carbonate on a Heated Surface in a Flow Through System with Mono Ethylene Glycol," *Norwegian University of Science and Technology.*

[80]   W. C. Cheong, P. H. Gaskell, and A. Neville, "Substrate effect on surface adhesion/crystallisation of calcium carbonate," *Journal of Crystal Growth,* 2012.

[81]   F. A. Setta, A. Neville, and H. J. Chen, "A surface kinetic scaling model for CaCO 3 on a stainless steel surface (316 L)," vol. 1, ed, 2012, pp. 285-303.

[82]   J. Chen and L. Xiang, "Controllable synthesis of calcium carbonate polymorphs at different temperatures," *Powder Technology,* vol. 189, pp. 64-69, 2008.

[83]   C. C. Patton, "Oilfield water Systems," *Cambell Petroleum Series, Norman, Oklahoma,* vol. 2nd Ed. , pp. 35-65, 1977.

[84]   L. N. Plummer and E. Busenberg, "The solubilities of calcite, aragonite and vaterite in CO_2-H_2O solutions between 0 and 90°C and an evaluation of the queous model for the system $CaCO_3$-CO_2-H_2O.," *Geochimica et Cosmochimica Acta,* vol. 46, pp. 1011-1040, 1982.

[85]   Y. Kitano, "Polymorphic Formation of Calcium Carbonate in thermal Springs with an Emphasis on the effect of Temperature," *Bull. Chem. Soc. Japan,* vol. 35, pp. 1973-1980, 1962.

[86]   M. B. Amor, et al., "Influence of water hardness, substrate nature and temperature on heterogeneous calcium carbonate nucleation," *Desalination,* vol. 166, pp. 79-84., 2004.

[87]   J. Gómez-Morales, J. Torrent-Burgués, and R. Rodríguez-Clemente, "Nucleation of calcium carbonate at different initial pH conditions," *Journal of Crystal Growth,* vol. 169, pp. 331-338, 1996.

[88]   D. Kralj and N. Vdovic, "The influence of some naturally occurring minerals on the precipitation of calcium carbonate polymorphs," *Water Research* vol. 34, pp. 179-184, 2000.

[89]   D. D. Verdoes, et al., "Determination of nucleation and growth rates from induction times in seeded and unseeded precipitation of calcium carbonate," *Journal of Crystal Growth,* vol. 118, pp. 401-413, 1992.

[90]   B. Cheng, et al., "Preparation of monodispersed cubic calcium carbonate particles via precipitation reaction," *Materials Letters,* vol. 58, pp. 1565-1570., 2004.

[91]   W. Cowan, and Donald, "Water-Formed Scale Deposits," *Houston, Texas: Golf publishing company,* 1976.

[92]   R. M. Pytkowicz and D. N. Conners, "High Pressure Solubility of Calcium Carbonate in Sea Water," *Science,* vol. 144, 1964.

[93]   Al-Anezi and N. Hilal, "Scale formation in desalination plants: effect of carbon dioxide solubility," *Desalination,* vol. 204, pp. 385-402., 2007.

[94]   J. Y. Gal, et al., "Mechanisms of scale formation and carbon dioxide partial pressure influence; Part II. Application in the study of mineral waters of reference. ," *Water Research,* vol. 36, pp. 764-773, 2002.

[95]   P. Walker and R. Sheikholeslami, "Assessment of the effect of velocity and residence time in CaSO4 precipitating flow reaction," *Chemical Engineering Science,* vol. 58, pp. 3807-3816, 2003.

[96]   Q. Yang, Y. Liu, A. Gu, J. Ding, and Z. Shen, "Investigation of calcium carbonate scaling inhibition and scale morphology by AFM," *Journal of Colloid and Interface Science,* vol. 240, pp. 608-621, 2001.

[97]   G. Trippa and R. J. J. Jachuck, "Process Intensification: Precipitation of Calcium Carbonate Using Narrow Channel Reactors," *Chemical Engineering Research and Design,* vol. 81, pp. 766-772, 2003.

[98]   A. J. Karabelas, "Scale formation in tubular heat exchangers--research priorities. ," *International Journal of Thermal Sciences,* vol. 41, pp. 682-692, 2002.

[99]   Q. Yang, Y. Liu, A. Gu, J. Ding, and Z. Shen, "Investigation of induction period and morphology of CaCO3 fouling on heated surface," *Chemical Engineering Science,* vol. 57, pp. 921-931, 2002.

[100]   T. G. Sabbides, "The crystallization of calcium carbonate in artificial seawater; role of the substrate," *Journal of Crystal Growth,* vol. 133, pp. 13-22, 1993.

[101]   J. Macadam and S. A. Parsons, "Calcium Carbonate Scale Control, Effect of Material and Inhibitors," vol. 49, ed, 2004, pp. 153-159.

[102]   F. Kan, and Tomson, "Mineral Scale Control in Subsea Completion," *Offshore Technology Conference, Houston,* 2001.

[103]   M. M. Reddy and G. H. Nancollas, "The crystallization of calcium carbonate. IV. The effect of magnesium, strontium and sulfate ions," *Journal of Crystal Growth,* vol. 35, pp. 33-38, 1976.

[104]   G. W. Akin and J. V. Lagerwerff, "Calcium carbonate equilibria in solutions open to the air. II. Enhanced solubility of CaCO3 in the

presence of Mg^{2+} and SO_4^{2-}," *Geochimica et Cosmochimica Acta,* vol. 29, pp. 353-360, 1965.

[105] W. A. House, M. R. Howson, and A. D. Pethybridge, "Crystallisation kinetics of calcite in the presence of magnesium ions," *Journal of the Chemical Society, Faraday Transactions 1: Physical Chemistry in Condensed Phases,* vol. 84, pp. 2723-2734, 1988.

[106] O. Devos, et al., "Nucleation-growth process of scale electrodeposition - Influence of the magnesium ions," *Crystal Growth,* 2009.

[107] N. Hamdona, and Hamza, "Spontaneous precipitation of Calcium Sulfate Dihydrate in the Presence of some Metal Ions," vol. 94, 1993.

[108] Y. Zhang and R. A. Dawe, "Influence of Mg^{2+} on the kinetics of calcite precipitation and calcite crystal morphology," *Chemical Geology,* vol. 163, pp. 129-138, 2000.

[109] S. Ghizellaoui and M. Euvrard, "Assessing the effect of zinc on the crystallization of calcium carbonate," *Desalination,* vol. 220, pp. 394-402, 2008.

[110] K. Zeppenfeld, "Prevention of CaCO3 scale formation by trace amounts of copper (II) in comparison to zinc (II). ," *Desalination,* vol. 252, pp. 60-65, 2010.

[111] B. H. Rankin and W. L. Adamson, "Scale formation as related to evaporator surface conditions," *Desalination,* vol. 13, pp. 63-87, 1973.

[112] M. Alahmad, "Factors affecting scale formation in sea water environments - An experimental approach.," *Chemical Engineering andTechnology,* vol. 31, pp. 149-156., 2008.

[113] Y. J. Sheng, S. Jiang, and H. K. Tsao, "Effects of geometrical characteristics of surface roughness on droplet wetting," *Journal of Chemical Physics,* vol. 127, 2007.

[114] B. Bhushan and Y. C. Jung, "Natural and biomimetic artificial surfaces for superhydrophobicity, self-cleaning, low adhesion, and drag reduction," *Progress in Materials Science,* vol. 56, pp. 1-108, 2010.

[115] M. Förster, Bohnet, M., "Influence of the transport properties of the crystal/heat transfer surface interfacial on fouling behavior," *Chemical Engineering and Technology,* vol. 26, pp. 1055-1060, 2003.

[116] Q. Yang, et al., "A theoretical analysis and experimental study of the induction period of calcium carbonate scaling," *Chemical Industry and Engineering,* vol. 45, pp. 199-205, 1994.

[117] M. Förster and W. Augustin, "Influence of the adhesion force crystal/heat exchanger surface on fouling mitigation," *Chemical Engineering and Processing, 1999.,* vol. 38, pp. 449-461., 1999.

[118] H. Müller-Steinhagen, Zhao, Q., "Investigation of low fouling surface alloys made by ion implantation technology," *Chemical Engineering Science,* vol. 52, pp. 3321-3332, 1997.

[119] H. Roques and A. Girou, "Kinetics of the formation conditions of carbonate tartars," *Water Research,* vol. 8, pp. 907-920, 1974.

[120] J. MacAdam and S. A. Parsons, "Calcium carbonate scale formation and control," *Reviews in Environmental Science and Biotechnology,* vol. 3, pp. 159-169, 2004.

[121] Y. Glater, and Cambell, "Scale Formation and Prevention. In: Principles of desalination," *Part B, 2nd ed., Academic Press,* vol. Chapter 10, p. 627, 1980.

[122] Z. Amjad, "Performance of Polymeric Additives as Hydroxyapatite Crystal Growth Inhibitor.," *Phosphorus Research Bulletin,* 1995.

[123] D. R. Sexsmith and E. Q. Petrey, "The use of polyelectrolytes for scale control in sea water evaporators," *Desalination,* vol. 13, pp. 89-90, 1973.

[124] X. Jianjun, et al., "The Fate of Scale Inhibitors in Oil/Gas Production," *Department of Environmental Science and Engineering, Rice University, Houston.*

[125] N. M. Farooqui and K. S. Sorbie, "Phase Behaviour of Poly-Phosphino Carboxylic Acid (PPCA) Scale Inhibitor for Application in Precipitation Squeeze Treatments.," *FAST, Institute of Petroleum Engineering, HeriotWatt University, Edinburgh.*

[126] A. Martinod, et al., "Progressing the understanding of chemical inhibition of mineral scale by green inhibitors," *Desalination,* vol. 220, pp. 345-352, 2008.

[127] T. N. Chen, Anne; Yuan, Mingdong; Sorbie, Ken, "Influence of PPCA inhibitor on CaCO3 scale surface deposition and bulk precipitation at elevated temperature " *Research gateway,* vol. 15, pp. 35-41, 2005.

[128] M. A. M.A. Quraishi, I. H. Farooqi, and P. A. Saini, "Natural Components as Corrosion Inhibitors for Cycled Systems," *NACE, Houston, Texas,* 1999.

[129] T. Chen, A. Neville, and M. Yuan, "Effect of PPCA and DETPMP Inhibitor Blends on CaCO$_3$ Scale Formation," *SPE International Symposium on Oilfield Scale, Aberdeen, UK,* 2004.

[130] N. Kohler, et al., "Polyaspartates: Biodegradable alternates to polyacrylates or noteworth multifuntional inhibitors?," *NACE International, Houston, Texas,* 2002.

[131] A. M. Kavanagh, et al., "Inhibitor Effects on Calcite Growth at Low Supersaturations," *Chemical Society, Faraday Trans,* vol. 86, pp. 965-972, 1990.

[132] S. Roweton, S. J. Huang, and G. Swift, "Polyaspartic acid : Synthesis, Biodegradation and Current Applications," *Polymers and the Environnement,* vol. 5, 1997.

[133] D. D. Alford, et al., "Biodegradation of Thermally Synthesized Polyaspartate. ," *Journal of Polymers and the Environment,* vol. 2, pp. 225-236, 1994.

[134] D. Verraest, et al. , "Carboxymethyl inulin: A new inhibitor for calcium carbonate precipitation. ," *The American Oil Chemists' Society,* vol. 73, pp. 55-62, 1996.

[135] C. V. Stevens, "Chemical Modification of Inulin, A Valuable Renewable Resource, and Its Industrial Applications, Biomacromolecules," *American Chemical Society,* vol. 2, pp. 1-16, 2001.

[136] C. M. Aurélie, "An Integrated Study of CaCO3 Formation and Inhibition," *University of Leeds PhD Thesis,* 2008.

[137] F. A. Setta and A. Neville, "Efficiency assessment of inhibitors on CaCO 3 precipitation kinetics in the bulk and deposition on a stainless steel surface (316L)," *Desalination,* vol. 281, pp. 340-347, 2011.

[138] C. E. Weinell, N. Marsh, and J. Roll, "Anti-Fouling Silicone Elastomers for Offshore Structures," 2006.

[139] I. R. Collins, "A New Model for Mineral Scale Adhesion," presented at the International Symposium on Oilfield Scale, Aberdeen, United Kingdom, 2002.

[140] Q. Zhao, S. Wang, and H. Müller-Steinhagen, "Tailored surface free energy of membrane diffusers to minimize microbial adhesion," *Applied Surface Science,* vol. 230, pp. 371-378, 2004.

[141] S. Krishnan, et al., "Comparison of the fouling release properties of hydrophobic fluorinated and hydrophilic PEGylated block copolymer surfaces: Attachment strength of the diatom Navicula and the green alga Ulva," *Biomacromolecules,* vol. 7, pp. 1449-1462, 2006.

[142] V. Eroini, N. Kapur, A. Neville, and M. Euvrard, "Preventing scale formation using modified surfaces," ed, 2011.

[143] A. Herz, M. R. Malayeri, and H. Müller-Steinhagen, "Fouling of roughened stainless steel surfaces during convective heat transfer to aqueous solutions," *Energy Conversion and Management,* vol. 49, pp. 3381-3386, 2008.

[144] I. R. Collins, "A New Model for Mineral Scale Adhesion," 2002, pp. 63-69.

[145] Q. Zhao and X. Wang, "Heat transfer surfaces coated with fluorinated diamond-like carbon films to minimize scale formation," *Surface and Coatings Technology,* vol. 192, pp. 77-80, 2005.

[146] J. MacAdam and S. A. Parsons, "Scaling on heat transfer surfaces: Chemical versus Non Chemical control," *NACE conference,* 2004.

[147] Q. Yang, J. Ding, and Z. Shen, "Investigation of calcium carbonate scaling on ELP surface," *Journal of Chemical Engineering of Japan,* vol. 33, pp. 591-596, 2000.

[148] Q. Yang, J. Ding, and Z. Shen, "Investigation on fouling behaviors of low-energy surface and fouling fractal characteristics," *Chemical Engineering Science,* vol. 55, pp. 797-805, 2000.

[149] A. Neville, et al., "Optimizing Inhibitor Efficiency Using Electrochemical Methods," 2002.

[150] H. U. Zettler, et al, "Influence of surface properties and characteristics on fouling in plate heat exchangers," *Heat Transfer Engineering,* vol. 26, 2005.

[151] J. M. Herri, et al., "Interest of in situ turbidimetry for the characterization of methane hydrate crystallization: Application to the study of kinetic inhibitors," *Chemical Engineering Science,* vol. 54, pp. 1849-1858, 1999.

[152] V. Tantayakom, et al., "Scale inhibition study by turbidity measurement," *Colloid and Interface Science,* vol. 284, pp. 57-65, 2005.

[153] P. G. a. C. G. K. Koutsoukos, "Precipitation of Calcium Carbonate in Aqueous Solutions," *Chem. Soc., Faraday Trans.1,* vol. 80, pp. 1181-1192, 1984.

[154] M. M. Reddy, G.H. Nancollas, "The crystallization of calcium carbonate : I. Isotopic exchange and kinetics," *Colloid and Interface Science,* vol. 36, pp. 166-172, 1971.

[155] S. He, A. T. Kan, and M. B. Tomson, "Inhibition of calcium carbonate precipitation in NaCl brines from 25 to 90°C," *Applied Geochemistry,* vol. 14, pp. 17-25, 1999.

[156] O. Sohnel and J. W. Mullin, "A method for the determination of precipitation induction periods," *Crystal Growth,* vol. 44, pp. 377-382, 1978.

[157] L. E. Holysz, et al., "Influence of impurity ions and magnetic field on the properties of freshly precipitated calcium carbonate. ," *Water Research,* vol. 37, pp. 3351-3360, 2003.

[158] J. R. Clarkson, T.J. Price, and C.J. Adams, "Role of Metastable Phases in the Spontaneous Precipitation of Calcium Carbonate," *Chem. Soc. Faraday Trans.1* vol. 88, pp. 243-249, 1992.

[159] C. W. Turner and D. W. Smith, "Calcium Carbonate Scaling Kinetics Determined from Radiotracer Experiments with Calcium-47," *Industrial and Engineering Chemistry Research,* vol. 37, pp. 439-448, 1998.

[160] C. Gabrielli, et al., "Quartz crystal microbalance investigation of electrochemical calcium carbonate scaling," *The Electrochemical Society,* vol. 145, pp. 2386-2396, 1998.

[161] G. H. Nancollas, "Kinetics of crystal growth from solution," *Journal of Crystal Growth,* vol. 3-4, pp. 335-339, 1968.

[162] P. G. Koutsoukos and C. G. Kontoyannis, "Prevention and inhibition of calcium carbonate scale," *Crystal Growth,* vol. 69, pp. 367-376, 1984.

[163] B. Bazin, N. Kohler, and A. Zaitoun, "Some Insights Into the Tube-Blocking-Test Method To Evaluate the Efficiency of Mineral Scale Inhibitors."

[164] A. L. Graham, et al., "How Minimum Inhibitor Concentration (MIC) and Sub-MIC Concentrations Affect Bulk Precipitation and Surface Scaling Rates," presented at the SPE International Symposium on Oilfield Chemistry, The Woodlands, Texas, 2005.

[165] C. Gabrielli, G. Maurin, G. Poindessous, and R. Rosset, "Nucleation and growth of calcium carbonate by an electrochemical scaling process," *Journal of Crystal Growth,* vol. 200, pp. 236-250, 1999.

[166] A. Neville, T. Hodgkiess, and A. P. Morizot, "Electrochemical assessment of calcium carbonate deposition using a rotating disc electrode (RDE)," *Journal of Applied Electrochemistry,* vol. 29, pp. 455-462, 1999.

[167] J. Rinat, E. Korin, L. Soifer, and A. Bettelheim, "Electrocrystallization of calcium carbonate on carbon-based electrodes," *Journal of Electroanalytical Chemistry,* vol. 575, pp. 195-202, 2005.

[168] W. Sun, G. Liu, L. Wang, and Y. Li, "A mathematical model for modeling the formation of calcareous deposits on cathodically protected steel in seawater," *Electrochimica Acta,* vol. 78, pp. 597-608, // 2012.

[169] W. a. M. Z. Frenier, "Formation, removal, and inhibition of inorganic scale in the oilfield environment.," *Society of Petroleum Engineers Journal,* 2008.

[170] W. F. Langlier, "The Analytical Control of Anti-Corrosion Water Treatment " *The American Water Works Association,* vol. 28, pp. 1500–1521, 1936.

[171] A. P. Morizot, Neville, A., & Hodgkiess, T, "Studies of the deposition of $CaCO_3$ on stainless steel surface by a novel electrochemical technique," *Journal of Crystal Growth,* pp. 198/199, 738/743., 1999a.

[172] A. P. Morizot and A. Neville, "Using an Electrochemical Approach for Monitoring Kinetics of CaCO3 and BaSO4 Scale Formation and Inhibition on Metal Surfaces," *SPE Journal,* vol. 6, pp. 220-223, 06/01/2001 2001.

[173] J. L. Semmlow, " Biosignal and biomedical image processing - Matlab based applications," 2004.

[174] H. E. Boyer and T. L. Gall, *Metals Handbook. Desk Edition ed. ,* 1997.

[175] T. Chen, A. Neville, and M. Yuan, "Influence of Mg2 + on CaCO3 formation-bulk precipitation and surface deposition," *Chemical Engineering Science,* vol. 61, pp. 5318-5327, 2006.

[176] W. C. Cheong, "Biomimetic Approach to Anti-Fouling Surfaces," *School of Mechanical Engineering. University of Leeds PhD. Thesis*

p. 256, 2011.

[177] P. C. Rieke, "Selection of phase and control of orientation during physisorption on surfaces on homogeneously formed calcium carbonate nuclei," *Materials Science and Engineering,* vol. C2, pp. 181-189, 1995.

[178] P. Kjellin, "X-ray diffraction and scanning electron microscopy studies of calcium carbonate electrodeposited on a steel surface," *Colloids and Surfaces A: Physicochemical and Engineering Aspects,* vol. 212, pp. 19-26, 1/1/ 2003.

[179] A. L. Graham, L. S. Boak, K. S. Sorbie, and A. Neville, "How Minimum Inhibitor Concentration (MIC) and Sub-MIC Concentrations Affect Bulk Precipitation and Surface Scaling Rates," *SPE Production & Operations,* vol. 21, pp. pp. 19-25, 02/01/2006 2006.

[180] T. Chen, A. Neville, and M. Yuan, "Assessing the effect of on scale formation–bulk precipitation and surface deposition," *Journal of Crystal Growth,* vol. 275, pp. e1341-e1347, 2005.

[181] C. Gabrielli, R. Jaouhari, S. Joiret, G. Maurin, and P. Rousseau, "Study of the electrochemical deposition of CaCO3 by in situ Raman spectroscopy. I. Influence of the substrate," *Journal of the Electrochemical Society,* vol. 150, pp. C478-C484, 2003.

[182] B. Tolaieb, R. Bingham, and A. Neville, "Barium Sulfate Kinetics on Steel Surfaces at Different Supersaturation Ratios."

[183] D. Hasson, D. Bramson, B. Limoni-Relis, and R. Semiat, "Influence of the flow system on the inhibitory action of CaCO 3 scale prevention additives," *Desalination,* vol. 108, pp. 67-79, 1997.

[184] V. A. Hao Wang, Juergen Tropsch, Roland Ettl, and Tommy Nylander, "Formation of $CaCO_3$ Deposits on Hard Surfaces·Effect of Bulk Solution Conditions and Surface Properties," *Applied Materials and Interfcaes,* vol. 5, pp. 4035-4045, 2013.

[185] A. J. Karabelas, "Scale formation in tubular heat exchangers—research priorities," *International Journal of Thermal Sciences,* vol. 41, pp. 682-692, 6// 2002.

[186] E. M. Flaten, M. Seiersten, and J.-P. Andreassen, "Induction time studies of calcium carbonate in ethylene glycol and water," *Chemical Engineering Research and Design,* vol. 88, pp. 1659-1668, 12// 2010.

[187] C. Yang, D. Xu, and Z. Shen, "Theoretical analysis and experimental study of the induction period of calcium carbonate scaling," *Huagong Xuebao/Journal of Chemical Industry and Engineering (China),* vol. 45, pp. 199-205, 1994.

[188] M. Kahlweit, "Ostwald ripening of precipitates," *Advances in Colloid and Interface Science,* vol. 5, pp. 1-35, 8// 1975.

[189] I. M. Lifshitz and V. V. Slyozov, "The kinetics of precipitation from supersaturated solid solutions," *Journal of Physics and Chemistry of Solids,* vol. 19, pp. 35-50, 4// 1961.

[190] A. Baldman, "Progress in Ostwald ripening theories and their applications to nickel-base superalloys," *Materials Science,* vol. 37, pp. 2171 – 2202, 2002.

[191] R. D. van der Weijden, A. E. van der Heijden, G. J. Witkamp, and G. M. van Rosmalen, "The influence of total calcium and total carbonate on the growth rate of calcite," *Journal of Crystal Growth,* vol. 171, pp. 190-196, 1997/01/02 1997.

[192] S. Muryanto, A. P. Bayuseno, H. Ma'mun, M. Usamah, and Jotho, "Calcium Carbonate Scale Formation in Pipes: Effect of Flow Rates, Temperature, and Malic Acid as Additives on the Mass and Morphology of the Scale," *Procedia Chemistry,* vol. 9, pp. 69-76, // 2014.

[193] M. C. XING Xiaokai, CHEN Yongchang, "Mechanism of Calcium Carbonate Scale Deposition under Subcooled Flow Boiling Conditions," *Chinese J. Chem. Eng,* vol. 13, pp. 464 - 470, 2005.

[194] A. L. Graham, L. S. Boak, K. S. Sorbie, and A. Neville, "How Minimum Inhibitor Concentration (MIC) and Sub-MIC Concentrations Affect Bulk Precipitation and Surface Scaling Rates," 2006/2/1/.

[195] S. Graham, and Jordan, "How Scale Inhibitors Work and How this Affects Test Methodology.," *Presented at the 3rd International Conference on Advances in Solving Oilfield Scaling, Aberdeen,* 1997.

[196] O. Sanni, T. Charpentier, N. Kapur, and A. Neville, "Study of Surface Deposition and Bulk Scaling Kinetics in Oilfield Conditions Using an In-Situ Flow Rig," 2015.

Appendix A.   Flow path and velocities by CFD

Max Reynold no. = 4.0187
Average velocity at centre = 0.0032580 m/s
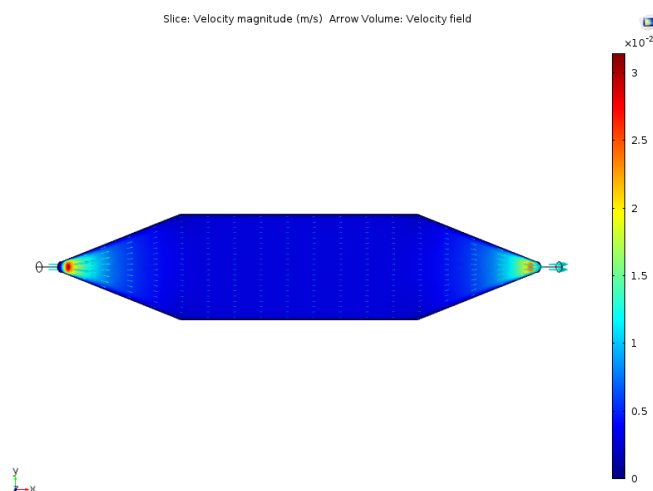
Figure S 1. Flow Characteristic at 10ml/min: velocity magnitude (m/s; Arrow volume indicates velocity field across flow cell

Max Reynold no. = 7.6089
Average velocity at centre = 0.0063454 m/s
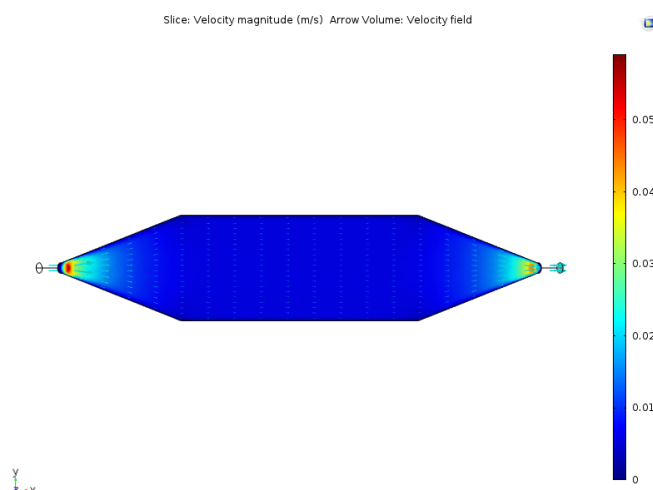
Figure S 2. Flow Characteristic at 20ml/min: velocity magnitude (m/s; Arrow volume indicates velocity field across flow cell

Max Reynold no. = 15.357
Average velocity at centre = 0.012770 m/s
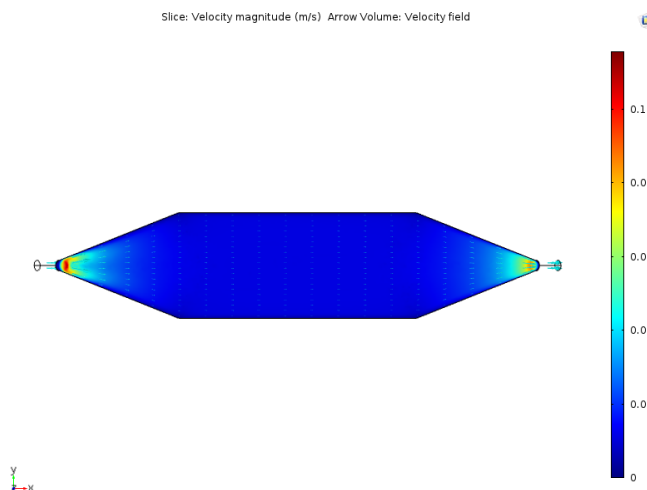
Figure S 3. Flow Characteristic at 40ml/min: velocity magnitude (m/s; Arrow volume indicates velocity field across flow cell

Max Reynold no. = 22.665
Average velocity at centre = 0.018773 m/s
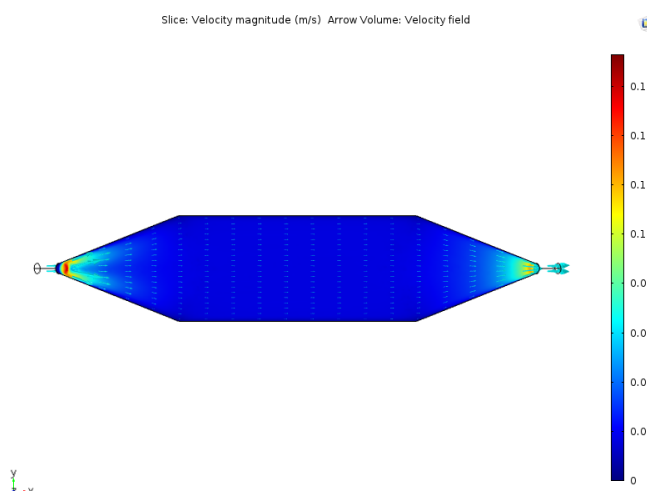
Figure S 4. Flow Characteristic at 60ml/min: velocity magnitude (m/s; Arrow volume indicates velocity field across flow cell
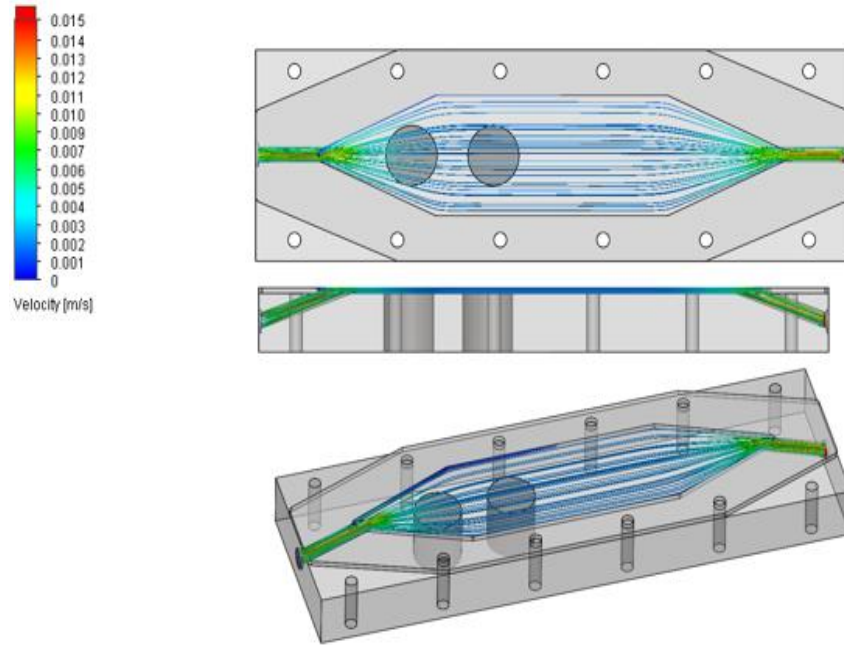
Flow path CFD – 10 ml/min
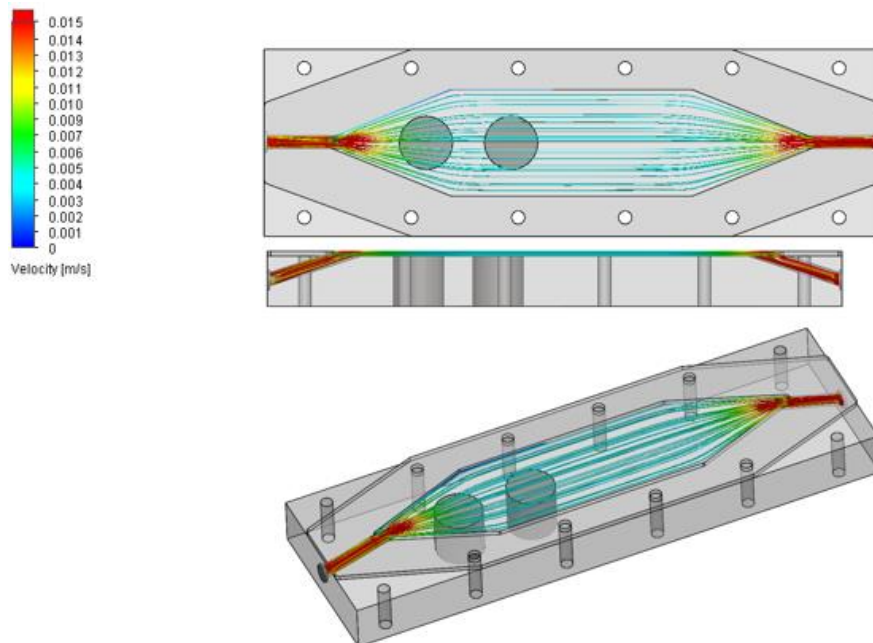
Figure S 5. Flow path CFD – 20 ml/min
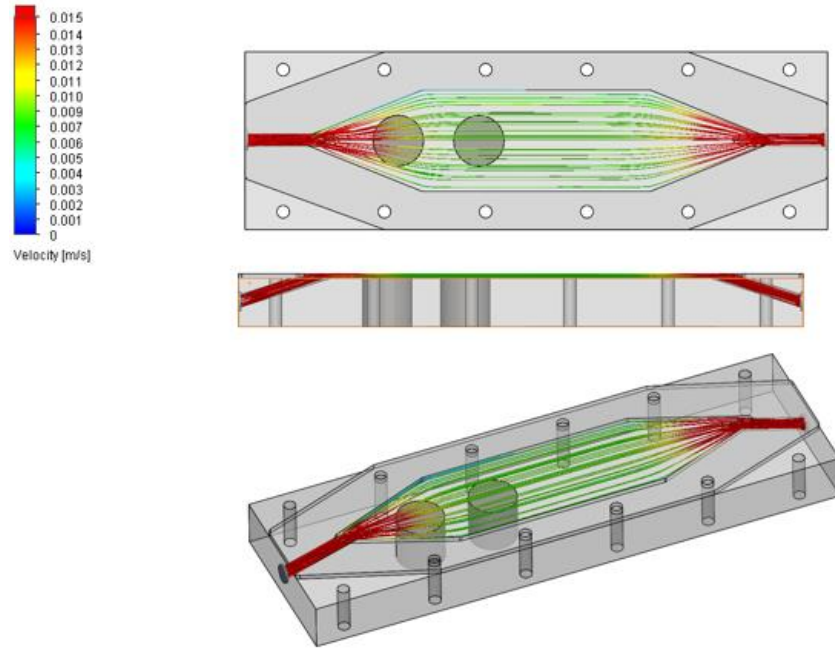
Figure S 6. Flow path CFD – 40 ml/min
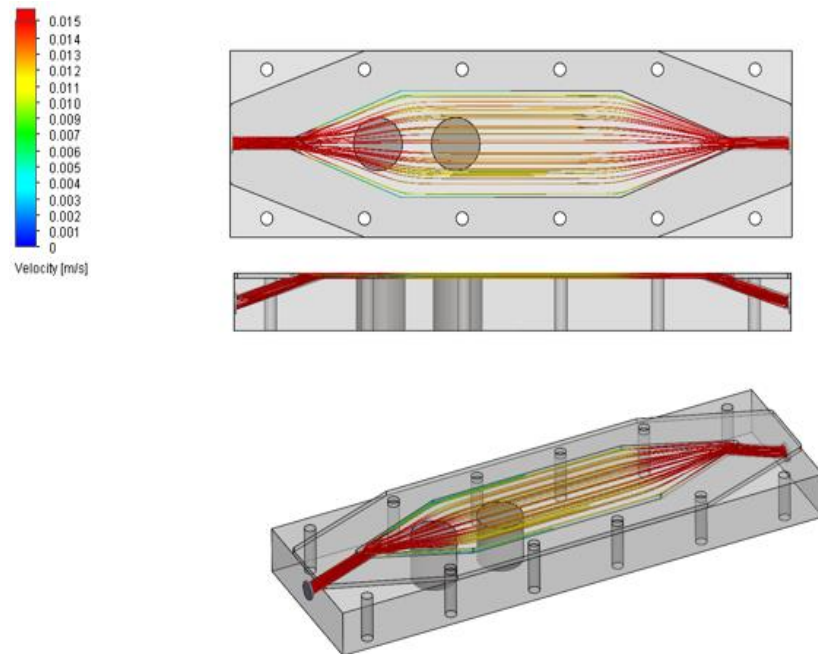
Figure S 7. Flow path CFD – 60 ml/min

Appendix B.   Algorithms for Image Processing

```
a = imread('calcium.jpg');

b = rgb2gray(a);
```

Thresholding

```
d = edge (b, 'sobel');

e = edge (b, 'canny');

f = edge (b, 'roberts');

g = edge (b, 'prewit');
```

Morphological Operation

```
e2 = bwmorph (e, 'bridge');

e3 = bwmorph (e2, 'close');

e4 = bwmorph (e3, 'fill');

e5 = bwmorph (e4, 'open');
```

Image counting and average Size

```
cc = bwconncomp (e5, 8);

cc.NumObjects

area = regionprops (cc, 'basic');

area.Area;

sizex=zeros(length(area),1);

i=1:length(area);

sizex(i) = area(i).Area;
```

```matlab
mn=mean(sizex);
```

Surface coverage

```matlab
nWhite = nnz (e5);

nBlack = numel (e5) - nWhite;

srfc = nBlack/nWhite;
```

Particle size distribution histogram

```matlab
part_area = [area.Area];

nbins = 20;

hist (part_area, 20)

xlabel ('Average sizes(area)','fontsize',15, 'color','k')

ylabel ('Frequency of distribution','fontsize',15, 'color','k')

grid on
```

Appendix C.   Quantitative analysis of surface scale build up
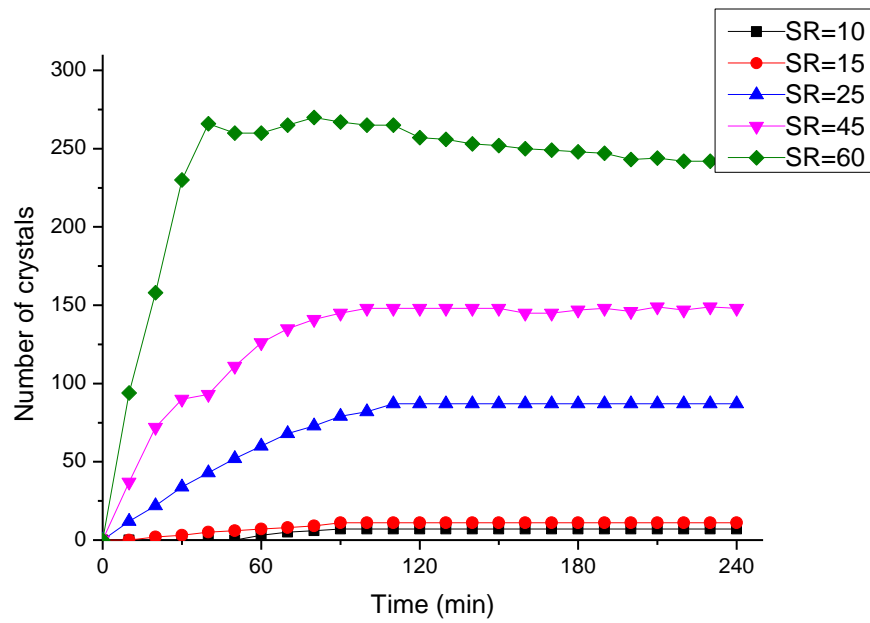
Figure S 8. Number of crystals as a function of time at different SR, T = 40ºC, Q = 20ml/min
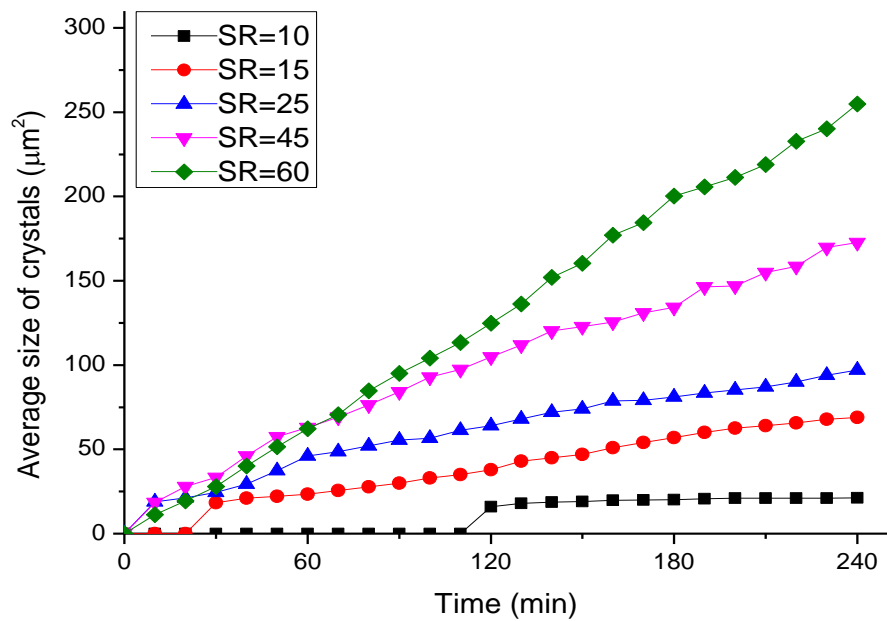
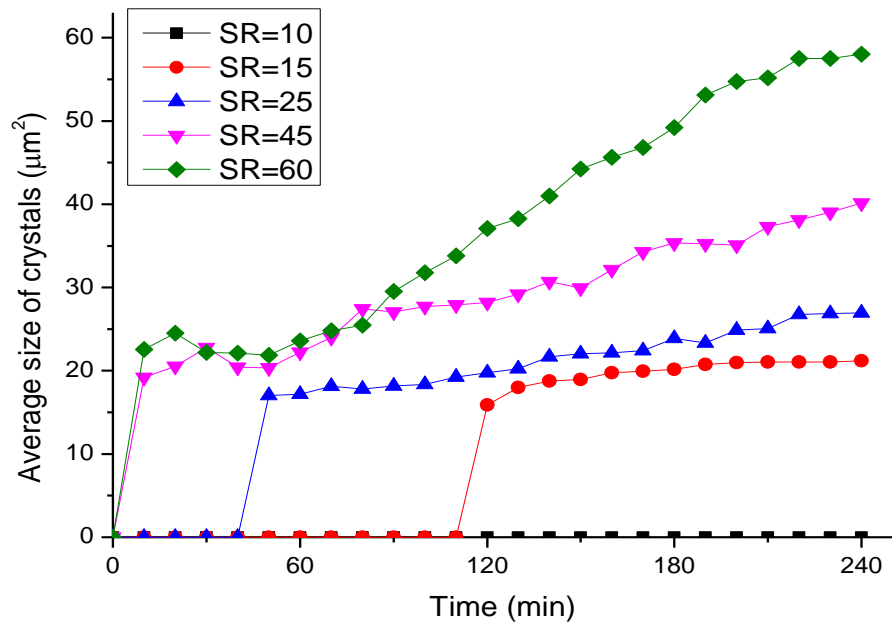**Figure S 9. Average size of crystals as a function of time at different SR, 40ºC, Q= 20ml/min**
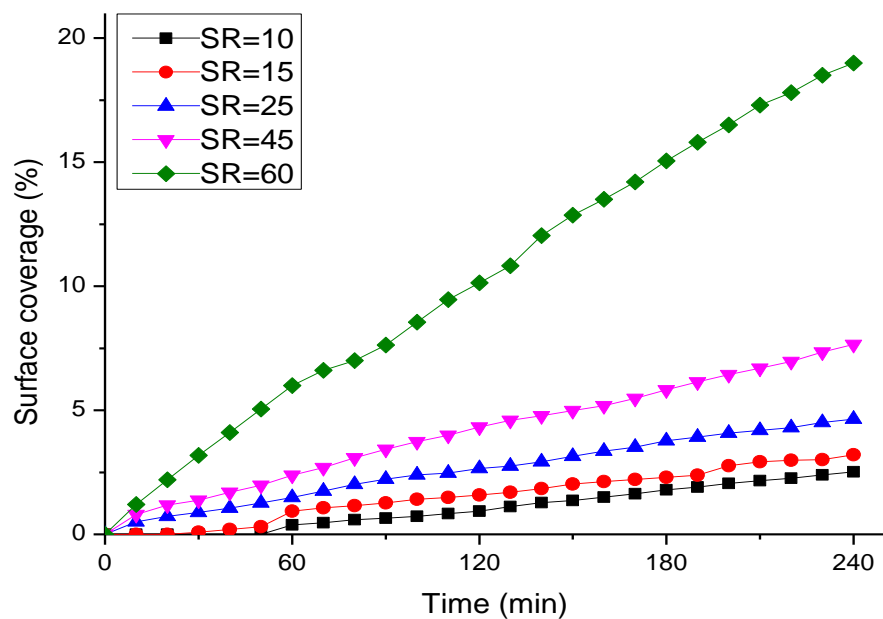
Figure S 10. Surface coverage of crystals as a function of time at different SR, T = 40⁰C, Q= 20ml/min

Effects of flow rates
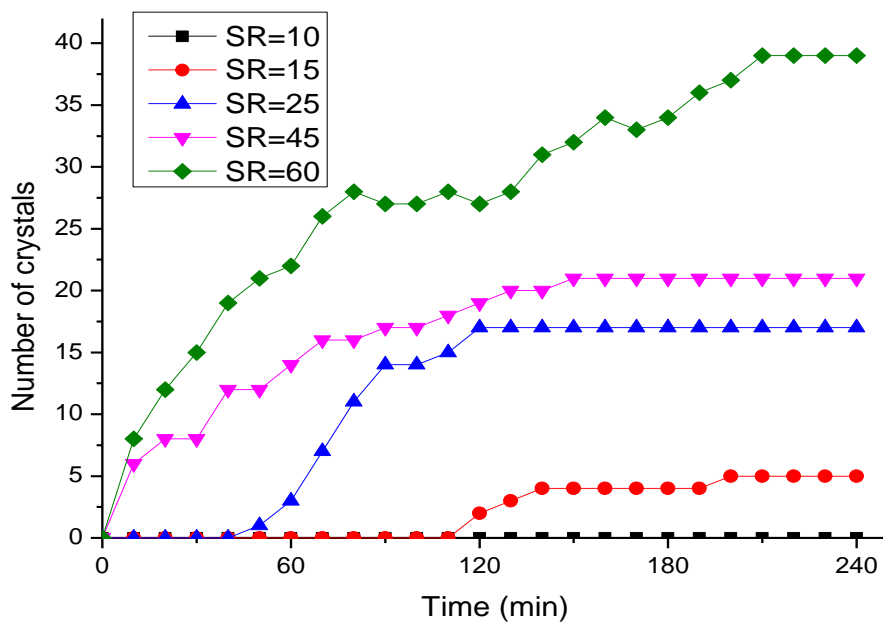
Figure S 11. Number of crystals as a function of time at different SR, T =25⁰C,

Figure S 12. Average size of surface crystals as a function of time at different SR,

T =25ºC, Q = 10ml/min

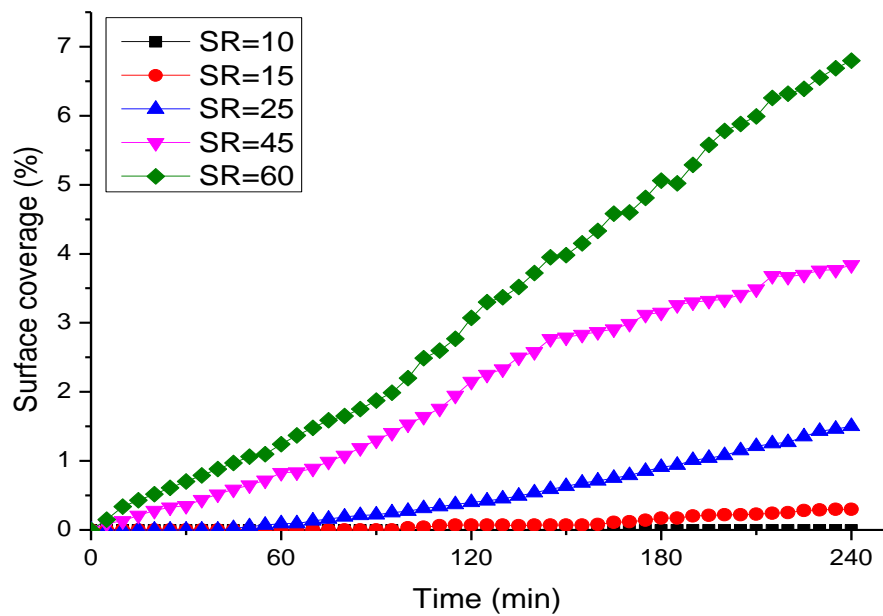**Figure S 13. Surface coverage of crystals as a function of time at different SR, T =25ºC, Q = 10ml/min**
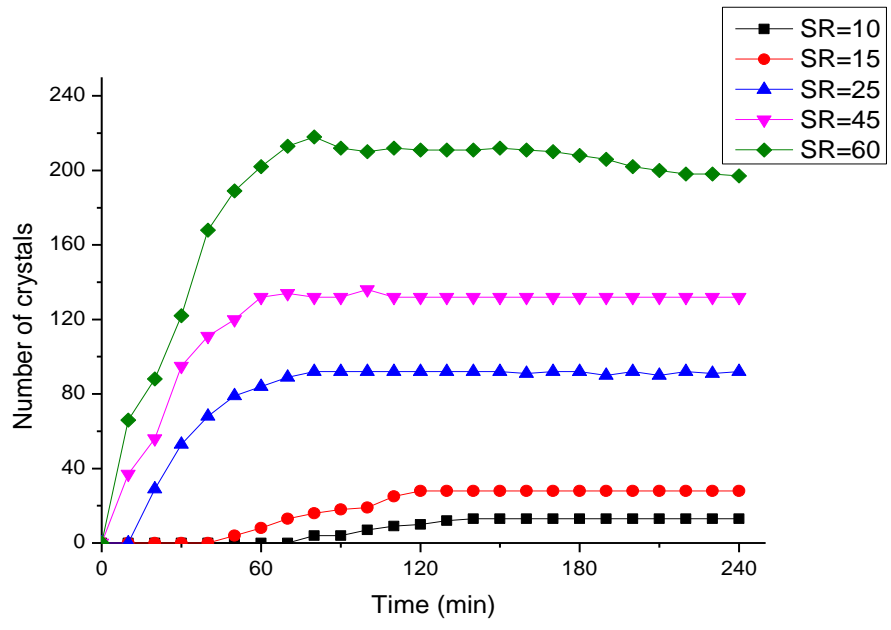
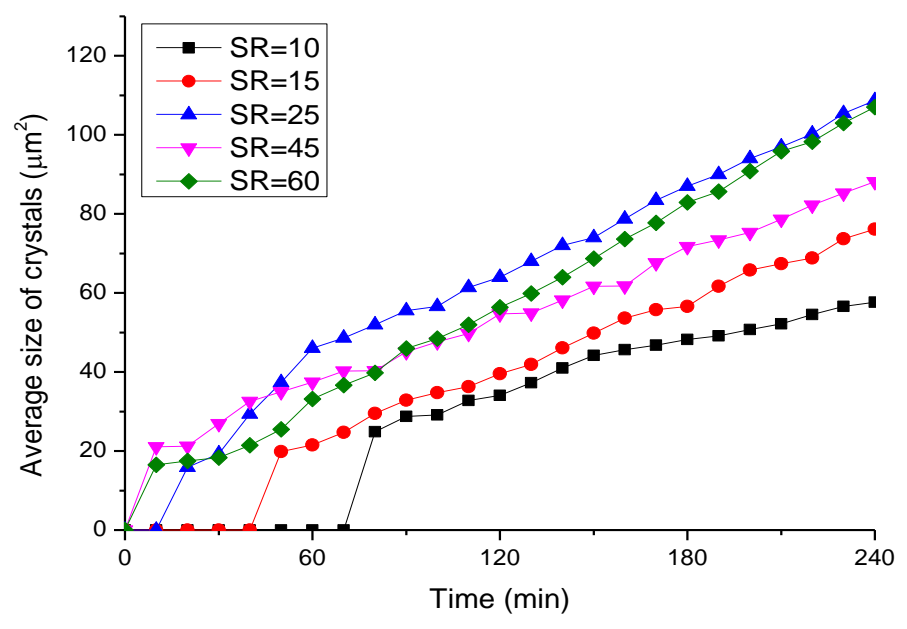**Figure S 14. Number of crystals as a function of time at different SR, T =25ºC, Q = 40ml/min**

Figure S 15: Average size of surface crystals as a function of time at different SR, T =25ºC, Q = 40ml/min
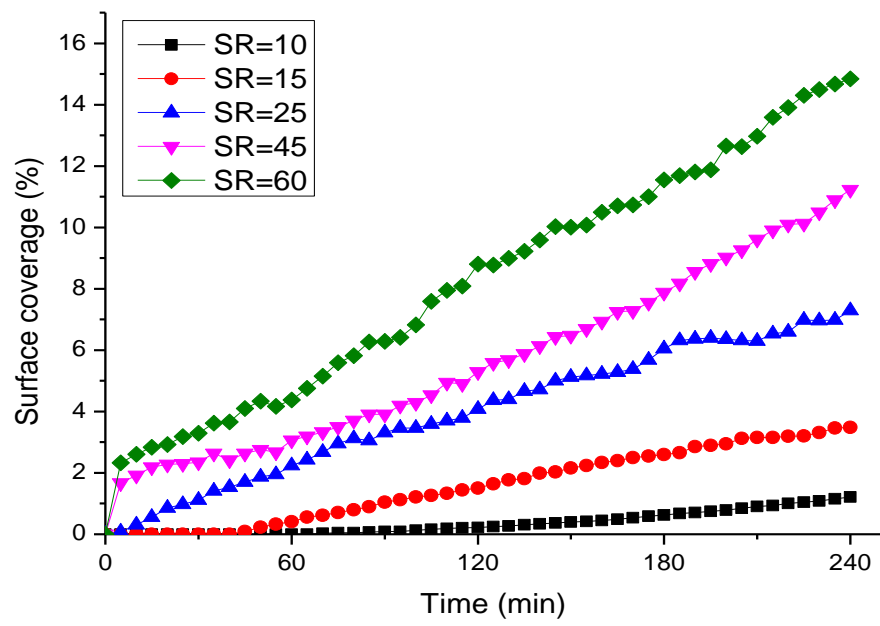
Figure S 16: Surface coverage of crystals as a function of time at different SR, T =25ºC, Q = 40ml/min